

Università degli Studi di Napoli Federico II

Thesis in Chemical Sciences

XXIV cycle



*Structure and function of hemoproteins  
from cold-adapted organism*

*Dissertation for the degree of "Doctor Philosophiae"*

**Candidate:**

**Roberta Russo**

**Tutors:**

**Dott. Cinzia Verde**

**Prof. Pompea Del Vecchio**

**Supervisor:**

**Prof. Alessandro Vergara**

**December 2011**

# ABSTRACT

Environmental oxygen availability certainly plays a key role in the evolution of polar marine life, as suggested by the physiological and biochemical strategies that the organisms have adopted to acquire, deliver and scavenge oxygen.

The psychrophilic Antarctic bacterium *Pseudoalteromonas haloplanktis* TAC125 gives the opportunity to explore the cellular strategies adopted *in vivo* by cold-adapted microorganisms to cope with cold and high oxygen concentration. Within vertebrates, the dominant suborder Notothenioidei of the Southern Ocean is one of the most interesting models to study the evolutionary biological responses to extreme environment.

Hemoproteins of cold-adapted organisms are likely to fulfil important physiological roles, not only in delivering oxygen to cells, but also in protecting them from the nitrosative and oxidative stress.

This thesis will in particular focus on: (i) the structural and functional features of globins of the Antarctic marine bacterium *Pseudoalteromonas haloplanktis* TAC125, (ii) the role of neuroglobin (Ngb) recently identified in the brain of Antarctic notothenioid fish.

The genome of the cold-adapted bacterium *P. haloplanktis* TAC125 contains multiple genes encoding three distinct monomeric hemoglobins (Hbs) exhibiting a 2/2  $\alpha$ -helical fold (2/2Hb). One of these 2/2Hb (*Ph-2/2HbO*) has been over-expressed and characterised by spectroscopic analysis, kinetic measurements and computer simulation approaches (Howes et al., 2011; Giordano et al., 2011). The results indicate unique adaptive structural properties, that overall confer higher flexibility to the protein and may facilitate its functioning in the cold by providing greater freedom for the correct positioning of ligand(s). Similar to Ngb, the recombinant protein is hexacoordinated in the ferric and ferrous forms, and shows a strong dependence on pH (Howes et al., 2011; Giordano et al., 2011).

Polar fish are a suitable model to learn more about the function of globins in the brain, and especially about their role in species devoid of Hb and Myoglobin (Mb). The finding that Antarctic icefishes retain the Ngb gene despite having lost Hb, and Mb in most species, suggests a crucial function. The function of Ngb needs to be ascertained, because it may have important implications in the physiology and pathology of the brain.

The first structural model of fish Ngb was described using molecular dynamics simulations. Specifically, Ngb genes from a colourless-blooded Antarctic icefish species (*Chaenocephalus aceratus*), and a related red-blooded species (*Dissostichus mawsoni*), were cloned, the recombinant proteins were expressed and purified, and then sequenced and analysed. Both Antarctic fish Ngbs are hexacoordinated, but have some peculiarities that differentiate them from mammalian counterparts: they have extensions in the N and C termini, interacting with the EF loop, and a gap in the alignment that changes the CD-region structure/dynamics, that has been found to play a key role in human Ngb.

The adaptive modifications to compensate for the effects of low temperature appear to primarily rely on a higher flexibility of key parts of the molecular structure and/or decreased overall stability. At all levels analysed, the functionally most crucial adaptation to permanently low temperatures apparently requires molecular flexibility to support cell functioning. Proteins are the major targets for the ensuing mechanisms of adaptation.

# TABLE OF CONTENTS

<b>ABSTRACT</b>	<b>1</b>
<b>LIST OF ABBREVIATIONS</b>	<b>6</b>
<b>ACKNOWLEDGEMENTS</b>	<b>9</b>
<b>Chapter 1: Introduction</b>	<b>10</b>
Summary	10
1.1 The Antarctic	10
1.2 Molecular adaptations in Notothenioidei	11
1.3 Molecular adaptations in polar bacteria: the <i>Pseudoalteromonas haloplanktis</i> TAC125 case	14
1.4 Hemoproteins	17
1.5 Neuroglobin: the search of function of a vertebrate Hb	21
1.6 “2-on-2” Hemoglobin	24
1.7 Hexacoordination in hemoproteins	28
1.8 Objectives of the Ph.D. project	30
<b>Chapter 2: Structural and functional characterization of the 2/2 Hb of cold-adapted bacterium <i>Pseudoalteromonas haloplanktis</i> TAC125</b>	<b>32</b>
Summary	32
2.1 Materials and Methods	32
2.1.1 Preparation <i>Ph-2/2HbO</i> : expression and purification	32
2.1.2 Sample preparation for RR and EPR experiments	33
2.1.3 Spectroscopy	34
2.1.4 Sequence alignment	35
2.1.5 Molecular dynamics simulations	35
2.1.6 Circular dichroism (CD) spectroscopy	35
2.1.7 Protein thermostability	36
2.1.8 Fluorescence measurements	36
2.1.9 High pressure spectroscopy	36
2.1.10 CO-bimolecular recombination rates by Laser Flash Photolysis (LFP)	37
2.2 Results and Discussion	38
2.2.1 Purification of <i>Ph-2/2HbO</i>	38

2.2.2 Sequence alignment	39
2.2.3 Spectroscopy at room temperature: ferric form	41
2.2.4 Spectroscopy at low temperature	44
2.2.5 Molecular dynamics simulations	45
2.2.6 Spectroscopy: ferrous form	47
2.2.7 CO-rebinding kinetic profile and determination of $k_{on}$ CO rates at different pH	50
2.2.8. Circular dichroism spectroscopy	53
2.2.9 High Pressure effects on <i>Ph-2/2HbO</i>	57
2.3. Conclusion	65
<b>Chapter 3: Neuroglobin from the brain and retina of Antarctic notothenioid fishes</b>	<b>68</b>
Summary	68
3.1 Materials and Methods	69
3.1.1 Cloning and sequencing of Ngbs cDNA	69
3.1.2 Site-directed mutagenesis	69
3.1.3 Expression and purification of Ngbs	69
3.1.4 Electronic absorption and RR spectroscopy	70
3.1.5 Multiple sequence alignment and structure modelling	70
3.1.6 Classical molecular dynamics	71
3.1.7 Essential dynamics (ED)	71
3.1.8 High pressure spectroscopy	72
3.2 Results and Discussion	72
3.2.1 Sequence alignment of mammal and fish Ngbs and structure Modeling	72
3.2.2 Molecular Dynamics (MDS): differences between <i>D. mawsoni</i> and <i>C. aceratus</i> Ngbs	73
3.2.3 Expression and purification of Antarctic fish Ngbs	77
3.2.4 UV-visible absorption and RR spectroscopy	78
3.2.5 High pressure effects on ferrous <i>C. acer</i> Ngb	80
3.3 Conclusion	83
<b>REFERENCES</b>	<b>86</b>

“The peculiar heme pocket of the 2/2 hemoglobin of cold adapted *Pseudoalteromonas haloplanktis* TAC125” Howes BD, Giordano D, Boechi L, **Russo R**, Mucciacciaro S, Ciaccio C, Sinibaldi F, Fittipaldi M, Martí MA, Estrin DA, di Prisco G, Coletta M, Verde C, Smulevich G, (2011). *J Biol Inorg Biochem* **16**, 299-311

“Ligand- and proton-linked conformational changes of the ferrous 2/2 hemoglobin of *Pseudoalteromonas haloplanktis* TAC125” Giordano D, **Russo R**, Ciaccio C, Howes BD, di Prisco G, Marden MC, Hui Bon Hoa G, Smulevich G, Coletta M, Verde C (2011). *IUBMB Life*, **63**(7), 566-573

“Structure and dynamics of Antarctic fish neuroglobin assessed by computer simulations” Boron, I., **Russo R**, Boechi L, Cheng C-H C, di Prisco G, Estrin D A, Verde C, Nadra AD, (2011) *IUBMB life* **633**, 206-213

## LIST OF ABBREVIATIONS

Å: Ångström

Abs: Absorbance

ACC: Antarctic Circumpolar Current

AFGP: Antifreeze Glycoproteins

Ala, A: Alanine

APF: Antarctic Polar Front

Arg, R: Arginine

Asn, N: Asparagine

Asp, D: Aspartic Acid

β-ME: beta-mercaptoethanol

bis-His: axially, by two histidine residues, coordinated heme group

*Bs*: *Bacillus subtilis*

CAPS: 3-(Cyclohexylamino)-1-propanesulfonic acid

*Ce*: *Chlamydomonas eugametos*

CD: Circular Dichroism

CO: carbon monoxide

CT: charge-transfer transition

Cys, C: Cysteine

D2: Second derivative

Da: dalton

DEAE: Diethylaminoethyl

DNA: Deoxyribonucleic acid

DTT: Dithiothreitol

ED: essential dynamic

EDTA: Ethylene-diamino-tetra-acetic acid

EPR: electron paramagnetic resonance

FAD: Flavin Adenine Dinucleotide

Fe (II): Iron atom (ferrous)

Fe (III): Iron atom (ferric)

FlavoHb: Flavohemoglobin

FPLC: Fast Protein Liquid Chromatography

Gln, Q: Glutamine  
Glu, E: Glutamic Acid  
Gly, G: Glycine  
*Gs: Geobacillus stearothermophilus*  
GuHCl: Guanidine Hydrochloride  
H<sub>2</sub>S: Dihydrogen monosulfide  
Hb: Hemoglobin  
His, H: Histidine  
HP: High Pressure  
HS: high spin  
Ile, I: Isoleucine  
IPTG Isopropyl β-D-thiogalactopyranoside  
Leu, L: Leucine  
LFP: Laser Flash Photolysis  
LS: low spin  
Lys, K: Lysine  
Met, M: Methionine  
Mb: Myoglobin  
MD: Molecular Dynamics  
MES: methyl ethyl sulfonate  
MK: marker  
MOPS: 3-(N-morpholino)propanesulfonic acid  
MPa: Megapascal  
mrw: mean residue weight  
*Mt: Mycobacterium tuberculosis*  
MW: molecular weight  
K: Kelvin  
Kbar: kilobar  
NaCl: Sodium Chloride  
Ngb: Neuroglobin  
nm: nanometer  
NMR: nuclear magnetic resonance  
NO: nitrogen monoxide  
ns: nanosecond

OD: optical density  
PAGE: Polyacrylamide gel electrophoresis  
*Pc: Paramecium caudatum*  
PCR: polymerase chain reaction  
pdb: protein data bank  
*Ph-2/2HbO*: 2-on-2 hemoglobin from *Pseudoalteromonas haloplanktis* TAC125  
*PhTAC125*: *Pseudoalteromonas haloplanktis* TAC125  
RMSD: Root Mean Square Deviation  
RMSF: Root Mean Square Fluctuation  
ROS: Reactive Oxygen Species  
rpm: revolutions per minute  
RR: Resonance Raman  
SDS: Sodium dodecylsulfate  
Ser, S: Serine  
TCEP: tris(2-carboxyethyl)phosphine  
Tm: melting temperature  
TRIS: hydroxymethyl-aminomethane  
Trp, W: Tryptophan  
Tyr, Y: Tyrosine  
Val, V: Valine  
UV-Vis: ultraviolet-visible  
 $\Delta G$ : Activation free Energy  
 $\Delta H$ : Enthalpy of Activation  
 $\lambda$ : Wavelength

## ACKNOWLEDGEMENTS

*Science is a team work and I feel indebted to many people who contribute significantly to the success of the work presented in this thesis.*

*Thanks very much to Dott. Cinzia Verde and Prof. Guido di Prisco. They accepted me in their laboratory twice, as a master degree student and then as a Ph.D. student, I thank them for believing in me and for always supporting me during these years. I have greatly benefited from this experience, scientifically and personally.*

*I would like to thank my Tutor, Prof. Pompea Del Vecchio for discussion, experimental assistance, infinite patience, and especially for personal and human support.*

*Thanks to all my group, Dr. Daniela Giordano, Dr. Alessia Riccio, Dr. Daniela Coppola, and all people in the laboratory for the technical and theoretical support and for the nice and friendly work atmosphere. I am particularly grateful to Dott. Donatella de Pascale, who shared with me her knowledge and taught me how to love this job and “life”, helping me in difficult moments, and to Dott. Ennio Cocca, for his balance, kindness, and for sharing with me one of the most exiting experience in my life....Antarctica! All this people was my second family in the last sixth years.*

*I express my gratitude to all people I have collaborated with, for the interest and fast feedback on the discussion of the data, the organization of all the steps of the scientific research. These collaborations were determinant for the success of this thesis. Particular thanks to Dott. Leonardo Boechi, for always supporting me first as a colleague, then as a big friend.*

*Most importantly, thanks to my big family, to my father and to my sweet sisters, who showed interest in my work, offering support in hard times, and very patient with my tiredness.*

# Chapter 1

## Introduction

### Summary

The Antarctic marine environment is one of the most extreme on Earth due to its stably low temperature and high oxygen content. Here in the first chapter I will discuss various aspects of the molecular adaptations evolved by Antarctic fish and marine microorganisms living in this environment. This chapter will in particular focus on: *(i)* the genetic/genomic bases of adaptation in Antarctic notothenioid fish and bacteria; *(ii)* the hemoproteins in vertebrate and bacteria; *(iii)* the role of neuroglobin recently identified in the brain of Antarctic icefish; *(iv)* the structural and functional features of the “2-on-2” globins; *(v)* the physiological role of hexacoordination in hemoproteins.

### 1.1 The Antarctic

Antarctica, more than any other habitat on Earth, offers a unique natural laboratory for fundamental research on the evolutionary processes that shape biological diversity. Over the past million years, the Antarctic shelf has been subjected to tectonic and oceanographic events that led to the isolation and cooling of the continent. Fragmentation of Gondwana into the modern southern continents and the displacement of the Antarctic continent to its current geographic location have been the most significant events responsible for these changes. The crucial opening of the Drake Passage between southern South America and the Antarctic Peninsula occurred 23.5–32.5 million years (My) before present (b.p.) (Thomson, 2004) and possibly even as early as 41 My (Scher and Martin, 2006). The Drake Passage lead to the development of the Antarctic Circumpolar Current (ACC) and this in turn was at least partially responsible for cooling of Antarctic waters from 20 °C to

the present extreme values near  $-1.8\text{ }^{\circ}\text{C}$  (Clarke, 1983). The Antarctic Polar Front (APF), the northern boundary of the ACC, is a well defined, roughly circular oceanic system, running between 50 and 60  $^{\circ}\text{S}$  and acts as a cold “wall” that prevents mixing of the waters of the Southern Ocean with those of the Indian, Pacific and Atlantic oceans and limits the opportunities for migration of the fauna of the cold-temperate ocean to the south, and *viceversa* (Coppes and Somero, 2007). Isolation and extreme environmental history have forged a unique biota, both on land and in the sea. Unlike deep oceans, polar marine environments are subject to large seasonal variations in sea-ice cover, greatly affecting the biology of organisms (Moline et al., 2008).

## **1.2 Molecular adaptations in Notothenioidei**

The expansion of the ice sheet due to abrupt cooling in the late Eocene scoured the continental margin of Antarctica, leading to shelf habitat loss and alterations in the marine fauna (Clarke and Crame, 1992; Clarke, 1993; Eastman and McCune, 2000; Aronson and Blake, 2001). Much of the Eocene fish fauna became extinct (Eastman, 1993; Eastman and McCune, 2000), providing vast ecological opportunities for species that succeeded to adapt to habitat change and could thus survive. The ancestral notothenioid, presumably a shallow benthic fish, was able to exploit the changing habitat, and, in the absence of significant niche competition, diversified into the dominant suborder that makes up almost half (46%) of today’s Antarctic fish species (Eastman, 2005). Bovichtidae, Pseudaphritidae, Eleginopidae, Nototheniidae, Harpagiferidae, Artedidraconidae, Bathydraconidae and Channichthyidae are the families of the suborder (Eastman, 2005). Bovichtidae, Pseudaphritidae and Eleginopidae, known as non-Antarctic notothenioids, never experienced near-freezing water temperatures because they presumably diverged and became established in waters around areas corresponding to New Zealand, Australia and South America before Antarctica became isolated (Near, 2004). Notothenioid species living in the Antarctic coastal regions, at the freezing point of sea water (near  $-1.9^{\circ}\text{C}$ ), are strictly stenothermal (Eastman, 1993, 2005) and highly specialised in their low and narrow temperature window (Somero and DeVries, 1967; Somero et al., 1996; Pörtner et al., 1999, 2000; Peck and Conway, 2000; Peck et al., 2002). The evolution of stenothermy in the Southern Ocean was certainly driven by the great constancy of water temperature, whose

variations rarely exceeds 2 °C (Somero and DeVries, 1967; Podrabsky and Somero, 2006; Pörtner, 2006; Cheng and Detrich, 2007).

Examples of cold adaptation include efficient microtubule assembly at temperatures as low as -1.9 °C (Detrich et al., 1989, 2000; Redeker et al., 2004), enzyme-structural constraints (Fields and Somero, 1998; Russell, 2000; Hochachka and Somero, 2002; Fields and Houseman, 2004; Johns and Somero, 2004), decreased membrane fluidity (Römisch et al., 2003), constraints in aerobic energy supply, mitochondrial functioning and the capacity of anaerobic energy production (Johnston et al., 1998; Pörtner, 2006), higher levels of ubiquitin-conjugated proteins in tissues as evidence for cold denaturation of proteins in vivo (Todgham et al., 2007).

One major example of adaptations evolved by Antarctic notothenioids is the acquisition of genes for antifreeze glycoproteins (AFGPs). AFGPs allow to avoid freezing by binding water molecules, thus preventing growth of ice crystals in the blood and other body fluids (DeVries, 1988; Cheng and DeVries, 1991).

Although Antarctic notothenioids are among the most stenothermal known, they still possess mechanisms to resist to acute heat stress. Their inability to acclimate to elevated temperatures within the long range may arise from their ineffectiveness to change gene expression as their body temperature changes and therefore from the failure of heat-shock response (HSR). The Antarctic notothenioid *Trematomus bernacchii*, for instance, is unable to increase the synthesis of any class of heat-shock proteins following thermal stress (Hofmann et al., 2000; Place et al., 2004).

The absence of a heat-shock response in Antarctic notothenioids, but its presence in temperate New Zealand notothenioids (Hofmann et al., 2005), suggests that evolution in a cold, stable environment has led to depletion of some genetic responses. The differences in gene regulation are accompanied by differences in the biochemical and functional features of constitutively expressed heat-shock proteins between Antarctic and cold-temperate notothenioids (Place and Hofmann, 2005).

Comparative analyses of same-tissue transcriptome profiles of the Antarctic notothenioid fish *Dissostichus mawsoni* and temperate/tropical fishes showed that evolution in the cold produced genomic expansions of specific protein gene families involved into physiological fitness of Antarctic notothenioids under the extreme polar conditions (Chen et al., 2008). Many of their up-regulated genes are involved in the antioxidant function, suggesting that augmented defenses against oxidative stress are fundamental in a cold and oxygen-rich environment.

*-Physiological adaptations and genomic losses in Antarctic notothenioid fishes: the icefish case*

Specialised hematological features are striking adaptations developed by the Antarctic ichthyofauna during evolution at low temperature. Red-blooded Antarctic notothenioids differ from temperate and tropical species in having fewer erythrocytes and reduced hemoglobin (Hb) concentration and multiplicity. In cold Antarctic waters, which have a much higher concentration of dissolved oxygen than elsewhere, and with the selective evolutionary pressure relaxing oxygen transport, red-blooded notothenioids have evolved a decrease in Hb oxygen affinity (Verde et al., 2006).

The blood of the 16 “icefish” species of Channichthyidae (Eastman, 1993), the most phyletically derived family, lacks Hb (Ruud, 1954). The increased solubility of oxygen in water allows icefish to transport sufficient oxygen in physical solution rather than by a specific oxygen carrier. Icefish retain genomic DNA sequences closely related to the adult  $\alpha$ -globin gene(s) of its redblooded notothenioid relatives, whereas its ancestral  $\beta$ -globin sequences have been deleted (Cocca et al., 1995; Zhao et al., 1998; di Prisco et al., 2002). The most parsimonious explanation for these observations is that the discovery within the icefish family of two distinct genomic rearrangement, both leading to the functional inactivation of the locus, seems to point towards a multistep mutational process (Near et al., 2006). These fish cope with the lack of an oxygen carrier with increased blood volume and higher cardiac output (Egginton et al., 2002); they have large gills, highly vascularised, scaleless skin, which favours cutaneous respiration, and enlarged heart with specialised volume pump performance. This heart is unable to cope with either increasing temperature fluctuations or cardiac wall stresses associated with higher systemic pressure demands. This vulnerability highlights the costs of cardiac cold adaptation in the icefish (Egginton et al., 2002; Johnston et al., 2003).

The loss of Hb in icefish is paralleled by the loss of myoglobin (Mb) in several icefish species through at least 4 mutational events (Sidell et al., 1997; Grove et al., 2004; Sidell and O’Brien, 2006). Mb has also been lost in many notothenioids, at least in certain tissues. No notothenioid has Mb in its skeletal locomotory muscle (Sidell et al., 1997). Recently, Hendgen-Cotta et al. (2008) have showed in Mb-knockout mice that Mb produces and scavenges nitrogen monoxide (NO) under deoxygenated and oxygenated conditions, respectively.

When it acts as a reductase (Hendgen-Cotta et al., 2008), deoxygenated Mb generates NO from circulating nitrite in cardiac muscle cells under hypoxic stress, where it suppresses the production of ROS in mitochondria, protecting the muscle cells from damage. Excess NO is reconverted to nitrate by oxy Mb acting as a dioxygenase.

The hearts of Mb-knockout mice do not recover from experimentally imposed ischemia; these mice show no evidence of nitrite-induced reduction in the damage to heart tissue caused by blood-vessel blockage (Cossins and Berenbrink, 2008). Since Hb and Mb are key proteins in NO homeostasis (Barouch et al., 2002), the icefish, as natural knockouts for Hb/Mb, represent a unique example to investigate whether these disruptive losses may have evolved cardiac modifications and susceptibility to NO taking into account the recent evidence provided by experimentally produced Mb knockout mice (Hendgen-Cotta et al., 2008).

These observations may help to better understand icefish physiology and the compensatory adaptations evolved in the cardiovascular system of these natural knockouts.

While there is no doubt about the adaptive value of AFGPs, Hb/Mb loss in icefish was suggested not to be selectively neutral, but rather maladaptive, as indicated by the development of compensatory adaptations that enhance oxygen delivery, such as cutaneous uptake of oxygen and decreases in metabolic oxygen demand (Sidell and O'Brien, 2006; Cheng and Detrich, 2007).

Recent studies highlight how the loss of Hb and Mb, their associated NO-oxygenase activity and subsequent elevation of NO levels (two fold those observed in red-blooded notothenioids) could explain the unique cardiovascular and physiological traits that have evolved in icefish (Sidell and O'Brien, 2006).

### **1.3 Molecular adaptations in polar bacteria: the *Pseudoalteromonas haloplanktis* TAC125 case**

Temperature-dependent gene expression and *in situ* comparative analyses will significantly progress taking advantage from microbial genomes. Microorganisms have been found in a great variety of icy environments (where they stay viable for very long times), e.g. permafrost, polar oceans, snow, sea ice, glacial ice, cryoconite holes. Examples

include ice-covered hypersaline and other lakes (Priscu et al., 1998) and cryptoendolithic communities colonising the pore spaces of exposed rocks in the Dry Valleys (de la Torre et al., 2003) and other Antarctic locations, methanogenic Archaea (Tung et al., 2005) and ultra-small microorganisms found in the deepest part of a 3053-m ice core in Greenland (Miteva and Brenchley, 2005).

Thanks to their short generation times and being most bacteria cultivable, they can be used in several experiments aimed to understand cold responses, since the responses of multiple generations to selective forces (e.g. environmental conditions and their changes) can be followed relatively easily and rapidly in selection experiments (Russo et al., 2010).

The knowledge of polar marine microorganisms from ecological and genomic perspectives is in the early phase of an exponential growth. Some bacterial polar microbial genomes are already present in GenBank, accompanied by publications: the Euryarchaeota *Methanogenium frigidum* and *Methanococoides burtonii* (Saunders et al., 2003), the  $\gamma$ -proteobacterium *Colwellia psychrerythraea* 34H (Méthé et al., 2005) and *Pseudoalteromonas haloplanktis* TAC125 (Médigue et al., 2005) and the  $\delta$  proteobacterium *Desulfotalea psychrophila* (Rabus et al., 2004).

Recently, the genome of the *Exiguobacterium sibiricum* strain isolated from 3 million year old permafrost was sequenced and annotated (Rodrigues et al., 2008). The authors showed that *E. sibiricum* is constitutively adapted to cold with differential gene expression between 4 °C and 28 °C (Rodrigues et al., 2008).

Evolution has allowed cold-adapted organisms not simply to survive, but to grow successfully under the extreme conditions of cold habitats, through a variety of structural and physiological adjustments in their genomes. These strategies include synthesis of factors, such as cold-shock proteins (Cavicchioli et al., 2000), molecular chaperones (Watanabe and Yoshida, 2004), compatible solutes (Pegg, 2007) and structural modifications leading to the maintenance of membrane fluidity (Russell, 1998; Chintalapati et al., 2004). In addition to adaptations at the cellular level, a key adaptive strategy is the modification of enzyme kinetics, allowing maintenance of sufficient reaction rates at thermal extremes. Enzyme catalysis is based on increased flexibility in certain regions of cold-active enzyme architecture and high activity with a concomitant increase in thermolability (Georlette et al., 2004).

However, the adaptations to protein architecture essential to cold-active enzymes are still not well understood, and this study is an active area of investigation (Marx et al., 2004). Nevertheless, the biochemical properties of cold-active enzymes make them

attractive for exploitation in biochemical, bioremediation, and industrial processes (Feller and Gerday, 2003).

Among cold-adapted bacteria, the genus *Colwellia* (Deming and Eicken, 2005), within  $\gamma$ -proteobacteria, provides an unusual case, i.e. all characterized members are strictly psychrophilic (requiring temperatures of  $-20\text{ }^{\circ}\text{C}$  to grow on solid media) living in stably cold marine environments, including deep sea and Arctic and Antarctic sea ice (Deming and Junge, 2005). Many members of this genus produce extracellular polymeric substances relevant to biofilm formation and cryoprotection (Krembs et al., 2002) and enzymes capable of degrading high-molecular-weight organic compounds.

Cold-adapted bacteria have developed programmed responses to strong oxidative stress. *C. psychrerythraea* (Méthé et al., 2005) seems to have faced high oxygen concentration by developing an enhanced antioxidant capacity owing to the presence of several genes that encode catalases and superoxide dismutases.

In contrast, the genome sequence of *P. haloplanktis* TAC125 reveals that the bacterium copes with increased oxygen solubility by enhancing production of oxygen-scavenging enzymes and deleting entire metabolic pathways, such as those which generate ROS as side products. The remarkable deletion of the ubiquitous molybdopterin-dependent metabolism in the *P. haloplanktis* TAC125 genome (Médigue et al., 2005) and the number of proteins involved in scavenging chemical groups can be seen in this perspective. Dioxygen-consuming lipid desaturases achieve both protection against oxygen and synthesis of lipids, making the membrane fluid.

A further sign, which may be related to the peculiar features of the Antarctic habitat, may be the synthesis of bacterial Hbs and flavoHbs (see below), surprisingly versatile proteins serving several biological functions. These molecules are bound to fulfil an important physiological role, including protection of the cell from nitrosative and oxidative stress and delivering oxygen to respiring cells.

## 1.4 Hemoproteins

### *-Vertebrate globins*

Few proteins have been studied in such a wide array of organisms as Hb, and recent discoveries on its structure–function relationship keep stimulating interest. Hbs are very ancient proteins; they probably evolved from enzymes that used to protect the tissues against toxic oxygen levels. Hbs have been found in bacteria, protists, fungi, plants and animals; they serve a wide array of physiological roles, from oxygen transport in vertebrates to catalysis of redox reactions (Gardner et al., 1998; Minning et al., 1999). These different functions suggest the acquisition of new roles by changes not only in the coding regions, but also in the regulatory elements in the preexisting structural gene (Hardison, 1998).

Hbs share a common structure comprising 5–8 helices. Thanks to genome sequencing, the evolutionary tree of globins went back to 1800 million years at the time when the oxygen began to accumulate in the atmosphere (Wajcman and Kiger, 2002). It is generally accepted that during the first 2000 million years of existence of the Earth, the oxygen levels in the atmosphere were very low until the advent of the “Great Oxidation” (Holland, 2006). The atmospheric oxygen content reached the present levels about 540 million years ago (mya) (Holland, 2006). At those times, the Hb-like ancestor was likely to have adapted to locally scavenge excessive oxygen concentration and/or, similar to bacterial flavoHbs to be involved in detoxification of nitrogen monoxide (Poole, 2005). The evolution of simple oxygen-binding proteins into multi-subunit proteins, in combination with the development of the circulatory system, made the transport of oxygen from the blood to metabolising cells possible on a significant scale (Wajcman and Kiger, 2002). Thus, the familiar vertebrate Hb, a tetramer of two identical  $\alpha$  and  $\beta$  globin chains, developed relatively recent adaptation to widely different environmental conditions (Vinogradov and Moens, 2008).

The amino-acid sequences of the  $\alpha$  and  $\beta$  globins are about 50% identical, suggesting a common ancestor (Hardison, 1998). The specialised function in higher vertebrates imposes severe structural constraints on the Hb molecule. Hence, it is not surprising that only a small fraction of the residues of the polypeptide chains are allowed to be replaced during evolution. According to the species-adaptation theory of Perutz (1983),

the replacement of few key residues may produce functional modulation. The first protein crystal structures of myoglobin (Mb), present in cytoplasm of skeletal and cardiac myocytes, and Hb provided the basis to understand the relationship between changes in amino-acid sequence and protein overall structure (Kendrew et al., 1958; Perutz et al., 1965). During the following four decades, studies of protein structure and function have led to a detailed understanding of these hemoproteins. In addition to tetrameric Hbs and monomeric Mbs, four vertebrate hemoproteins have been recently discovered. These are cytoglobin (Cygb) which is widely expressed in vertebrate tissues (Trent and Hargrove, 2002; Burmester et al., 2002), globin E (GbE) (Kugelstadt et al., 2004) in the chicken eye (absent in mammals), globin X (GbX) recently found in fish and amphibians (Roesner et al., 2005) and neuroglobin (Ngb) (Burmester et al., 2000). The latter has received the most attention for its hypothetical role in protecting neurons from several injuries (Greenberg et al., 2008).

Phylogenetic analysis of vertebrate globins suggest a common ancestor, but confirm an ancient evolutionary relationship between GbX and Ngb, suggesting the existence of two distinct globin types in the last common ancestor of Protostomia and Deuterostomia (700 mya) (Roesner et al., 2005) as shown in Figure 1.1. Recently, other authors pointed out that these proteins are more modern than originally believed, in contrast to earlier suggestions (Brittain et al., 2010).

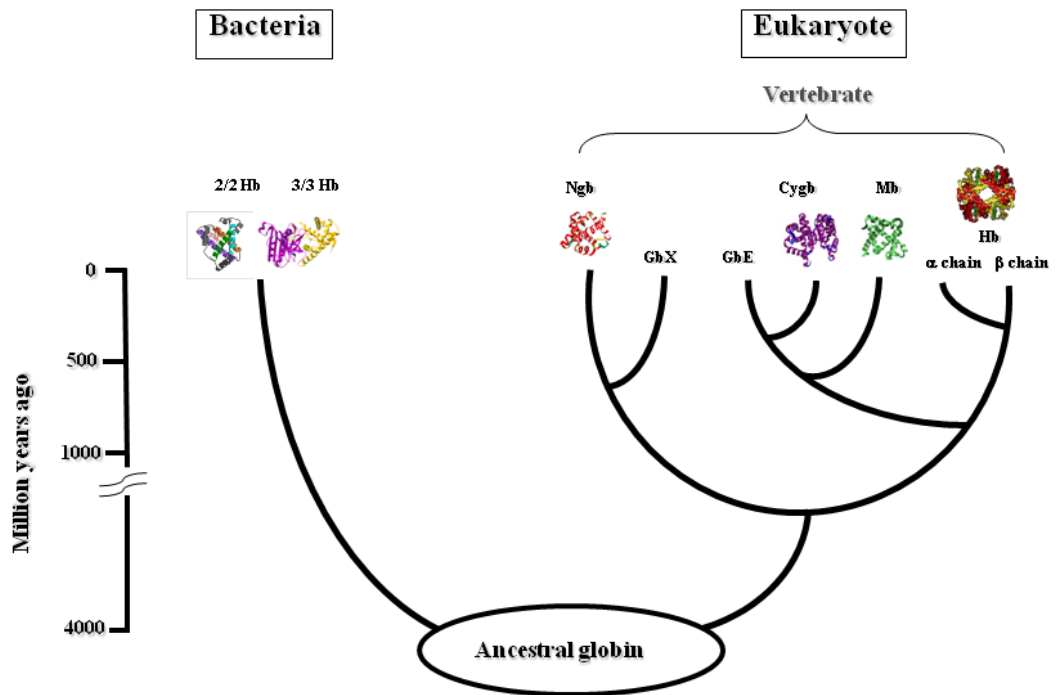


Figure 1.1: A simplified phylogenetic tree of vertebrate globins. After Brunori and Vallone, 2007; Vinogradov et al., 2005. (Verde et al., 2009)

In fact, GbX sequences are distinct from vertebrate Hb, Mb, Ngb, and Cygb, but display the highest identity scores with Ngb (26% to 35%). For the first time in vertebrate globins, analysis of the gene structure showed an intron in helix E of Ngb and GbX, supporting the assignment of Ngb and GbX to a gene family different from that including Mb, Hb and Cygb. Only two introns, positioned at B12.2 and G7.0, are present in most vertebrate genes and are phylogenetically ancient (Wajcman and Kiger, 2002; Roesner et al., 2005).

### *-Bacterial globins*

The variety of recently discovered bacterial Hbs has dramatically changed our view of the globin family. Bacterial Hbs highlight that oxygen transport in vertebrate Hbs is a

relatively recent evolutionary acquisition and that the early Hb functions have been enzymatic and oxygen sensing (Vinogradov and Moens, 2008). The bacterial superfamily comprises three families distributed in two structural classes (Figure 1.2).

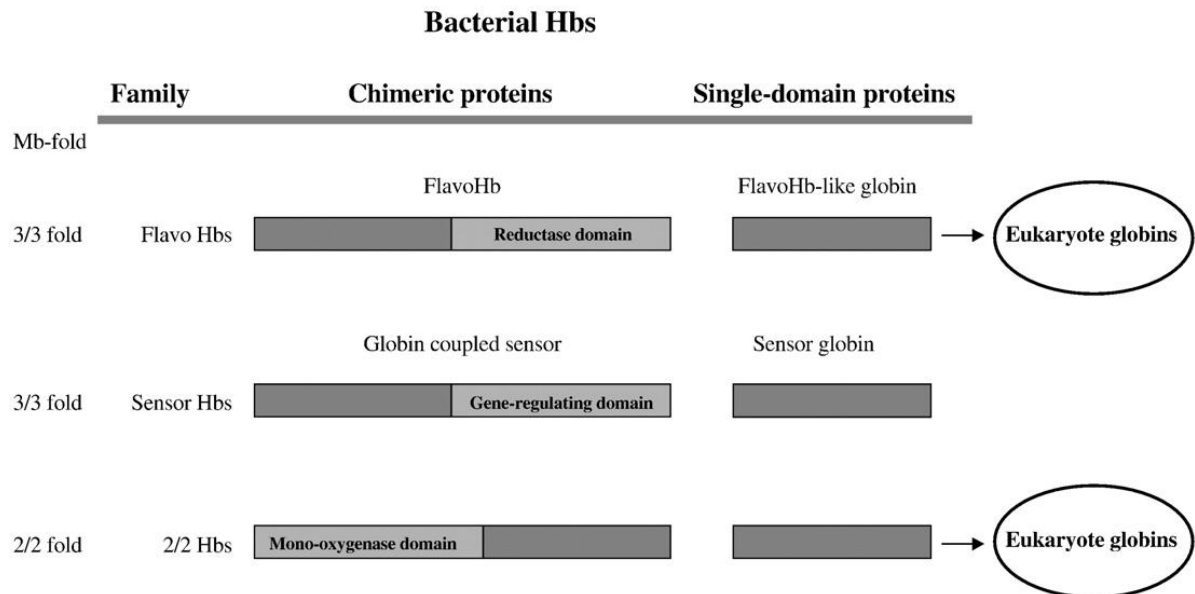


Figure 1.2: The three bacterial globin families and their relationships to eukaryotic globins. After Vinogradov and Moens, 2008 (Verde et al., 2009).

Within each family a given globin may occur in a chimeric or in a single-domain structure (Vinogradov and Moens, 2008). The first class, including the two families of flavoHbs and sensor Hbs, respectively involved in nitrosative stress and in adaptive responses to fluctuations of gaseous physiological messengers, displays the “3- on-3” classical Mb-like folding (3/3 Hbs). Historically, the first members of the two families were found to be chimeric. Single domain flavoHbs are present in eukaryotic globins unlike singledomain sensor globins. The second class includes the third family of “2 -on-2” Hbs (2/2 Hbs), and is widely distributed in bacteria, microbial eukaryotes and plants. Currently, there are still some uncertainties about the evolutionary relationship between the three families. The 2/2 Hbs and the sensor globins seem to have kept their original enzymatic functions in prokaryotes, plants and some unicellular eukaryotes. Therefore, the flavoHb family has been the only one able to adapt to different functions more extensively than the other two families (Vinogradov and Moens, 2008). Vinogradov et al. (2005)

proposed that all eukaryotic Hbs, including vertebrate  $\alpha/\beta$  globins, Mb, Ngb, and Cygb and invertebrate, bacterial and plant Hbs, emerged from a common ancestor (Figure 1.1).

## **1.5 Neuroglobin: the search of function of a vertebrate Hb**

Ngb, a structurally very related protein to Mb, is one of the newly discovered globins. Ngb is a monomeric heme-containing globin displaying the classical vertebrate folding “3-on-3” (Burmester et al., 2000; Pesce et al., 2003; Vallone et al., 2004a).

The protein is able to bind oxygen and other ligands, and is transcriptionally induced by hypoxia and ischemia (Brunori and Vallone, 2007). Ngb is mainly expressed in retinal neurons and fibroblast-like cells and plays a neuroprotective role during hypoxic stress (Brunori and Vallone, 2007). Evidence includes the observations that neuronal hypoxia and cerebral ischemia induce Ngb expression; knocking down Ngb expression increases hypoxic neuronal injury in vitro and ischemic cerebral injury in vivo (Greenberg et al., 2008). However, enhanced expression of Ngb does not seem to be a universal response to all forms of neuronal injury, because some insults do not produce such response (Greenberg et al., 2008).

However, so far, its exact physiological function remains uncertain. Suggested functional roles and their rationale can be divided into the following groups: Oxygen was found to bind reversibly to Ngb with an affinity which is within the range of Mb (Burmester et al., 2000; Dewilde et al., 2001). It binds the ligand under a high oxygen pressure and releases it again when the pressure is lowered. Ngb resides in metabolically active neuronal cells and subcellular compartments and was suggested to enhanced oxygen supply in these locations (Schmidt et al., 2003).

Cell cultures exposed to hypoxic conditions were found to moderately induce Ngb expression (Schmidt-Kastner et al., 2006). Additionally, goldfish, an animal that survives extended periods of reduced oxygen availability, maintains an approximately fivefold higher Ngb concentration than the less hypoxia-tolerant zebrafish (Roesner et al., 2008). Given these facts, it was proposed that Ngb is involved in the regulation of hypoxia. In analogy to Mb, Ngb was found to protect neurons from reactive oxygen or nitrogen species like NO and H<sub>2</sub>O<sub>2</sub> in vitro (Herold et al., 2004; Brunori et al., 2005). It was suggested that depending on the oxygen partial pressure, Ngb may either decompose or produce NO. This

mechanism is important to the control of vaso-constriction or -relaxation and the level of mitochondrial respiration (Petersen et al., 2008). Under a reduced oxygen flow reactive oxygen species are known to be formed in neuronal cells (Flögel et al., 2004). This observation is in line with a neuroprotective effect of Ngb discovered after ischemia and reperfusion (Khan et al., 2006).

Several studies considered Ngb to interact with other proteins. An observed binding of Ngb to the  $\alpha$  subunit of heterotrimeric G proteins proposed an inhibition of the dissociation of guanosine diphosphate from  $G\alpha$  (Watanabe and Wakasugi, 2008). This fact qualifies Ngb to protect the cell from apoptosis. Recent studies suggested that Ngbs neuroprotective effect is the result of the reduction of ferric cytochrome *c* by ferrous Ngb, thereby preventing cytochrome *c*-induced apoptosis (Raychaudhuri et al., 2010, Fago et al., 2006).

Ngb was originally identified in mammalian species, but then it was also found in fish, e.g. the zebrafish *Danio rerio* (Awenius et al., 2001). Watanabe and Wakasugi have suggested that zebrafish Ngb is a cell-membrane penetrating globin (Watanabe and Wakasugi, 2008).

A comparison of the primary structures of Ngb with Mb and Hb show that Ngb shares less than 25% of conserved residues with Mb and Hb. Among the conserved amino acids B10-Phe, CD1-Phe, CD3-Tyr, E11-Val, F4-Leu, FG1-Val, FG3-Val and G5-Phe are located in the heme binding or ligand interaction sites (Pesce et al., 2003, Vallone et al., 2004). In spite of the low sequence homology between Mb and Ngb, the tertiary structure of both proteins display the same three over three  $\alpha$ -helical sandwich fold.

Nevertheless, the X-ray structure of metNgb has a particular feature setting it apart from Mb. While the heme iron atom in Mb, in the absence of an exogenous ligand, is pentacoordinated to the four porphyrin nitrogen atoms and to the F8-His side-chain on the proximal side of the protein the same position is additionally bound to the distal E7-His side-chain (His64) in metNgb resulting in a hexacoordinated configuration (Figure 1.3) (Pesce et al., 2004). This feature, which is meant to control the affinity for external ligand binding, lead to many speculations about the physiological function of neuroglobin. More details on hexacoordination will be provided in section 1.7.

Ngb has recently been discovered in the tissues of two notothenioids (Cheng et al., 2009a,b), namely from the brain of the icefish *Chaenocephalus aceratus* (Channichthyidae) and the retina of the closely related, red-blooded *Dissosticus mawsoni* (Nototheniidae). Mammalian and fish Ngbs show about 50% amino-acid sequence identity.

This lack of significant structural change during evolution suggests that Ngb may play a conserved, beneficial function to neurons (Burmester and Hankeln, 2009). In an extreme oxygen-rich environment, this neuroprotective role has potential implications in our understanding of the function of this protein and suggests future avenues of investigation (Russo et al., 2010).

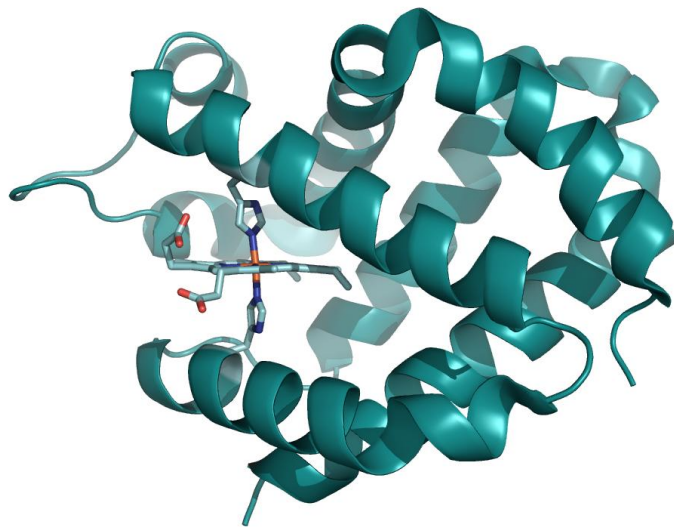


Figure 1.3: X-ray structure of human Ngb (pdb 1OJ6, Pesce et al., 2003), that shows the typical hexacoordinate state

## 1.6 “2 -on- 2” Hemoglobins

2/2Hbs represent a distinct set of proteins within the Hb superfamily (Wittenberg et al. 2002). These proteins can be found in a variety of plants, unicellular eukaryotes and bacteria. Compared to other non-vertebrate Hbs, 2/2Hb sequences are shorter by 20-30 residues, with deletions and additions occurring in specific regions of the primary structure. Differences in 2/2Hb structure include shortened A helices and elimination of the D helix to form a compact CD loop.

Sequence analysis indicates that 2/2Hbs can be separated into three groups: I (N), II (O), and III (P) (Wittenberg et al. 2002). Invariant among these groups is HisF8, the proximal

histidine ligand conserved across all Hbs (Dickerson and Geis 1983). A PheB9-TyrB10 pair is strongly conserved among 2/2Hb sequences with only a few exceptions (Wittenberg et al. 2002). Within these 2/2Hb groups, specific patterns of conservation are seen. Within group I and II 2/2Hbs, Gly-Gly motifs are found in the AB and EF interhelical regions. PheCD1 is strictly conserved in group I and III trHbs but His and Tyr residues are also observed at this position in group II members. An apolar region in the heme pocket is maintained by the predominance of Phe at position E14. Like other Hbs, 2/2Hbs are capable of binding oxygen. The rate constant of O<sub>2</sub> association is comparable for most globins ( $1.7 \times 10^7$  -  $2.4 \times 10^8$  M<sup>-1</sup> s<sup>-1</sup>) and is high, close to the diffusion limit (Hvitved et al. 2001, Springer et al. 1989 and references therein); as a result, dissociation rate constants are often used to indicate affinity. The 2/2Hb from *Paramecium caudatum* has an oxygen dissociation rate constant of 25 s<sup>-1</sup>, similar to that of Mb (Das et al. 2000), and the rate constant reported for *Nostoc commune* 2/2Hb is 79 s<sup>-1</sup> (Thorsteinsson et al. 1999). These rates are comparable to the oxygen dissociation rate constants from mammalian Mb, which vary from 15 s<sup>-1</sup> to 40 s<sup>-1</sup> (Carver et al. 1992). In contrast, the rate constants for O<sub>2</sub> dissociation for *Mycobacterium tuberculosis* 2/2HbO and *Chlamydomonas eugametos* 2/2Hb are 0.0014 s<sup>-1</sup> and 0.0141 s<sup>-1</sup>, respectively (Couture et al. 1999a, Ouellet et al. 2003). Differences in ligand binding are likely influenced by the heme pocket characteristics of each protein.

Crystal structures are available for a number of 2/2Hbs: *Chlamydomonas eugametos* 2/2Hb (*Ce* 2/2Hb, 1dly, Pesce et al. 2000), *Paramecium caudatum* 2/2Hb (*Pc* 2/2Hb, 1dlw, Pesce et al. 2000), *Mycobacterium tuberculosis* (*Mt*) 2/2HbN (1idr, Milani et al., 2001) and *Mt* 2/2HbO (1ngk, Milani et al., 2003b). The structures reveal that the “3 -on- 3” helical fold found in full-length Hbs has been reduced to a “2 -on- 2” helical sandwich (Pesce et al., 2000).

The first 3D structure of 2/2Hb from *P. caudatum* was determined by Bolognesi and coworkers (Milani et al., 2004), and in Figure 1.3 it is compared to the sperm whale Mb fold. The crystal structure shows that the *P. caudatum* globin fold is based on a subset of the “classical” globin fold (the so called “3 -on- 3”  $\alpha$ -helical sandwich (3/3) typical of sperm whale myoglobin (Mb) (Figure 1.3 left). Indeed, *P. caudatum* globin fold hosts the heme in a “2 -on- 2”  $\alpha$ -helical sandwich (2/2) based on four  $\alpha$ -helices, corresponding to the B-, E-, G-, and H-helices of the classical globin fold. The antiparallel helix pairs (B/E and G/H) are arranged in a sort of  $\alpha$ -helical bundle which surrounds and protects the heme group from the solvent phase (Figure 1.3 right) (Nardini et al., 2007).

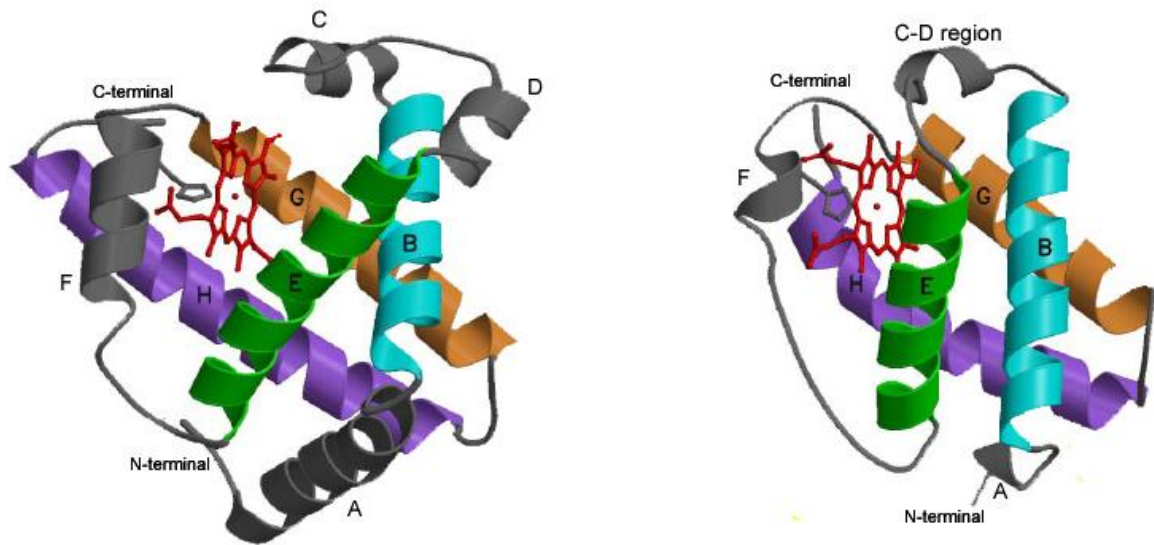


Figure 1.4: The  $\alpha$ -helical sandwich fold in sperm whale Mb (3/3Hb, left) (pdb 1ebc) and in 2/2Hb from *P. caudatum* (2/2Hb, right) (pdb 1dlw). The figure has been taken from lecture by Prof. Bolognesi during the XII School of Pure and Applied Biophysics (*The ever changing world of (hemo)globins*, Venice 28 January - 2 February 2008).

The presence of TrpG8 as part of the network also serves to control ligand access to the distal site by maintaining hydrophobic contacts in the heme pocket (Milani et al., 2003, Ouellet et al., 2003).

The *Ce* and *Pc* 2/2Hb structures reveal a long tunnel near the AB and GH corner of the distal pocket (Pesce et al. 2000). A shorter tunnel is found between the G and H helices. These tunnels are lined with hydrophobic residues. Ligand binding studies indicate that these tunnels facilitate ligand access to the heme iron (Milani et al., 2004b, Samuni et al., 2003).

The polarity of the distal residues is the common properties of the 2/2Hbs, but the residues involved in the building of the heme architecture switch over the three groups. In group I, for example, the hydrogen-bond network involves residues at B10, E7 and E11 topological positions. The strongly conserved tyrosine (Tyr B10) in position B10 plays a key role in the ligand stabilization through its OH group pointing directly to the heme ligand. Normally, the complete stabilization by hydrogen-bond network is realized by a Glu residue located at E7 or E11, or at both positions. In group II, another residue, the Trp

G8 is fully conserved; it contributes to the heme-bound ligand stabilization by the hydrogen bond linking the indole nitrogen atom and the ligand. Furthermore, the presence of a tyrosine at position CD1 in some 2/2HbO proteins drastically modifies the interaction network. In particular, structure and sequence analysis suggests that the nature of residues at CD1 is correlated with the nature of the site E11, at least for the group II 2/2Hbs.

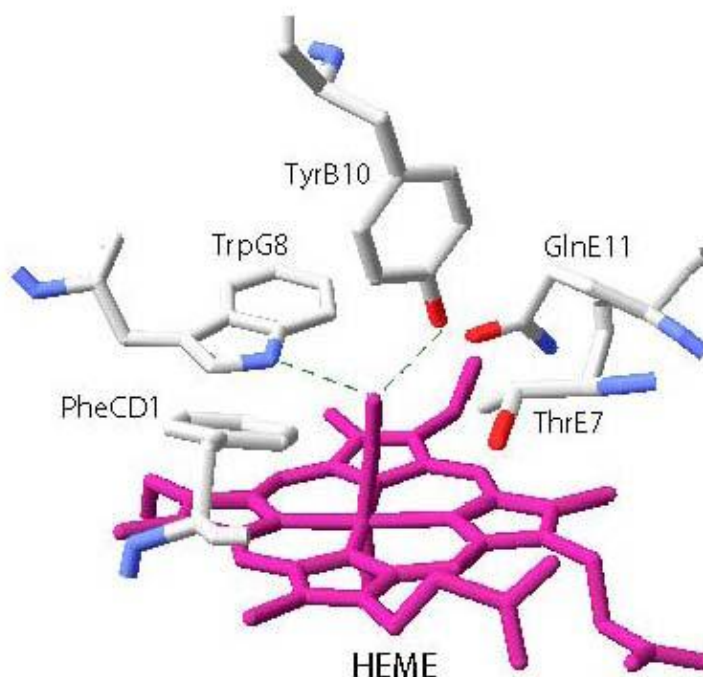


Figure 1.5: Scheme of the distal site of the CO complex of *Bacillus subtilis* 2/2HbO, in which the main residues discussed in the text and their topological positions are displayed. The green dashed lines show possible hydrogen-bonding interactions (Feis et al., 2008).

The functions of 2/2Hbs are not well understood and appear to vary. Limited information is available for the purified members. In the cyanobacterium *N. commune*, cyanoglobin, a group I 2/2Hb, is believed to sequester oxygen for reaction by a terminal cytochrome oxidase complex under nitrogen fixing conditions (Thorsteinsson et al., 1996). Studies on *Mycobacterium bovis* 2/2HbN show that the protein is able to convert nitric oxide to nitrate (Ouellet et al. 2002). Milani and co-workers have suggested that nitric oxide detoxification by *Mt* 2/2HbN is a defense mechanism by the pathogen during infection (Milani et al., 2003a). In the case of *Ce* 2/2Hb, the protein is expressed as a response to photosynthesis, but additional action is unclear (Couture et al., 1994).

Multiple genes encoding 2/2Hbs (annotated as *PSHAa0030*, *PSHAa0458*, *PSHAa2217*) and one for flavoHbs (*PSHAa2880*) have been discovered in the genome of *P. haloplanktis* TAC125, suggesting that specific and distinct functions may be associated to these two classes of proteins (Giordano et al., 2007).

## 1.7 Hexacoordination in hemoproteins

Crystallographic evidence for endogenous coordination at the sixth coordination site of the heme iron has been reported in both the ferrous (hemochrome) and ferric (hemichrome) oxidation state (Vergara et al., 2008). Usually, the sixth ligand is provided by the imidazole side chain of a His in E7, normally present in the distal site of the heme pocket. The occurrence of hemichrome/hemochrome states in members of the Hb superfamily is not uniform suggesting that the functional roles of these oxidation states are multiple, possibly being a tool for modulating ligand-binding or redox properties.

Over the years, hemichromes in tetramers have been considered as precursors of Hb denaturation, since their formation is accelerated by denaturing agents (Rifkind et al., 1994). It has been shown that hemichromes can be obtained under non-denaturing as well as physiological conditions (Vergara et al., 2008). Recently, it has also been suggested that hemichromes can be involved in Hb protection from peroxide attack (Feng et al., 2005), given that the hemichrome species of human  $\alpha$  subunits complexed with the  $\alpha$ -helix-stabilising protein (AHSP) do not exhibit peroxidase activity (Feng et al., 2005). Structural and spectroscopic evidence has shown endogenous coordination at the sixth coordination site in several tetrameric Hbs isolated from Antarctic notothenioid fish (Riccio et al., 2002; Vitagliano et al., 2004; Vergara et al., 2007, 2008; Vitagliano et al., 2008). Under physiological conditions, the oxidation of Antarctic fish Hbs leads to the formation of an endogenous bis-histidyl complex ( $\beta$ -hemichrome) in the ferric state. The bis-His coordination in the ferrous state has never been observed. Thus, under reduction, the hemichrome species is reversibly converted to the classical pentacoordinated deoxy form both in solution (Vitagliano et al., 2004) and in the crystal state (Merlino et al., 2008). Another example of bis-His coordination in tetrameric Hbs regards horse met-Hb. Notably, bis-His formation invariably involves the  $\alpha$  heme in horse Hb (Robinson et al., 2003; Feng et al., 2005). In comparison with horse Hb, bis-histidyl adducts in Antarctic fish Hbs exhibit large differences in the quaternary structure rearrangement. Horse Hb develops the bis-His form within the R quaternary structure, whereas Antarctic fish Hbs in the bis-His form adopt a quaternary structure that is intermediate between the R and T states (Vergara et al., 2007, 2008). According to the evidence of higher peroxidase activity in Antarctic

fish Hbs, the exchange between hemichrome and pentacoordinated forms may play a distinctive physiological role in Antarctic teleosts (Vergara et al., unpublished).

Hexacoordinated Hbs are also expressed at low structural complexity and observed in bacteria, unicellular eukaryotes (Wittenberg et al., 2002), plants (Watts et al., 2001), invertebrates (Dewilde et al., 2006) and in some tissues of higher vertebrates. In the absence of exogenous ligands, also Ngb (Pesce et al., 2004) and Cygb (de Sanctis et al., 2004) display hexacoordination with distal His E7 coordinating directly with the heme iron, either in ferrous or ferric forms.

The UV–vis spectra of ferric and ferrous form of both *C. aceratus* and *D. mawsoni* Ngbs proteins are typical of hexacoordinate state in analogy with other Ngbs (Dewilde et al., 2001).

The physiological role of these hexacoordinated Hbs is not well understood. Several roles have been suggested. Firstly, these proteins may scavenge oxygen under hypoxic conditions and supply it for aerobic respiration (Burmester et al., 2000, 2002). Sun et al. (2001, 2003) demonstrated that Ngb is upregulated under hypoxic conditions, in vivo and in vitro, and that it protects neurons against the deleterious effects of the hypoxia and ischemia. Formation and cleavage of a disulfide bond influences the functional characteristics of the protein and the formation of the hexacoordinated form. Under hypoxic conditions, the disulfide bond in Ngb will be reduced, with subsequent release of oxygen counteracting hypoxia. Secondly, they may function as terminal oxidases by oxidizing NADH under hypoxic conditions and hence enhance ATP production by glycolysis (Sowa et al., 1999). Thirdly, they might be oxygen-sensor proteins, activating other proteins with regulatory function (Hargrove et al., 2000; Kriegl et al., 2002). Fourthly, they may be involved in nitric oxide metabolism (Smagghe et al., 2008).

Hexacoordination, found in monomeric and dimeric Hbs, shows tendency for bis-histidyl hexacoordination and generally exhibit reversible bis-histidyl coordination of the heme iron while retaining the ability to bind exogenous ligands (Weiland et al., 2004). It has been suggested that bis-His adducts can be involved in nitric oxide NO detoxification by acting as NO scavengers. However, there does not seem to exist a distinguishing predisposition in NO scavenging for hexacoordinated Hbs but any Hb may play this role in the presence of a mechanism for heme iron re-reduction (Smagghe et al., 2008). Currently, some monomeric and dimeric Hb 3D structures, which show the bis-histidyl endogenous coordination, have been deposited in pdb (Mitchell et al., 1995; Hargrove et al., 2000; Hoy et al., 2004; Pesce et al., 2004; Vallone et al., 2004; de Sanctis et al., 2004, 2005).

However, in some Hbs with lower structural complexity, Tyr B10 has been found to act as the sixth ligand at the iron site in the ferrous (Couture et al., 1999) and ferric states (Das et al., 1999; Milani et al., 2005). In general, bacterial 2/2Hbs do not show tendency for hexacoordination but few cases have been examined and are reported in the literature. The ferrous heme iron atom of deoxygenated *Mycobacterium leprae* 2/2Hb appears to be hexacoordinated (Visca et al., 2002). Ferric 2/2Hb from the cyanobacterium *Synechococcus* sp. PCC 7002 (Scott et al., 2002) shares several physical properties with 2/2Hb from of *Synechocystis* sp. PCC 6803 (Falzone et al., 2002). Both Hbs readily form a hexacoordinate, low-spin complex in the absence of exogenous ligands. Spectral studies support a bis-histidyl ligation to the heme on the distal side.

The 2/2 Hb of the bacterium *Herbaspirillum seropedicae* undergoes transition from an aquomet form in the ferric state, with equilibrium between high and lowspin, to a hexacoordinated low-spin form in the ferrous state (Razzera et al., 2008).

Spectroscopic studies of *P. haloplanktis* TAC125 recombinant 2/2Hb, encoded by the PSHAA0030 gene, show a predominance of a sixcoordinated species in the ferric and ferrous forms. The hexacoordinate form is strongly dependent on pH (Giordano et al., 2011).

## 1.8 Objectives of the Ph.D. project

The research activities during my Ph.D. thesis have been focused mainly on the structure and function of hemoproteins. In order to carry out these studies, I have used techniques of considerable importance in the characterization of the active sites of biomolecules: UV-Vis electronic absorption, Resonance Raman (RR), Circular Dichroism (CD), kinetic measurements, High Pressure spectroscopy and different bio-informatic approaches. I have studied hemoproteins of different organisms: a) the 2/2Hb (*Ph-2/2HbO*) from the Antarctic bacterium *Pseudoalteromonas haloplanktis* TAC125, already object of my degree thesis and then further investigated during my Ph.D.; b) the Ngbs from the Antarctic fishes *Chaenocephalus aceratus* and *Dissosticus mawsoni*.

- a) The 2/2Hb of *Pseudoalteromonas haloplanktis* TAC125, encoded by the PSHAA0030 gene (named *Ph-2/2HbO*) was structurally and functionally characterized. In the second chapter, the results obtained on the ferric and ferrous

forms of *Ph-2/2HbO* in collaboration with Prof. Smulevich (University of Florence), Prof. Estrin (University of Buenos Aires), Prof. Hui Bon Hoa (CNRS of Paris), and Prof. Del Vecchio are described.

- b) The recent discovery of the *Ngb* gene in the brain of red-blooded notothenioids and icefish species suggests a crucial biological function of *Ngb*. The finding that icefish retain the *Ngb* gene despite having lost Hb, and Mb in most species, may potentially have important implications in the physiology and pathology of the brain. Therefore, in collaboration with Prof. Smulevich (University of Florence), Prof. Estrin (University of Buenos Aires), further objectives of the Ph.D. project, illustrated in the third chapter, are focussed on the comparative analysis of *Ngbs* isolated from the brain of the icefish *Chaenocephalus aceratus* (white-blooded fish) and from the retina of the closely related Antarctic notothenioid *Dissostichus mawsoni* (red-blooded fish). These results have been analysed and discussed with respect to the best investigated human *Ngb*.

## Chapter 2

### **Structural and functional characterization of the 2/2 Hb of cold-adapted bacterium *Pseudoalteromonas haloplanktis* TAC125**

#### **Summary**

The genome of the Antarctic marine eubacterium *Pseudoalteromonas haloplanktis* TAC125 (*Ph*TAC125) contains multiple genes encoding three different 2/2Hb, at distinct positions on chromosome I, namely *PSHAa0030*, *PSHAa2217* and *PSHAa0458*. The proteins exhibit a 2/2  $\alpha$ -helical fold (Giordano et al., 2007). The unusually high number of 2/2 Hbs strongly suggests that these proteins are bound to fulfil important physiological roles that are perhaps related to the peculiar features of the Antarctic habitat.

The 2/2Hb encoded by the *PSHAa0030* gene (named *Ph*-2/2HbO) was overexpressed as described previously (Giordano et al., 2007).

In this chapter the structural characterization of *Ph*-2/2HbO in ferric form is described. A detailed characterization was obtained by Resonance Raman (RR), electronic absorption spectroscopy, Electronic Paramagnetic Resonance spectroscopy (EPR), Circular Dichroism spectroscopy (CD), High Pressure spectroscopy and computer simulation approaches. The spectroscopic and ligand-binding properties have been also studied in the ferrous state and here described.

#### **2.1 Materials and Methods**

##### **2.1.1 Preparation of *Ph*-2/2HbO: expression and purification**

The strain BL21(DE3) of *Escherichia coli* was successfully transformed with the recombinant expression plasmid pET28a-2/2HbO. The cells were grown overnight in a flask at 37°C and shaken at 180 rpm. Fifty microliters of the growth medium were inoculated in an Applikon fermentor with a working volume of 1 l. The culture was grown

using a mineral medium according to a standard procedure from CPC Biotech. The first growth phase occurred in fed-batch mode at 30 °C. After 23 h, the temperature was decreased to 25 °C. The culture was induced at  $OD_{600} = 32$  by the addition of isopropyl-1-thio-D-galactopyranoside to a final concentration of 0.5 mM, and 0.3 mM  $\delta$ -aminolevulinic acid; expression was continued overnight. The cells were harvested by centrifugation at 4 °C. For purification, the frozen cells were thawed, suspended in 50 mM Tris-HCl pH 7.6, 1.0 mM EDTA, 1.0 mM phenylmethylsulfonylfluoride and protease-inhibitor cocktail (SIGMA P8465) and disrupted in a French press until the supernatant was reddish and clear. The cell debris was removed by centrifugation at 30,000 rpm for 1 h at 4 °C. The supernatant was loaded onto an anion-exchange column (Q Sepharose Fast Flow, GE Healthcare Biosciences), equilibrated with 20 mM Tris-HCl pH 7.6 and 1.0 mM EDTA (Akta Explorer system, GE Healthcare Biosciences, Amersham Biosciences Ltd, UK). *Ph-2/2HbO* was eluted with a NaCl gradient (from 0 to 0.25 M) in 20 mM Tris-HCl pH 7.6, 1.0 mM EDTA (Giordano et al., 2007). The fraction was chosen on the basis of the absorbance of heme at 407 nm and protein at 280 nm. The collected protein was concentrated, dialyzed against 50 mM 2-(*N*-morpholino) ethanesulfonic acid (MES) pH 6.0, and further purified with a SP (sulfopropyl) Sepharose Fast Flow column (GE Healthcare Biosciences) equilibrated with 50 mM MES pH 6.0. The protein was eluted with a NaCl gradient (from 0 to 0.35 M). Final purification was performed by using another strong cation-exchange column, Mono S (GE Healthcare Biosciences) equilibrated with 50 mM MES pH 6.0 and applying a NaCl gradient (from 0 to 0.50 M). The protein obtained was over 98% pure, as judged from sodium dodecyl sulfate polyacrylamide gel electrophoresis (SDSPAGE), and was stored at -20 °C. The N-terminal sequence was elucidated by automatic sequencing performed with an Applied Biosystems Procise 494 Automatic Sequencer, equipped with on-line detection of phenylthiohydantoin amino acids.

### **2.1.2 Sample preparation for RR and EPR experiments**

The samples of *Ph-2/2HbO* at pH 5.6 and 7.6 were prepared in 0.1 M MES and 0.1 M Tris-HCl or 0.1 M 3-morpholinopropane-1-sulfonic acid (MOPS) buffers, respectively. Protein concentrations in the range 10–70  $\mu$ M were used for the electronic absorption and RR samples.

Sample concentration for low-temperature RR was between 30 and 100  $\mu\text{M}$ . The concentration of the electron paramagnetic resonance (EPR) sample was 160  $\mu\text{M}$ . The protein concentration was determined on the basis of the molar absorptivity,  $\epsilon = 131 \text{ mM}^{-1} \text{ cm}^{-1}$  at 408 nm.

The ferrous samples were prepared by adding 2  $\mu\text{l}$  of sodium dithionite ( $10 \text{ mg ml}^{-1}$ ) to 50  $\mu\text{l}$  of deoxygenated buffered solution of Met-Hb. The carbomonoxy complex was prepared by flushing Met- *Ph-2/2HbO* with nitrogen, then with CO, and reducing the protein as described above (Droghetti et al., 2010) The protein concentration of all samples, for RR and electronic absorption spectroscopy, was 30  $\mu\text{M}$  on a heme basis.

### 2.1.3 Spectroscopy

Electronic absorption spectra were measured with a double-beam Cary 5 spectrophotometer (Varian, Palo Alto, CA, USA) using a 5-mm NMR tube and a  $600 \text{ nm min}^{-1}$  scan rate. A detailed description of the room and low-temperature RR, and EPR experimental procedures has been reported previously (Nicoletti et al., 2010). The measurements at 4  $^{\circ}\text{C}$  were obtained using a thermostatically controlled water bath. More detailed information on RR and EPR procedures are reported in Howes et al., 2011.

### 2.1.4 Sequence alignment

Sequence alignments were performed between *Ph-2/2HbO* and four Hbs belonging to Group II for which the crystal structures are available, namely *Mycobacterium tuberculosis* (*Mt-2/2HbO*) (pdb Id: 1NGK), *Bacillus subtilis* (*Bs-2/2HbO*) (1ux8), *Geobacillus stearothermophilus* (*Gs-2/2HbO*) (2bKm), *Thermobifida fusca* (*Tf-2/2HbO*) (2bMM). *Shewanella oneidensis* 2/2HbO was selected due to the presence of an extension at the N-terminus of the primary structure, similar to *Ph-2/2HbO*. Sequence identities are 34, 37, 34, 33 and 39%, respectively.

To align these sequences, different computational programs have been used, namely Modeller (Sali 1993) BLAST (Tatusova and Madden 1999) and ClustalX (Thompson et al., 1997). Based on the present and previous alignments (Giordano et al., 2007), we constructed 3D models using *Mt-2/ 2HbO* and *Bs-2/2HbO* proteins as templates,

and the Modeller program with default parameters. Several putative *Ph-2/2HbO* structures were obtained.

### **2.1.5 Molecular dynamics simulations**

To evaluate the stabilities of the different structures, molecular dynamics simulations (MD) were performed for each structure using the Amber 9 force field ff99SB (Pearlman et al., 1995).

Detailed information are reported in Howes et al., 2011.

### **2.1.6 Circular dichroism (CD) spectroscopy**

CD spectra were recorded with a Jasco J-715 spectropolarimeter equipped with a Peltier type temperature control system (Model PTC-348WI). Molar ellipticity per mean residue,  $[\theta]$  in  $\text{deg cm}^2 \text{ dmol}^{-1}$ , was calculated from the equation:  $[\theta] = [\theta]_{\text{obs}} \text{mrw}/10 \times l \times C$ , where  $[\theta]_{\text{obs}}$  is the ellipticity measured in degrees, mrw is the mean residue molecular weight,  $C$  is the protein concentration in  $\text{g mL}^{-1}$  and  $l$  is the optical path length of the cell in cm. A 0.1 cm path length cell was used in the far-UV region. CD spectra were recorded with a time constant of 4 s, a 2.0 nm band width, and a scan rate of  $20 \text{ nm min}^{-1}$ , were signal-averaged over at least five scans, and baseline corrected by subtracting a buffer spectrum.

Each spectrum represented the average of three accumulations recorded between wavelengths of 190 and 260 nm, with a 0.2 nm resolution, a response time of 4 s and a scan speed of 20 nm/min.

The GuHCl-induced denaturation curves at constant temperature were obtained by recording the CD signal at 222 nm for each independent sample. The protein solutions were prepared in a 100 mM Tris HCl pH 7.6/ 8.5 and 1mM TCEP. The protein concentration was determined by UV spectra using a theoretical, extinction coefficient of  $17780 \text{ M}^{-1} \text{ cm}^{-1}$  at 280 nm. For chemical denaturation stock solutions of GuHCl (a commercial 8 M solution), in different amounts, were mixed with protein solution to obtain constant, fixed final protein concentration. The final concentrations ranged from 0.2 to 6 M for GuHCl. Each sample was mixed by vortex and incubated at  $5^\circ\text{C}$  for a day.

### **2.1.7 Protein thermostability**

The protein was subjected to the thermal melting profile by monitoring the changes of circular dichroism spectra at 222 nm at different pH. For thermal unfolding, curves were recorded from 2 to 90°C (heating plate temperature), and samples were continuously scanned at 1 °C/min. The temperature was programmed using a Jasco (Peltier PTC-348WI) thermoelectric temperature controller.

### **2.1.8 Fluorescence measurements**

Steady-state fluorescence measurements were conducted with a Perkin Elmer LS50B spectrofluorimeter equipped with thermostat-controlled cell holders and the temperature was kept constant using a circulating water bath. The protein concentration was 0.1 mg ml<sup>-1</sup>. The excitation wavelength was set at 280 nm in order to include the contribution of tyrosine residues to the overall fluorescence emission. The experiments were performed at 20 °C by using a 0.2 cm sealed cell and a 5 nm emission slit width, and corrected for background signal. Both the change in fluorescence intensity and the shift in fluorescence maximum wavelength were recorded to monitor the unfolding transition.

### **2.1.9 High pressure spectroscopy**

Spectral measurements were made with 4-×10-mm quartz cuvettes using a Cary 50 spectrophotometer. Samples were 10 μM (on a heme basis) in 100 mM Tris-HCl at pH 8.5. The ferrous deoxy sample was obtained by equilibration under nitrogen and adding an excess of sodium dithionite.

High Pressure Apparatus, capable of generating 7000 bar, employs a 5-×5-mm quartz cuvette contained within the high pressure cell (Mentré and Hui Bon Hoa, 2001), made of maraging steel and surrounded by a copper jacket for temperature control. The high pressure bomb fit snugly into a Cary 3E spectrophotometer sample compartment thus minimizing any movement relative to the light path. The sample previously equilibrated in the appropriate condition was introduced into the high pressure quartz optical cuvette of volume of 500 μl and an optical path of 5 mm. The globin solution was isolated from the

compression fluid (pentane) through two thin (0.1 mm) teflon membranes. The high pressure was generated with a modified 700 MPa pump (Top Industry, Vaux le Pénil, France) of volume 4 cm<sup>3</sup> with a piston possessing a double Bridgman seal. The pressure was increased in 50 MPa increments and held for 3 min before the spectral measurements to assure a stability of the final pressure. The temperature of the high pressure cell was maintained by a circulating water bath. The absorption spectra (between 280 and 700 nm) of ferric, CO and deoxy *Ph-2/2HbO* were measured at room temperature as a function of hydrostatic pressure up to 700 megapascal (MPa). Because the high pressure system is all liquid, there is no change *versus* P in the total amount of protein or ligand. The samples were corrected for the solvent compressibility (Vedam and Holton, 1968), which (for water) is initially 4% per kilobar (kbar) and a total of 15% at 6 kbar. The shift *versus* pressure of the Soret band to determine the fraction dissociated (based on the observed signal amplitude) was taking into account.

#### 2.1.10 CO-bimolecular recombination rates by Laser Flash Photolysis (LFP)

The kinetics of ligand binding to the heme iron was measured by the LFP technique. The photolysis setup consists of a 10-ns ND:YAG (neodymium-doped yttrium aluminum garnet) laser, delivering pulses of 120 mJ at 532 nm (Quantel, France) and a detection beam. The standard detection wavelength was 436 nm, in the Soret band. The protein concentration was 5 μM on a heme basis. Samples were in 100 mM buffer in the pH range from 6.0 to 11.0, at 25 °C, and were equilibrated under CO (0.01, 0.1, or 1 atm) in 1-cm optical path length cuvettes. Additional CO levels were obtained by mixing one of the standards (0.01, 0.1, or 1 atm CO) with nitrogen (Uzan et al., 2004). A typical kinetic curve was obtained from the average of 10 measurements, with at least 4 sec lapsing between photolysis pulses to allow sample recovery. Before and after laser exposure, the samples were checked by visible absorption spectra. Simulation of a series of curves, using Eqs. (1) and (2), at different CO concentrations allows a determination of the CO on rate. Kinetic progress curves of ligand dissociation–association to Fe(II)-*Ph-2/2HbO* have been analyzed according to:

$$A_{\text{obs}} = A_0 + \sum_{i=1}^{i=n} \Delta A_i \times \exp(-k_{\text{obs}}^i \times t) \quad \text{Eq. (1)}$$

The CO concentration dependence of  $k_{\text{obs}}$  was analyzed according to:

$$k_{\text{obs}} = k_{\text{on}} \times [\text{CO}] + k_{\text{off}} \quad \text{Eq. (2)}$$

Simulations were made with up to three phases, but only two dominant phases were retained, as the third component was small in amplitude and showed no clear pH or temperature dependence.

The kinetic data were reproducible; the main error of about 20% is due to separation of the phases.

## 2.2 Results and Discussion

### 2.2.1 Purification of *Ph-2/2HbO*

In this thesis the reported expression and purification methods (Giordano et al., 2007) were replaced by an alternative procedure to improve the biomass yield of *Ph-2/2HbO*, and avoid sulfide binding (Nicoletti et al., 2010a). The recombinant *Ph-2/2HbO* was shown to form high affinity complexes with hydrogen sulfide in its ferric state. The presence of a ferric sulfide adduct with a typical visible absorption spectrum peaked at 427 nm was also reproducibly observed in *2/2Hb* from *Bacillus subtilis* and from *Thermobifida fusca* preparations immediately after cell disruption, thus indicating that these proteins were at least partially saturated with sulfide within the *Escherichia coli* expression vector and were endowed with a high affinity for this ligand (Nicoletti et al., 2010).

The Resonance Raman spectroscopy of *Ph-2/2HbO* showed a sulfide ligation of the protein in a low-spin iron complex. Further experiments have shown that the exogenous sulfide ligand is an artefact derived from the purification procedure. The low spin ferric adduct, present within beta-mercaptoethanol ( $\beta$ -ME) containing solutions, was attributed to the formation of a stable ferric derivative with some byproduct, possibly sulfide. Sulfide may coordinate to the heme iron in the monoprotonated form,  $\text{HS}^-$ , or in the diprotonated one,  $\text{H}_2\text{S}$ , since the pK for this equilibrium is reportedly  $\sim 7$ .

Figure 2.1 shows the different spectra with and without sulfide. The sulfide bound spectrum (dotted line) displays an absorption profile which is characteristic of the low-spin

sulfide adduct as reported for *Lucina pectinata* HbI, with a Soret band centred at 427 nm and a broad visible band at 550-575 nm (Kraus et al., 1990, Boffi et al., 1997).

To avoid sulfide binding to the protein, an alternative purification method was used. As shown in the spectrum (continuous line) after this procedure, the protein displays the absorption profile characteristic of a ferric form.

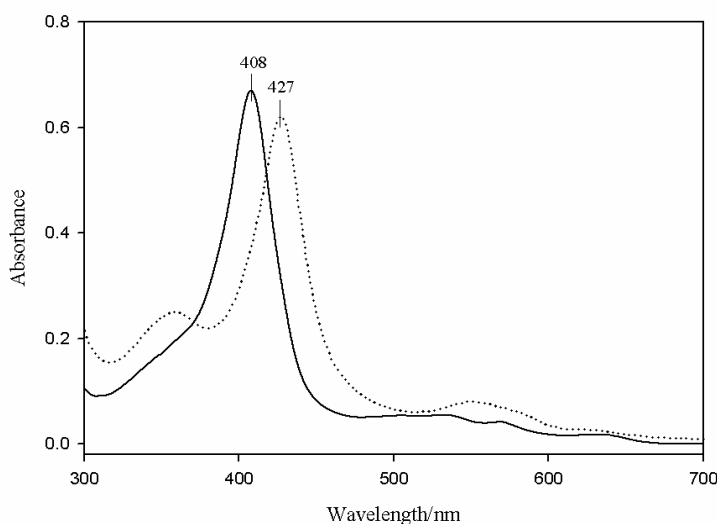


Figure 2.1: Electronic absorption spectra of ferric *Ph-2/2HbO* (25°C, pH 7.6), purified in the presence (dotted line) and absence of 1.0 mM  $\beta$ -ME (solid line). The shift of the Soret band to 427 nm was caused by sulfide impurities present in  $\beta$ -ME; upon omission of  $\beta$ -ME during the purification, *Ph-2/2HbO* was isolated in a ferric form characterized by a Soret band at 408 nm and bands in the visible region as reported in the text and Figure 2.1 of the chapter.

The high affinity for hydrogen sulfide is thought to have a possible physiological significance as  $H_2S$  is present in marine sediments containing bacteria. The potential sulfide binding properties of Hbs and the sulphur metabolism of microorganisms, biochemical functions other than transport of the gaseous ligand could be hypothesized. However there is no evidence of a potential physiological role of hydrogen disulfide in the metabolism of the Antarctic bacterium.

### 2.2.2 Sequence alignment

The sequence alignment indicates that *Ph-2/2HbO* has structural features typical of 2/2 Hbs, and especially those belonging to Group II. In particular, *Ph-2/2HbO* has Trp at position G8, and both the CD1 and the B10 positions are occupied by Tyr (see Figure 2.2).

These three positions are the most important for oxygen stabilization in this family of Hbs (Milani et al., 2005). In contrast to Group I of 2/2Hbs, the E7 and E11 positions are occupied by non-polar aminoacid residues, Ile and Phe, respectively, precluding ligand stabilization by these two residues. Several structures of *Ph*-2/2HbO were obtained (see ‘‘Materials and methods’’) starting from different alignments, with proteins of Group II giving rise to different initial structural models. The global fold of the models was very good, and the most significant structural differences were located in the CD loop, due to the insertion of three residues (Figures 2.2 and 2.3). In all of the obtained alignments, the important heme cavity residues (HisF8, TyrB10, TrpG8, TyrCD1, IleE7, PheE11) are in the positions originally proposed by Wittenberg (Wittenberg et al., 2002) and subsequently confirmed by Vuletich and Lecomte (Vuletich and Lecomte, 2006) for Group II proteins. This alignment differs from that obtained in a previous study with other Group II proteins, where the residue at CD1 was His (Giordano et al., 2007). The latter did not take into account the insertion of three residues in the CD loop, so the CD loop of the current alignment is longer than in other Group II Hbs.

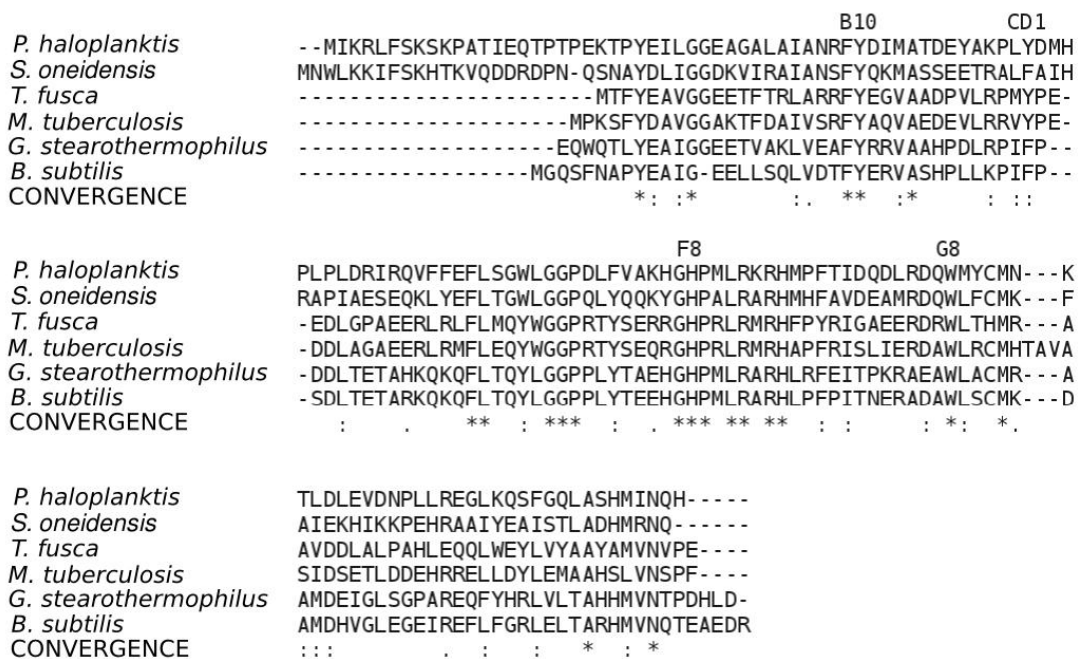


Figure 2.2: Sequence alignment of *Ph*-2/2HbO compared with other 2/2HbO. An insertion is present in the *Ph*-2/2HbO sequence after the CD1 position, and in the GH loop of *Mt*-2/2HbO. *S. oneidensis* 2/2HbO was added to the data set as it has an extension at the N-terminus similar to *Ph*-2/2HbO.

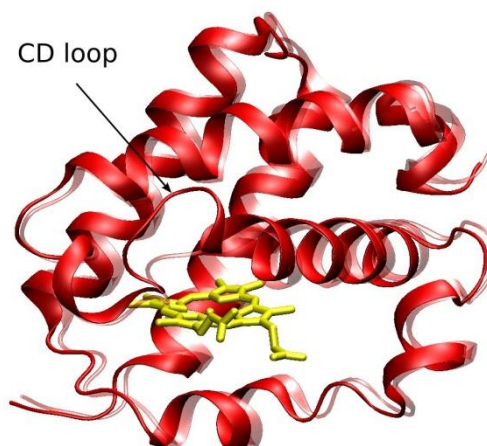


Figure 2.3: Overlay of the backbone and the heme group of the model of *Ph-2/2HbO* and the *Bs-2/2HbO* (*ghost*). The main differences between both structures are located in the CD loop.

*Ph-2/2HbO* presents an unusual extension of 15 residues at the N-terminus (pre-A helix). A similar situation had also been found in *M. tuberculosis* HbN (Group I) and appears to occur in many slow-growing species of mycobacterium, such as *M. bovis*, *M. avium*, *M. microti*, *M. marinum* (Lama et al., 2009) and *S. oneidensis* (Vuletich and Lecomte, 2006). The X-ray structure of *M. tuberculosis* HbN (1IDR) showed that the pre-A motif does not significantly contribute to the structural integrity of the protein, protruding out of the compact globin fold, but rather confers a vital contribution in regulating the efficient nitrogen-monoxide-dioxygenase activity of HbN (Lama et al., 2009).

### 2.2.3 Spectroscopy at room temperature: ferric form

The electronic absorption spectrum of ferric *Ph-2/2HbO* and its second-derivative spectrum (D2, dotted line) are invariant over the pH range 5.6–7.6. The spectrum obtained at pH 7.6 (Figure 1a, bottom) is characterized by a Soret band at 408 nm and bands in the visible region at 503, 533 (538 in D2), 570, and 635 nm (638 in D2). The wavelength maxima suggest the presence of various species, namely a His–Fe–H<sub>2</sub>O six-coordinate high-spin (6cHS) form [bands at 503 and charge-transfer transition (CT1) at 635 nm] and at least one 6c-low-spin (LS) heme (bands at 533 and 570 nm). The absorption maxima of the LS forms are quite unusual, reminiscent of those of ferric *Chlamydomonas* Hb (Das et

al., 1999) and the hemophore HasA proteins from *Serratia marcescens* and *Pseudomonas aeruginosa* (Caillet-Saguy et al., 2008; Alontaga et al., 2009) and they are very different from either a LS His–Fe–His (that exhibits well-defined absorption bands at about 535 and 565 nm) or a His–Fe–OH heme complex (that exhibits well-defined absorption bands at about 540 and 580 nm) (Smulevich et al., 1991).

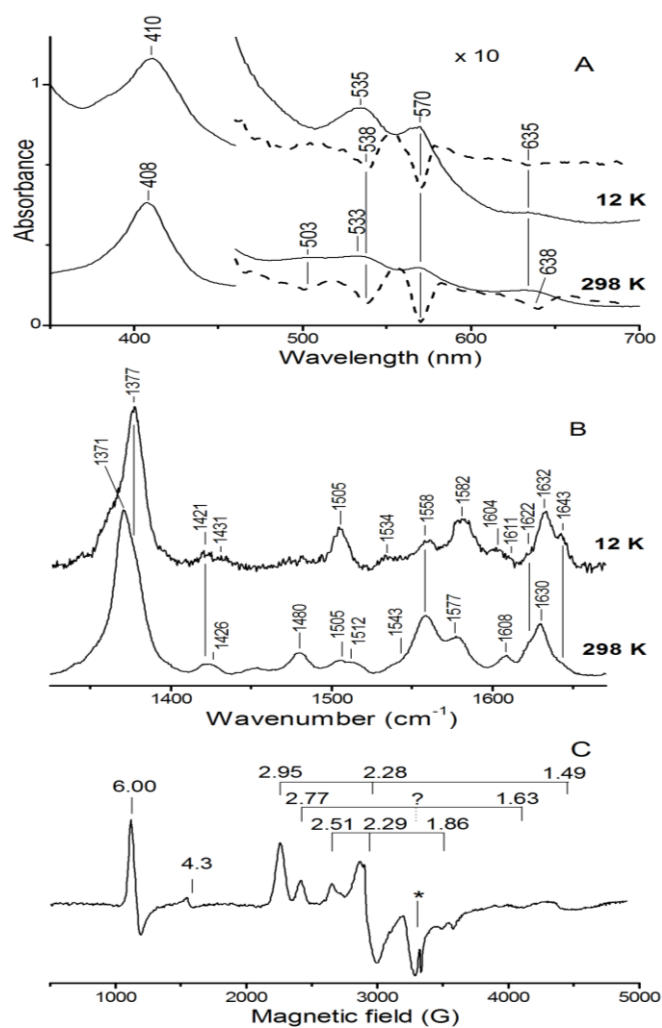


Figure 2.4 Ferric *Ph-2/2HbO* at pH 7.6. A) UV–vis absorption (continuous line) and D2 (dotted line) spectra in 20 mM Tris–HCl at 298 (bottom) and 12 K (top). The visible region has been expanded ten-fold. Spectra have been shifted along the ordinate axis to allow better visualization. B) RR spectra taken with the 413.1 nm excitation wavelength in the high-wavenumber region in 0.1 M MOPS at 298 K (bottom) and in 20 mM Tris–HCl at 12 K (top). C) X-band EPR spectrum in 0.1 M Tris–HCl. The feature at  $g = 4.3$  results from a non-heme iron impurity

Therefore, on the basis of the similarity with the UV–vis spectrum of ferric *Chlamydomonas* Hb and HasA hemophores, a His and a Tyr ligand are suggested to occupy the fifth and sixth coordination positions, respectively. In agreement with the electronic absorption spectra, the Raman excitation profile at pH 7.6 (Figure 2.4 A, bottom), together with the spectra in polarized light (Figure 2.5 B), allow the identification

of three species: a 6cHS species ( $\nu_3$  at  $1,480\text{ cm}^{-1}$ ,  $\nu_{10}$  at  $1,608\text{ cm}^{-1}$ ), and two 6cLS species. In particular, with Soret excitation, two 6cLS  $\nu_3$  bands at  $1,505$  and  $1,512\text{ cm}^{-1}$  were observed (Figure 2.4 B, bottom; Figure 2.5 B, bottom trace), and in the  $1,600\text{--}1,650\text{ cm}^{-1}$  region the spectra in polarized light enable the identification of two polarized bands at  $1,622$  and  $1,630\text{ cm}^{-1}$  assigned to the  $\nu(\text{C}=\text{C})$  vinyl stretching modes (Figure 2.5 B, bottom trace). Upon excitation with the  $514.5\text{ nm}$  line (i.e., in resonance with the visible bands), two depolarized bands at  $1,635$  and  $1,643\text{ cm}^{-1}$  were identified and assigned to two m10 modes of 6cLS hemes (Figure 2.5 B).

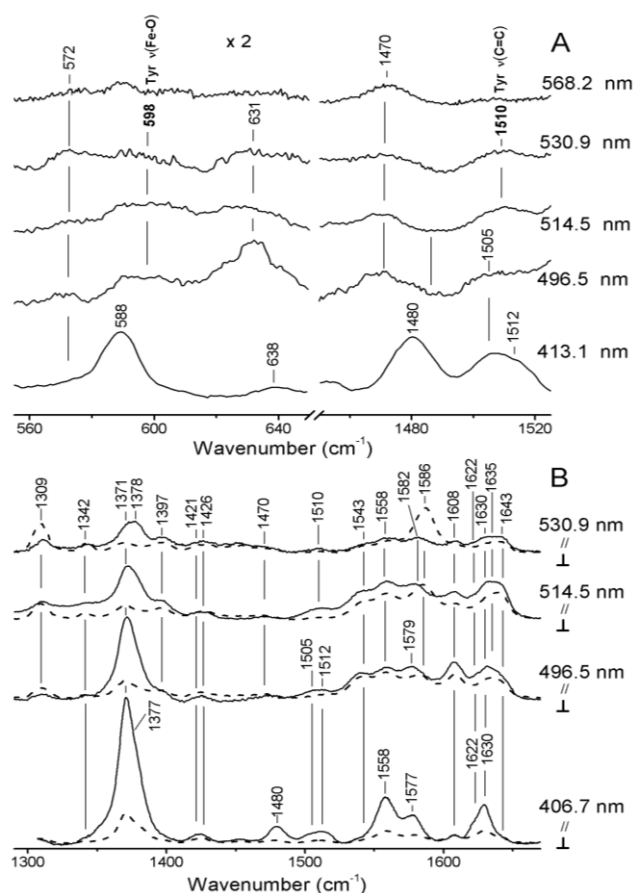


Figure 2.5 RR spectra of ferric *Ph-2/2HbO* at 298 K, in 20 mM Tris-HCl, pH 7.6 obtained with various excitation wavelengths: 406.7 nm, 496.5 nm, 514.5 nm, 530.9 nm, 568.2 nm. Experimental conditions are reported in Howes et al., 2011

A Tyr coordinated to a heme iron can often be identified by RR experiments. In fact, excitation in the tyrosinate-Fe(III) CT band (near 500 nm) yields characteristic vibrational frequencies of the bound phenolate (Que, 1988). In the  $400\text{--}1,700\text{ cm}^{-1}$  region, the spectra taken with excitation wavelengths in the visible region (Figure 2.5 A) clearly show the enhancement of two bands at  $598$  and  $1,510\text{ cm}^{-1}$  (which are polarized, data not

shown), displaying maximum intensification for excitation at 514.5 nm. Figure 2.5 a shows the two spectral regions expanded to better visualize the bands. These bands are assigned to the  $m(\text{Fe}-\text{OTyr})$  and  $m\text{Tyr}(\text{C}=\text{C})$  tyrosinate modes, respectively. Note that, despite the observation of two low spin forms in the RR spectra, only one  $m(\text{Fe}-\text{OTyr})$  stretching mode at  $598\text{ cm}^{-1}$  is clearly evident.

#### 2.2.4 Spectroscopy at low temperature

The electronic absorption and the D2 spectra of ferric *Ph-2/2HbO* in the low-temperature range 220–12 K (Figure 2.4 A, top) are essentially those of 6cLS hemes. The LS Q-bands observed at room temperature (535 and 570 nm) are intensified, whereas the Soret band red-shifts by 2 nm and the 6cHS bands at 503 and 635 nm (638 nm in the D2 spectrum) are considerably reduced. In accord with the low-temperature absorption spectrum, the high-frequency RR spectrum at 12 K pH 7.6 shows an intensification of the LS form ( $\nu_3$  1,505,  $\nu_2$  1,582,  $\nu_{10}$  1,643  $\text{cm}^{-1}$ ) at the expense of the 6cHS form ( $\nu_3$  1,480,  $\nu_2$  1,558,  $\nu_{10}$  1,608  $\text{cm}^{-1}$ ) observed at 298 K (Figure 2.3 B), which is considerably reduced at 12 K. Moreover, of the two LS forms observed at 298 K, characterized by  $m_3$  bands at 1,505 and 1,512  $\text{cm}^{-1}$ , only one form appears to be particularly enhanced at 12 K ( $m_3$  at 1,505  $\text{cm}^{-1}$ ). Interestingly, at the physiological temperature for the bacterium (4 °C), a slight increase in the relative intensity of the RR  $\nu_3$  LS band at 1,505 with respect to that at 1,512  $\text{cm}^{-1}$  has been observed. Nevertheless, the broad  $\nu_2$  band (1,582  $\text{cm}^{-1}$ ) at 12 K suggests the presence of two LS forms. This interpretation is supported by the presence of the bands at 1,604 and 1,611  $\text{cm}^{-1}$ , assigned to two  $\nu_{37}$  LS modes. X-band EPR spectroscopy (at 5 K) was carried out to gain further insight into the spin state and heme coordination environment of the protein (Figure 2.3 C). The  $g$  values of EPR spectrum should be considered to be average values, as at each  $g$  value there is evidence of more than one species with very similar  $g$  values, likely indicative of some structural flexibility at this site. A detailed analysis of EPR data (see Howes et al., 2011) proposed a tyrosinate LS heme species that is strongly H-bonded with a neighboring residue.

### 2.2.5 Molecular dynamics simulations

The most stable structure found by homology modeling was used to perform 40 ns of MD simulations. To elucidate the potential residue(s) involved in the hexacoordinated conformation, selected key distances during the simulation were monitored. As reported for other Group II Hbs, the oxygen atom of TyrB10 was found to be close to the Fe(III) atom (Milani et al., 2005; Das et al., 1999). However, TyrCD1 was found to be even closer to the Fe(III) atom than TyrB10 (Howes et al., 2011).

This is the first reported case in which the TyrCD1 may be bound to the Fe(III) atom. On this basis, two models were constructed in which either TyrCD1 or TyrB10 was coordinated to the Fe(III). MD simulations of these models were performed in order to determine the stabilities of these potential structures. The results show that both systems were stable during the 20 ns of the MD. When TyrCD1 is coordinated to the iron atom, TrpG8 is H-bonded to the O<sup>-</sup> of TyrCD1, highlighting the important role of this residue (Figure 2.5). On the other hand, when TyrB10 is coordinated to the iron, both TrpG8 and TyrCD1 are H-bonded to the O<sup>-</sup> of TyrB10 (Figure 2.6). These results are fully in keeping with the presence of multiple LS forms displaying different heme binding affinities and spectroscopic properties.

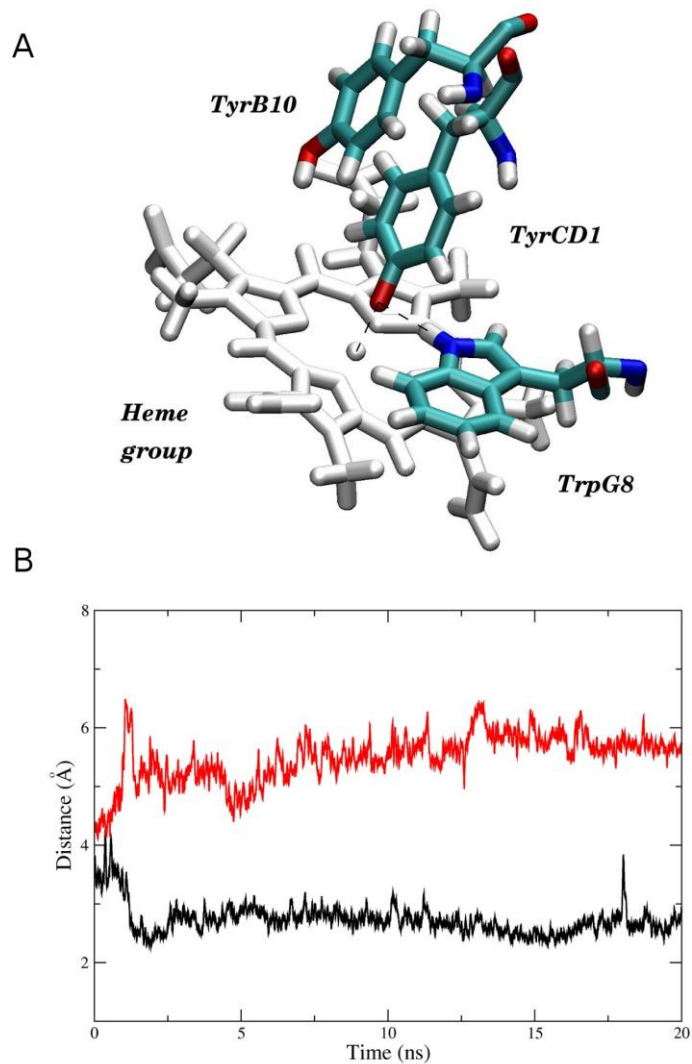


Figure 2.5: *Ph-2/2HbO* with TyrCD1-O- coordinated to the heme iron. A) Schematic representation of the distal site of the protein showing the coordinated TyrCD1-O- stabilized by a H-bond with the TrpG8. As shown in b, the distance between TyrCD1-O- and the hydroxylic proton of TyrB10 is too long to form a H-bond. B) Time evolution of selected distances between the O- atom of the coordinated TyrCD1 and the indole N $\epsilon$  proton of TrpG8 (black), and the hydroxylic proton of TyrB10 (red)

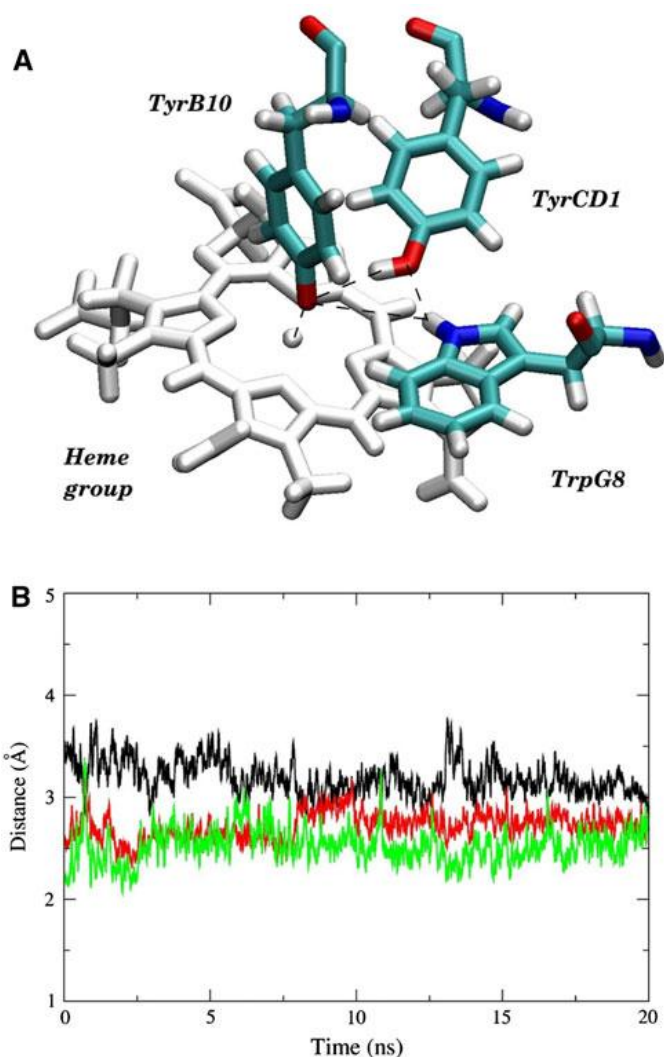


Figure 2.6: *Ph-2/2HbO* with TyrB10-O<sup>-</sup> coordinated to the heme iron. A) Schematic representation of the distal site of the protein, showing the coordinated TyrB10-O<sup>-</sup> stabilized by H-bonds with both TyrCD1 and TrpG8. Interaction between TyrCD1 and TrpG8 is also indicated. B) Time evolution of selected distances between the TyrB10-O<sup>-</sup> atom with the indole N<sub>ε</sub> proton of TrpG8 (black), the TyrB10-O<sup>-</sup> atom with the hydroxylic proton of TyrCD1 (red), and the indole Ne proton of TrpG8 with the hydroxylic oxygen of TyrCD1 (green)

### 2.2.6 Spectroscopy: ferrous form

The electronic-absorption spectrum of ferrous *Ph-2/2HbO*, in the pH range 5.8–10.9 at 25 °C, varied as a function of pH. In particular, the spectra were characterized by a mixture of a predominant 6cLS heme (Soret band at 421 and Q bands at 528 and 559 nm) and a 5cHS form (shoulder at about 440 nm; Figure 2.7). The fraction of the LS form increased with increasing pH from 5.8 to 11.0 (Figure 1A, traces a–c). Accordingly, the RR spectra in the high-frequency region, obtained in resonance with the Soret maximum at 440 nm (Figure 2.7, traces a–c) showed core size marker bands typical of a 5cHS form ( $\nu_3$

at  $1,468\text{ cm}^{-1}$  and  $\nu_2$  at  $1,559\text{ cm}^{-1}$ ), predominant at acid pH, and a 6cLS form ( $\nu_3$  at  $1,491\text{ cm}^{-1}$ ,  $\nu_2$  at  $1,580\text{ cm}^{-1}$ ) which markedly increased at alkaline pH. Therefore, the low-frequency region of the RR spectra (Figure 2.7 C, trace a) yields information about the Fe-proximal His bond strength from the frequency of the corresponding m(Fe-His) stretching mode, which is active only in the ferrous 5cHS form upon excitation in the Soret absorption band (Hori and Kitagawa, 1980; Stein and Spiro, 1980).

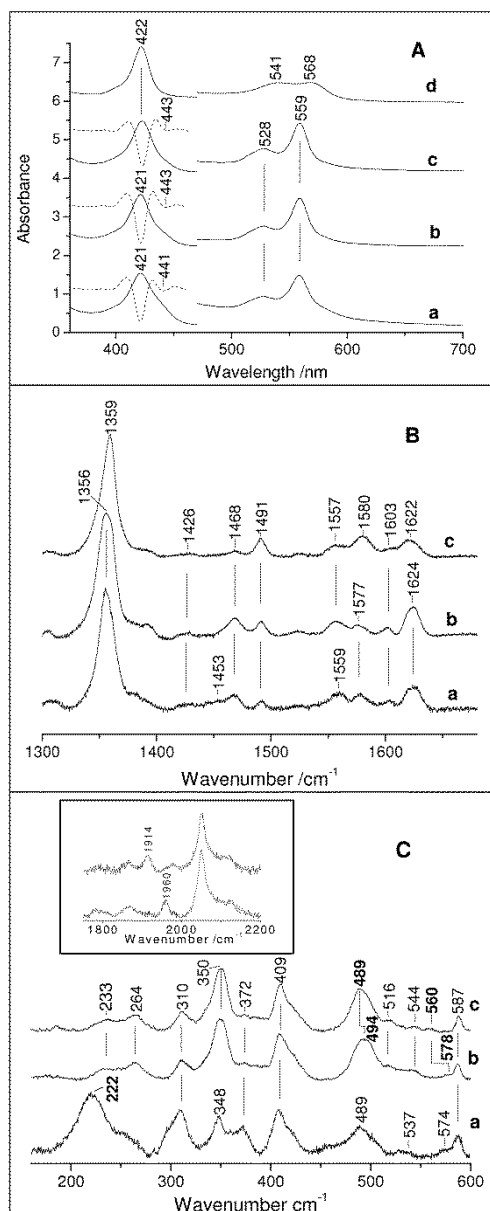


Figure 2.7. A) Absorption spectra of the deoxy form of *Ph-2/2HbO* at pH 5.8 in 0.1 M MES (a), pH 7.6 in 0.1 M Tris-HCl (b), and pH 11.0 in 0.1 M CAPS (c), and the CO complex at pH 5.8 in 0.1 M MES (d); the spectrum of the CO complex is invariant in the pH range 5.8–10.9. The second derivative and absorption spectra are shown superimposed on the Soret region. The visible region was expanded fivefold. Spectra were shifted along the ordinate axis to allow better visualization. B) RR spectra of the deoxy form recorded with the 441.6-nm excitation wavelength in the high-wavenumber region at pH 5.8 (a), 7.6 (b) and 11.0 (c). C) RR spectra of the deoxy form (a) and its CO complex for  $^{12}\text{CO}$  (b) and  $^{13}\text{CO}$  (c) recorded with the 441.6- and 413.1-nm excitation wavelengths, respectively, in the low-wavenumber region at pH 7.6; the spectrum of the CO complex is invariant in the pH range 5.8–11.0. The inset shows the  $\nu(\text{CO})$  stretching mode at  $1960\text{ cm}^{-1}$ , which shifts to  $1914\text{ cm}^{-1}$  for the  $^{13}\text{CO}$  adduct. Experimental conditions: see Giordano et al., 2011

The intense band at  $222\text{ cm}^{-1}$ , whose intensity decreases at alkaline pH, was assigned to the  $\nu(\text{Fe-Im})$  stretching mode. Its frequency is similar to that of Mb. A definitive determination of the nature of the sixth ligand is not possible, however, based on

the results previously obtained for the ferric form, we suggest that either the TyrCD1-O<sub>2</sub> or TyrB10-O<sub>2</sub> are coordinated to the heme Fe (II) atom. Upon addition of CO, the UV–visible absorption spectra (Figure 2.7 A, trace d; with Soret and Q bands at 422, 541, and 568 nm, respectively) and the high-frequency RR spectra obtained with 413.1 nm excitation (data not shown) were characteristic of the 6cLS form. The spectra did not change between pH 5.8 and 10.9. In the low-frequency region RR spectrum (Figure 2.7 C, traces b and c) two isotope-sensitive peaks were observed. The band at 494 cm<sup>-1</sup>, which shifted to 489 cm<sup>-1</sup> for the <sup>13</sup>CO complex, was assigned to a  $\nu(\text{Fe—C})$  stretching mode, and the band at 578 cm<sup>-1</sup>, which shifted to 560 cm<sup>-1</sup>, was assigned to the corresponding  $\delta(\text{Fe—C—O})$  bending mode. Accordingly, it was possible to identify one  $\nu(\text{CO})$  stretching mode at 1,960 cm<sup>-1</sup> (inset Figure 2.7 C), which shifted to 1,914 cm<sup>-1</sup> upon isotopic substitution.

### 2.2.7 CO-rebinding kinetic profile and determination of $k_{\text{on}}$ CO rates at different pH

The CO-rebinding kinetics following nanosecond laser photolysis of *Ph-2/2HbO* were recorded as a function of CO concentration at different pH values and at 25 °C. A two-exponential decay model was sufficient to explain the kinetic curves. With this model, two CO-dependent kinetic phases were obtained. Table 1 reports the CO-association constants obtained from Eq. (2) for the fast (i.e.,  $^f k_{\text{on}}$ ) and slow rates (i.e.,  $^s k_{\text{on}}$ ) at different pH values. The data demonstrate that  $^f k_{\text{on}}$  is very fast, in the range of 10<sup>7</sup> M<sup>-1</sup> sec<sup>-1</sup>, and close to that of human Ngb (Uzan et al., 2004), whereas  $^s k_{\text{on}}$  is compatible to the rates obtained for Mb, in the range of 10<sup>5</sup> M<sup>-1</sup> sec<sup>-1</sup> (Springer et al., 1994).

pH	$^f k_{\text{on}}$ (10 <sup>7</sup> M <sup>-1</sup> s <sup>-1</sup> )	$^s k_{\text{on}}$ (10 <sup>5</sup> M <sup>-1</sup> s <sup>-1</sup> )
6.0	0.8±0.1 (25)	4.6±0.9 (75)
7.6	1.2±0.2 (29)	6.9±1.3 (71)
8.5	1.2±0.2 (35)	7.8±1.5 (65)
11.0	1.2±0.2 (52)	5.8±1.1 (48)

Table 1: CO-association rate constants obtained by LFP at different pH values at 25 °C (in parentheses the relative percentage of the two rate constants at 1 atm CO). Weighted standard deviations are determined from five different experiments

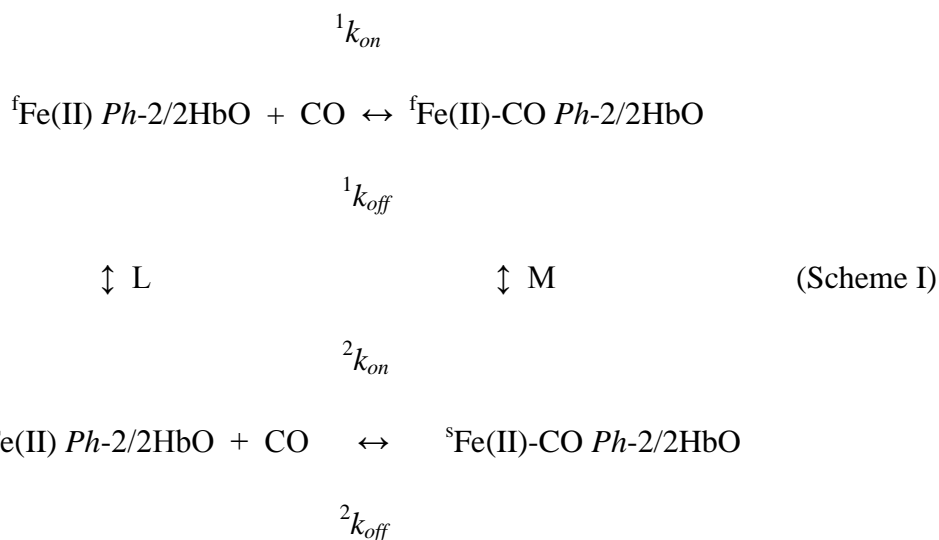
The CO-dependent kinetic phases are unusual for a 2/2 bacterial Hb of group II. In the 2/2HbO of *M. tuberculosis*, the slow phase is in the range of 10<sup>4</sup> M<sup>-1</sup> sec<sup>-1</sup>, whereas the fast phase is in the range of 10<sup>5</sup> M<sup>-1</sup> sec<sup>-1</sup> (Ouellet et al., 2003). Both proteins display two

conformations that differ greatly in ligand association rate, suggesting that these proteins may switch between two distinct functional levels.

Table 1 shows that the amplitude of the slow phase dominated (75%) at pH 6.0, but decreased to 48% at pH 11.0. There is apparently an equilibrium between the two conformations, and pH strongly modulates such an equilibrium. The amplitude of the fast phase increased with increasing pH, whereas the amplitude of the slow phase decreased in such a way that at pH 11.0, each conformation accounted for almost 50%.

In collaboration with Prof. Coletta, stopped flow experiments were performed showing that CO dissociation was characterized at all pH values by a two exponential pattern (data not shown) with essentially pH-independent rates (but not the relative amplitudes), which ranged for the faster rate constant (i.e.,  $^f k_{\text{off}}$ ) around  $1.0(\pm 0.5) \text{ sec}^{-1}$  and for the slower rate constant (i.e.,  $^s k_{\text{off}}$ ) around  $0.03(\pm 0.02) \text{ sec}^{-1}$ . Interestingly, the percentage of the absorption amplitude for the faster CO dissociation process increased with pH, shifting from about 16% at pH 6.0 to about 39% at pH 11.0. This behavior suggested the coexistence of two CO-bound forms, whose relative percentage is pH-dependent, and the fast CO-dissociating form was stabilized by alkaline pH.

On the basis of stopped flow and laser photolysis data, we can reasonably envisage the existence in Fe(II)-*Ph-2/2HbO* of a ligand- and pH-linked conformational transition between two tertiary arrangements. The unliganded form showed a large predominance of the slow-reacting form, which was characterized by the following kinetic parameters at pH 7.0 and 20°C:  $k_{\text{on}} = 4.25(\pm 0.5) \times 10^5 \text{ M}^{-1} \text{ sec}^{-1}$  and  $k_{\text{off}} = 0.023 \pm 0.004 \text{ sec}^{-1}$ . Upon CO binding the equilibrium was partially displaced (in a pH-dependent fashion) toward a fast-reacting form (coexisting with the slow reacting forms predominant in the unliganded form), which was characterized by the following parameters at pH 7.6 and 25°C:  $k_{\text{on}} = 1.16(\pm 0.32) \times 10^7 \text{ M}^{-1} \text{ sec}^{-1}$  and  $k_{\text{off}} = 0.45 \pm 0.06 \text{ sec}^{-1}$ . This mechanism may be sketched according to the following Scheme:



where  ${}^f\text{Fe(II)-}Ph\text{-}2/2\text{HbO}$  and  ${}^f\text{Fe(II)-CO-}Ph\text{-}2/2\text{HbO}$  are the unliganded and the CO-bound forms, respectively, of the fast reacting species, whereas  ${}^s\text{Fe(II)-}Ph\text{-}2/2\text{HbO}$  and  ${}^s\text{Fe(II)-CO-}Ph\text{-}2/2\text{HbO}$  are the unliganded and the CO-bound forms, respectively, of the slow-reacting species,  $L = [{}^s\text{Fe(II)-}Ph\text{-}2/2\text{HbO}]/[{}^f\text{Fe(II)-}Ph\text{-}2/2\text{HbO}]$  and  $M = [{}^s\text{Fe(II)-CO-}Ph\text{-}2/2\text{HbO}]/[{}^f\text{Fe(II)-CO-}Ph\text{-}2/2\text{HbO}]$  are the equilibrium constants of the tertiary conformational equilibrium in the unliganded and in the CO bound forms, respectively. The extent of the two phases rather than the rate constants of  ${}^f\text{Fe(II)-}Ph\text{-}2/2\text{HbO}$  (see Table 1) appeared to be slightly proton linked both for the association and the dissociation rate constants. However, this proton linkage does not support any relevant role played by pH on the functional modulation over the physiological pH range (i.e., between pH 6.5 and 8.0). Furthermore, at a given pH value the amplitude of the slow phase increased as the CO concentration decreased (data not shown), suggesting that after photolysis there is competition between CO rebinding of  ${}^f\text{Fe(II)-}Ph\text{-}2/2\text{HbO}$  and the transition between  ${}^f\text{Fe(II)-}Ph\text{-}2/2\text{HbO}$  and  ${}^s\text{Fe(II)-}Ph\text{-}2/2\text{HbO}$  (corresponding to equilibrium L, see Scheme I). This behavior is perfectly in line with the mechanism sketched in Scheme I, suggesting that  $L > M$  and the existence of a CO linked tertiary equilibrium.

### 2.2.8. Circular dichroism spectroscopy

CD has become increasingly recognized as a valuable spectroscopic technique for studying protein structure in solution because all the protein secondary structure components display characteristic far-UV (178—250 nm) CD spectra. The spectrum of a protein is basically the sum of the spectra of its conformational elements, and thus CD can be used to estimate secondary structure (Greenfield, 1999). The effects of pH and temperature on the secondary structure of ferric *Ph-2/2HbO* were investigated by far-UV CD spectroscopy, to understand the basic chemical biology properties of the protein.

The far-UV CD spectrum (190–260 nm) of ferric *Ph-2/2HbO* was typical of the globin family showing mainly an alpha helical secondary structure. The spectra for native *Ph-2/2HbO* had negative bands at 208 and 222 nm (data not shown), as expected for a high percentage of alpha helix.

Molar ellipticity at 222 nm was used to follow the thermal unfolding at pH 7.6 and pH 8.5. The melting profiles are shown in Figure 2.8

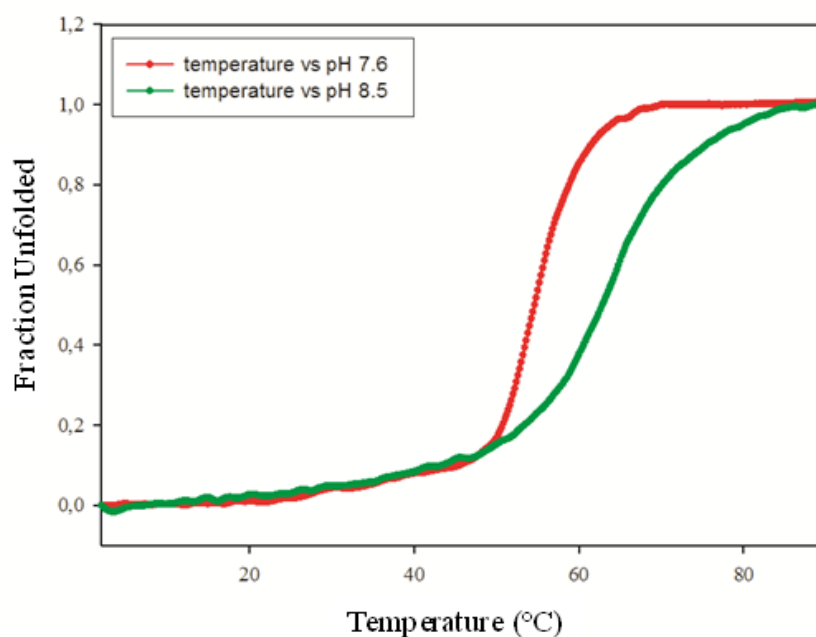


Figure 2.8: Melting profiles (Fraction Unfolded vs. Temperature) of *Ph-2/2HbO* at different pH. Experiments were performed from 2 °C to 90°C in 100 mM TrisHCl pH 7.6 (in red) and 100 mM Tris HCl pH 8.5 (in green) in presence of 1mM TCEP.

The secondary structure of *Ph-2/2HbO* is sensitive to its environment, in particular to pH. The melting profile of *Ph-2/2HbO* (Figure 2.8) showed a sigmoidal transition at 54 °C (pH

7.6) and 64 °C (pH 8.5), the values of the temperature induced unfolding of the native structure.

After cooling back from 90 °C to 2 °C, the spectrum recorded at pH 7.6 was not completely superimposable to that obtained from the initial acquisition at 2 °C, demonstrating that unfolding is largely irreversible. Although the thermal denaturation was irreversible at pH 7.6, we observed a significant thermal reversibility at pH 8.5. These results may be attributed to the hexacoordinated heme structure of *Ph-2/2HbO*, as demonstrated for human Ngb and human Cygb (Hamdane et al., 2005). These values are lower respect human Ngb ( $T_m = 100$  °C) and horse heart Mb ( $T_m = 85$ °C) (Hamdane et al., 2005). Ngb and Cygb show an unusually high  $T_m$  relative to other hemoproteins, probably due to their possible enhanced stability promoted by disulfide bond formation (Hamdane et al., 2005).

Although the high thermostability of a cold adapted protein was unexpected, other similar cases have been reported. One example is psychrophilic L-glutamate dehydrogenase from the Antarctic bacterium *Psychrobacter* sp. TAD1, which becomes irreversibly denatured only at temperatures higher than 55 °C (Di Fraia et al., 2000), namely the same typical of the bovine enzyme. The stability of mesophilic globins in vertebrates and invertebrates has been investigated in the past (Wittenberg et al., 2002; Hughson and Baldwin, 1989; Hughson et al., 1991). Mbs are very stable to thermal denaturation when they are in the holo-structure ( $T_m \sim 85$ °C). In the absence of heme, some intra-protein interactions may not be strong enough to preserve the stability of the classical eight-helix globin fold (Harrison and Blout, 1965). Apo-globins generally display lower resistance to thermal or chemical denaturation.

Hb recently identified in *Aquifex aeolicus* is called thermoglobin because it is resistant to thermal denaturation, still containing ~ 75% of its physiological  $\alpha$ -helical content at 90 °C (Miranda et al., 2005). Similar to thermoglobin, 2/2Hb from the thermophilic actinobacterium *Thermobifida fusca* is significantly more thermostable (as expected) than its mesophilic homologue (Bonamore et al., 2005). However, it currently seems virtually impossible to ascribe thermostability of these two 2/2Hbs to substitution of some residues, or to invoke a single explanation to distinguish between mesophile and psychrophile proteins. A commonly accepted view for protein cold adaptation is the activity–stability–flexibility relationships. Active site sequences are generally highly conserved among homologous proteins due to structural constraints in ligand/substrate binding. In some proteins, e.g. enzymes, adaptive changes in the structure may occur at subunit interfaces,

distant from the active site (Johns and Somero, 2004). These alterations in the strength of subunit interactions may affect thermal stability and energy changes associated with conformational transitions due to ligand binding (Somero, 1995; D'Amico et al., 2006).

The conformational stability of *Ph-2/2HbO* against the denaturing action of GuHCl has been investigated by steady-state fluorescence measurements at pH 7.6, 100 mM Tris HCl. The protein possesses several fluorophore residues with two Trp residues and five Tyr residues in its primary structure. Fluorescence measurements were performed by using a 280 nm excitation wavelength in order to detect the contribution of both Tyr and Trp residues. Measurements were performed after an overnight incubation of the samples at 4 °C. The fluorescence emission spectrum of *Ph-2/2HbO* shows a maximum at 345 nm that, when the tertiary structure is completely unfolded, shifts to 352 nm in 6 M GuHCl (see Figure 2.9).

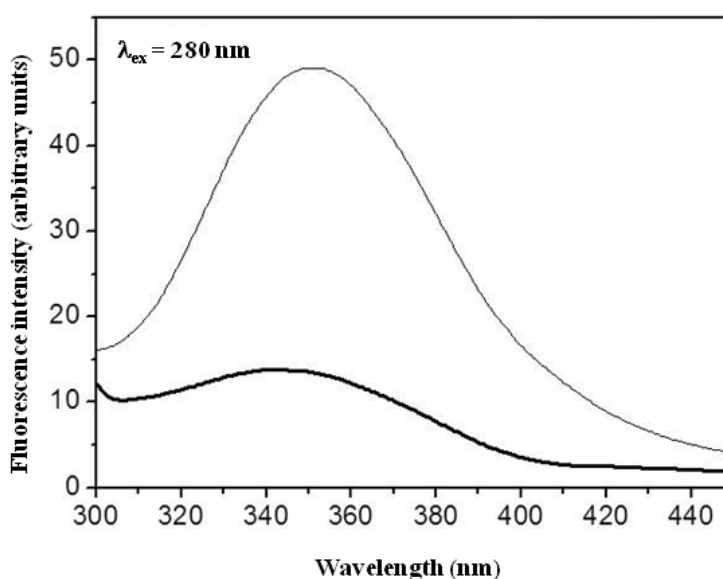


Figure 2.9: Fluorescence emission spectra of native *Ph-2/2HbO* (in bold) and of unfolded *Ph-2/2HbO* in 6 M GuHCl

Upon increasing the concentration of the denaturant, the signal intensity increases. It is well known that fluorescence spectra of proteins with a maximum around 335 nm are characteristic of Trp residues well buried in the hydrophobic core, whereas fluorescence spectra with a maximum around 350 nm are characteristic of Trp residues exposed to the aqueous solvent (Lakowicz, J. R., 1983). Therefore, *Ph-2/2HbO* seems to have the tryptophan side chains nearly exposed to the aqueous solvent in the native structure, but well exposed to the aqueous solvent in the denaturant-induced unfolded state. *Ph-2/2HbO*

shows sigmoidal transition curves recording the change in fluorescence intensity at 345. The GuHCl-induced transition curves are shown in Figure 2.10.

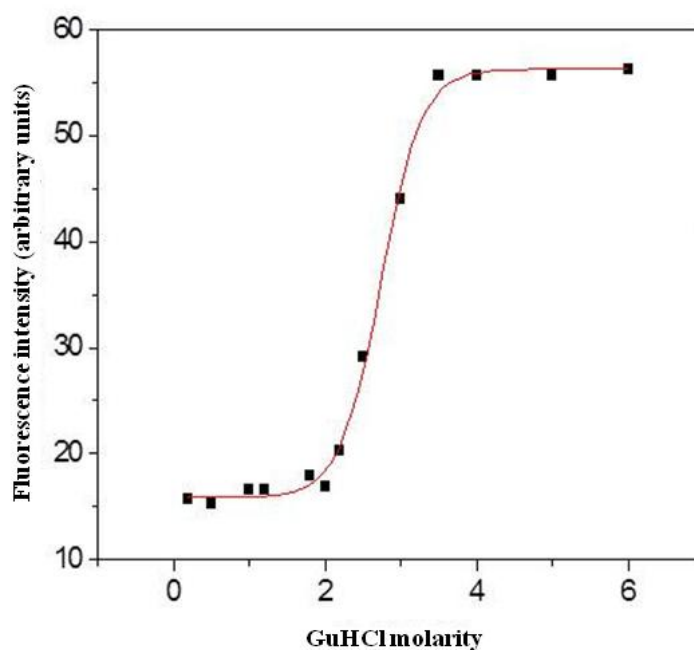


Figure 2.10: GuHCl-induced equilibrium unfolding curves of *Ph-2/2HbO* obtained by recording shift in the wavelength corresponding to the maximum of the fluorescence spectrum

The values of the denaturant concentration at half-completion of the transition, indicated as  $[\text{den}]_{1/2}$ , correspond to  $[\text{GuHCl}]_{1/2} = 2.7 \text{ M}$ . Moreover, this value agree with those previously determined by recording the molar ellipticity at 222 nm in CD measurements (Figure 2.11) :  $[\text{GuHCl}]_{1/2} = 2.7 \text{ M}$ . We can conclude that the protein is endowed with good chemical stability when compared to compared with Mb where  $[\text{GuHCl}]_{1/2} = 1.5 \text{ M}$  (Ahmad et al., 1992).

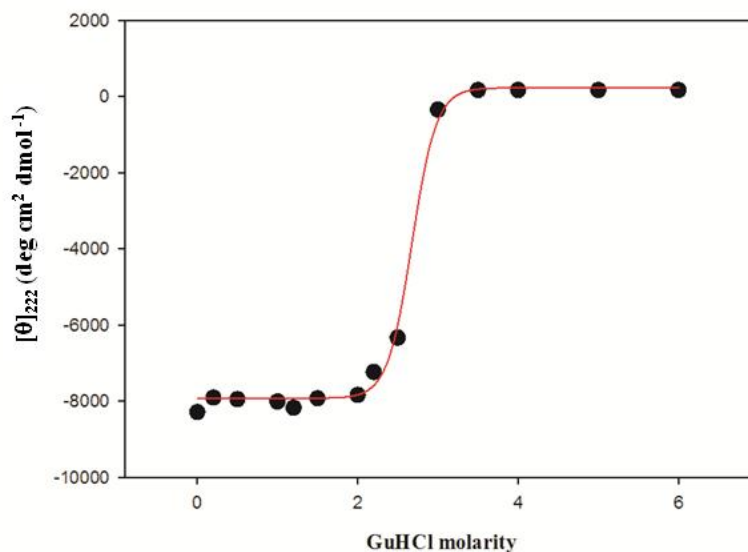


Figure 2.11: GuHCl-induced equilibrium unfolding curves of *Ph-2/2HbO* obtained by recording the molar ellipticity at 222 nm in CD measurements

## 2.2.9 High Pressure effects on *Ph-2/2HbO*

### *-Ferric Ph-2/2HbO*

High pressure is an interesting and suitable thermodynamic parameter in the characterisation of the dynamics and stability of proteins, allowing study the modification dependent on volume changes. The effects of high pressure indicate the volume ( $\Delta V^\circ$ ) and energy ( $\Delta G^\circ$ ) parameters of the molecule.

This technique was used to study hydration, stability and dynamics of the active site of *Ph-2/2HbO*. In this section were reported results obtained at pH 8.5. The absorption spectra of ferric *Ph-2/2HbO* at pressures from 0.1 MPa to 600 MPa are shown in Figure 2.12 and 2.14. In the visible region (Figure 2.12) the spectra are normalized to zero at 700 nm. As shown in the figure there is a transition induced by high pressure from 0.1 MPa until 600 MPa. *Ph-2/2HbO* Fe (III) shifts from a mixture of low spin- high spin (LS-HS) at 0.1 MPa (with 2 maxima at 533nm, 570nm and a charge-transfer state at 633 nm) to a completely high spin state at 600 MPa (with 2 maxima at 540 nm and 573 nm). At 600 MPa the charge-transfer state is considerably smaller.

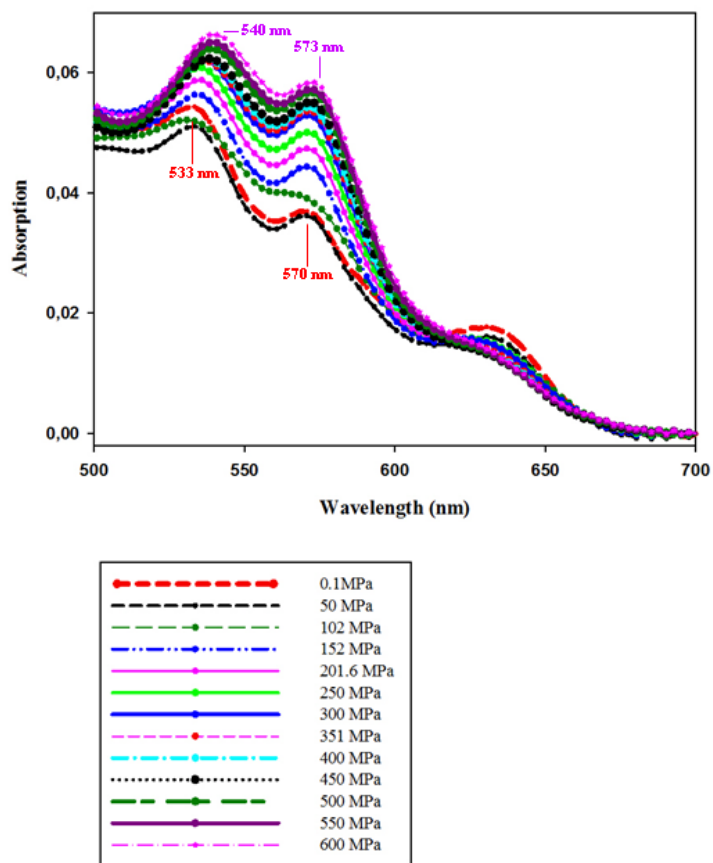


Figure 2.12: Absorption spectra *versus* pressure for ferric *Ph-2/2HbO* in the visible region

The measured molar reaction volume change ( $\Delta V^0$ ) associated with iron spin state transition (high to low spin) was obtained from the plot of  $\ln(\text{Keq} = \text{LS/HS})$  *versus* pressure (Figure 2.13).

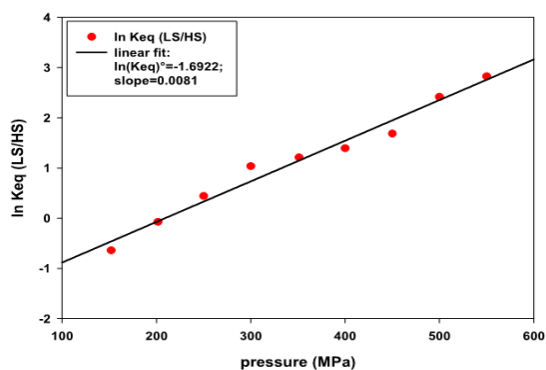


Figure 2.13: Determination of the standard volume change: pressure induces LS to HS transition in ferric *Ph-2/2HbO*, pH 8.5.  $\Delta V^0 = -RT\delta\ln K/\delta P = -0.0081 \times 2477.57 = -20.1 \text{ cm}^3 \text{ mol}^{-1}$

The slope of the linear behavior of  $\ln K_{eq}$  versus pressure gives the standard volume change:

$$\Delta V^\circ = -RT \delta \ln K / \delta \ln P$$

The  $\Delta V^\circ$  of the iron spin transition was  $-20.1 \text{ cm}^3 \text{ mole}^{-1}$ , which is roughly the equivalent of one water molecules ( $18 \text{ cm}^3 \text{ mol}^{-1}$  at 1 atm). This value of  $\Delta V^\circ$  is similar to those previously reported for other hemoproteins, which was estimated in general between  $-10$  and  $-50 \text{ cm}^3 \text{ mol}^{-1}$  (Ogunmola et al., 1976; Alden et al., 1989).

In the Soret region, the absorbance of the Soret spectrum at 0.1MPa is 407 nm and shifts to 414 nm at 600 MPa with a concomitant decrease of the amplitude. There is a partial reversibility of the process. The recovery is about 99.91% (Figure 2.14)

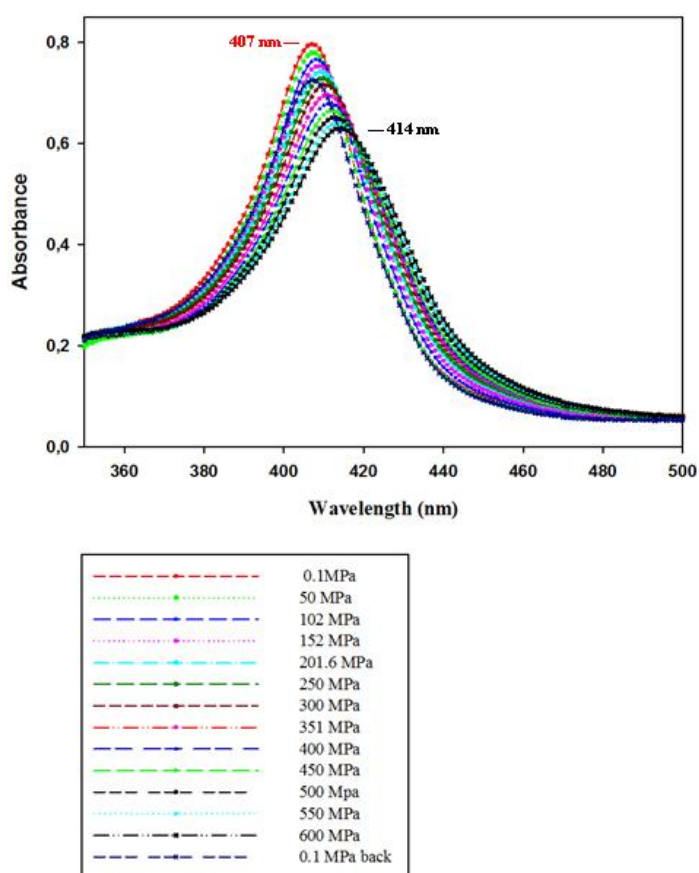


Figure 2.14: Absorption spectra versus pressure for ferric *Ph-2/2HbO* in the Soret region

The observed behaviour can be attributed to two processes: (i) a shift of the amplitude from the pentacoordinated to the hexacoordinated state induced by the binding of molecules of water, and (ii) a red shift of the wavelengths induced by high pressure which is presumably related to some compressibility of the heme pocket.

The results indicate that Soret amplitude is sensitive to ligand coordination and also to polar environment changes. The amplitude of the Soret peaks depend on protein's structure and environment near the sixth ligand. Pressure effects are shown to hydrate the heme pocket leading in general to a decrease of the electronic transition of the heme iron except when the sixth ligation is occupied by an internal ligand. For ferric *Ph-2/2HbO*, the pressure rather strengthens the binding of water molecules to the sixth ligand of the iron. Figure 2.14 shows also an important red shift of the Soret maximum peaks versus pressure. In fact, the wavelength shifts from 407 nm to 414 nm, a total of 7 nm, this  $\Delta\lambda$  is higher than that observed with ferric Mb and with ferric Ngb (with a  $\Delta\lambda = 2$  nm). This effect may be interpreted as a pressure-induced heme pocket compressibility, due to increase of the polarity of the heme pocket.

To calculate the isothermal compressibility coefficient of proteins ( $\beta$ ), we assume that (i) because the heme is buried in the protein, the environment of the heme is not the solvent but the protein including active-site water molecules and (ii) the pressure-induced red-shift of the Soret band is mainly due to the increase of the interaction between the heme and the water molecules and/or polar amino acid residues near the heme (Jung et al., 1995). In the following quantitative estimations of the compressibilities only the Soret band red-shift data were used.

The wavenumber at any pressure ( $\nu_P$ ) minus the wavenumber at 0.1MPa ( $\nu_0$ ), taking as a reference, varies linearly with the pressure (Figure 2.15).

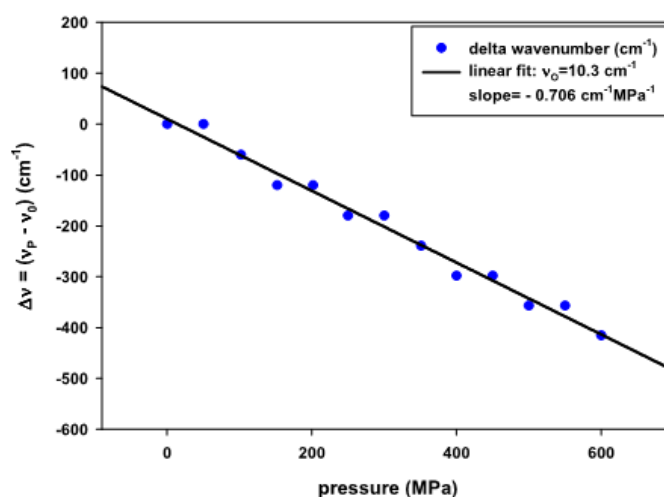


Figure 2.15: Delta wavenumber plot ( $\Delta V$ ) versus pressure (MPa)

The slope of such a linear plot is equal to  $-0.706 \text{ cm}^{-1} \text{ MPa}^{-1}$ . This value is equal or proportional to  $\beta_{(T)} = -1/V * [\delta V / \delta P]$ , the isothermal compressibility coefficient of proteins. Ferric *Ph-2/2HbO* heme pocket results to be compressible as the ferric and ferrous-CO form of human Ngb ( $\beta_{\text{hNgb}} = -0.72 \text{ cm}^{-1} \text{ MPa}^{-1}$ ). Horse Mb in its ferrous-CO form is less compressible ( $\beta_{\text{Mb}} = -0.214 \text{ cm}^{-1} \text{ MPa}^{-1}$ ). The difference between *Ph-2/2HbO* and both Mb and human Ngb resides in the amplitude behaviour: there is a decrease of the Soret absorbance maxima for ferric *Ph-2/2HbO* while, for ferric and ferrous-CO Mb and human Ngb there is an increase of the Soret peaks as the pressure increases. Such behaviours emphasized a large difference in the structure and the environment of the heme pocket.

In conclusion the results show that pressure increases hydration of the heme pocket of ferric *Ph-2/2HbO* at pH 8.5 and 25 °C leading to LS to HS spectra transition in the visible region, as shown by absorbance increase. A plot of the absorbance at selected wavelength in the visible region allowed to calculate the  $K_{\text{eq}}$  and thus the volume change ( $\Delta V^\circ$ ) of the pressure-induced structural as well as hydration transitions. The study on the Soret spectra leads to the conclusion that high pressure acts to increase the hydration content of the heme pocket, presumably favouring the binding of some molecules of water to the sixth coordination of the heme iron in the ferric state. Additional dynamic informations are extracted from the study on the pressure-induced Soret spectra changes. The protein in its ferric state is shown to be very compressible similar to human Ngb but more than Mb, indicating more dynamic flexibility of the heme pocket of the bacterial

protein. As a consequence, an increase of pressure could decrease enough the atomic distance between the heme iron and some internal ligand leading to a pressure-induced hexacoordination. It is evident that increase pressure can favour the binding of the distal internal His to the iron Fe (II) in tomato Hb (Hamdane 2003). At physiological pressure this ligand is too far away from the iron to form ligation.

*-Ferrous Ph-2/2HbO*

Experiments also on ferrous *Ph-2/2HbO* were performed. *Ph-2/2HbO* is a good example for the visualization of the pressure effect on the coordination state at the distal position, because this globin in the ferrous form is not completely hexacoordinated. As shown in Figure 2.16, pressure increases the fraction of hexacoordination, as indicated by the enhanced alpha absorption band. There is not an observable spectral difference of this band for example in human Ngb, because the protein is already 99% hexacoordinated at 1 atm (Hamdane et al., 2005).

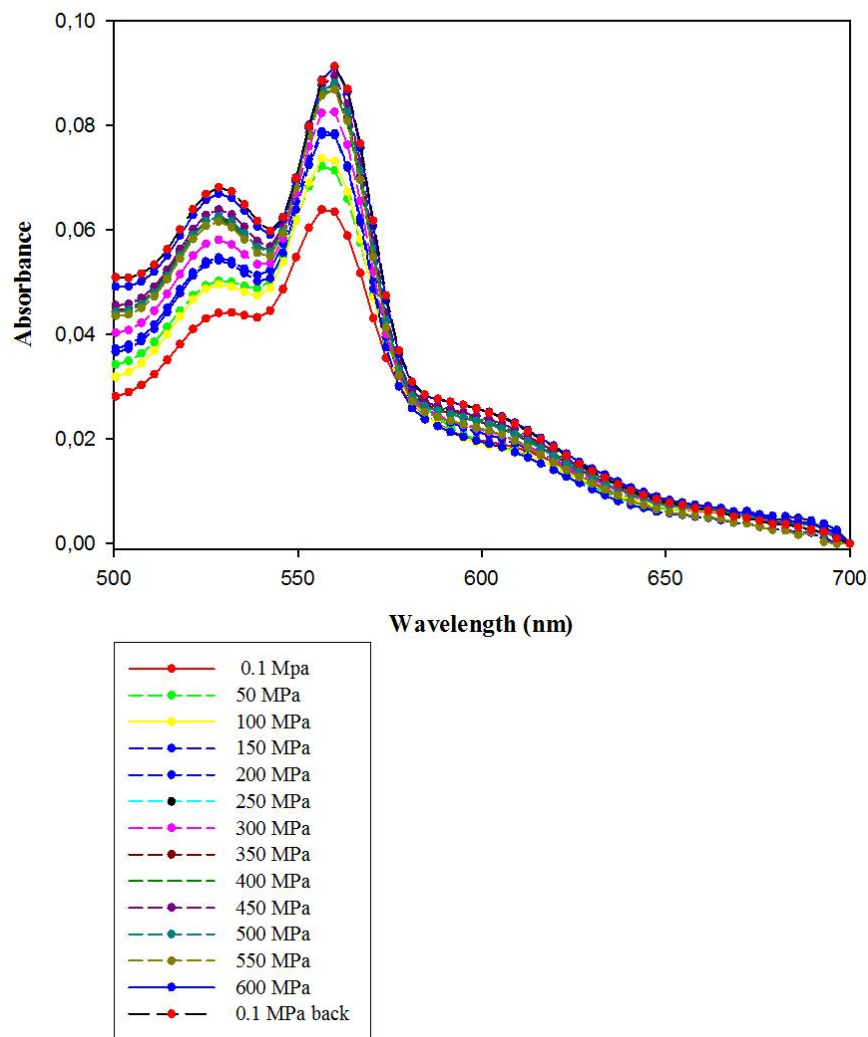


Figure 2.16: Absorption spectra in the visible region *versus* pressure for ferrous deoxy *Ph-2/2HbO*

In the Soret region (Figure 2.17), there is a continue increase of the absorbance, there is only the effect of pressure on the electronic transition without structural transition.

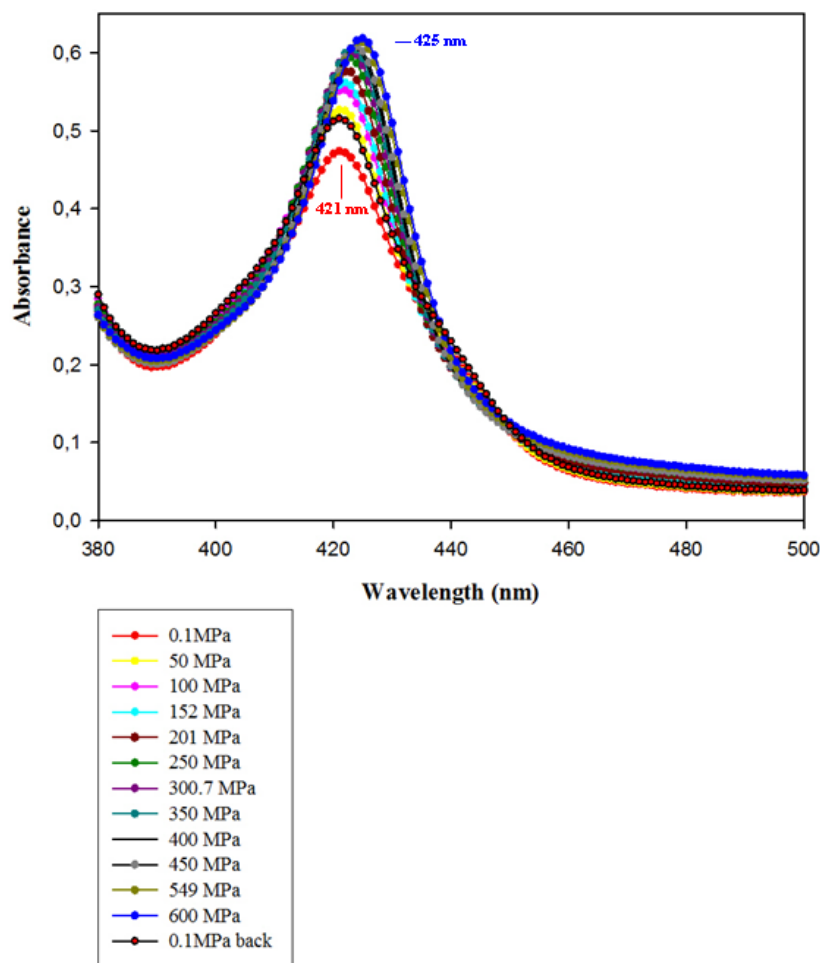


Figure 2.17: Absorption spectra in the Soret *versus* pressure for ferrous deoxy *Ph-2/2HbO*

Pressure induces red shift of the Soret ferrous spectra of *Ph-2/2HbO* as for most of the heme proteins (Gibson and Carey, 1977) such as human Ngb, cytochrome *c* and cytochrome *b5*. The effect is smaller,  $\Delta\lambda$  shift is 4 nm as compare to ferrous human Ngb which exhibits a red shift of 6.14 nm. Thus, we can conclude that ferrous *Ph-2/2HbO* is less compressible than human Ngb, presumably because less cavities are present in the heme pocket of *Ph-2/2HbO* respect to human Ngb. However the protein is more compressible in comparison with cytochrome *c* where  $\Delta\lambda = 1.5\text{nm}$ . After the pressure release from 600 MPa to 0.1 MPa, the protein exhibits the original form without any loss of heme, indicating a full reversibility. Other proteins such as the Hb chains, or cytochrome *P450*, did not show reversible changes *versus* pressure (Jung et al., 1995).

### 2.3. Conclusion

Unlike the large majority of bacteria, *PhTAC125* possesses three genes encoding 2/2 Hbs, two of which belong to the Group II, and one gene encoding flavoHb. Sequence alignment of *Ph-2/2HbO* with other 2/2 Hbs, indicates that the conserved residues HisF8, TyrB10, TrpG8, TyrCD1, IleE7, PheE11 are in the typical positions for Group II Hbs (Wittenberg et al., 2002; Vuletich and Lecomte, 2006). *Ph-2/2HbO* presents an unusual extension of 15 residues at the N terminus (pre-A helix). A similar situation had also been found in *M. tuberculosis* HbN (Group I) and appears to occur in many slow-growing species of mycobacterium, e.g. *M. bovis*, *M. avium*, *M. microti*, *M. marinum* (Lama et al., 2009) and *S. oneidensis* (Vuletich and Lecomte, 2006). The X-ray structure of *M. tuberculosis* HbN showed that pre-A motif, that does not significantly contribute to the structural integrity of the protein, confers a vital contribution in regulating the nitrogen-monoxide-dioxygenase activity of HbN (Lama et al., 2009).

At neutral pH, the heme population of ferric *Ph-2/2HbO* contains a mixture of 6cHS (aquo) and different 6cLS heme forms. The LS forms are all characterized by a non-protonated tyrosinate bound to the heme iron, which experience different degrees of H-bonding with neighbouring H-bond donors. Either TyrCD1-O<sup>-</sup> or TyrB10-O<sup>-</sup>, are suggested to be coordinated to the heme Fe(III) atom. The first residue is stabilized by TrpG8 and the second by both TrpG8 and TyrCD1. Clearly, TrpG8 has a very important role in the stabilization of the coordinated tyrosyl residues. This is the first example in which both TyrCD1 and TyrB10 are proposed to be the residues alternatively involved in heme hexacoordination by endogenous ligands.

In agreement with the coordination of Tyr residues thermal stability experiments show higher  $T_m$  at pH 8.5 respect to pH 7.6, probably linked to an enhanced hexacoordination at this pH. This condition seems to be the most stable in the protein as shown also in the reversibility of the process under pressure.

The reduced state, the hexacoordination, likely due to the tyrosyl residue, seems very weak and does not disturb the ligand-binding reaction. As for Ngb, potential *in vivo* interactions could influence the function via the strength of the six-coordination. A shift in the equilibrium between the two conformations could also provide a large change in the ligand affinities.

All of the results presented indicate that *Ph-2/2HbO* displays potential adaptive structural properties conferring higher flexibility to the protein that may facilitate the functioning in the cold providing greater freedom for the correct positioning of ligand(s), even at low temperatures. Alternatively, the multiple hexacoordinated states may account for multiple functions in the same molecule. Hexacoordinated Hbs are observed in unicellular eukaryotes (Wittenberg et al., 2002), plants (Watts et al., 2001), invertebrates (Dewilde et al., 2006) and in some tissues of higher vertebrates (De Santis et al., 2007; Pesce et al., 2004), but only a few cases have been examined and reported in the literature for bacterial 2/2Hbs (Visca et al., 2002; Razzera et al., 2008). The physiological role of these hexacoordinated Hbs is not well understood. Several roles have been suggested, such as that of an oxygen scavenger under hypoxic conditions (Burmester et al., 2000; 2002), of a terminal oxidase (Sowa et al., 1999), of an oxygen sensor (Hargrove et al., 2000; Kriegl et al., 2002) and of being involved in nitrogen monoxide metabolism (Smagghe et al., 2008). The discovery of hexacoordinated Ngb and Cygb in man and other vertebrates suggests that in different phylogenetically unrelated groups of organisms, these proteins may be endowed with a common function mainly linked to production of ROS and NO. The sixth ligand is usually provided by the imidazole side chain of a His E7, normally present at the distal site of the heme pocket and only few examples have been reported where TyrB10 has been found to act as the sixth ligand at the iron site in the ferrous (Razzera et al., 2008) and ferric states (Milani et al., 2005, Das et al., 1999). Indeed, the amino-acid sequence, the MD simulations and the spectroscopic data of *Ph-2/2HbO* indicate that the distal ligands of the LS ferric form can be either TyrCD1 or TyrB10. Hexacoordination may suggest a common physiological mechanism for protecting cells against oxidative chemistry in response to high oxygen concentration.

A further confirmation of involvement of *Ph-2/2HbO* in the protection against the stress induced by high oxygen concentration comes from recent results on genomic mutant strain, in which the *Ph-2/2HbO* encoding gene (*PSHAa0030*) was inactivated by insertional mutagenesis (Parrilli et al., 2010). Inactivation makes the mutant bacterial strain sensitive to high oxygen pressure, and to nitrosating agents, suggesting a potential role of the protein in oxidative and nitrosative stress. Disk diffusion assays display a hydrogen peroxidase sensitivity of *PhTAC125(-0030)* mutant in comparison with the wild-type suggesting that *Ph-2/2HbO* may be endowed also of peroxidase activity (Parrilli et al., 2010).

In conclusion *Ph-2/2HbO* displays multiple conformations and a partial hexacoordination, which are key factors that need to be considered when determining its functional properties.

Material in this chapter has been presented in the following publications:

“The peculiar heme pocket of the 2/2 hemoglobin of cold adapted *Pseudoalteromonas haloplanktis* TAC125” Howes BD, Giordano D, Boechi L, **Russo R**, Mucciacciaro S, Ciaccio C, Sinibaldi F, Fittipaldi M, Martí MA, Estrin DA, di Prisco G, Coletta M, Verde C, Smulevich G, (2011). *J Biol Inorg Biochem* **16**, 299-311

“Ligand- and proton-linked conformational changes of the ferrous 2/2 hemoglobin of *Pseudoalteromonas haloplanktis* TAC125” Giordano D, **Russo R**, Ciaccio C, Howes BD, di Prisco G, Marden MC, Hui Bon Hoa G, Smulevich G, Coletta M, Verde C (2011). *IUBMB Life*, **63**(7): 566-573.

### Collaborations

Raman Resonance and EPR data were collected by Dr. B. D. Howes and Prof. G. Smulevich from University of Florence.

Molecular dynamics simulations were provided by L. Boechi, M. A. Martì and D. A. Estrin from Universidad de Buenos Aires.

High pressure and Laser Flash Photolysis (LFP) experiments were performed at National Institute of Health and Medical Research (INSERM), Dept “Pathologie de la polymerisation des proteines substitut du sang- U779”, Le Kremlin Bicêtre, Paris, France, under the supervision of Dr. Gaston Hui Bon Hoa and Prof. Michael Marden. This research period was financially supported by a fellowship of the Transfer of Knowledge Grants-2009, funded by CAREX FP7 (Coordination Action for Research Activities on Life in Extreme Environments) and by a Short-Term Mobility 2010 scholarship of CNR.

## Chapter 3

### Neuroglobin from the brain and retina of Antarctic notothenioid fishes

#### Summary

To prevent cellular damage, adjustments in antioxidant defences are needed to maintain the steady-state concentration of reactive oxygen species. Polar marine species potentially experience increased oxidative pressure and metabolic costs associated with antioxidant defences.

Globins are probably involved in many disease-related oxidative-stress conditions. Ngb, recently discovered in vertebrates, is a monomeric globin expressed in retinal neurons and fibroblast-like cells: It displays the classical “3-on-3” vertebrate folding (Burmester et al., 2000; Vallone et al., 2004) and can bind oxygen and NO. Previous studies demonstrated that expression of Ngb increases in response of oxygen deprivation and that it is neuroprotective against hypoxic/ischemic brain injuries (Liu et al., 2011; Sun et al., 2001). Although a number of hypotheses (signal transduction, involvement in Alzheimer’s disease) have been proposed, its role is uncertain.

The finding that colourless-blooded Antarctic icefish (family Channichthyidae, suborder Notothenioidei) retain the Ngb gene despite the loss of Hb, and of Mb in most species, may have important implications in the physiology of the brain and may help the elucidation of Ngb function (Cheng et al., 2009a, b).

Red-blooded *Dissostichus mawsoni* and icefish *Chaenocephalus aceratus* Ngb cDNAs from retina and brain, respectively, were cloned, expressed in *Escherichia coli* and the recombinant proteins were purified. Their structural characterisation was performed by spectroscopic measurements, and dynamic simulation. Both fish Ngbs are hexacoordinated, but have some peculiarities in regions considered relevant for protein function, that differentiate them from mammalian counterparts (Boron et al., 2011). The peculiarities showed by these proteins are a new challenge for understanding the role of

Ngb in brain and retina physiology and for the interpretation of the structure/function relationship.

### **3.1 Materials and Methods**

#### **3.1.1. Cloning and sequencing of Ngbs cDNA**

To obtain notothenioid-specific primers for Ngb cDNA, a partial Ngb gene was PCR-amplified from genomic DNA of several Antarctic notothenioid species.

The Ngb cDNA of *C. aceratus* and *D. mawsoni* was subcloned in the expression vector pET3a as follows. A PCR was performed on the plasmid using the 5' primer (GCGCATATGGAGAAGCTGTCAGAGAAAG), containing an *Nde*I restriction site that covers the initiating Met codon of the globin gene, and the 3' primer (GCGGGATCCTCAGTCGGCCTTGTCTCCC), containing a *Bam*HI restriction site. The amplified product was cleaned and cut with *Nde*I and *Bam*HI and subsequently ligated into the equivalently cleaved expression vector pET3a.

*In silico* translation of the cDNA sequences provided the Ngb protein sequences used for homology modeling and were submitted to UniProt Knowledgebase under accession numbers P86880 (*C. aceratus*Ngb) and P86881 (*D. mawsoni*Ngb) respectively.

#### **3.1.2 Site-directed mutagenesis**

Three mutations were made on the cDNA of Ngb resulting in the replacement of Cys51(CD5), Cys57(D6), and Cys121(G15) with Ser using the QuikChange<sup>TM</sup> site-directed mutagenesis method (Stratagene). The mutants bearing the Cys→Ser substitutions are annotated in the chapter as *C. ace*Ngb and *D. maw*Ngb respectively.

#### **3.1.3 Expression and purification of Ngbs**

Recombinant expression plasmid was successfully transformed in the *Escherichia coli* strain BL21(DE3)pLysS (Invitrogen). The growth of the transformed bacteria and the overexpression of *C. ace*Ngb and *D. maw*Ngb were performed as described in (Dewilde et al., 2008). After expression, the cells were harvested and resuspended in lysis buffer [50 mM Tris-HCl pH 8.0, 5 mM EDTA, 1 mM phenylmethylsulfonyl fluoride (PMSF), 0.5

mM DTT]. The resuspended cells were exposed to three freeze-thaw steps and sonically disrupted. The extract was clarified by low- (10 min at 10,700 x g, 4°C) and high- (60 min at 105,000 x g, 4°C) speed centrifugation and fractionated with ammonium sulfate. The 40-60%-ammonium-sulfate pellet was dissolved in 5 mM sodium phosphate pH 6.9 and dialysed. A DEAE-Sepharose Fast-Flow column (Amersham Biosciences) was equilibrated with 50 mM Tris-HCl pH 8.5, 150 mM NaCl, 0.5 mM EDTA; bound Ngb was eluted with 5 mM sodium phosphate pH 6.9, 300 mM NaCl. The dialysed and concentrated material was loaded on a Hitrap<sup>TM</sup> DEAE fast flow (GE Healthcare) and the protein was eluted using a gradient (buffer A: 5 mM sodium phosphate pH 6.8; buffer B: 5 mM sodium phosphate pH 6.8, 1M NaCl; 25 min 100% A, linear gradient in 40 min to 60% B). The Ngb fractions were dialysed and the concentrated material was run on a Superdex<sup>TM</sup>75 column (1.5 x 100 cm) in gel-filtration buffer. A sample of both proteins was taken for analyses on SDS-PAGE.

### **3.1.4 Electronic absorption and RR spectroscopy**

Electronic absorption spectra were measured with a double-beam Cary 5 spectrophotometer (Varian, Palo Alto, CA) using a 5-mm NMR tube or a 1-cm cuvette, and a 600 nm/min scan rate.

*D. mawsoni* and *C. aceratus* Ngbs were isolated in the Fe (III) form. The Ngbs Fe (II) samples were prepared by adding sodium dithionite to Ngbs Fe (III) in 50 mM Tris-HCl at pH 7.6. All CO-heme complexes were prepared by degassing Fe (III) samples by flushing first with nitrogen and then with CO and reducing the heme by addition of sodium dithionite solution.

The spectra were recorded both before and after the RR measurements.

### **3.1.5 Multiple sequence alignment and structure modelling**

Antarctic fish Ngb sequences together to those of mammalian and other fish species, downloaded from Swiss-prot (Boeckmann et al., 2003), were aligned by the 3DCoffee programme (Notredame et al., 2000) following standard parameters. The model of hexacoordinated *D. mawsoni* Ngb was generated with the Modeller9 programme (Sali et al., 1993), using the human X-ray structure (pdb entry 1OJ6) as a template. The resulting structure was then used as starting point to generate the complete set of simulations.

### 3.1.6 Classical molecular dynamics

All simulations were performed at 300 K and pressures of 1 bar using Berendsen thermostat and barostat. The Amber99 force field (Cheatham et al., 1999) was used for all residues but not for the heme, whose parameters had been developed and thoroughly tested in previous work (Martì et al., 2006; Bidon-Chanal et al., 2006; Capece et al., 2009; Boechi et al., 2010). The simulations were performed with the PMEMD module of the AMBER9 package (Pearlman et al., 1995). Equilibration consisted of energy minimization of the initial structures, followed by slow heating up to 300 K (4 steps of 50 ps at 150, 200, 250, and 300 K). The structure was considered to be stabilised after a 20-ns MD run of the hexacoordinated *D. mawsoni* Ngb. From this equilibrated structure, the other structures where generated by deleting the His-Fe bond (pentacoordinated-state) and/or introducing the two point mutations that differentiate the Antarctic Ngbs, followed by the same 4-step equilibration protocol. For each structure, 80-ns long MD production runs were performed where the backbone root mean square distance does not exceed 1.9 Å with respect to the initial frame. Detailed information on procedure are reported in Boron et al., 2011.

### 3.1.7 Essential dynamics (ED)

Dynamical differences between *D. mawsoni* iNgb and *C. aceratus* Ngbs in their pentacoordinated state were studied using essential dynamics (ED) analysis. (Amadei et al., 1993). ED analysis was performed with the ptraj module of the AMBER suite and consisted in the diagonalisation of the covariance matrices of atomic positions along the trajectory. From them we obtained the eigenvectors that define the essential motions of the protein. To analyse the configurational space explored by the proteins, projections of their essential modes onto the last 50 ns of the MD trajectory were performed. Only backbone atoms were considered.

### 3.1.8 High pressure spectroscopy

Spectral measurements on *C. ace*Ngb and *D. maw*Ngb were made with 4-×10-mm quartz cuvettes using a Cary 50 spectrophotometer. Samples were 10 μM (on a heme basis) in 100mM Tris-HCl at pH 7.6. The ferrous deoxy sample was obtained by equilibration under nitrogen and adding an excess of sodium dithionite.

High pressure apparatus and experimental procedure are described in the previous chapter in the section 2.1.9.

## 3.2 Results and Discussion

### 3.2.1 Sequence alignment of mammal and fish Ngbs and structure modeling

When compared with mammalian counterparts in a multiple sequence alignment (Figure 3.1), fish Ngbs display some striking peculiarities.

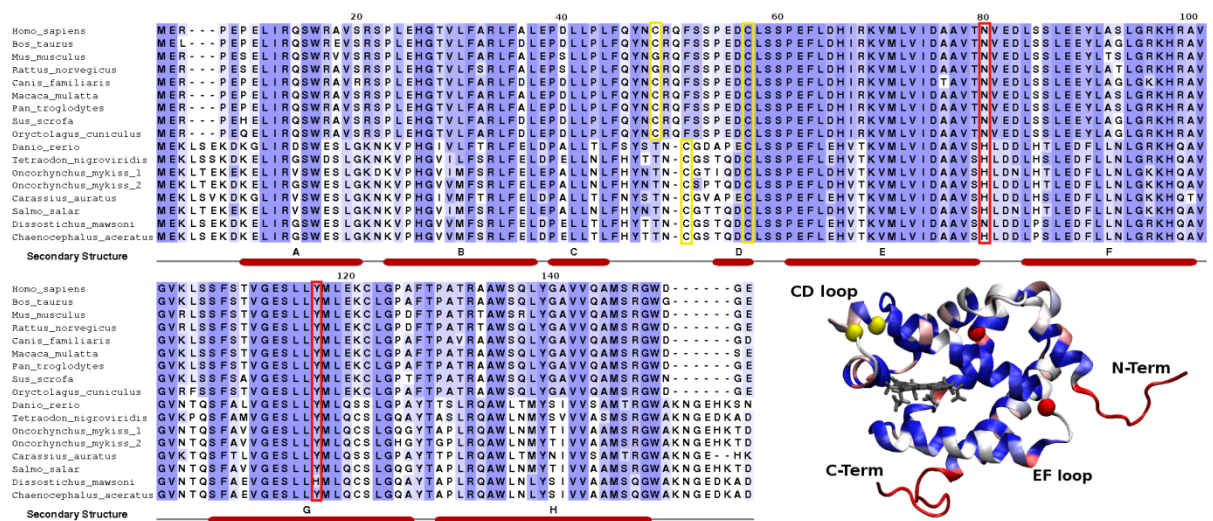


Figure 3.1: Sequence alignment of mammal and fish Ngbs. Residues are shaded according to sequence conservation. Relevant positions, e.g., mutations between Antarctic fish proteins or conserved Cys residues, are boxed. A scheme of the secondary structure found in human Ngb with helices A-H is below the alignment. Inset: Modeled structure of fish Ngb colored by sequence conservation with human Ngb. N- and C-terminal extensions are in red, residues 80 and 117 in red circles and Cys in yellow circles.

They all show three- and six-residue extensions, composed of charged residues, in their N and C termini, respectively. In the zebrafish *D. rerio*, the N-terminal region was demonstrated to be implied in cell-penetrating capability (Watanabe and Wakasugi, 2008).

Crucial for this activity appears to be the presence of three Lys residues at the N terminus (Watanabe and Wakasugi, 2010), which can be used as a building block to create novel cell-membrane penetrating folded proteins (Watanabe and Wakasugi, 2011). In Antarctic fish Ngbs the extra residues protrude toward the EF loop causing potentially relevant interactions, as discussed below. The alignment also shows a gap (position 51) in the CD region, which may be involved in aiding heme coordination and shows correlated motions with the so-called His-gate (Nadra et al., 2008, Anselmi et al., 2007).

In fish Ngbs, the average Cys-Cys distance in the CD loop is several-Å shorter than in the human protein, in which Cys46-CD7 and Cys55-D5 are known to form a disulfide bridge and appear to be involved in redox-state sensing (Fuchs et al., 2004, Nadra et al., 2008, Astudillo et al., 2010). Thus, although the residues are in the reduced form, they remain very close to each other during the time scale of the simulations (data not shown). This short distance allows the protein to adopt a conformation, which is more suitable to form a disulfide bridge than in human Ngb, where a more important rearrangement is needed. Disulfide formation in human Ngb has been experimentally shown to decrease protein flexibility (Ishikawa et al., 2007), particularly, in the CD region. This in turn enhances oxygen affinity about 10-fold by stabilizing the pentacoordinated state, making the protein adopt a conformation prone to bind exogenous ligands (Hamdane et al., 2003, Nadra et al., 2008).

Apart from these differences, conservation is high in the rest of the Ngb sequences between mammals and fish, with Antarctic fish Ngbs about 55% identical to human, as well as between members of each group. Notably, sequence conservation is significantly higher among mammals than among fish species as previously described (Awenius et al., 2001).

### **3.2.2 Molecular Dynamics (MDS): differences between *D. mawsoni* and *C. aceratus* Ngbs**

Sequence analysis of *D. mawsoni* and *C. aceratus* Ngbs shows that the only differences between these proteins are at positions 80 and 117, the icefish *C. aceratus* having His and Tyr and red-blooded *D. mawsoni* Asn and His, respectively.

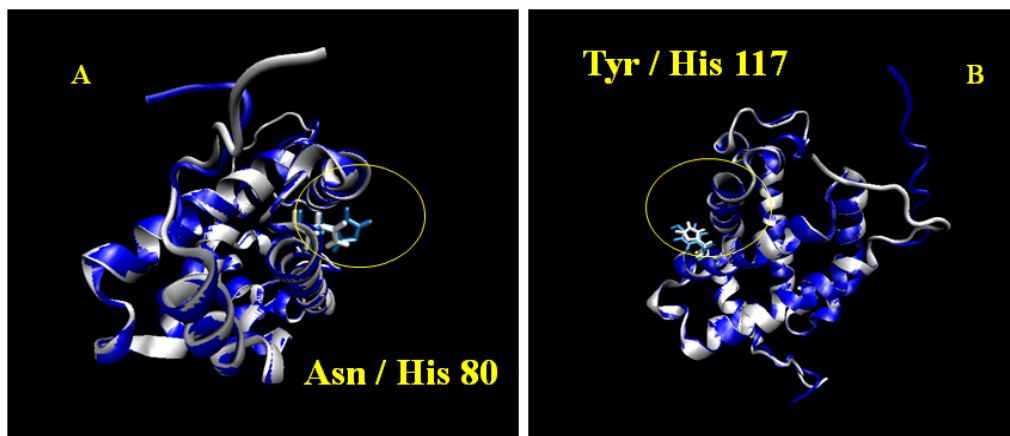


Figure 3.2: View of constructed model of *D. mawsoni* (in grey) and *C. aceratus* (in blue) Ngbs, showing residues 80 (A) and residues 117 (B).

As shown in the Figure 3.2 both residues are located away from the heme, exposed to the solvent and distant from the dynamically relevant CD corner. MDS shows that the two proteins differ in loop structure and flexibility (Figures 3.3 A and 3.3 B).

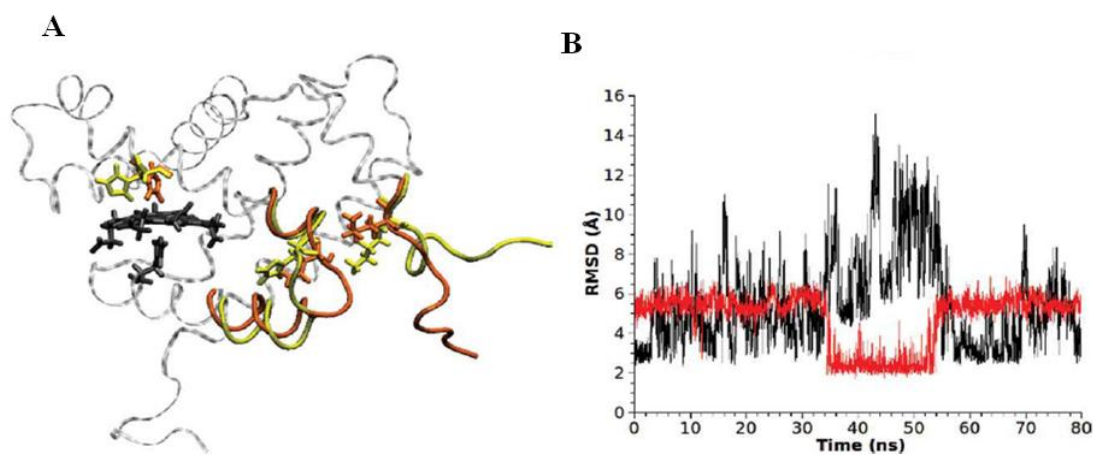


Figure 3.3: A) Backbone representation of *D. mawsoni* Ngb (orange) and *C. aceratus* Ngb (yellow), highlighting the changes in EF-loop conformation and its interaction with the N-terminal region in colored sticks. B) Time trace for two selected distances in *D. mawsoni* Ngb (Asn80:O-Asp83:H in red; Lys9:HD2-Asn80:O in black) illustrating the interaction between the EF loop and N termini.

Moreover, different interactions are established between the EF loop and its N-terminal region of *D. mawsoni* Ngb and the corresponding regions of *C. aceratus* Ngb. This interaction, absent in human Ngb, helps to stabilize an incipient  $\alpha$ -helical structure in

the N-terminal region. In *D. mawsoni* Ngb, formation of the H bond between Lys9:HD2 and Asn80:O involves disruption of that between Asn80:O and Asp83:H, and vice versa (Figures 3.3 A and 3.3 B). In contrast, in *C. aceratus* Ngb, the EF loop and N-terminal interaction is present but is less specific and fluctuates contacting different residues. A static view of the conformation adopted by the proteins can be obtained by comparing average structures (Figure 3.3). Furthermore, this difference is not only static but also affects the dynamics of the protein (Figure 3.4), where root mean square fluctuations (RMSF) and ED projections show a remarkably higher flexibility in the *C. aceratus* EF loop, whereas in *D. mawsoni* Ngb, the overall flexibility is spread along different loops (Figures 3.4 A and 3.4 B). In the distal site, the main consequence is that His is able to open in a “His-gate”-like movement only in *C. aceratus* Ngb in the time frame under consideration. Notably, the His opening modifies the CD-region conformation and flexibility. RMSD values for this region (data not shown) show that *C. aceratus* Ngb is significantly different in the 5c state after His opening. Furthermore, RMSF values and ED analysis show that CD region becomes less flexible (Figures 3.4 A and 3.4 B). All these conformational and dynamical differences are dictated by the replacement of Asn 80 by His, as they can be reverted by mutating these residues. This experiment consisted in converting *C. aceratus* Ngb to *D. mawsoni* Ngb at position 80 after the conformational change that the loop suffer was acquired and stabilized. Within 5 ns after reversion, the EF loop readopted the conformation consistent with the corresponding residue at position 80. This implies that the single mutation modifies EF loop conformation and dynamics and propagates, through the heme-coordinating His, up to the CD region in the opposite part of the protein.

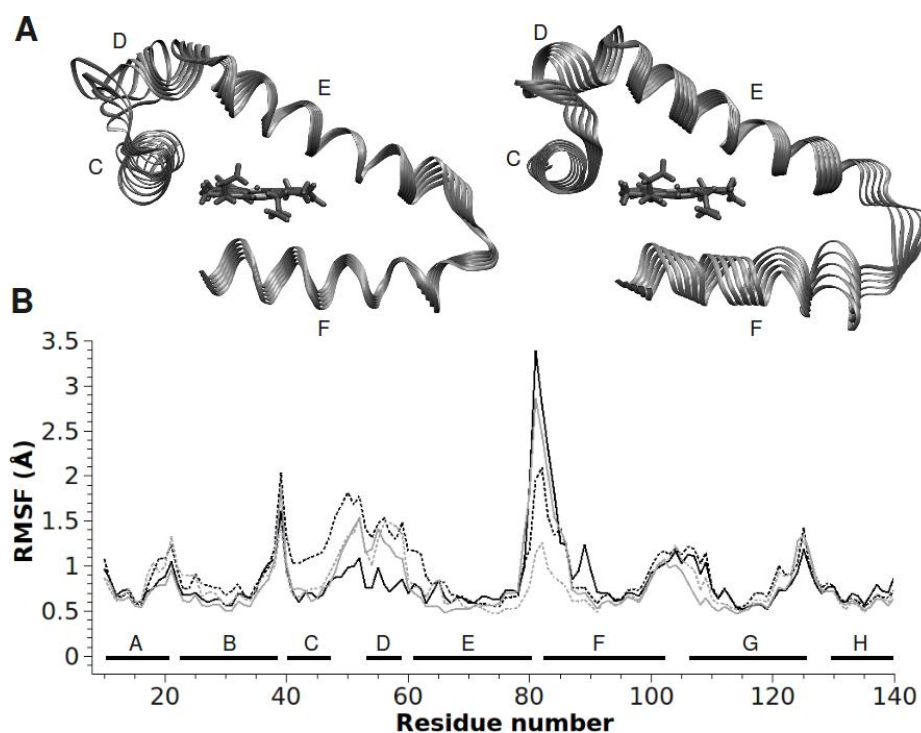


Figure 3.4: Dynamical differences between fish Ngbs. A) Projection of the normal mode with highest amplitude in *D. mawsoni* Ngb (left) and *C. aceratus* Ngb (right). B) Root mean square fluctuations along the last 50 ns in *D. mawsoni* Ngb (dotted line) and *C. aceratus* Ngb (continuous line). Pentacoordinated species are in black and hexacoordinated species in gray.

The UV–vis spectra of ferric and ferrous form of both *C. aceratus* and *D. mawsoni* Ngbs proteins are typical of hexacoordinated state (see section 3.2.4) in analogy with other Ngbs (Dewilde et al., 2001). Preliminary results obtained using multiple steered molecular dynamics and the Jarzynski equality as in Nadra et al. 2008, show that the hexacoordinated-state is preferred in both Ngbs by about  $6 \text{ kcal mol}^{-1}$ . Unexpectedly, but consistent with the Cys-Cys distance, the overall conformation of the pentacoordinated state for both proteins is much more similar to the oxidised state of human Ngb (with the Cys residues forming an intramolecular disulfide bond). A single amino-acid replacement appears sufficient to induce much higher flexibility in *C. aceratus* Ngb in comparison with red-blooded *D. mawsoni* Ngb. MDS analysis suggests that the Asn→His substitution in position 80 produces changes in the conformational and dynamical features in the icefish protein. In the distal domain, the main consequence is the “His-gate”-like movement, causing rearrangement of the CD region that correlates with EF-loop movements. These differences are dictated by this replacement, because they disappear by reversal mutation. No effect is associated to the Tyr→His replacement at position 117.

Adaptive changes appear restricted to regions that influence conformational mobility. This finding has important implications for rates of protein evolutionary adaptation, because a single substitution is sufficient for potential functional shifts. As these sequence differences are far from the active site or previously described relevant regions for protein function, in principle, we did not expect these mutations to be very functionally relevant. To our surprise, this appeared to be true only for the Tyr117→His mutation but not for His80→Asn. The latter is located in the EF loop, which connects the helices, which include heme-coordinated His, and is very close to the N-terminal extension. Although this loop is less variable in sequence than the CD region, it displays flexibility (Nadra et al., 2008, Anselmi et al., 2007) and may indeed have a relevant role in heme coordination.

### **3.2.3 Expression and purification of Antarctic fish Ngbs**

As Ngb is present in the cell at very low concentration, it is impossible to obtain the proteins from the tissues. For the biochemical characterization of the proteins and functional studies, the cloning and the expression were the best alternative approach.

The Antarctic fish Ngbs triple mutant (CysCD5Ser, CysD6Ser and CysG15Ser) were used in this expression cloning for a preliminary characterization and for crystallization trials. The Cys residues were mutated to prevent aggregation and formation of insoluble precipitates that were already observed in human Ngb.

Ngbs mutant, *C. acer*Ngb and *D. maw*Ngb, were cloned and over-expressed in *E. coli*, then purified by ion-exchange and gel-filtration chromatographies (not shown). Analysis of the fractions by 15% SDS-PAGE in presence of  $\beta$ -mercaptoethanol reveals a major monomeric Ngb band for both recombinant proteins, at an apparent MW of  $\sim 17,000$  Da as expected. In the leading edge of the peak, a band with an apparent MW of  $\sim 32,000$  Da, together with minor non-globin impurities can be seen (Figure 3.5). The top fractions and trailing edge of the peak contain the purest Ngbs. The bands of MW  $\sim 32,000$  Da may represent a dimeric Ngb fraction, as already shown for human Ngb (Dewilde et al., 2008)

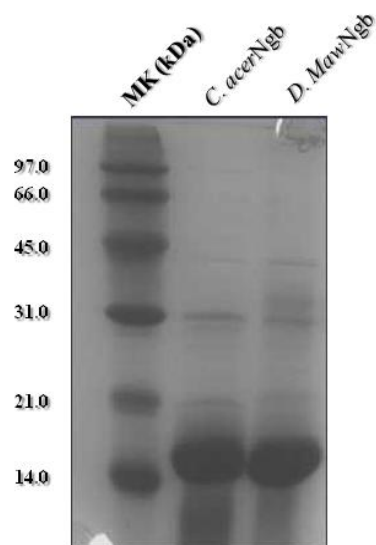


Figure 3.5: Purity of the obtained Ngbs preparation by 15% SDS-PAGE

The final purity and the accurate molecular weight of both Ngbs were checked by mass spectrometry (data not shown).

### 3.2.4 UV-visible absorption and RR spectroscopy

The UV-visible absorption spectra of ferric and ferrous *C. acerNgb* are typical of hexacoordinated low-spin hemes (6cLS) (Figure 3.6, panels A and B).

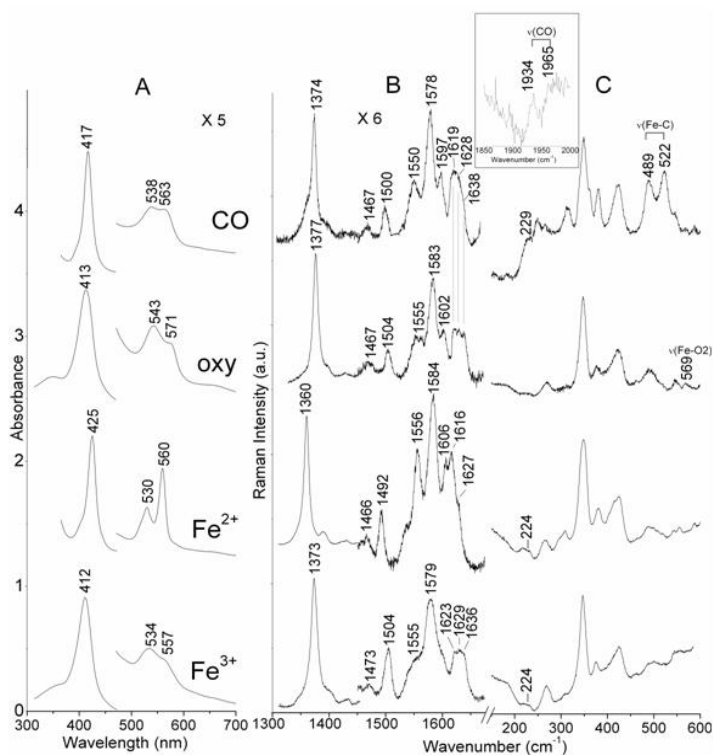


Figure 3.6: UV-Vis (A) and RR spectra of Fe (III), Fe (II), oxy, and CO complex of *C. acerNgb* in the high (B) and low (C) frequency regions. Spectra have been shifted along the ordinate axis to allow better visualisation. In the inset: RR spectra of the CO adducts in the  $\nu(\text{CO})$  stretching region, average of 3 spectra with 3600-sec integration time, and  $3.3 \text{ cm}^{-1}$  spectral resolution.

In particular, the UV-vis spectra of the ferric (Soret band at 411 nm,  $\beta$  and  $\alpha$  bands at 534 and 557 nm, respectively) and deoxy (Soret band at 425 nm,  $\beta$  and  $\alpha$  bands at 530 and 560 nm, respectively) ferrous forms, unequivocally indicated the presence of a bis-His heme-iron coordination, in analogy with other Ngbs (Dewilde et al., 2001). The UV-vis and RR spectra of *D. mawNgb* and *C. acerNgb* were almost identical (1-nm shift of the Soret band in the ferric form). The spectroscopic data of *D. mawNgb* are shown in the Figure 3.7.

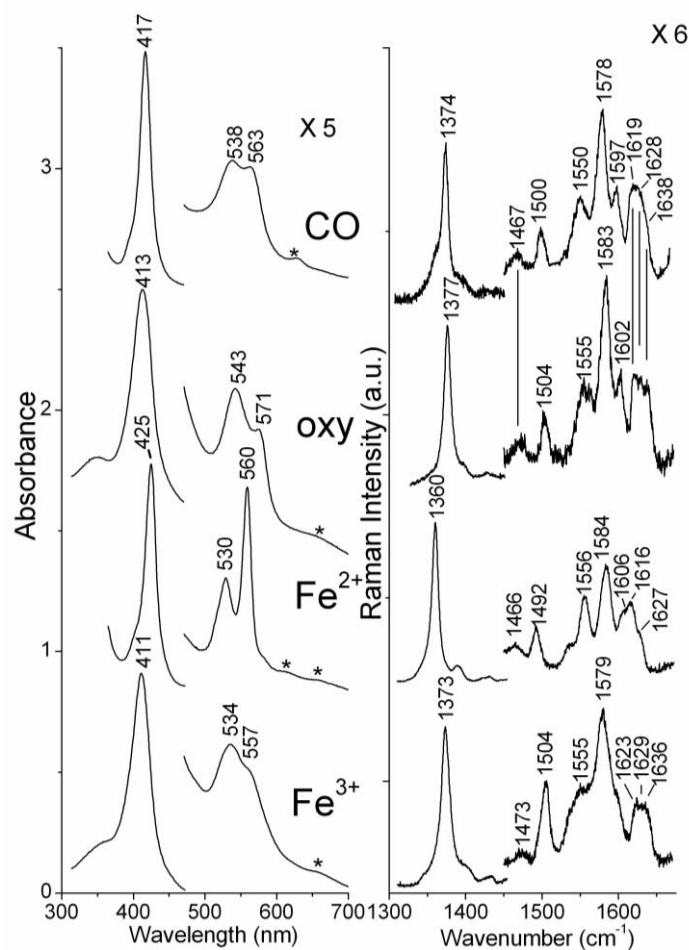


Figure 3.7: UV-vis (left) and RR (right) spectra of Fe (III), Fe (II), oxy, and CO complex of *D. mawNgb*, pH 7.6, in 20 mM TRIS-HCl. The asterisks in the spectrum of the CO adduct indicate impurities. Experimental conditions are identical to those of *C. acerNgb* (see Figure 3.6).

Upon addition of oxygen and CO to the ferrous form, the diatomic ligands replaced distal His and gave rise to the oxy (Soret at 413 nm,  $\beta$  and  $\alpha$  at 543 e 571 nm, respectively) and CO (Soret at 417 nm,  $\beta$  and  $\alpha$  at 538 e 563 nm) adducts (Dewilde et al., 2001, Couture et al., 2001, Uno et al., 2004). The oxygenated proteins remained stable over the time scale necessary to acquire absorption and RR spectra.

### 3.2.5 High pressure effects on ferrous *C. acerNgb*

High pressure experiments on ferrous *C. acerNgb* were performed to investigate pressure effects on the hexacoordinated protein.

Pressure has no effects on the ferrous spectra or structural transition of *C. acerNgb*, as indicated by the progressive increase of the absorbance (Figure 3.8), and with only a

slight effect on the epsilon. The same results were observed in human Ngb, which is completely hexacoordinated at 1 atm (Hamdane et al., 2005). Under pressure, the ferrous state of *C. acer*Ngb remains hexacoordinated (Figure 3.8) with a ratio between  $\alpha$  and  $\beta$  peaks equal to 1.79 at 0.1MPa and 1.68 at 600MPa. These values are similar to the ferrous hexacoordinated cytochrome *c* ( $r = 1.715$ ), cytochrome *b5* ( $r = 1.86$ ) and human Ngb, the most highly hexacoordinated heme protein in its ferrous state ( $r = 2.159$ ). This would suggest that the binding of the sixth ligand to the iron is weaker in *C. acer*Ngb than in humanNgb.

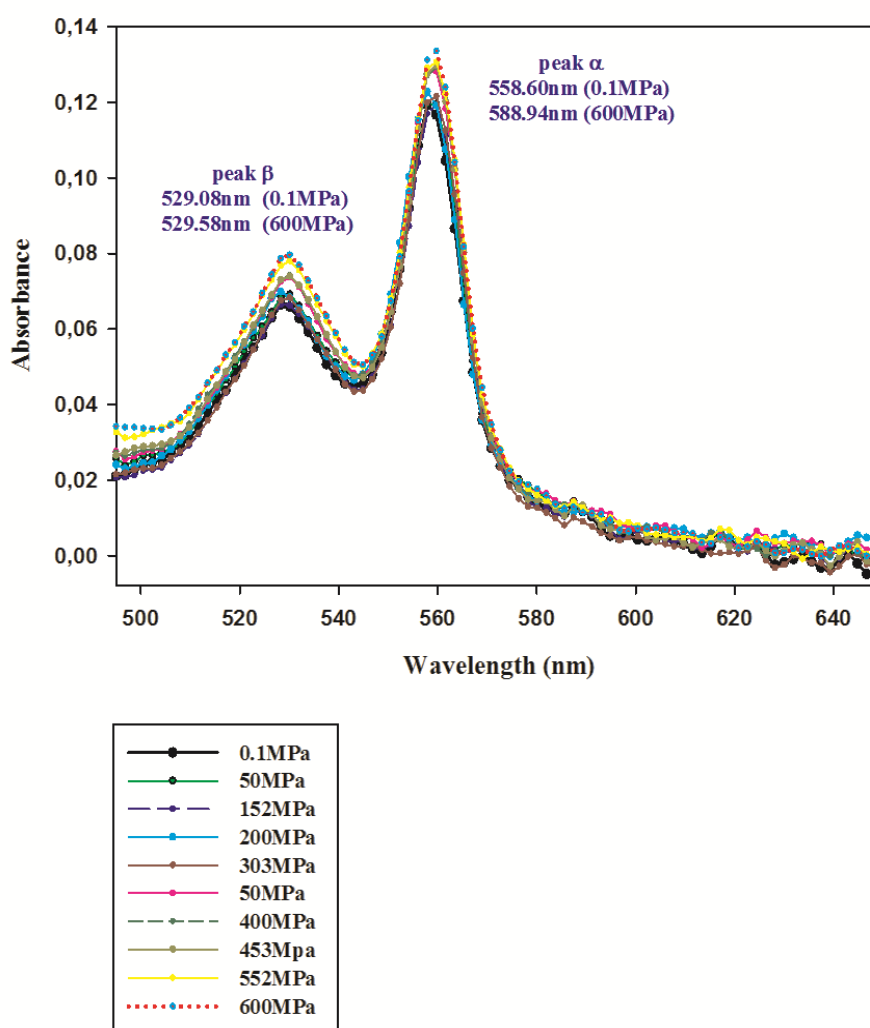


Figure 3.8: Absorption spectra in the visible region *versus* pressure for ferrous deoxy *C. acer*Ngb

In the Soret spectra of ferrous *C. acer*Ngb (Figure 3.9) pressure has an effect only on the amplitude.

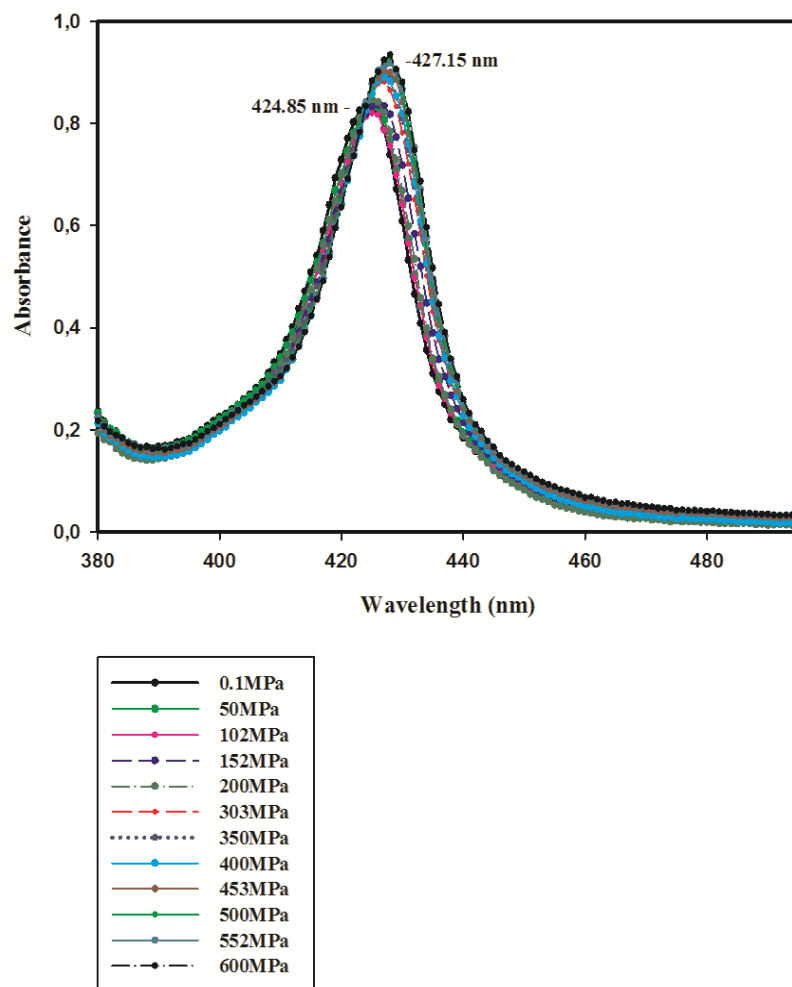


Figure 3.9: Absorption spectra in the Soret *versus* pressure for ferrous deoxy *C. acer*Ngb

Pressure induces a red shift of the Soret band as it happens in most hemoproteins, such as human Ngb, cytochrome *c* and cytochrome *b5*. The  $\Delta\lambda$  shift is only 2.3 nm as compared to human Ngb which exhibits a red shift of 6.14 nm. Thus, we can conclude that *C. acer*Ngb is probably less compressible than human Ngb (probably endowed with less cavities in the heme pocket) but more compressible than cytochrome *c* ( $\Delta\lambda = 1.5\text{nm}$ ). The ferrous *C. acer*Ngb remains hexacoordinated presumably through the sixth internal ligand, with a partial reversibility at pH 7.6.

### 3.3 Conclusion

Isolation and environmental history have shaped a unique Antarctic marine biota. Many fish groups became extinct because of the constraints of increasingly cold and icy conditions, and the cold adapted and antifreeze-protected notothenioids emerged as the predominant teleost taxon (Eastman, 1993, 2005). In the modern notothenioid family Channichthyidae, mutational events led to remnant  $\alpha$  globin genes and complete deletion of the genes encoding the  $\beta$  globins of Hb (Cocca et al., 1995; Near et al., 2006). Six of the 16 species of icefish species including *C. aceratus* also fail to produce cardiac Mb (Sidell and O'Brien, 2006). The lack of these globins is closely correlated with compensatory changes in the icefish anatomy, e.g. larger heart and gills and blood volume (Egginton et al., 2002). Because oxygen transport and supply must be achieved without Hb and Mb, icefishes are an excellent system to investigate possible enhancement of other factors to compensate for the loss of these essential hemoprotein functions. Icefishes serve as the natural knock-outs for functional studies of oxygen-binding hemoproteins and the correlated nitrogen-monoxide-oxygenase activity. Current research in mammals suggests that nearly all icefish hallmark traits are linked to high levels of NO (Beers et al., 2010).

The UV-vis spectra of ferric and ferrous form of both *C. acer*Ngb and *D. maw*Ngb mutant proteins are typical of hexacoordinated-state (Giordano et al., in preparation) in analogy with other Ngbs (Dewilde et al., 2001), and pressure effects show no significant differences with human Ngb because both proteins are already hexacoordinated at atmospheric pressure.

This is the first structural study on such proteins from Antarctic fish. When compared to mammals, fish Ngbs display some striking peculiarities in regions considered relevant for protein function: (i) Ngbs of Antarctic and temperate fish have extensions of charged amino-acid residues at the N and C termini (ii) Antarctic and temperate fish Ngbs are shorter by one residue in the CD region, involved in heme coordination and in the "His-gate". The shorter loop approaches the two Cys that form the disulfide bridge in human Ngb so that the Cys-Cys distance is several-Å shorter.

A single amino-acid replacement appears sufficient to induce much higher flexibility in *C. aceratus* Ngb in comparison with red-blooded *D. mawsoni* Ngb. MDS analysis suggests that the Asn→His substitution in position 80 produces changes in the

conformational and dynamical features in the icefish protein. In the distal domain, the main consequence is the “His-gate”-like movement, causing rearrangement of the CD region that correlates with EF-loop movements. These differences are dictated by this replacement, because they disappear by reversal mutation.

These results support the general hypothesis that alterations in protein conformational mobility can happen through one/few substitutions, providing insights into the evolutionary rates at which adaptive change may occur (Fields and Somero, 1998; Somero, 2010). They also indicate that a small change in the primary structure, namely a short term response, may be very efficient as such for generating an adaptive response to a challenge. The icefish is an exceptional oxygen-transport system to take into account. In the icefish brain and retina, the delivery of oxygen by diffusion could be highly insufficient. Thus, Ngb may also have the task to fulfill the role of a classical oxygen carrier, and the conformational flexibility of Ngb can be included into the suite of anatomical and physiological compensations that icefish had to engineer as a result of the evolutionary loss of hemoglobin and Mb.

Material in this chapter has been presented in the following publication:

“Structure and dynamics of Antarctic fish neuroglobin assessed by computer simulations”  
Boron, I., **Russo R**, Boechi L, Cheng C-H C, di Prisco G, Estrin D A, Verde C, Nadra AD,  
(2011) *IUBMB life* **633**, 206-213.

### **Collaborations**

Cloning, sequencing process and expression were performed in collaboration with Prof. C.-H. C. Cheng from University of Illinois and with Prof. Silvia Dewilde from University of Antwerp.

Raman Resonance data were collected by Dott. Francesco Nicoletti and Prof. G. Smulevich from University of Florence.

Molecular dynamics simulations were provided by L. Boechi, I. Boron and D. A. Estrin from Universidad de Buenos Aires.

High pressure experiments, were performed at National Institute of Health and Medical Research (INSERM), Dept “Pathologie de la polymerisation des proteines substitut du sang- U779”, Le Kremlin Bicêtre, Paris, France, under the supervision of Dr. Gaston Hui Bon Hoa and Prof. Michael Marden. The visit was financially supported by a Short-Term Mobility 2010 scholarship of CNR.

## REFERENCES

- Ahmad F, Yadav S, Taneja S (1992). Determining stability of proteins from guanidinium chloride transition curves. *Biochem J* **287**: 481-485.
- Alden RG, Satterlee JD, Mintorovitch J, Constantinidis I, Ondrias MR, Swanson BI (1989). The effects of high pressure upon ligated and deoxyhemoglobins and myoglobin. An optical spectroscopic study. *J Biol Chem* **264**: 1933-1940.
- Alontaga AY, Rodriguez JC, Schönbrunn E, Becker A, Funke T, Yukl ET, Hayashi T, Stobaugh J, Moënné-Loccoz P, Rivera M (2009). Structural characterization of the hemophore HasAp from *Pseudomonas aeruginosa*: NMR spectroscopy reveals protein-protein interactions between Holo-HasAp and hemoglobin. *Biochemistry* **48**: 96-109.
- Amadei A, Linssen AB, Berendsen HJ (1993) Essential dynamics of proteins. *Proteins* **17**: 412-425.
- Anselmi M, Brunori M, Vallone B, Di Nola A (2007). Molecular dynamics simulation of deoxy and carboxy murine neuroglobin in water. *Biophys J* **93**: 434-441.
- Antonini E and Brunori M (1971). Hemoglobin and myoglobin in their reactions with ligands. North-Holland Publishing Co., Amsterdam.
- Aronson RB, Blake DB (2001). Global climate change and the origin of modern benthic communities in Antarctica. *Am Zool* **41**: 27-39.
- Astudillo L, Bernad S, Derrien V, Sebban P, Miksovská J (2010) Probing the role of the internal disulfide bond in regulating conformational dynamics in neuroglobin. *Biophys J* **99**: L16-L18.
- Awenius C, Hankeln T, Burmester T (2001). Neuroglobins from the zebrafish *Danio rerio* and the pufferfish *Tetraodon nigroviridis*. *Biochem Biophys Res Commun* **287**: 418-421.

Barouch LA, Harrison RW, Skaf MW, Rosas GO, Cappola TP, Kobeissi ZA, Hobai IA, Lemmon CA, Burnett AL, O'Rourke B, Rodriguez ER, Huang PL, Lima JA, Berkowitz DE, Hare JM (2002). Nitric oxide regulates the heart by spatial confinement of nitric oxide synthase isoforms. *Nature* **416**: 337-339.

Beers JM, Borley KA, Sidell BD (2010). Relationship among circulating hemoglobin, nitric oxide synthase activities and angiogenic poise in red- and white-blooded Antarctic notothenioid fishes. *Comp Biochem Physiol A Mol Integr Physiol* **156**: 422-429.

Bidon-Chanal A, Marti MA, Crespo A, Milani M, Orozco M, Bolognesi M, Luque FJ, Estrin DA (2006). Ligand-induced dynamical regulation of NO conversion in *Mycobacterium tuberculosis* truncated hemoglobin-N. *Proteins* **64**: 457-464.

Boechi L, Mañez PA, Luque FJ, Marti MA, Estrin DA (2010). Unraveling the molecular basis for ligand binding in truncated hemoglobins: the trHbO *Bacillus subtilis* case. *Proteins* **78**, 962-70.

Boeckmann B, Bairoch A, Apweiler R, Blatter M-C, Estreicher A, Gasteiger E, Martin MJ, Michoud K, O'Donovan C, Phan I, Pilbout S, Schneider M (2003). The Swiss-Prot Protein Knowledgebase and its supplement TrEMBL in 2003. *Nucleic Acids Res* **31**: 365-370.

Boffi A, Wittenberg JB, Chiancone E (1997). Circular dichroism spectroscopy of Lucina I hemoglobin. *FEBS Lett* **411**: 335-338.

Bonamore A, Ilari A, Giangiacomo L, Bellelli A, Morea V, Boffi A (2005). A novel thermostable hemoglobin from the actinobacterium *Thermobifida fusca*. *FEBS J* **272**: 4189-4201.

Boron I, Russo R, Boechi L, Cheng C-HC, di Prisco G, Estrin DA, Verde C, Nadra AD, (2011). Structure and dynamics of Antarctic fish neuroglobin assessed by computer simulations. *IUBMB life* **633**: 206-213.

Brittain T, Yosaatmadja Y, Henty K (2008). The interaction of human neuroglobin with hydrogen sulphide. *IUBMB Life* **60**: 135-138.

Brittain T, Skommer J, Raychaudhuri S, Birch N (2010) An Antiapoptotic Neuroprotective Role for Neuroglobin. *Int. J. Mol. Sci.* **11**: 2306-2321.

Brunori M, Giuffrè A, Nienhaus K, Nienhaus GU, Scandurra FM, Vallone B (2005). Neuroglobin, nitric oxide, and oxygen: functional pathways and conformational changes. *Proc Natl Acad Sci USA* **102**: 8483-8488.

Brunori M and Vallone B (2007). Neuroglobin, seven years after. *Cell Mol Life Sci* **64**: 1259-1268.

Burmester T, Weich B, Reinhardt S, Hankeln T (2000). A vertebrate globin expressed in the brain. *Nature* **407**: 520-523.

Burmester T, Ebner B, Weich B, Hankeln T (2002). Cytoglobin: a novel globin type ubiquitously expressed in vertebrate tissues. *Mol Biol Evol* **19**: 416-421.

Caillet-Saguy C, Turano P, Piccioli M, Lukat-Rodgers GS, Czjzek M, Guigliarelli B, Izadi-Pruneyre N, Rodgers KR, Delepierre M, Lecroisey A (2008). Deciphering the structural role of histidine 83 for heme binding in hemophore HasA. *J Biol Chem* **283**: 5960-5970.

Capece L, Martì MA, Bidon-Chanal A, Nadra A, Luque FJ, Estrin DA (2009). High pressure reveals structural determinants for globin hexacoordination: neuroglobin and myoglobin cases. *Proteins* **75**: 885-94.

Carver TE, Brantley RE Jr, Singleton EW, Arduini RM, Quillin ML, Phillips GN Jr, Olson JS (1992). A novel site-directed mutant of myoglobin with an unusually high O<sub>2</sub> affinity and low autooxidation rate. *J Biol Chem* **267**, 14443-14450.

Cheatham TE III, Cieplak P, Kollman PA (1999). A modified version of the Cornell et al. force field with improved sugar pucker phases and helical repeat. *J Biomol Struct Dyn* **16**: 845-862.

- Chen Z, Cheng C-HC, Zhang J, Cao L, Chen L, Zhou L, Jin Y, Ye H, Deng C, Dai Z, Xu Q, Hu P, Sun S, Shen Y, Chen L (2008). Transcriptomic and genomic evolution under constant cold in Antarctic notothenioid fish. *Proc Natl Acad Sci USA* **105**: 12944-12949.
- Cheng C-HC and DeVries AL (1991). The role of antifreeze glycopeptides and peptides in the freezing avoidance of cold water fishes. In: di Prisco G (Ed.), *Life Under Extreme Conditions*. Springer-Verlag, Berlin-Heidelberg, pp. 1-14.
- Cheng C-HC, Chen L, Near T, Jin Y (2003). Functional antifreeze glycoprotein genes in temperate-water New Zealand nototheniid fish infer an Antarctic evolutionary origin. *Mol Biol Evol* **20**: 1897-1908.
- Cheng C-HC, Cziko PA, Evans CW (2006). Non-hepatic origin of notothenioid antifreeze reveals pancreatic synthesis as common mechanism in polar fish freezing avoidance. *Proc Natl Acad Sci USA* **103**: 10491-10496.
- Cheng C-HC and Detrich III HW (2007). Molecular ecophysiology of Antarctic notothenioid fishes. *Philos Trans R Soc Lond B Biol Sci* **362**: 2215-2232.
- Cheng C-HC, di Prisco G, Verde C (2009a). Cold-adapted Antarctic fish: the discovery of neuroglobin in the dominant suborder Notothenioidei. *Gene* **433**: 100-101.
- Cheng C-HC, di Prisco G, Verde C (2009b). The “icefish paradox”. Which is the task of neuroglobin in Antarctic haemoglobin-less icefish? *IUBMB Life* **61**: 184-188.
- Clarke A (1983). Life in cold water: the physiological ecology of polar marine ectotherms. *Oceanography and Marine Biology Annual Reviews* **21**: 341-453.
- Clarke A (1993). Temperature and extinction in the sea: a physiologist’s view. *Paleobiology* **19**: 499-518.
- Clarke A and Crame JA (1992). The Southern Ocean benthic fauna and climate change: a historical perspective. *Philos Trans R Soc Lond B Biol Sci* **338**: 299-309.

Cocca E, Ratnayake-Lecamwasam M, Parker SK, Camardella L, Ciaramella M, di Prisco G, Detrich III HW (1995). Genomic remnants of  $\alpha$ -globin genes in the hemoglobinless Antarctic icefishes. *Proc Natl Acad Sci USA* **92**: 1817-1821.

Cossins A and Berenbrink M (2008). Physiology: myoglobin's new clothes. *Nature* **454**: 416-417.

Couture M, Chamberland H, St-Pierre B, Lafontaine J, Guertin M (1994). Nuclear genes encoding chloroplast hemoglobins in the unicellular green alga *Chlamydomonas eugametos*. *Mol Gen Genet* **243**: 185-197.

Couture M, Yeh SR, Wittenberg BA, Wittenberg JB, Ouellet Y, Rousseau DL, Guertin M (1999). A cooperative oxygen-binding hemoglobin from *Mycobacterium tuberculosis*. *Proc Natl Acad Sci USA* **96**: 11223-11228.

Couture M, Das TK, Lee HC, Peisach J, Rousseau DL, Wittenberg BA, Wittenberg JB, Guertin M (1999). *Chlamydomonas* chloroplast ferrous hemoglobin. *J Biol Chem* **274**: 6898-6910.

Couture M, Burmester T, Hankeln T, Rousseau DL (2001). The heme environment of mouse neuroglobin. Evidence for the presence of two conformations of the heme pocket. *J Biol Chem* **276**: 36377-36382.

D'Amico S, Collins T, Marx JC, Feller G, Gerday C (2006). Psychrophilic microorganisms: challenges for life. *EMBO Rep* **7**: 385-389.

Das TK, Couture M, Lee HC, Peisach J, Rousseau DL, Wittenberg BA, Wittenberg JB, Guertin M (1999). Identification of the ligands to the ferric heme of *Chlamydomonas* chloroplast hemoglobin: evidence for ligation of tyrosine-63 (B10) to the heme. *Biochemistry* **38**: 15360-15368.

Deming JW and Eicken H (2005). *Life in Ice*. Cambridge Univ Press, Cambridge.

Deming JW and Junge K (2005). *Bergey's Manual of Systematic Bacteriology*, vol. 2. Bergey's Manual Trust, East Lansing.

de Sanctis D, Dewilde S, Pesce A, Moens L, Ascenzi P, Hankeln T, Burmester T, Bolognesi M (2004). Crystal structure of cytoglobin: the fourth globin type discovered in man displays heme hexa-coordination. *J Mol Biol* **336**: 917-927.

de Sanctis D, Dewilde S, Vornrhein C, Pesce A, Moens L, Ascenzi P, Hankeln T, Burmester T, Ponassi M, Nardini M, Bolognesi M (2005). Bishistidyl heme hexacoordination, a key structural property in *Drosophila melanogaster* hemoglobin. *J Biol Chem* **280**: 27222-27229.

De Sanctis G, Petrella G, Ciaccio C, Feis A, Smulevich G, Coletta M (2007). A comparative study on axial coordination and ligand binding in ferric mini myoglobin and horse heart myoglobin. *Biophys J* **93**: 2135–2142

Detrich III HW, Johnson KA, Marchese-Ragona SP (1989). Polymerization of Antarctic fish tubulins at low temperatures: energetic aspects. *Biochemistry* **28**: 10085-10093.

Detrich III HW, Parker SK; Williams RCJ, Nogales E, Downing KH (2000). Cold adaptation of microtubule assembly and dynamics. Structural interpretation of primary sequence changes present in the alpha- and beta-tubulins of Antarctic fishes. *J Biol Chem* **275**: 37038-37040.

DeVries AL (1988). The role of glycopeptide and peptide antifreeze in the freezing avoidance of Antarctic fishes. *Comput Biochem Physiol B* **90**: 611-621.

Dewilde S, Kiger L, Burmester T, Hankeln T, Baudin-Creuzat V, Aerts T, Marden MC, Caubergs R, Moens L (2001). Biochemical characterization and ligand-binding properties of neuroglobin, a novel member of the globin family. *J Biol Chem* **276**: 38949-38955.

Dewilde S, Ebner B, Vinck E, Gilany K, Hankeln T, Burmester T, Kreiling J, Reinisch C, Vanfleteren JR, Kiger L, Marden MC, Hundahl C, Fago A, Van Doorslaer S, Moens L

- (2006). The nerve hemoglobin of the bivalve mollusc *Spisula solidissima*: molecular cloning, ligand binding studies, and phylogenetic analysis. *J Biol Chem* **281**: 5364-5372.
- Dewilde S, Mees K, Kiger L, Lechauve C, Marden MC, Pesce A, Bolognesi M, Moens L (2008). Expression, purification, and crystallization of neuro- and cytoglobin. *Meth Enzymol* **436**: 341-357.
- Dickerson RE and Geis I (1983). Hemoglobin : structure, function, evolution, and pathology. Benjamin/Cummings Pub Co, Menlo Park Calif.
- Di Fraia R, Wilquet V, Ciardiello MA, Carratore V, Antignani A, Camardella L, Glansdorff N, Di Prisco G (2000). NADP<sup>+</sup>-dependent glutamate dehydrogenase in the Antarctic psychrotolerant bacterium *Psychrobacter* sp. TAD1. *Eur J Biochem* **267**: 121-131.
- di Prisco G, Cocca E, Parker SK, Detrich III HW (2002). Tracking the evolutionary loss of hemoglobin expression by the white-blooded Antarctic icefishes. *Gene* **295**: 185-191.
- Droghetti E, Nicoletti FP, Bonamore A, Boechi L, Mañez PA, Estrin DA, Boffi A, Smulevich G, Feis A (2010). Heme pocket structural properties of a bacterial truncated hemoglobin from *Thermobifida fusca*. *Biochemistry* **49**: 10394-10402.
- Eastman JT (1993). Antarctic fish biology. Evolution in a unique environment. Academic Press, San Diego.
- Eastman JT (2005). The nature of the diversity of Antarctic fishes. *Polar Biol* **28**: 93-107.
- Eastman JT and MCCune AR (2000). Fishes on the Antarctic shelf: evolution of a marine species flock? *J Fish Biol* **57**: 84-102.
- Egginton S, Skilbeck C, Hoofd L, Calvo J, Johnston IA (2002). Peripheral oxygen transport in skeletal muscle of Antarctic and sub-Antarctic notothenioid fish. *J Exp Biol* **205**: 769-779.

Fago A, Mathews AJ, Moens L, Dewilde S, Brittain T (2006). The reaction of neuroglobin with potential redox protein partners cytochrome *b*(5) and cytochrome *c*. *FEBS Lett*, **580**(20): 4884-4888.

Falzone CJ, Christie Vu B, Scott NL, Lecomte JT (2002). The solution structure of the recombinant hemoglobin from the cyanobacterium *Synechocystis* sp. PCC 6803 in its hemichrome state. *J Mol Biol* **324**: 1015-1029.

Feis A, Lapini A, Catacchio B, Brogioni S, Foggi P, Chiancone E, Boffi A, Smulevich G (2008). Unusually strong H-bonding to the heme ligand and fast geminate recombination dynamics of the carbon monoxide complex of *Bacillus subtilis* truncated hemoglobin. *Biochemistry* **47**(3): 902-910.

Feller G and Gerday C (2003). Psychrophilic enzymes: hot topics in cold adaptation. *Nature Rev Microbiol* **1**: 200-208.

Feng L, Zhou S, Gu L, Gell D, Mackay J, Weiss M, Gow A, Shi Y (2005). Structure of oxidized  $\alpha$ -haemoglobin bound to AHSP reveals a protective mechanism for heme. *Nature* **435**: 697-701.

Fields PA and Somero GN (1998). Hot spots in cold adaptation: localized increases in conformational flexibility in lactate dehydrogenase A4 orthologs of Antarctic notothenioid fishes. *Proc Natl Acad Sci USA* **95**: 11476-11481.

Fields PA and Houseman DE (2004). Decreases in activation energy and substrate affinity in cold-adapted A4-LDH dehydrogenase: evidence from the Antarctic notothenioid fish *Chaenocephalus aceratus*. *Mol Biol Evol* **21**: 2246-2255.

Flögel U, Gödecke A, Klotz LO, Schrader J (2004). Role of myoglobin in the antioxidant defense of the heart. *FASEB J* **18**(10): 1156-1158.

Fuchs C, Heib V, Kiger L, Haberkamp M, Roesner A, Schmidt M, Hamdane D, Marden MC, Hankeln T, Burmester T (2004). Zebrafish reveals different and conserved features of

vertebrate neuroglobin gene structure, expression pattern, and ligand binding. *J Biol Chem* **279**: 24116-24122.

Gardner PR, Gardner AM, Martin LA, Salzman AL (1998). Nitric oxide dioxygenase: an enzymic function for flavohemoglobin. *Proc Natl Acad Sci USA* **95**: 10378-10383.

Georlette D, Blaise V, Collins T, D'Amico S, Gratia E, Hoyoux A, Marx JC, Sonan G, Feller G, Gerday C (2004). Some like it cold: biocatalysis at low temperatures. *FEMS Microbiol Rev* **28**: 25-42.

Gibson QH and Carey FG (1977). Effect of hydrostatic pressure on spectra of heme compounds. *J Biol Chem* **252**: 4098-4101.

Giordano D, Parrilli E, Dettai A, Russo R, Barbiero G, Marino G, Lecointre G, di Prisco G, Tutino ML, Verde C (2007). The truncated hemoglobins in the Antarctic psychrophilic bacterium *Pseudoalteromonas haloplanktis* TAC125. *Gene* **398**: 69-77.

Giordano D, Russo R, Ciaccio C, Howes BD, di Prisco G, Marden MC, Hui Bon Hoa G, Smulevich G, Coletta M, Verde C (2011). Ligand- and proton-linked conformational changes of the ferrous 2/2 hemoglobin of *Pseudoalteromonas haloplanktis* TAC125. *IUBMB Life* **63**(7): 566-573.

Greenberg DA, Jin K, Khan AA (2008). Neuroglobin: an endogenous neuroprotectant. *Curr Opin Pharmacol* **8**: 20-24.

Greenfield Norma J (1999). Applications of circular dichroism in protein and peptide analysis. *TrAC* **18**: 236-244.

Grove TJ, Hendrickson JW, Sidell BD (2004). Two species of Antarctic icefishes (genus *Champscephalus*) share a common genetic lesion leading to the loss of myoglobin expression. *Polar Biol* **27**: 579-585.

Hamdane D, Kiger L, Dewilde S, Green BN, Pesce A, Uzan J, Burmester T, Hankeln T, Bolognesi M, Moens L, Marden MC (2003). The redox state of the cell regulates the ligand binding affinity of human neuroglobin and cytoglobin. *J Biol Chem* **278**: 51713-51721.

Hamdane D, Kiger L, Hoa GH, Dewilde S, Uzan J, Burmester T, Hankeln T, Moens L, Marden MC (2005). High pressure enhances hexacoordination in neuroglobin and other globins. *J Biol Chem* **280**: 36809-36814.

Hardison R (1998). Hemoglobins from bacteria to man: evolution of different patterns of gene expression. *J Exp Biol* **201**: 1099-1117.

Hargrove MS, Brucker EA, Stec B, Sarath G, Arredondo-Peter R, Klucas RV, Olson JS, Phillips GN (2000). Crystal structure of a nonsymbiotic plant hemoglobin. *Structure* **8**: 1005-1014.

Harrison SC and Blout ER (1965). Reversible conformational changes of myoglobin and apomyoglobin. *J Biol Chem* **240**: 299-303.

Hendgen-Cotta UB, Merx MW, Shiva S, Schmitz J, Becher S, Klare JP, Steinhoff HJ, Goedecke A, Schrader J, Gladwin MT, Kelm M, Rassaf T (2008). Nitrite reductase activity of myoglobin regulates respiration and cellular viability in myocardial ischemia-reperfusion injury. *Proc Natl Acad Sci USA* **105**: 10256-10261.

Herold S, Fago A, Weber RE, Dewilde S, Moens L (2004). Reactivity studies of the Fe(III) and Fe(II)NO forms of human neuroglobin reveal a potential role against oxidative stress. *J Biol Chem* **279**(22): 22841-22847.

Hochachka PW and Somero GN (2002). Biochemical Adaptation. Mechanism and Process in Physiological Evolution. Oxford University Press, New York.

Hofmann GE, Buckley BA, Airaksinen S, Keen JE, Somero GN (2000). Heat-shock protein expression is absent in the Antarctic fish *Trematomus bernacchii* (family Nototheniidae). *J Exper Biol* **203**: 2331-2339.

Hofmann GE, Lund SG, Place SP, Whitmer AC (2005). Some like it hot, some like it cold: the heat shock response is found in New Zealand but not Antarctic notothenioid fishes. *J Exper Marin Biol Ecol* **316**: 79-89.

Holland HD (2006) The oxygenation of the atmosphere and oceans. *Philos Trans R Soc* **B361**: 903-916.

Hori H and Kitagawa T (1980). Iron-ligand stretching band in the resonance Raman spectra of ferrous iron porphyrin derivatives. Importance as a probe band for quaternary structure of hemoglobin. *J Am Chem Soc* **102**: 3608-3613.

Howes BD, Giordano D, Boechi L, Russo R, Mucciacciaro S, Ciaccio C, Sinibaldi F, Fittipaldi M, Martí MA, Estrin DA, di Prisco G, Coletta M, Verde C, Smulevich G (2011). The peculiar heme pocket of the 2/2 hemoglobin of cold adapted *Pseudoalteromonas haloplanktis* TAC125. *J Biol Inorg Chem* **16**: 299-311.

Hoy JA, Kundu S, Trent III JT, Ramaswamy S, Hargrove MS (2004). The crystal structure of *Synechocystis* hemoglobin with a covalent heme linkage. *J Biol Chem* **279**: 16535-16542.

Hughson FM and Baldwin RL (1989). Use of site-directed mutagenesis to destabilize native apomyoglobin relative to folding intermediates. *Biochemistry* **28**: 4415-4422.

Hughson FM, Barrick D, Baldwin RL (1991). Probing the stability of a partly folded apomyoglobin intermediate by site-directed mutagenesis. *Biochemistry* **30**: 4113-4118.

Hvitved AN, Trent JT III, Premer SA, Hargrove MS (2001). Ligand binding and hexacoordination in *synechocystis* hemoglobin. *J Biol Chem* **276**: 34714-34721.

Ishikawa H, Kim S, Kwak K, Wakasugi K, Fayer MD (2007). Disulfide bond influence on protein structural dynamics probed with 2D-IR vibrational echo spectroscopy. *Proc Natl Acad Sci USA* **104**: 19309-19314.

Johns GC and Somero GN (2004). Evolutionary convergence in adaptation of proteins to temperature: A4-lactate dehydrogenases of Pacific damselfishes (*Chromis spp.*). *Molecular Biology and Evolution* **21**: 314-320.

Johnston IA, Calvo J, Guderley H, Fernandez D, Palmer L (1998). Latitudinal variation in the abundance and oxidative capacities of muscle mitochondria in perciform fishes. *Journal of Experimental Biology* **201**: 1-12.

Johnston IA, Fernández DA, Calvo J, Vieira VL, North AW, Abercromby M, Garland Jr T (2003). Reduction in muscle fibre number during adaptive radiation of notothenioid fishes: a phylogenetic perspective. *J Exp Biol* **206**: 2595-2609.

Jung C, Hui Bon Hoa G, Davydov D, Gill E, Heremans K (1995). Compressibility of the heme pocket of substrate analogue complexes of cytochrome P-450cam-CO. The effect of hydrostatic pressure on the Soret band. *Eur J Biochem* **233**: 600-606.

Kendrew JC, Bodo G, Dintzis HM, Parrish RG, Wyckoff H, Phillips DC (1958). A three-dimensional model of the myoglobin molecule obtained by X-ray analysis. *Nature* **181**: 662-666.

Khan AA, Wang YM, Sun YJ, Mao XO, Xie L, Miles E, Graboski J, Chen S, Ellerby LM, Jin KL, Greenberg DA (2006). Neuroglobin-overexpressing transgenic mice are resistant to cerebral and myocardial ischemia. *Proc Nat Acad Sci USA* **103**(47): 17944-17948.

Kraus DW and Wittenberg JB (1990). Hemoglobins of the *Lucina pectinata*/bacteria symbiosis. I. Molecular properties, kinetics and equilibria of reactions with ligands. *J Biol Chem* **265**: 16043-16053.

Kraus DW, Wittenberg JB, Lu JF, Peisach J (1990). Hemoglobins of the *Lucina pectinata*/bacteria symbiosis. II. An electron paramagnetic resonance and optical spectral study of the ferric proteins. *J Biol Chem* **265**: 16054-16059.

Krembs C, Eicken H, Junge K, Deming JW (2002). High concentrations of exopolymeric substances in Arctic winter sea ice: implications for the polar ocean carbon cycle and cryoprotection of diatoms. *Deep Sea Res A* **49**: 2163-2181.

Kriegel JM, Bhattacharyya AJ, Nienhaus K, Deng P, Minkow O, Nienhaus GU (2002). Ligand binding and protein dynamics in neuroglobin. *Proc Natl Acad Sci USA* **99**: 7992-7997.

Lakowicz JR (1983). Principles of Fluorescence Spectroscopy. Plenum Press, New York.

Lama A, Pawaria S, Bidon-Chanal A, Anand A, Gelpí JL, Arya S, Martí M, Estrin DA, Luque FJ, Dikshit KL (2009). Role of Pre-A motif in nitric oxide scavenging by truncated hemoglobin, HbN, of Mycobacterium tuberculosis. *J Biol Chem* **284**: 14457-14468.

Liu J, Yu Z, Guo S, Lee SR, Xing C, Zhang C, Gao Y, Nicholls DG, Lo EH, Wang X (2011). Effects of neuroglobin overexpression on mitochondrial function and oxidative stress following hypoxia/reoxygenation in cultured neurons. *J Neurosci Res* **87**: 164-170.

Martí MA, Crespo A, Capece L, Boechi L, Bikiel DE, Scherlis DA, Estrin DA (2006). Dioxygen affinity in heme proteins investigated by computer simulation. *J Inorg Biochem* **100**: 761-770.

Martí MA, Capece L, Bidon-Chanal A, Crespo A, Guallar V, Luque FJ, Estrin DA (2008). Nitric Oxide Reactivity with Globins as Investigated Through Computer Simulation. *Methods Enzymol* **437**: 477-498.

Marx JC, Blaise V, Collins T, D'Amico S, Delille D, Gratia E, Hoyoux A, Huston AL, Sonan G, Feller G, Gerday C (2004). A perspective on cold enzymes: current knowledge and frequently asked questions. *Cell Mol Biol (Noisy-le-grand)* **50**: 643-655.

Médigue C, Krin E, Pascal G, Barbe V, Bernsel A, Bertin PN, Cheung F, Cruveiller S, D'Amico S, Duilio A, Fang G, Feller G, Ho C, Mangenot S, Marino G, Nilsson J, Parrilli E, Rocha EP, Rouy Z, Sekowska A, Tutino ML, Vallenet D, von Heijne G, Danchin A

(2005). Coping with cold: the genome of the versatile marine Antarctica bacterium *Pseudoalteromonas haloplanktis* TAC125. *Genome Res* **15**: 1325-1335.

Mentré P and Hui Bon Hoa G (2001). Effects of high hydrostatic pressures on living cells: a consequence of the properties of macromolecules and macromolecule-associated water. *Int Rev Cytology* **201**: 1-84.

Merlino A, Verde C, di Prisco G, Mazzarella L, Vergara A (2008). Reduction of ferric hemoglobin from *Trematomus bernacchii* in a partial bis-histidyl state produces a deoxy coordination even when encapsulated into the crystal phase. *Spectroscopy: Biomed Appl* **22** (2-3): 143-152.

Methe BA, Nelson KE, Deming JW, Momen B, Melamud E, Zhang X, Moulton J, Madupu R, Nelson WC, Dodson RJ, Brinkac LM, Daugherty SC, Durkin AS, DeBoy RT, Kolonay JF, Sullivan SA, Zhou L, Davidsen TM, Wu M, Huston AL, Lewis M, Weaver B, Weidman JF, Khouri H, Utterback TR, Feldblyum TV, Fraser CM (2005). The psychrophilic lifestyle as revealed by the genome sequence of *Colwellia psychrerythraea* 34H through genomic and proteomic analyses. *Proc Natl Acad Sci USA* **102**: 10913-10918.

Milani M, Pesce A, Ouellet Y, Ascenzi P, Guertin M, Bolognesi M (2001). *Mycobacterium tuberculosis* hemoglobin N displays a protein tunnel suited for O<sub>2</sub> diffusion to the heme. *Embo J* **20**: 3902-3909.

Milani M, Pesce A, Ouellet H, Guertin M, Bolognesi M (2003a) Truncated hemoglobins and nitric oxide action. *IUBMB Life* **55**: 623-627.

Milani M, Savard PY, Ouellet H, Ascenzi P, Guertin M, Bolognesi M (2003b). A TyrCD1/TrpG8 hydrogen bond network and a TyrB10TyrCD1 covalent link shape the heme distal site of *Mycobacterium tuberculosis* hemoglobin O. *Proc Natl Acad Sci USA* **100**: 5766-5771.

Milani M, Ouellet Y, Ouellet H, Guertin M, Boffi A, Antonini G, Bocedi A, Mattu M, Bolognesi M, Ascenzi P (2004a). Cyanide binding to truncated hemoglobins: a crystallographic and kinetic study. *Biochemistry* **43**: 5213-5221.

Milani, M., Pesce, A., Ouellet, Y., Dewilde, S., Friedman, J., Ascenzi, P., Guertin, M., and Bolognesi, M. (2004b). Heme-ligand tunneling in group I truncated hemoglobins. *J Biol Chem* **279**: 21520-21525.

Milani M, Pesce A, Nardini M, Ouellet H, Ouellet Y, Dewilde S, Bocedi A, Ascenzi P, Guertin M, Moens L, Friedman JM, Wittenberg JB, Bolognesi M (2005). Structural bases for heme binding and diatomic ligand recognition in truncated hemoglobins. *J Inorg Biochem* **99**: 97-109.

Minning DM, Gow AJ, Bonaventura J, Braun R, Dewhirst M, Goldberg DE, Stamler JS, (1999). Ascaris haemoglobin is a nitric oxide-activated “deoxygenase”. *Nature* **401**: 497-502.

Miranda JLL, Maillett DH, Soman J, Olson JS (2005). Thermoglobin, oxygen-avid hemoglobin in a bacterial hyperthermophile. *J Biol Chem* **280**: 36754-36761.

Nadra AD, Marti MA, Pesce A, Bolognesi M, Estrin DA (2008). Exploring the molecular basis of heme hexacoordination in human neuroglobin. *Proteins* **71**: 695-705.

Nardini M, Pesce A, Milani M, Bolognesi M (2007). Protein fold and structure in the truncated (2/2) globin family. *Gene* **398**: 2-11.

Near T (2004). Estimating divergence times of notothenioid fishes using a fossil-calibrated molecular clock. *Antarctic Science* **16**: 37-44.

Near TJ, Parker SW, Detrich HW III (2006). A Genomic fossil reveals key steps in hemoglobin loss by the Antarctic icefishes. *Mol Biol Evol* **23**: 2008-2016.

Nicoletti FP, Comandini A, Bonamore A, Boechi L, Boubeta F, Feis A, Smulevich G, Boffi A (2010). Sulfide binding properties of truncated hemoglobins. *Biochemistry* **49**: 2269-2278.

Nicoletti FP, Thompson M, Howes BD, Franzen S, Smulevich G (2010). New insights into the role of distal histidine flexibility in ligand stabilization of dehaloperoxidase-hemoglobin from *Amphitrite ornata*. *Biochemistry* **49**: 1903-1912.

Notredame C, Higgins DG, Heringa J (2000). T-Coffee: a novel method for fast and accurate multiple sequence alignment. *J Mol Biol* **302**: 205-217.

Ogunmola GB, Kauzmann W, and Zipp A (1976). Volume changes in binding of ligands to methemoglobin and metmyoglobin. *Proc Natl Acad Sci USA* **73**: 4271-4273.

Ouellet H, Ouellet Y, Richard C, Labarre M, Wittenberg B, Wittenberg J, Guertin M (2002). Truncated hemoglobin HbN protects *Mycobacterium bovis* from nitric oxide. *Proc Natl Acad Sci USA* **99**: 5902-5907.

Ouellet H, Juszczak L, Dantsker D, Samuni U, Ouellet YH, Savard PY, Wittenberg JB, Wittenberg BA, Friedman JM, Guertin M (2003). Reactions of *Mycobacterium tuberculosis* truncated hemoglobin O with ligands reveal a novel ligand-inclusive hydrogen bond network. *Biochemistry* **42**: 5764-5774.

Parrilli E, Giuliani M, Giordano D, Russo R, Marino G, Verde C, Tutino ML (2010). The role of a 2-on-2 haemoglobin in oxidative and nitrosative stress resistance of Antarctic *Pseudoalteromonas haloplanktis* TAC125. *Biochimie* **92**: 1003-1009.

Pearlman DA, Case DA, Caldwell JW, Ross WS, Cheatham TE, Debolt S, Ferguson D, Seibel G, Kollman P (1995). AMBER, a package of computer programs for applying molecular mechanics, normal mode analysis, molecular dynamics and free energy calculations to simulate the structural and energetic properties of molecules. *Comput Phys Commun* **91**: 1-41.

Peck LS and Conway LZ (2000). The myth of metabolic cold adaptation: oxygen consumption in stenothermal Antarctic bivalves. In: Harper EM, Taylor JD, Crame JA (Eds), *The Evolutionary Biology of the Bivalvia*. Special publications, London, UK, Geological Society, vol. 177, pp 441-445.

Peck LS, Pörtner HO, Hardewig I (2002). Metabolic demand, oxygen supply and critical temperatures in the Antarctic bivalve, *Laternula elliptica*. *Physiol Biochem Zool* **75**: 123-133.

Perutz MF (1983) Species adaptation in a protein molecule. *Mol Biol Evol* **1**: 1-28.

Perutz MF, Kendrew JC, Watson HC (1965). Structure and function of haemoglobin. II. Some relations between polypeptide chain configuration and amino acid sequence. *J Mol Biol* **13**: 669-678.

Pesce A, Couture M, Dewilde S, Guertin M, Yamauchi K, Ascenzi P, Moens L, Bolognesi M (2000). A novel two-over-two  $\alpha$ -helical sandwich fold is characteristic of the truncated hemoglobin family. *EMBO J* **19**: 2424-2434.

Pesce A, Dewilde S, Nardini M, Moens L, Ascenzi P, Hankeln T, Burmester T, Bolognesi M (2003). Human brain neuroglobin structure reveals a distinct mode of controlling oxygen affinity. *Structure* **11**: 1087-1095.

Pesce A, Dewilde S, Nardini M, Moens L, Ascenzi P, Hankeln T, Burmester T, Bolognesi M. The human brain hexacoordinated neuroglobin three-dimensional structure. (2004). *Micron* **35**: 63-65.

Petersen MG, Dewilde S, Fago A (2008). Reactions of ferrous neuroglobin and cytoglobin with nitrite under anaerobic conditions. *J Inorg Biochem* **102**(9): 1777-1782.

Place SP, Zippay ML, Hofmann GE (2004). Constitutive roles for inducible genes: evidence for the alteration in expression of the inducible hsp70 gene in Antarctic notothenioid species. *Am J Physiol Regul Integr Comp Physiol* **287**: R429-R436.

Place SP and Hofmann GE (2005). Comparison of Hsc70 orthologues from polar and temperate notothenioid fishes: differences in the prevention of aggregation and refolding of denatured proteins. *Am J Physiol Regul Integr Comp Physiol* **288**: R1195-R1202.

Podrabsky JE and Somero GN (2006). Inducible heat tolerance in Antarctic notothenioid fishes. *Polar Biol* **30**: 39-43.

Poole RK (2005). Nitric oxide and nitrosative stress tolerance in bacteria. *Biochem Soc Trans* **33**: 176-180.

Pörtner HO (2006). Climate dependent evolution of Antarctic ectotherms: an integrative analysis. *Deep Sea Res II* **53** 1071-1104.

Pörtner HO, Peck LS, Zielinski S, Conway LZ (1999). Intracellular pH and energy metabolism in the highly stenothermal Antarctic bivalve *Limopsis marionensis* as a function of ambient temperature. *Polar Biol* **22**: 17-30.

Pörtner HO, Van Dijk PLM, Hardewig I, Sommer A (2000). Levels of metabolic cold adaptation: tradeoffs in eurythermal and stenothermal ectotherms. In: Davison V and Williams CW (Eds), *Antarctic Ecosystems: Models for a Wider Understanding*. Caxton Press, Christchurch, New Zealand, pp 109-122.

Rabus R, Ruepp A, Frickey T, Rattei T, Fartmann B, Stark M, Bauer M, Zibat A, Lombardot T, Becker I, Amann J, Gellner K, Teeling H, Leuschner WD, Glockner FO, Lupas AN, Amann R, Klenk HP (2004). The genome of *Desulfotalea psychrophila*, a sulfate-reducing bacterium from permanently cold Arctic sediments. *Environ Microbiol* **6**: 887-902.

Raychaudhuri S, Skommer J, Henty K, Birch N, Brittain T (2010). Neuroglobin protects nerve cells from apoptosis by inhibiting the intrinsic pathway of cell death. *Apoptosis* **15(4)**: 401-411.

Razzera G, Vernal J, Baruh D, Serpa VI, Tavares C, Lara F, Souza EM, Pedrosa FO, Almeida FC, Terenzi H, Valente AP (2008). Spectroscopic characterization of a truncated

hemoglobin from the nitrogen-fixing bacterium *Herbaspirillum seropedicae*. *J Biol Inorg Chem* **13**: 1085-1096.

Redeker V, Frankfurter A, Parker SK, Rossier J, Detrich III HW (2004). Posttranslational modification of brain tubulins from the Antarctic Fish *Notothenia coriiceps*: reduced Cterminal glutamylation correlates with efficient microtubule assembly at low temperature. *Biochemistry* **43**: 12265-12274.

Riccio A, Vitagliano L, di Prisco G, Zagari A, Mazzarella L (2002). The crystal structure of a tetrameric hemoglobin in a partial hemichrome state. *Proc Natl Acad Sci USA* **99**: 9801-9806.

Rifkind JM, Abugo O, Levy A, Heim JM (1994). Detection, formation, and relevance of hemichrome and hemochrome. *Methods Enzymol* **231**: 449-480.

Robinson VL, Smith BB, Arnone A (2003). A pH-dependent aquomet-to-hemichrome transition in crystalline horse methemoglobin. *Biochemistry* **42**: 10113-10125.

Rodrigues D, Ivanova N, He Z, Huebner M, Zhou J, Tiedje M (2008). Architecture of thermal adaptation in an *Exiguobacterium sibiricum* strain isolated from 3 million year old permafrost: a genome and transcriptome approach. *BMC Gen* **9**: 547.

Roesner A, Fuchs C, Hankeln T, Burmester T (2005). A globin gene of ancient evolutionary origin in lower vertebrates: evidence for two distinct globin families in animals. *Mol Biol Evol* **22**: 12-20.

Roesner A, Mitz SA, Hankeln T, Burmester T (2008). Globins and hypoxia adaptation in the goldfish, *Carassius auratus*. *FEBS J*, **275**(14): 3633-3643.

Römisch K, Collie N, Soto N, Logue J, Lindsay M, Scheper W, Cheng C-HC (2003). Protein translocation across the endoplasmic reticulum membrane in cold-adapted organisms. *Journal of Cell Science* **116**: 2875-2883.

- Russell NJ (2000). Toward a molecular understanding of cold activity of enzymes from psychrophiles. *Extremophiles* **4**: 83-90.
- Ruud JT (1954). Vertebrates without erythrocytes and blood pigment. *Nature* **173**: 848-850.
- Sali A and Blundell TL (1993). Comparative protein modelling by satisfaction of spatial restraints. *J Mol Biol* **234**: 779-815.
- Samuni U, Dantsker D, Ray A, Wittenberg JB, Wittenberg BA, Dewilde S, Moens L, Ouellet Y, Guertin M, Friedman JM (2003). Kinetic modulation in carbonmonoxy derivatives of truncated hemoglobins: the role of distal heme pocket residues and extended apolar tunnel. *J Biol Chem* **278**: 27241-27250.
- Saunders NF, Thomas T, Curmi PM, Mattick JS, Kuczek E, Slade R, Davis J, Franzmann PD, Boone D, Rusterholtz K, Feldman R, Gates C, Bench S, Sowers K, Kadner K, Aerts A, Dehal P, Detter C, Glavina T, Lucas S, Richardson P, Larimer F, Hauser L, Land M, Cavicchioli R (2003). Mechanisms of thermal adaptation revealed from the genomes of the Antarctic Archaea *Methanogenium frigidum* and *Methanococcoides burtonii*. *Genome Res* **13**: 1580-1588.
- Scher HD and Martin EE (2006). Timing and climatic consequences of the opening of Drake Passage. *Science* **312**: 428-430.
- Schmidt-Kastner R, Haberkamp M, Schmitz C, Hankeln T, Burmester T (2006). Neuroglobin mRNA expression after transient global brain ischemia and prolonged hypoxia in cell culture. *Brain Res* **1103**: 173-180.
- Schmidt M, Giessler A, Laufs T, Hankeln T, Wolfrum U, Burmester T.(2003). How does the eye breathe? Evidence for neuroglobin-mediated oxygen supply in the mammalian retina. *J Biol Chem* **278**(3):1932-1935.
- Scott NL, Falzone CJ, Vuletich DA, Zhao J, Bryant DA, Lecomte JT (2002). Truncated hemoglobin from the cyanobacterium *Synechococcus* sp. PCC 7002: evidence for

hexacoordination and covalent adduct formation in the ferric recombinant protein. *Biochemistry* **41**: 6902-6910.

Sidell BD, Vayda ME, Small DJ, Moylan TJ, Londraville RL, Yuan ML, Rodnick KJ, Eppley ZA, Costello L (1997). Variable expression of myoglobin among the hemoglobinless Antarctic icefishes. *Proc Natl Acad Sci USA* **94**: 3420-3424.

Sidell BD and O'Brien KM (2006). When bad things happen to good fish: the loss of hemoglobin and myoglobin expression in Antarctic icefishes. *J Exp Biol* **209**: 1791-1802.

Smagghe BJ, Trent III JT, Hargrove MS (2008). NO dioxygenase activity in hemoglobins is ubiquitous *in vitro*, but limited by reduction *in vivo*. *PLoS ONE* **3**(4): e2039.

Smulevich G, Miller MA, Kraut J, Spiro TG (1991). Conformational change and histidine control of heme chemistry in cytochrome *c* peroxidase: resonance Raman evidence from Leu-52 and Gly-181 mutants of cytochrome *c* peroxidase. *Biochemistry* **30**: 9546-9558.

Somero GN (1995). Proteins and temperature. *Annu Rev Physiol* **57**: 43-68.

Somero GN (2010) The physiology of climate change: how potentials for acclimatization and genetic adaptation will determine winners and losers. *J Exp Biol* **213**: 912-920.

Somero GN and DeVries AL (1967). Temperature tolerance of some Antarctic fish. *Science* **156**: 257-258.

Somero GN, Dahlhoff E, Lin JJ (1996). Stenotherms and eurytherms: mechanisms establishing thermal optima and tolerance ranges. In: Johnston IA and Bennett AF (Eds) *Animals and temperature: Phenotypic and Evolutionary Adaptation*. Cambridge University Press, Cambridge UK, pp. 53-57.

- Sowa AW, Guy PA, Sowa S, Hill RD (1999). Nonsymbiotic haemoglobins in plants. *Acta Biochim Pol* 46: 431-445.
- Springer BA, Egeberg KD, Sligar SG, Rohlfs RJ, Mathews AJ, Olson JS (1989). Discrimination between oxygen and carbon monoxide and inhibition of autooxidation by myoglobin. Site-directed mutagenesis of the distal histidine. *J Biol Chem* **264**: 3057-3060.
- Springer BA, Sligar SG, Olson JS, Phillips GN Jr (1994). Mechanisms of ligand recognition in myoglobin. *Chem Rev* **94**: 699-714.
- Stein P and Spiro TG (1980). Hydrogen-bond and deprotonation effects on the resonance Raman iron-imidazole mode in deoxy hemoglobin models: implication for hemoglobin cooperativity. *J Am Chem Soc* **102**: 7795-7797.
- Sun Y, Jin K, Mao XO, Zhu Y, Greenberg DA (2001). Neuroglobin protects the brain from experimental stroke *in vivo*. *Proc Natl Acad Sci USA* **98**: 15306-15311.
- Tatusova TA and Madden TL (1999). BLAST 2 Sequences, a new tool for comparing protein and nucleotide sequences. *FEMS Microbiol Lett* **174**: 247-250.
- Thompson JD, Gibson TJ, Plewniak F, Jeanmougin F, Higgins DG (1997). The CLUSTAL\_X windows interface: flexible strategies for multiple sequence alignment aided by quality analysis tools. *Nucleic Acids Res* **25**: 4876-4882.
- Thomson MRA (2004). Geological and palaeoenvironmental history of the Scotia Sea region as a basis for biological interpretation. *Deep Sea Research Part II* **51**: 1467-1487.
- Thorsteinsson MV, Bevan DR, Ebel RE, Weber RE, Potts M (1996). Spectroscopical and functional characterization of the hemoglobin of *Nostoc commune* (UTEX 584 (Cyanobacterial)). *Biochim Biophys Acta* **1292**: 133-139.

Thorsteinsson MV, Bevan DR, Potts M, Dou Y, Eich RF, Hargrove MS, Gibson QH, Olson JS (1999). A cyanobacterial hemoglobin with unusual ligand binding kinetics and stability properties. *Biochemistry* **38**: 2117-2126.

Todgham AE, Hoaglund EA, Hofmann GE (2007). Is cold the new hot? Elevated ubiquitin-conjugated protein levels in tissues of Antarctic fish as evidence for cold-denaturation of proteins in vivo. *J Comp Physiol B Biochem Syst Environ Physiol* **177**: 857-866.

Trent III JT and Hargrove MS (2002). A ubiquitously expressed human hexacoordinate haemoglobin. *J Biol Chem* **277**: 19538-19545.

Uno T, Ryu D, Tsutsumi H, Tomisugi Y, Ishikawa Y, Wilkinson AJ, Sato H, Hayashi T (2004). Residues in the distal heme pocket of neuroglobin. Implications for the multiple ligand binding steps. *J Biol Chem* **279**: 5886-5893.

Uzan J, Dewilde S, Burmester T, Hankeln T, Moens L, Hamdane D, Marden MC, Kiger L (2004). Neuroglobin and other hexacoordinated hemoglobins show a weak temperature dependence of oxygen binding. *Biophys J* **2**: 1196-1204.

Vallone B, Nienhaus K, Brunori M, Nienhaus GU (2004a). The structure of murine neuroglobin: Novel pathways for ligand migration and binding. *Proteins* **56**: 85-92.

Vallone B, Nienhaus K, Matthes A, Brunori M, Nienhaus GU (2004b). The structure of carbonmonoxy neuroglobin reveals a heme-sliding mechanism for control of ligand affinity. *Proc Natl Acad Sci USA* **101**: 17351-17356.

Vedam R and Holton G (1968). Specific Volumes of Water at High Pressures, Obtained from Ultrasonic-Propagation Measurements. *J Acoust Soc Am* **43**: 108-116.

Verde C, Parisi E, di Prisco G (2006). The evolution of thermal adaptation in polar fish. *Gene* **385**: 137-145.

Verde C, Giordano D, Russo R, Riccio A, Vergara A, Mazzarella L, di Prisco G (2009). Hemoproteins in the cold. *Mar Gen* **2**: 67-73.

Vergara A, Franzese M, Merlino A, Vitagliano L, di Prisco G, Verde C, Lee HC, Peisach J, Mazzarella L (2007). Structural characterization of ferric hemoglobins from three Antarctic fish species of the suborder Notothenioidei. *Biophys J* **93**: 2822-2829.

Vergara A, Vitagliano L, Verde C, di Prisco G, Mazzarella L (2008). Spectroscopic and crystallographic characterization of bis-histidyl adducts in tetrameric hemoglobins. *Methods Enzymol* **436**: 425-444.

Vinogradov S, Hoogewijs D, Bailly X, Arredondo-Peter R, Gough J, Dewilde S, Moens L, Vanfleteren J (2005). Three globin lineages belonging to two structural classes in genomes from the three kingdoms of life. *Proc Natl Acad Sci USA* **102**: 11385-11389.

Vinogradov S and Moens L (2008). Diversity of globin function: enzymatic, transport, storage, and sensing. *J Biol Chem* **283**: 8773-8777.

Visca P, Fabozzi G, Petrucca A, Ciaccio C, Coletta M, De Sanctis G, Bolognesi M, Milani M, Ascenzi P (2002). The truncated hemoglobin from *Mycobacterium leprae*. *Biochem Biophys Res Commun* **294**: 1064-1070.

Vitagliano L, Bonomi G, Riccio A, di Prisco G, Smulevich G, Mazzarella L (2004). The oxidation process of Antarctic fish hemoglobins. *Eur J Biochem* **271**: 1651-1659.

Vitagliano L, Vergara A, Bonomi G, Merlino A, Smulevich G, Howes B, di Prisco G, Verde C, Mazzarella L (2008). Spectroscopic and crystallographic analysis of a tetrameric hemoglobin oxidation pathway reveals features of an intermediate R/T state. *J Am Chem Soc* **130**: 10527-10535.

Vuletich DA and Lecomte JT (2006). A phylogenetic and structural analysis of truncated hemoglobins. *J Mol Evol* **62**: 196-210.

- Wajcman H, Kiger L (2002). Hemoglobin, from microorganisms to man: a single structural motif, multiple functions. *C R Biol* **325**: 1159-1174 (Article in French).
- Watanabe S and Wakasugi K (2008). Zebrafish neuroglobin is a cellmembrane-penetrating globin. *Biochemistry* **47**: 5266-5270.
- Watanabe S and Wakasugi K (2010). Identification of residues critical for the cell-membrane-penetrating activity of zebrafish neuroglobin. *FEBS Lett* **584**: 2467-2472.
- Watanabe S and Wakasugi K (2011). Module M1 of zebrafish neuroglobin acts as a structural and functional protein building block for a cell-membrane-penetrating activity. *PloS ONE* **6(2)**: e16808.
- Watts RA, Hunt PW, Hvitved AN, Hargrove MS, Peacock WJ, Dennis ES (2001). A hemoglobin from plants homologous to truncated hemoglobins of microorganisms. *Proc Natl Acad Sci USA* **98**: 10119-10124.
- Weiland TR, Kundu S, Trent III JT, Hoy JA, Hargrove MS (2004). Bis-Histidyl Hexacoordination in hemoglobins facilitates heme reduction kinetics. *J Am Chem Soc* **126**: 11930-11935.
- Wittenberg JB, Bolognesi M, Wittenberg BA, Guertin M (2002). Truncated hemoglobins: a new family of hemoglobins widely distributed in bacteria, unicellular eukaryotes, and plants. *J Biol Chem* **277**: 871-874.
- Zhao Y, Ratnayake-Lecamwasam M, Parker SK, Cocca E, Camardella L, di Prisco G, Detrich III HW (1998). The major adult  $\alpha$ -globin gene of Antarctic teleosts and its remnants in the hemoglobinless icefishes. Calibration of the mutational clock for nuclear genes. *J Biol Chem* **273**: 14745-14752.

## The peculiar heme pocket of the 2/2 hemoglobin of cold-adapted *Pseudoalteromonas haloplanktis* TAC125

Barry D. Howes · Daniela Giordano · Leonardo Boechi · Roberta Russo · Simona Mucciacciaro · Chiara Ciaccio · Federica Sinibaldi · Maria Fittipaldi · Marcelo A. Martí · Darío A. Estrin · Guido di Prisco · Massimo Coletta · Cinzia Verde · Giulietta Smulevich

Received: 7 September 2010 / Accepted: 11 October 2010 / Published online: 13 November 2010  
© SBIC 2010

**Abstract** The genome of the cold-adapted bacterium *Pseudoalteromonas haloplanktis* TAC125 contains multiple genes encoding three distinct monomeric hemoglobins exhibiting a 2/2  $\alpha$ -helical fold. In the present work, one of these hemoglobins is studied by resonance Raman, electronic absorption and electronic paramagnetic resonance spectroscopies, kinetic measurements, and different bioinformatic approaches. It is the first cold-adapted bacterial hemoglobin to be characterized. The results indicate that this protein belongs to the 2/2 hemoglobin family, Group II, characterized by the presence of a tryptophanyl residue on the bottom of the heme distal pocket in position G8 and

two tyrosyl residues (TyrCD1 and TyrB10). However, unlike other bacterial hemoglobins, the ferric state, in addition to the aquo hexacoordinated high-spin form, shows multiple hexacoordinated low-spin forms, where either TyrCD1 or TyrB10 can likely coordinate the iron. This is the first example in which both TyrCD1 and TyrB10 are proposed to be the residues that are alternatively involved in heme hexacoordination by endogenous ligands.

**Keywords** Resonance Raman · EPR · Molecular dynamics · Tyrosinate ligand · Antarctic bacterium

---

D. Giordano and L. Boechi contributed equally to this work.

**Electronic supplementary material** The online version of this article (doi:10.1007/s00775-010-0726-y) contains supplementary material, which is available to authorized users.

---

B. D. Howes · S. Mucciacciaro · M. Fittipaldi · G. Smulevich (✉)  
Dipartimento di Chimica, Università di Firenze,  
50019 Sesto Fiorentino (FI), Italy  
e-mail: giulietta.smulevich@unifi.it

M. Fittipaldi  
INSTM (Consorzio Interuniversitario per la Scienza  
e Tecnologia dei Materiali), 50019 Sesto Fiorentino (FI), Italy

D. Giordano · R. Russo · G. di Prisco · C. Verde  
Institute of Protein Biochemistry,  
CNR, 80131 Naples, Italy

L. Boechi · M. A. Martí · D. A. Estrin  
Departamento de Química Inorgánica,  
Analítica y Química Física/INQUIMAE-CONICET,  
Facultad de Ciencias Exactas y Naturales,  
Universidad de Buenos Aires,  
C1428EHA Buenos Aires, Argentina

### Abbreviations

*Ph*-2/2HbO *Pseudoalteromonas haloplanktis* 2/2 Hb  
encoded by the *PSHAA0030* gene  
RR Resonance Raman

C. Ciaccio · F. Sinibaldi · M. Coletta  
Dipartimento di Medicina Sperimentale e Scienze Biochimiche,  
Università di Roma Tor Vergata, 00133 Rome, Italy

C. Ciaccio · M. Coletta · G. Smulevich  
Consorzio Interuniversitario di Ricerca in Chimica dei Metalli  
nei Sistemi Biologici, 70126 Bari, Italy

## Introduction

Most ocean waters are permanently at temperatures ranging between 2 and 4 °C. Therefore, marine organisms have been exposed to a permanent excess of oxygen, due to the high solubility of this gas at cold temperatures, leading to oxygen reserves that are larger than those available in warmer waters. Although many cold-adapted marine species have been studied [1], we still have limited knowledge about molecular adaptations at low temperatures. The genome of the Antarctic marine eubacterium *Pseudoalteromonas haloplanktis* TAC125 (*Ph*TAC125) has been sequenced and annotated [2], shedding light on several molecular features that have selectively developed in cold environments. The genome contains multiple genes encoding three different truncated hemoglobins (Hbs) at distinct positions on chromosome I, namely *PSHAa0030*, *PSHAa2217* and *PSHAa0458*, which exhibit a 2/2  $\alpha$ -helical fold [3]. The unusually high number of 2/2 Hbs strongly suggests that these proteins are bound to fulfil important physiological roles that are perhaps related to the peculiar features of the Antarctic habitat.

In the present study, we cloned and overexpressed the 2/2 Hb encoded by the *PSHAa0030* gene (hereafter named *Ph-2/2HbO*). The ferric form was investigated by spectroscopy, kinetic measurements and different computer simulation approaches. This work represents the first detailed characterization of a cold-adapted bacterial Hb. The results highlight the unique features of the ferric state among 2/2 Hbs of Group II. The ensemble of results indicates high protein structural flexibility, which may be linked to the cold environment.

## Materials and methods

### Protein expression and purification

The gene encoding *Ph-2/2HbO* was cloned as described previously [3]. The reported expression and purification methods were replaced by an alternative procedure to (a) improve the biomass yield of *Ph-2/2HbO*, and (b) avoid sulfide binding [4].

Using the previous purification procedure, in the presence of 1.0 mM  $\beta$ -ME, *Ph-2/2HbO* was isolated in a ferric form with a Soret band at 427 nm and a broad band at 550 nm. The close similarities of this unusual spectrum to that of sulfide-bound heme proteins suggested that an exogenous sulfide ligand was bound to the heme Fe atom [4–6], possibly derived from sulfide impurities contained in  $\beta$ -ME used during the purification steps. Accordingly, in the present work, in the absence of  $\beta$ -ME, ferric *Ph-2/2HbO* displays quite different spectral

characteristics (see Fig. S1 of the Electronic supplementary material, ESM).

The strain BL21(DE3) of *Escherichia coli* was successfully transformed with the recombinant expression plasmid pET28a-2/2HbO. The cells were grown overnight in a flask at 37 °C and shaken at 180 rpm. Fifty microliters of the growth medium were inoculated in an Applikon fermentor with a working volume of 1 l. The culture was grown using a mineral medium according to a standard procedure from CPC Biotech. The first growth phase occurred in fed-batch mode at 30 °C. After 23 h, the temperature was decreased to 25 °C. The culture was induced at  $OD_{600} = 32$  by the addition of isopropyl-1-thio-D-galactopyranoside to a final concentration of 0.5 mM, and 0.3 mM  $\delta$ -aminolevulinic acid; expression was continued overnight. The cells were harvested by centrifugation at 4 °C.

For purification, the frozen cells were thawed, suspended in 50 mM Tris–HCl pH 7.6, 1.0 mM EDTA, 1.0 mM phenylmethylsulfonyl fluoride and protease-inhibitor cocktail (SIGMA P8465) and disrupted in a French press until the supernatant was reddish and clear. The cell debris was removed by centrifugation at 30,000 rpm for 1 h at 4 °C. The supernatant was loaded onto an anion-exchange column (Q Sepharose Fast Flow, GE Healthcare Biosciences), equilibrated with 20 mM Tris–HCl pH 7.6 and 1.0 mM EDTA (Akta Explorer system, GE Healthcare Biosciences, Amersham Biosciences Ltd, UK). *Ph-2/2HbO* was eluted with a NaCl gradient (from 0 to 0.25 M) in 20 mM Tris–HCl pH 7.6, 1.0 mM EDTA [3]. The fraction was chosen on the basis of the absorbance of heme at 407 nm and protein at 280 nm. The collected protein was concentrated, dialyzed against 50 mM 2-(*N*-morpholino)ethanesulfonic acid (MES) pH 6.0, and further purified with a SP (sulfopropyl) Sepharose Fast Flow column (GE Healthcare Biosciences) equilibrated with 50 mM MES pH 6.0. The protein was eluted with a NaCl gradient (from 0 to 0.35 M). Final purification was performed by using another strong cation-exchange column, Mono S (GE Healthcare Biosciences) equilibrated with 50 mM MES pH 6.0 and applying a NaCl gradient (from 0 to 0.50 M). The protein obtained was over 98% pure, as judged from sodium dodecyl sulfate polyacrylamide gel electrophoresis (SDS-PAGE), and was stored at –20 °C. The N-terminal sequence was elucidated by automatic sequencing performed with an Applied Biosystems Procise 494 Automatic Sequencer, equipped with on-line detection of phenylthiohydantoin amino acids.

### Sample preparation

The samples of *Ph-2/2HbO* at pH 5.6 and 7.6 were prepared in 0.1 M MES and 0.1 M Tris–HCl or 0.1 M

3-morpholinopropane-1-sulfonic acid (MOPS) buffers, respectively. Protein concentrations in the range 10–70  $\mu\text{M}$  were used for the electronic absorption and RR samples. Sample concentration for low-temperature RR was between 30 and 100  $\mu\text{M}$ . For kinetics measurements, the final protein concentration was 5  $\mu\text{M}$ . The concentration of the electron paramagnetic resonance (EPR) sample was 160  $\mu\text{M}$ . The protein concentration was determined on the basis of the molar absorptivity,  $\varepsilon = 131 \text{ mM}^{-1} \text{ cm}^{-1}$  at 408 nm.

### Electrochemistry

Direct current cyclic voltammetry was carried out at 25 °C using an AMEL (Milan, Italy) 433 multipolarograph. A saturated calomel electrode (+244 mV vs. NHE at 25 °C; AMEL) was the reference electrode and a pyrolytic graphite electrode was the working electrode (3-mm diameter, AMEL), modified as previously described [7]. Cyclic voltammograms were run at 25 °C in the potential range +200 to –600 mV (vs. the standard calomel electrode), at scan rates of 0.05–1.00 V/s. Measurements were carried out in 0.1 M phosphate pH 7.0.

### Spectroscopy

Electronic absorption spectra were measured with a double-beam Cary 5 spectrophotometer (Varian, Palo Alto, CA, USA) using a 5-mm NMR tube and a 600  $\text{nm min}^{-1}$  scan rate. The RR spectra were obtained using a 5-mm NMR tube and by excitation with the 406.7, 530.9 and 568.2 nm lines of a  $\text{Kr}^+$  laser (Innova 300 C, Coherent, Santa Clara, CA, USA), and the 496.5 and 514.5 nm lines of an  $\text{Ar}^+$  laser (Innova 90/5, Coherent). A detailed description of the room and low-temperature RR experimental procedures has been reported previously [8]. The measurements at 4 °C were obtained using a thermostatically controlled water bath. All RR measurements were repeated several times under the same conditions to ensure reproducibility. The RR spectra were calibrated with indene and  $\text{CCl}_4$  as standards to an accuracy of 1  $\text{cm}^{-1}$  for intense isolated bands. The RR spectrum of water was subtracted from all spectra obtained with excitation at wavelengths in the visible region (496.5–568.2 nm). Spectra in polarized light were obtained by inserting a Polaroid analyzer between the sample and the entrance slit of the monochromator. The depolarization ratios,  $\rho = I_{\perp}/I_{\parallel}$ , of the bands at 314 and 460  $\text{cm}^{-1}$  of  $\text{CCl}_4$  were measured to check the reliability of the polarization measurements. The values obtained, 0.73 and 0.00, respectively, compare well with the theoretical values of 0.75 and 0.00. To determine peak intensities and positions, a curve-fitting program (Lab Calc, Galactic) was used to simulate

experimental spectra, using a Lorentzian line shape. The frequencies of the bands were optimized with an accuracy of 1  $\text{cm}^{-1}$ , and the bandwidths with an accuracy of 0.5  $\text{cm}^{-1}$ .

EPR spectra were recorded as reported previously [8].

Kinetic measurements were carried out employing a rapid-mixing stopped flow (SX.18MV, Applied Photophysics, Salisbury, UK) with a 1 ms dead time. The Fe(III) form of *Ph-2/2HbO* was mixed with different concentrations of sodium azide in 0.1 M phosphate buffer pH 7.0 at 20 °C, and transient absorption spectra were collected between 350 and 700 nm. Kinetic progress curves were fitted according to the following equation:

$$\text{OD}_{\text{obs}} = \text{OD}_{t=\infty} \pm \sum_{i=1}^{i=n} \Delta\text{OD}_i \exp(-ik_{\text{obs}}t), \quad (1)$$

where  $\text{OD}_{\text{obs}}$  is the absorption at 408 nm at a given time from the start of the reaction,  $\text{OD}_{\infty}$  is the absorption at longer times from the start of the reaction (when it is completed),  $\Delta\text{OD}_i$  is the signal change for phase  $i$ ,  $k_i$  is the rate constant for phase  $i$ , and  $t$  is time. The sign  $\pm$  indicates that, depending on the wavelength, the signal may either decrease or increase.

### Sequence alignment

Sequence alignments were performed between *Ph-2/2HbO* and four Hbs belonging to Group II for which the crystal structures are available, namely *Mycobacterium tuberculosis* (*Mt-2/2HbO*) (pdb Id: 1NGK), *Bacillus subtilis* (*Bs-2/2HbO*) (1ux8), *Geobacillus stearothermophilus* (*Gs-2/2HbO*) (2bKm), *Thermobifida fusca* (*Tf-2/2HbO*) (2bMM), *Shewanella oneidensis 2/2HbO* (see Fig. S2 of the ESM) was selected due to the presence of an extension at the N-terminus of the primary structure, similar to *Ph-2/2HbO*. Sequence identities are 34, 37, 34, 33 and 39%, respectively.

To align these sequences, different computational programs have been used, namely Modeller [9], BLAST [10] and ClustalX [11]. Based on the present and previous alignments [3], we constructed 3D models using *Mt-2/2HbO* and *Bs-2/2HbO* proteins as templates, and the Modeller program with default parameters. Several putative *Ph-2/2HbO* structures were obtained.

### Molecular dynamics simulations

To evaluate the stabilities of the different structures, molecular dynamics simulations (MD) were performed for each structure using the Amber 9 force field ff99SB [12]. Initially, every system was minimized to avoid any possible structural clashes. Subsequently, the systems were

heated slowly from 0 to 300 K using a time step of 0.1 fs, and with a constraint on the  $\alpha$ -C of the protein backbone. A short simulation at the constant temperature of 300 K under a constant pressure of 1 bar was then performed using a time step of 0.1 fs to allow the systems to reach proper density, as shown previously [13, 14]. Finally, 2 ns of MD using a time step of 2 fs was performed for each structure. The majority of the structures were found to be unstable and unfolded during the time scale of these short simulations. The most stable structure was obtained by using the X-ray structure of *Bs-2/2HbO* as a template and sequence alignments with ClustalX. This model structure was used to perform 40 ns of MD simulation. The structure was found to be stable during the time scale of the simulation (Fig. S3 of the ESM).

To build the Tyr hexacoordinated structures, we pushed the tyrosine oxygen toward the Fe(III) atom until typical binding distances were reached, and we used the generated structure to start a new simulation with TyrO<sup>−</sup> coordinated to Fe(III), including the Fe–TyrO<sup>−</sup> bond in the force field. We carried out minimization and thermalization as described above, and 20 ns of MD were performed for the protein with TyrCD1–O<sup>−</sup> and with TyrB10–O<sup>−</sup> coordinated to Fe(III). The charges and parameters of the active site were determined as reported previously [15] using the isolated heme with a coordinated Tyr–O<sup>−</sup> as the model at the DFT/B3LYP level with a 6-31G\*\* basis set to compute the active-site electronic structure. Since no reliable structural information can be obtained for the pre-A helix, all simulations were performed without this motif at the N-terminus.

## Results

### Sequence alignment

The sequence alignment indicates that *Ph-2/2HbO* has structural features typical of 2/2 Hbs, and especially those belonging to Group II. In particular, *Ph-2/2HbO* has Trp at position G8, and both the CD1 and the B10 positions are occupied by Tyr (see Fig. S2 of the ESM). These three positions are the most important for oxygen stabilization in this family of Hbs [16]. In contrast to Group I of 2/2 Hbs, the E7 and E11 positions are occupied by nonpolar amino-acid residues, Ile and Phe, respectively, precluding ligand stabilization by these two residues.

Several structures of *Ph-2/2HbO* were obtained (see “Materials and methods”) starting from different alignments, with proteins of Group II giving rise to different initial structural models. The global fold of the models was very good, and the most significant structural differences were located in the CD loop, due to the insertion of three

residues (Figs. S2, S4 of the ESM). In all of the obtained alignments, the important heme cavity residues (HisF8, TyrB10, TrpG8, TyrCD1, IleE7, PheE11) are in the positions originally proposed by Wittenberg et al. [17] and subsequently confirmed by Vuletich and Lecomte [18] for Group II proteins.

This alignment differs from that obtained in a previous study with other Group II proteins, where the residue at CD1 was His [3]. The latter did not take into account the insertion of three residues in the CD loop, so the CD loop of the current alignment is longer than in other Group II Hbs.

### Redox potential measurements

The redox potential of *Ph-2/2HbO* at pH 7.0 [−80 mV vs. standard hydrogen electrode (SHE)] is low compared to that of horse heart myoglobin (Mb) and human Hb (+50 and +135 mV, respectively) [19].

### Spectroscopy at room temperature

The electronic absorption spectrum of ferric *Ph-2/2HbO* and its second-derivative spectrum ( $D^2$ , dotted line) are invariant over the pH range 5.6–7.6. The spectrum obtained at pH 7.6 (Fig. 1a, bottom) is characterized by a Soret band at 408 nm and bands in the visible region at 503, 533 (538 in  $D^2$ ), 570, and 635 nm (638 in  $D^2$ ). The wavelength maxima suggest the presence of various species, namely a His–Fe–H<sub>2</sub>O six-coordinate high-spin (6cHS) form [bands at 503 and charge-transfer transition (CT1) at 635 nm] and at least one 6c-low-spin (LS) heme (bands at 533 and 570 nm). The absorption maxima of the LS forms are quite unusual, reminiscent of those of ferric *Chlamydomonas* Hb [20] and the hemophore HasA proteins from *Serratia marcescens* and *Pseudomonas aeruginosa* [21, 22], and they are very different from either a LS His–Fe–His (that exhibits well-defined absorption bands at about 535 and 565 nm) or a His–Fe–OH heme complex (that exhibits well-defined absorption bands at about 540 and 580 nm) [23]. Therefore, on the basis of the similarity with the UV–vis spectrum of ferric *Chlamydomonas* Hb and HasA hemophores, a His and a Tyr ligand are suggested to occupy the fifth and sixth coordination positions, respectively.

In agreement with the electronic absorption spectra, the Raman excitation profile at pH 7.6 (Fig. 1b, bottom; Fig. S5 of the ESM), together with the spectra in polarized light (Fig. 2b), allow the identification of three species: a 6cHS species ( $\nu_3$  at 1,480 cm<sup>−1</sup>,  $\nu_{10}$  at 1,608 cm<sup>−1</sup>), and two 6cLS species. In particular, with Soret excitation, two 6cLS  $\nu_3$  bands at 1,505 and 1,512 cm<sup>−1</sup> were observed (Fig. 1b, bottom; Fig. S5 of the ESM; Fig. 2b, bottom trace), and in the 1,600–1,650 cm<sup>−1</sup> region the spectra in polarized light

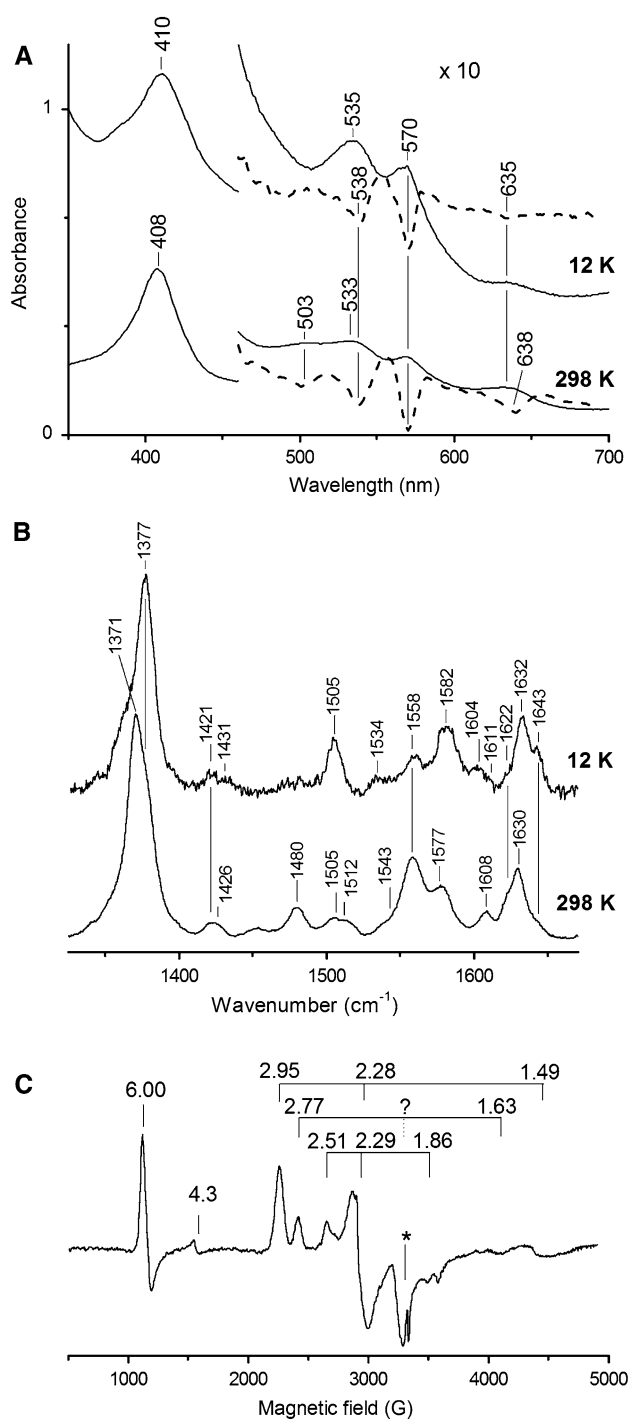


**Fig. 1** Ferric *Ph-2/2HbO* at pH 7.6. **a** UV-vis absorption (continuous line) and  $D^2$  (dotted line) spectra in 20 mM Tris-HCl at 298 (bottom) and 12 K (top). The visible region has been expanded tenfold. Spectra have been shifted along the ordinate axis to allow better visualization. **b** RR spectra taken with the 413.1 nm excitation wavelength in the high-wavenumber region in 0.1 M MOPS at 298 K (bottom) and in 20 mM Tris-HCl at 12 K (top). Experimental conditions: 15 mW laser power at the sample,  $1\text{ cm}^{-1}$  (298 K) and  $5\text{ cm}^{-1}$  (12 K) spectral resolution; average of seven spectra with 600 s integration time (298 K), 10 s/ $0.5\text{ cm}^{-1}$  (12 K). The intensities are normalized to that of the  $1,371\text{ cm}^{-1}$  band. **c** X-band EPR spectrum in 0.1 M Tris-HCl. The spectra were recorded at 5 K, 9.36 GHz microwave frequency, 0.1 mW microwave power and 10 G modulation amplitude. The asterisk indicates a spurious signal. The feature at  $g = 4.3$  results from a non-heme iron impurity

these bands are also observed in Q band excitation. This is consistent with previous observations for various heme containing peroxidases—namely CcP [24], HRPc [25], and *Coprinus cinereus* peroxidase (CIP) [26]—despite the fact that vinyl stretching modes are not expected to be enhanced a priori with visible excitation. The complete assignment of the high-frequency region is reported in Table S1 of the ESM.

A Tyr coordinated to a heme iron can often be identified by RR experiments. In fact, excitation in the tyrosinate-Fe(III) CT band (near 500 nm) yields characteristic vibrational frequencies of the bound phenolate [27]. In the  $400\text{--}1,700\text{ cm}^{-1}$  region, the spectra taken with excitation wavelengths in the visible region (Fig. 2a; Fig. S5 of the ESM) clearly show the enhancement of two bands at 598 and  $1,510\text{ cm}^{-1}$  (which are polarized, data not shown), displaying maximum intensification for excitation at 514.5 nm. Figure 2a shows the two spectral regions expanded to better visualize the bands. These bands are assigned to the  $\nu(\text{Fe-O}_{\text{Tyr}})$  and  $\nu_{\text{Tyr}}(\text{C}=\text{C})$  tyrosinate modes, respectively. Note that, despite the observation of two low-spin forms in the RR spectra, only one  $\nu(\text{Fe-O}_{\text{Tyr}})$  stretching mode at  $598\text{ cm}^{-1}$  is clearly evident. However, we cannot exclude that a second mode is hidden under the polarized band at  $572\text{ cm}^{-1}$  observed in both Soret and visible excitations (Fig. 2a; Fig. S5 of the ESM), assigned to the  $\nu_{48}(E_u)$  in analogy to Mb [28].

The frequencies of the phenolate modes observed for a number of heme iron-tyrosinate proteins are listed in Table 1 [20, 29–34]. In general, ferric-heme proteins with tyrosinate ligation have been found to have penta- or hexa-HS heme states. The only exceptions are *Chlamydomonas* Hb and the HasA hemophores, which have 6cLS hemes. The tyrosinate 6cLS heme of the protein studied herein, *Ph-2/2HbO*, is now added to this list. Table 1 shows that while the  $\nu_{\text{Tyr}}(\text{C}=\text{C})$  modes occur in a narrow frequency range, the  $\nu_{\text{Tyr}}(\text{C}-\text{O})$  and  $\nu(\text{Fe-O}_{\text{Tyr}})$  modes are markedly variable, ranging from 1,260 to 1,310, and from 502 to  $623\text{ cm}^{-1}$ , respectively. The comparison between the data

enable the identification of two polarized bands at 1,622 and  $1,630\text{ cm}^{-1}$  assigned to the  $\nu(\text{C}=\text{C})$  vinyl stretching modes (Fig. 2b, bottom trace). Upon excitation with the 514.5 nm line (i.e., in resonance with the visible bands), two depolarized bands at 1,635 and  $1,643\text{ cm}^{-1}$  were identified and assigned to two  $\nu_{10}$  modes of 6cLS hemes (Fig. 2b). The  $\nu(\text{C}=\text{C})$  vinyl stretching modes are enhanced via the A-term (Franck-Condon mechanism); however,

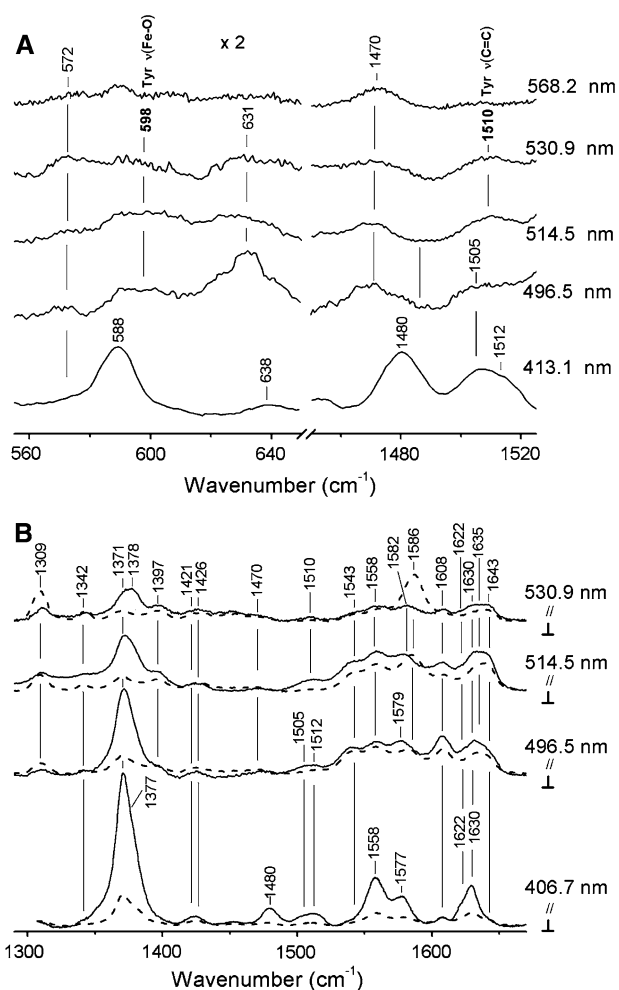


**Fig. 2** RR spectra of ferric *Ph-2/2HbO* at 298 K, in 20 mM Tris-HCl, pH 7.6 obtained with various excitation wavelengths: 406.7 nm, 10 mW laser power at the sample,  $1\text{ cm}^{-1}$  spectral resolution; 413.1 nm, 15 mW laser power at the sample,  $1\text{ cm}^{-1}$  spectral resolution; 496.5 nm, 100 mW laser power at the sample,  $2.4\text{ cm}^{-1}$  spectral resolution; 514.5 nm, 150 mW laser power at the sample,  $2.2\text{ cm}^{-1}$  spectral resolution; 530.9 nm, 36 mW laser power at the sample,  $2.5\text{ cm}^{-1}$  spectral resolution; 568.2 nm, 23 mW laser power at the sample,  $2\text{ cm}^{-1}$  spectral resolution and in polarized light at room temperature. **a** Experimental conditions: 413.1 nm, average of 18 spectra with 180 s integration time; 496.5 nm, average of 4 spectra with 720 s integration time; 514.5 nm, average of 15 spectra with 720 s integration time; 530.9 nm, average of 15 spectra with 600 s integration time (low frequency) and average of 6 spectra with 720 s integration time (high frequency); 568.2 nm, average of 7 spectra with 600 s integration time. The 520–740  $\text{cm}^{-1}$  region has been expanded twofold. The intensities are normalized to that of the  $1,230\text{ cm}^{-1}$  band ( $\nu_{13}$ ). **b** RR spectra in polarized light taken with excitation wavelengths at 406.7 and 530.9 nm in 0.1 M MOPS and with excitation wavelengths at 496.5 and 514.5 nm in 20 mM Tris-HCl at pH 7.6. Experimental conditions: 406.7 nm, average of 8 spectra (continuous line, parallel, //) and of 27 spectra (dotted line, perpendicular,  $\perp$ ) with 600 s integration time; 496.5 nm, average of 5 spectra (//) and of 8 spectra ( $\perp$ ) with 720 s integration time; 514.5 nm, average of six spectra (//) and of 8 spectra ( $\perp$ ) with 720 s integration time; 530.9 nm, average of 12 spectra (//) and of 13 spectra ( $\perp$ ) with 600 s integration time. The intensities are normalized to that of the  $1,230\text{ cm}^{-1}$  band ( $\nu_{13}$ )

reported in Table 1 for various heme proteins allows us to exclude a trans-axial effect altering the frequencies of these latter modes. However, different factors can affect these frequencies, namely (a) the TyrO-Fe bond angle via the interaction between the  $\pi$  orbitals of phenolate and the porphyrin, (b) the relative orientation between the tyrosinate ring and the heme plane, and (c) the Fe-O bond strength via the donation of electrons from phenolate to the heme with consequent weakening of the Fe-O bond. Formation of H-bonds between the tyrosinate and neighboring groups strongly affects the frequency of the  $\nu(\text{Fe-O}_{\text{Tyr}})$  modes. In the 6cLS *Chlamydomonas* Hb, the band at  $502\text{ cm}^{-1}$  was assigned to a tyrosinate H-bonded to a Lys residue. Recently, for the natural mutant, Hb M Saskatoon, in which the distal E7 His is replaced by a Tyr residue giving rise to a 6cHS species, two  $\nu(\text{Fe-O}_{\text{Tyr}})$  modes at 581 and  $598\text{ cm}^{-1}$  have been observed (Table 1) [34]. These bands were assigned to a Fe-O (protonated Tyr) ( $581\text{ cm}^{-1}$ ) and a Fe-O (deprotonated Tyr) ( $598\text{ cm}^{-1}$ ) stretching mode, respectively, on the basis of variations in their relative intensities at alkaline pH. The frequency of  $598\text{ cm}^{-1}$  is close to the Fe-(deprotonated Tyr) stretching frequency of another natural Hb mutant, Hb M Boston ( $603\text{ cm}^{-1}$ ) [30], and identical to that reported herein for the  $\nu(\text{Fe-O}_{\text{Tyr}})$  mode. This outstanding coincidence of frequencies suggests that, for at least one of the LS forms observed in the RR spectra, the heme-bound *Ph-2/2HbO* distal Tyr residue corresponds to a deprotonated species at pH 7.6.

#### Azide binding kinetics

Figure 3a shows the progress curves at 408 nm for sodium azide binding to ferric *Ph-2/2HbO* at pH 7.0 and  $20^\circ\text{C}$ . The continuous lines correspond to the nonlinear least-squares fitting of the data according to Eq. 1, employing three exponentials (i.e.,  $i = 3$  in Eq. 1).

In particular, two of these exponentials correspond to azide-dependent bimolecular processes, whereas a third process displays a rate which does not seem to depend on azide concentration. As is evident from Fig. 3a, the optical density change resulting from the reaction with azide increases as the concentration is increased. The  $\Delta\text{OD}$  at 408 nm for the two bimolecular processes is reported in Fig. 3b as a function of azide concentration. Optical density changes were analyzed according to the following equation:

$$\Delta\text{OD}_{\text{obs}} = \Delta\text{OD}_{\text{tot}} \frac{K[N_3^-]}{1 + K[N_3^-]}, \quad (2)$$

where  $\Delta\text{OD}_{\text{obs}}$  is the optical density change at 408 nm corresponding to the exponential process,  $\Delta\text{OD}_{\text{tot}}$  is the total optical density change at 408 nm (corresponding to

**Table 1** Tyrosinate vibrational bands ( $\text{cm}^{-1}$ ) for ferric heme proteins with tyrosinate ligation

Protein	Spin state	$\nu_{\text{Tyr}}(\text{C}=\text{C})$	$\nu_{\text{Tyr}}(\text{C}=\text{C})$	$\nu_{\text{Tyr}}(\text{C}-\text{O})$	$\nu(\text{Fe}-\text{O}_{\text{Tyr}})$	Reference
<i>Ph-2/2HbO</i>	6cLS	1,601 <sup>a</sup>	1,510	n.d. <sup>b</sup>	598	This work
<i>Chlamydomonas</i> Hb	6cLS	1,595	1,500	1,308	502	20
Hb M Saskatoon	6cHS	1,607	1,504	1,300	581/598	29, 30, 34
Hb M Boston	5cHS	1,603	1,504	1,279	603	29, 30
Human Mb (H93Y)	5cHS	1,603	1,504	1,302	585	31
Human HO-1(H25Y)	5cHS	1,605	1,504	1,258	591	32
ShuT	5cHS	1,601	1,502	1,301/1,265	613	33

<sup>a</sup> This band overlaps with the 6cHS  $\nu_{10}$  observed at  $1,608 \text{ cm}^{-1}$ . A polarized band at  $1,601 \text{ cm}^{-1}$  has been observed by curve fitting (bandwidth  $13 \text{ cm}^{-1}$ ) the spectra obtained with  $514.5 \text{ nm}$  excitation in polarized light (data not shown)

<sup>b</sup> This band overlaps with a mode observed at  $1,309 \text{ cm}^{-1}$  and assigned to the  $\nu_{21}$  (see Table S1 of the ESM)

complete saturation of the binding site),  $K$  is the equilibrium constant, and  $[\text{N}_3^-]$  is the azide concentration. In this way, it was possible to determine the apparent equilibrium constant of azide binding to the two Fe(III) forms of *Ph-2/2HbO*, which are characterized by the two bimolecular processes (corresponding to  $K = 9.8 \pm 1.2 \times 10^1 \text{ M}^{-1}$  for the faster bimolecular process 1, and  $K = 5.5 \pm 0.7 \times 10^2 \text{ M}^{-1}$  for the slower bimolecular process 2, respectively). This information is particularly important since it allows the concentration dependence of the two bimolecular rate constants (Fig. 3c) to be fitted in a constrained way with physically meaningful parameters. In this respect, the ligand concentration dependence of kinetic rate constants has been fitted using a classical bimolecular scheme:

$$k_{\text{obs}} = k_{\text{on}}[\text{N}_3^-] + k_{\text{off}} \quad (3)$$

The nonlinear least-squares fitting of the two bimolecular rate constants is reported in Fig. 3c. It is noted that only for the faster bimolecular process does the use of Eq. 3 give a satisfactory description of the azide-concentration dependence, with values of  $k_{\text{on}}$  ( $=2.4 \pm 0.3 \times 10^2 \text{ M}^{-1} \text{ s}^{-1}$ ) and  $k_{\text{off}}$  ( $=2.44 \pm 0.38 \text{ s}^{-1}$ ) compatible with the value of  $K$  [ $=9.8(\pm 1.2) \times 10^1 \text{ M}^{-1}$ ] obtained from optical density changes (Fig. 3b). In the case of the slower bimolecular rate constant, we must use a different reaction scheme (Scheme S1 of the ESM). The nonlinear least-squares fits of the rates for the two bimolecular processes are reported in Fig. 3c; the corresponding parameters are reported in Table 2.

Clearly, the fact that these data need three exponentials indicates that the azide ligand encounters three different hexacoordinated forms in the heme pocket. Two of these forms allow a fairly fast ligand binding, such that the process maintains its bimolecular nature (probably because the originally bound ligand dissociates quickly), whereas the third one, which is the slowest concentration-independent process, seems to reflect a situation where the heme Fe(III) atom is hexacoordinated by a ligand which dissociates very

slowly (with a  $k_{\text{obs}} \cong 7.0 \pm 1.5 \times 10^{-4} \text{ s}^{-1}$ ), such that the dissociation process is rate limiting under all conditions [i.e., when  $k_2' \cdot [\text{N}_3^-] \gg k_1', k_1$ ; see Scheme S1 of the ESM].

#### Spectroscopy at low temperature

The electronic absorption and the  $\text{D}^2$  spectra of ferric *Ph-2/2HbO* in the low-temperature range 220–12 K (Fig. 1a, top) are essentially those of 6cLS hemes. The LS Q-bands observed at room temperature (535 and 570 nm) are intensified, whereas the Soret band redshifts by 2 nm and the 6cHS bands at 503 and 635 nm (638 nm in the  $\text{D}^2$  spectrum) are considerably reduced. In accord with the low-temperature absorption spectrum, the high-frequency RR spectrum at 12 K pH 7.6 shows an intensification of the LS form ( $\nu_3$  1,505,  $\nu_2$  1,582,  $\nu_{10}$  1,643  $\text{cm}^{-1}$ ) at the expense of the 6cHS form ( $\nu_3$  1,480,  $\nu_2$  1,558,  $\nu_{10}$  1,608  $\text{cm}^{-1}$ ) observed at 298 K (Fig. 1b), which is considerably reduced at 12 K. Moreover, of the two LS forms observed at 298 K, characterized by  $\nu_3$  bands at 1,505 and 1,512  $\text{cm}^{-1}$ , only one form appears to be particularly enhanced at 12 K ( $\nu_3$  at 1,505  $\text{cm}^{-1}$ ). Interestingly, at the physiological temperature for the bacterium (4 °C), a slight increase in the relative intensity of the RR  $\nu_3$  LS band at 1,505 with respect to that at 1,512  $\text{cm}^{-1}$  has been observed, together with an intensification (of ca. 20%) of the UV-vis Soret band (Fig. S6 of the ESM). Nevertheless, the broad  $\nu_2$  band (1,582  $\text{cm}^{-1}$ ) at 12 K suggests the presence of two LS forms. This interpretation is supported by the presence of the bands at 1,604 and 1,611  $\text{cm}^{-1}$ , assigned to two  $\nu_{37}$  LS modes.

X-band EPR spectroscopy (at 5 K) was carried out to gain further insight into the spin state and heme coordination environment of the protein (Fig. 1c). In agreement with the electronic absorption and RR spectra, the EPR spectrum at pH 7.6 is characterized by an axial HS ferric signal ( $g_{\perp} \sim 6.0$ ,  $g_{\parallel} \sim 2.0$ ) and three rhombic LS forms:

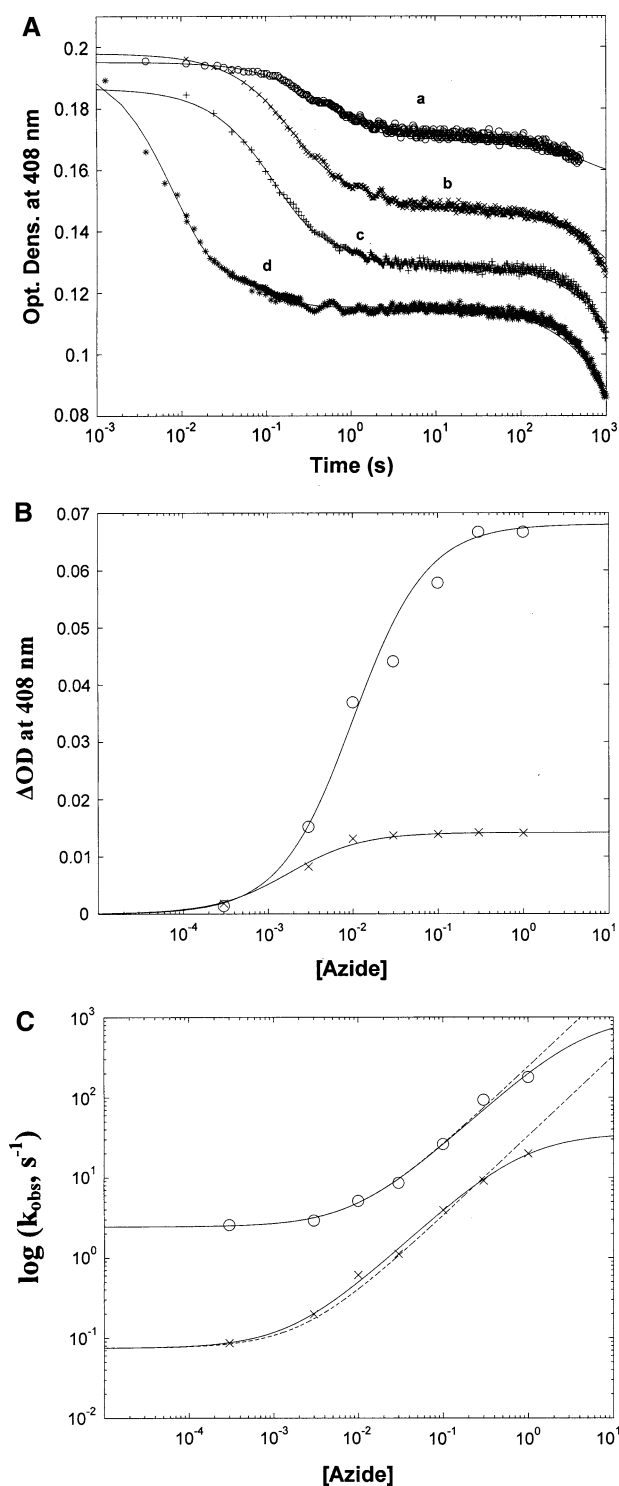


**Fig. 3** **a** Kinetic progress curves at 408 nm of  $3 \times 10^{-6}$  M Fe(III) *Ph-2/2HbO* for different concentrations of  $\text{N}_3^-$ ; i.e.,  $3 \times 10^{-4}$  M (curve *a*),  $3 \times 10^{-3}$  M (curve *b*),  $1 \times 10^{-2}$  M (curve *c*) and  $3 \times 10^{-1}$  M (curve *d*) at pH 7.0 and 20 °C. Continuous lines represent nonlinear least-squares fits to data employing Eq. 1 with three exponentials (i.e.,  $i = 3$  in Eq. 1). **b** Amplitude of optical-density changes at 408 nm for the first two exponentials (open circle *r1* and asterisk *r2*) of  $\text{N}_3^-$  binding to  $3 \times 10^{-6}$  M Fe(III) *Ph-2/2HbO* as a function of  $[\text{N}_3^-]$ . Continuous lines show nonlinear least-squares fits to data employing Eq. 2. **c** Dependence on  $[\text{N}_3^-]$  of the observed rate constants for the first two exponentials of azide binding to Fe(III) *Ph-2/2HbO* (symbols are the same as those used in the middle panel). Continuous lines show nonlinear least-squares fits to data employing Eq. S1 (see the ESM) and parameters reported in Table 2; dashed lines show nonlinear least-squares fits to data employing Eq. 3

**Table 2** Kinetic parameters for azide binding to bimolecular species of Fe(III) *Ph-2/2HbO* (indicated as *r1* and *r2*) at pH 7.0 and 20 °C, according to Scheme S1, employing Eq. S1 (see the ESM)

	<i>r1</i>	<i>r2</i>
$k_1$ ( $\text{s}^{-1}$ )	$1.0 (\pm 0.2) \times 10^3$	$3.6 (\pm 0.5) \times 10^1$
$k_2/k_1'$ ( $\text{M}^{-1}$ )	$0.23 \pm 0.04$	$1.2 \pm 0.3$
$k_2$ ( $\text{s}^{-1}$ )	$2.4 \pm 0.4$	$0.07 \pm 0.01$

hidden by the bands of the other two species at  $g \sim 2.2$  or by the spurious band.

The  $g$  tensor anisotropy of these LS forms is typical of N and O ligation to the heme (Table 3) [5, 20, 35–41]. The Blumberg–Peisach diagram [36] can provide some empirical guidance to obtain an indication of possible LS heme iron axial ligands, although it should be kept in mind that a number of pitfalls have been found in the use of this diagram, and it should not be used as the only criterion for ligand assignment [42]. The rhombicity ( $V/\Delta$ ) and tetragonality ( $\Delta/\lambda$ ) parameters determined from the  $g$  values [43, 44] of the predominant LS form at pH 7.6 (form 1;  $V/\Delta = 0.59$ ,  $\Delta/\lambda \pm = 3.30$ ) place it in the H-type group of the Blumberg–Peisach diagrams [36], characterized by systems with bis-His axial coordination. Nevertheless, the  $g$  values of form 1 are quite similar to those of the human serum albumin–ibuprofen complex (2.93, 2.27, 1.55), which is characterized by His–Fe–Tyr axial coordination [41] (Table 3). A similar assignment to the H group of the Blumberg–Peisach diagram was also reported for the HasA proteins from *S. marcescens* and *P. aeruginosa* at neutral pH ( $g = 2.86, 2.21, 1.71$ ), which are characterized by His–Fe–Tyr axial coordination. It is noted that the original EPR study of *S. marcescens* HasA, prior to the determination of the crystal structure, mistakenly assigned a bis-His axial heme coordination [39, 40]. Furthermore, the rhombicity and tetragonality crystal parameters determined from the  $g$  values of *Chlamydomonas* Hb, which is assigned to His–Fe–Tyr axial coordination, place it in the H structural group [20]. In all the cited cases, the tyrosinate ligand is

form 1,  $g = 2.95, 2.28, 1.49$ , form 2,  $g = 2.51, \sim 2.29, 1.86$ , and form 3,  $g = 2.77, -, 1.63$  (Table 3). The  $g$  values reported for form 2 should be considered to be average values, as at each  $g$  value there is evidence of more than one species with very similar  $g$  values, likely indicative of some structural flexibility at this site (see Fig. S7 of the ESM). The band corresponding to  $g_2$  of form 3 is likely

**Table 3** Comparison of the EPR spectral parameters of various low-spin heme proteins

Protein	$g_1$	$g_2$	$g_3$	pH	Coordination	Reference
<i>Ph-2/2HbO</i>	2.95	2.28	1.49	7.6	His/Tyr <sup>-a</sup>	This work
<i>Ph-2/2HbO</i>	2.51	~2.29	1.86	7.6	His/Tyr <sup>-</sup>	This work
<i>Ph-2/2HbO</i>	2.77	–	1.63	7.6	His/Tyr <sup>-a</sup>	This work
HRPA2	2.96	2.13	1.66	Alkaline	His/OH <sup>-a</sup>	[35]
Mb	2.55	2.17	1.85	Alkaline	His/OH <sup>-</sup>	[5]
<i>L. pectinata</i> Hb II	2.61	2.20	1.82	Alkaline	His/OH <sup>-</sup>	[5]
Various heme proteins <sup>b</sup>	~2.8	2.4	1.5		His/His	[36, 37]
Cytochrome <i>b</i>	>3				His/His <sup>c</sup>	[38]
<i>Chlamydomonas</i> Hb	2.52	2.31	1.86	Alkaline	His/Tyr <sup>-a</sup>	[20]
<i>S. marcescens</i> HasA	2.85	2.21	1.71	7.5	His/Tyr <sup>-a</sup>	[39, 40]
HSA ibuprofen	2.93	2.27	1.55	6.9	His/Tyr <sup>-a</sup>	[41]
<i>L. pectinata</i> Hb II	2.76	2.20	1.75	Alkaline	His/Tyr <sup>-</sup>	[5]
HH cytochrome <i>c</i>	3.06	2.25	1.25	7.0	Met/His	[37]
<i>Euglena</i> cytochrome	3.20	2.05	1.39	7.0	Met/His <sup>d</sup>	[37]
HH cytochrome <i>c</i>	3.37	2.1		Alkaline	Lys/His	[37]
HH cytochrome <i>c</i>	3.58			Alkaline	Lys/Lys	[37]

HRPA<sub>2</sub> horseradish peroxidase isoenzyme A<sub>2</sub>, HSA human serum albumin, HH horse heart

<sup>a</sup> OH<sup>-</sup> strongly H-bonded

<sup>b</sup> Approximate  $g$  values

<sup>c</sup> Imidazole planes, nonparallel

<sup>d</sup> Imidazole with enhanced H-bonding

strongly H-bonded with a nearby residue, which has been suggested to be the origin of the atypical crystal field parameters for O heme ligation [20, 40]. Hence, by analogy with these three cases, form 1 is proposed to be a tyrosinate LS heme species that is strongly H-bonded with a neighboring residue.

The crystal field parameters of form 2 ( $V/\Delta = 0.82$ ,  $\Delta/\lambda = 5.17$ ) are consistent with normal O coordination of the heme based on the Blumberg–Peisach diagram [36]. Thus, it is suggested that in this case the bound Tyr residue is not involved in H-bonding interactions and, consequently, is deprotonated. It cannot be completely excluded that form 2 corresponds to His–Fe–OH<sup>-</sup> coordination (see Table 3), although this possibility is considered unlikely as there is no evidence for a hydroxyl complex in the UV–vis spectrum at 12 K at pH 7.6 (Fig. 1a) [23]. The heme coordination of form 3 ( $g_1 = 2.77$ ,  $g_2 = -$ ,  $g_3 = 1.63$ ) is uncertain due to the absence of  $g_2$ ; however, the  $g$  tensor anisotropy suggests a probable assignment to the H group of the Blumberg–Peisach diagram and, therefore, bis-His coordination. This can be ruled out, as there are no histidine residues in the near vicinity of the distal heme pocket of *Ph-2/2HbO*, suggesting that the coordination is His–Fe–Tyr, with the tyrosinate ligand involved in a H-bonding interaction with neighboring residues distinct from that of form 1. Thus, in accord with the UV–vis and RR data, all of the LS forms are assigned to His–Fe–Tyr heme coordination.

The apparent absence in the RR spectrum of a third LS form observed in the EPR spectrum at 5 K is likely due to two forms having very similar RR frequencies.

#### Molecular dynamics simulations

The most stable structure found by homology modeling was used to perform 40 ns of MD simulations. To elucidate the potential residue(s) involved in the hexacoordinated conformation, we monitored selected key distances during the simulation. As reported for other Group II Hbs, the oxygen atom of TyrB10 was found to be close to the Fe(III) atom [16, 20]. However, TyrCD1 was found to be even closer to the Fe(III) atom than TyrB10 (Fig. 4). This is the first reported case in which the TyrCD1 may be bound to the Fe(III) atom.

On this basis, we constructed two models in which either TyrCD1 or TyrB10 was coordinated to the Fe(III). MD simulations of these models were performed in order to determine the stabilities of these potential structures. The results show that both systems were stable during the 20 ns of the MD (see Figs. S8, S9 of the ESM). We also found that when TyrCD1 is coordinated to the iron atom, TrpG8 is H-bonded to the O<sup>-</sup> of TyrCD1, highlighting the important role of this residue (Fig. 5). On the other hand, when TyrB10 is coordinated to the iron, both TrpG8 and TyrCD1 are H-bonded to the O<sup>-</sup> of TyrB10 (Fig. 6). These

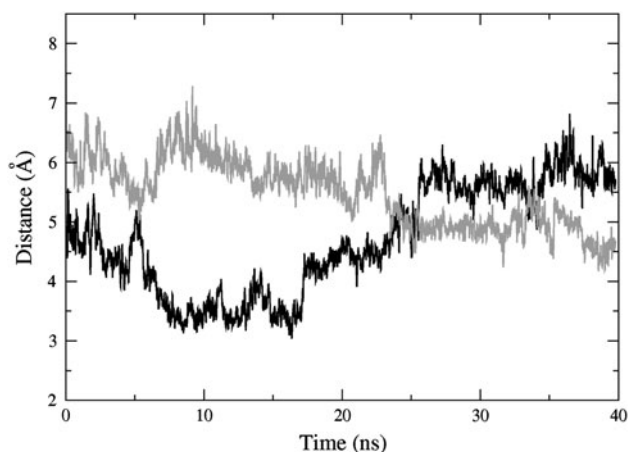


**Fig. 4** *Ph-2/2HbO* Fe(III). Time evolution of selected distances between distal residues of the protein. The distances are defined as the distances between the iron and the hydroxylic oxygen of TyrCD1 (black), or the iron and the hydroxylic oxygen of TyrB10 (dark gray)

results are fully in keeping with the presence of multiple LS forms displaying different heme binding affinities and spectroscopic properties.

## Discussion

Unlike the great majority of bacteria, *PhTAC125* possesses three genes encoding 2/2 Hbs, two of which belong to Group II, and one gene encoding flavoHb. Sequence alignment (Fig. S2 of the ESM) of *Ph-2/2HbO* with other 2/2 Hbs indicates that the conserved residues HisF8, TyrB10, TrpG8, TyrCD1, IleE7, and PheE11 are at the typical positions for Group II Hbs [17, 18]. On the proximal side, HisF8 is coordinated to the heme iron, as confirmed by the  $\nu(\text{Fe-Im})$  stretching mode at  $223\text{ cm}^{-1}$  in the RR spectrum of the deoxy form (data not shown).

*Ph-2/2HbO* presents an unusual extension of 15 residues at the N-terminus (pre-A helix). A similar situation had also been found in *M. tuberculosis* HbN (Group I) and appears to occur in many slow-growing species of mycobacterium, such as *M. bovis*, *M. avium*, *M. microti*, *M. marinum* [45], and *S. oneidensis* [18]. The X-ray structure of *M. tuberculosis* HbN (1IDR) showed that the pre-A motif does not significantly contribute to the structural integrity of the protein, protruding out of the compact globin fold, but rather confers a vital contribution in regulating the efficient nitrogen-monoxide-dioxygenase activity of HbN [45].

Inactivation of the *Ph-2/2HbO* encoding gene makes the mutant bacterial strain sensitive to high oxygen pressure, to  $\text{H}_2\text{O}_2$  and to nitrosating agents, suggesting a potential role of the protein in oxidative and nitrosative stress [46].

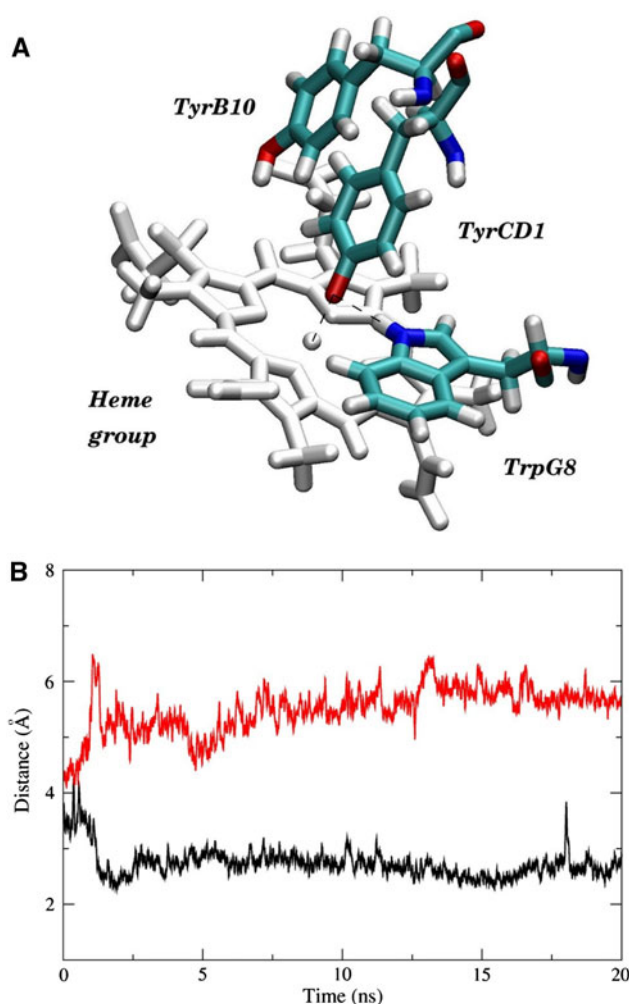


**Fig. 5** *Ph-2/2HbO* with TyrCD1-O<sup>-</sup> coordinated to the heme iron. **a** Schematic representation of the distal site of the protein showing the coordinated TyrCD1-O<sup>-</sup> stabilized by a H-bond with the TrpG8. As shown in **b**, the distance between TyrCD1-O<sup>-</sup> and the hydroxylic proton of TyrB10 is too long to form a H-bond. **b** Time evolution of selected distances between the O<sup>-</sup> atom of the coordinated TyrCD1 and the indole Ne proton of TrpG8 (black), and the hydroxylic proton of TyrB10 (red)

At neutral pH, the heme population of *Ph-2/2HbO* contains a mixture of 6cHS (aquo) and different 6cLS heme forms. The LS forms are all characterized by a nonprotonated tyrosinate bound to the heme iron, which experience different degrees of H-bonding with neighboring H-bond donors. Either TyrCD1-O<sup>-</sup> or TyrB10-O<sup>-</sup> are suggested to be coordinated to the heme Fe(III) atom. The first residue is stabilized by TrpG8 and the second by both TrpG8 and TyrCD1. Clearly, TrpG8 plays a very important role in the stabilization of the coordinated tyrosyl residues. The lower redox potential of *Ph-2/2HbO* at pH 7.0 (i.e.,  $-80\text{ mV}$  vs. SHE) compared to that of horse heart Mb and human Hb ( $+50$  and  $+135\text{ mV}$ , respectively) [19] does indeed agree with the presence of Tyr as axial ligand.

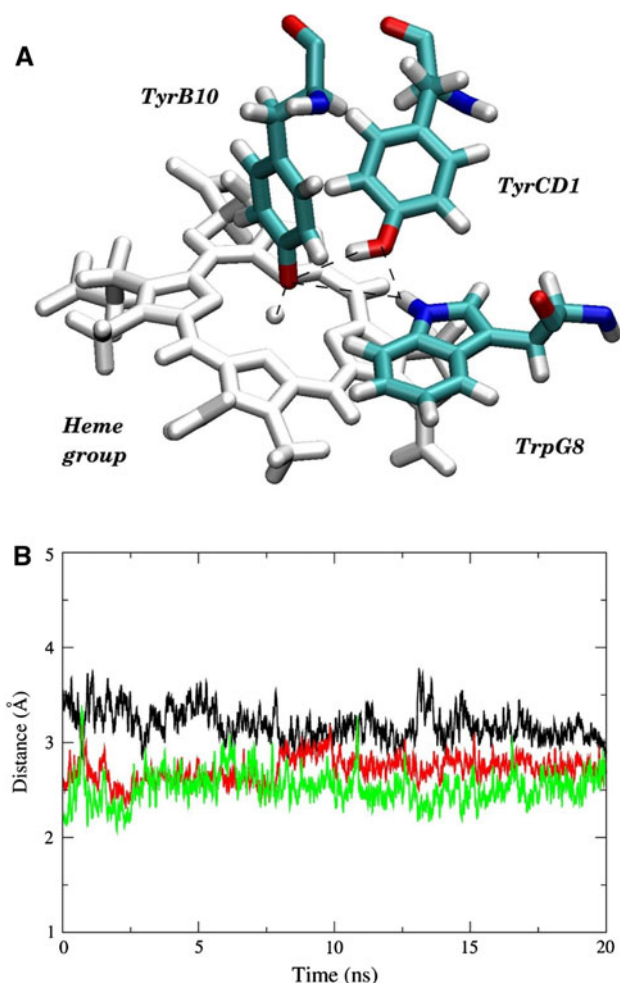


**Fig. 6** *Ph-2/2HbO* with TyrB10-O<sup>-</sup> coordinated to the heme iron. **a** Schematic representation of the distal site of the protein, showing the coordinated TyrB10-O<sup>-</sup> stabilized by H-bonds with both TyrCD1 and TrpG8. Interaction between TyrCD1 and TrpG8 is also indicated. **b** Time evolution of selected distances between the TyrB10-O<sup>-</sup> atom with the indole N $\epsilon$  proton of TrpG8 (black), the TyrB10-O<sup>-</sup> atom with the hydroxylic proton of TyrCD1 (red), and the indole N $\epsilon$  proton of TrpG8 with the hydroxylic oxygen of TyrCD1 (green)

Moreover, the kinetic behavior observed for azide binding indicates the presence of three reacting forms, suggesting that the HS and LS hexacoordinated forms do not interchange quickly. The faster component displays a fairly fast dissociation rate (likely corresponding to the hexacoordinated HS species with a water molecule coordinated to the heme), even faster than those reported for water dissociation from Mbs [47, 48]. The slight redshift of the CT1 in *Ph-2/2HbO* compared to Mbs [48] suggests that this feature might be accounted for by the lack of a H-bond between the water molecule and distal residues of the heme pocket. Thus, in Mbs the water molecule is H-bonded with distal His that stabilizes the Fe(III)–H<sub>2</sub>O interaction, slowing down its dissociation rate; this H-bonding is not present (or

is much weaker) in the distal pocket of *Ph-2/2HbO*, rendering the water dissociation much faster. The slower bimolecular component is characterized by a very slow dissociation rate of the hexacoordinating ligand (Table 2), a behavior that is in keeping with a stronger interaction between this endogenous ligand (possibly one of the two Tyr residues, TyrCD1 or TyrB10) and the heme. The slowest azide-independent rate constant could instead correspond to a form where the hexacoordination by Tyr is stabilized by the H-bond network mentioned above.

All of the results presented here indicate that *Ph-2/2HbO* displays unique adaptive structural properties conferring higher flexibility to the protein that may facilitate the functioning in the cold by providing greater freedom for the correct positioning of ligand(s), even at low temperatures. Alternatively, the multiple hexacoordinated states may account for multiple functions in the same molecule. Hexacoordinated Hbs are observed in unicellular eukaryotes [17], plants [49], invertebrates [50], and in some tissues of higher vertebrates [48, 51], but only a few cases have been examined and reported in the literature for bacterial 2/2 Hbs [52–55]. The physiological role of these hexacoordinated Hbs is not well understood. Several roles have been suggested for them: oxygen scavengers under hypoxic conditions [56, 57], terminal oxidases [58], oxygen sensors [59, 60], and that they are involved in nitrogen monoxide metabolism [61].

The discovery of hexacoordinated neuroglobin and cytoglobin in man and other vertebrates suggests that in different phylogenetically unrelated groups of organisms, these proteins may be endowed with a common function that is mainly linked to the production of reactive oxygen species (ROS) and nitrogen monoxide. The sixth ligand is usually provided by the imidazole side chain of a His, normally present at the distal site of the heme pocket, and only a few examples have been reported where TyrB10 has been found to act as the sixth ligand at the iron site in the ferrous [55] and ferric states [16, 20]. Indeed, the amino-acid sequence, the MD simulations, and the spectroscopic data of *Ph-2/2HbO* indicate that the distal ligands of the LS ferric form can be either TyrCD1 or TyrB10.

In summary, the existence of several similar LS forms suggests that the protein has a high degree of structural flexibility that gives rise to conformers which may be distinguished by the strength of the H-bond interactions with the Tyr ligand and/or the disposition of the H-bonding partner.

**Acknowledgments** This work was financially supported by grants from the Italian Ministero dell’Istruzione, dell’Università e della Ricerca (MIUR) (PRIN 2007SFZXXZ7, “Structure, function and evolution of heme proteins from Arctic and Antarctic marine organisms: cold adaptation mechanisms and acquisition of new functions”) to G.S., M.C. and C.V., by the research programme ‘rientro dei

cervelli' to M.F., and by the Italian National Programme for Antarctic Research (PNRA). It is included in the framework of the SCAR program Evolution and Biodiversity in the Antarctic (EBA), and in that of the project CAREX (Coordination Action for Research Activities on Life in Extreme Environments), European Commission FP7 call ENV.2007.2.2.1.6. Support from the ANPCyT (PICT 06-25667), the EU FP7 programme INQUIMAE-CONICET, and the University of Buenos Aires (to L.B., M.A.M. and D.A.E.) is gratefully acknowledged. The authors thank the Centre de Ressources Biologiques de l'Institut Pasteur, Paris (<http://www.crbip.pasteur.fr>) for supplying the *P. haloplanktis* CIP 108707 strain.

## References

- Deming JW (2002) *Curr Opin Microbiol* 5:301–309
- Médigue C, Krin E, Pascal G, Barbe V, Bernsel A, Bertin PN, Cheung F, Cruveiller S, D'Amico S, Duilio A, Fang G, Feller G, Ho C, Mangelot S, Marino G, Nilsson J, Parrilli E, Rocha EP, Rouy Z, Sekowska A, Tutino ML, Vallenet D, von Heijne G, Danchin A (2005) *Genome Res* 15:1325–1335
- Giordano D, Parrilli E, Dettai A, Russo R, Barbiero G, Marino G, Lecointre G, di Prisco G, Tutino ML, Verde C (2007) *Gene* 398:69–77
- Nicoletti FP, Comandini A, Bonamore A, Boechi L, Boubeta F, Feis A, Smulevich G, Boffi A (2010) *Biochemistry* 49:2269–2278
- Kraus DW, Wittenberg JB, Lu JF, Peisach J (1990) *J Biol Chem* 265:16054–16059
- Brittain T, Yosaatmadja Y, Henty K (2008) *IUBMB Life* 60:135–138
- Ferri T, Poscia A, Santucci R (1998) *Bioelectrochem Bioenerg* 44:177–181
- Nicoletti FP, Thompson M, Howes BD, Franzen S, Smulevich G (2010) *Biochemistry* 49:1903–1912
- Sali A, Blundell TL (1993) *J Mol Biol* 234:779–815
- Tatusova TA, Madden TL (1999) *FEMS Microbiol Lett* 174:247–250
- Thompson JD, Gibson TJ, Plewniak F, Jeanmougin F, Higgins DG (1997) *Nucleic Acids Res* 25:4876–4882
- Pearlman DA, Case DA, Caldwell JW, Ross WS, Cheatham TE, Debolt S, Ferguson D, Seibel G, Kollman P (1995) *Comput Phys Commun* 91:1–41
- Boechi L, Martí MA, Milani M, Bolognesi M, Luque FJ, Estrin DA (2008) *Proteins* 73:372–379
- Boechi L, Manez PA, Luque FJ, Martí MA, Estrin DA (2010) *Proteins* 78:962–970
- Martí MA, Capece L, Bidon-Chanal A, Crespo A, Guallar V, Luque FJ, Estrin DA (2008) *Methods Enzymol* 437:477–498
- Milani M, Pesce A, Nardini M, Ouellet H, Ouellet Y, Dewilde S, Bocedi A, Ascenzi P, Guertin M, Moens L, Friedman JM, Wittenberg JB, Bolognesi M (2005) *J Inorg Biochem* 99:97–109
- Wittenberg JB, Bolognesi M, Wittenberg BA, Guertin M (2002) *J Biol Chem* 277:871–874
- Vuletich DA, Lecomte JT (2006) *J Mol Evol* 62:196–210
- Antonini E, Brunori M (1971) Hemoglobin and myoglobin in their reactions with ligands. North-Holland, Amsterdam
- Das TK, Couture M, Lee HC, Peisach J, Rousseau DL, Wittenberg BA, Wittenberg JB, Guertin M (1999) *Biochemistry* 38:15360–15368
- Caillet-Saguy C, Turano P, Piccioli M, Lukat-Rodgers GS, Czjzek M, Guigliarelli B, Izadi-Pruneyre N, Rodgers KR, Delepierre M, Lecroisey A (2008) *J Biol Chem* 283:5960–5970
- Alontaga AY, Rodriguez JC, Schonbrunn E, Becker A, Funke T, Yuki ET, Hayashi T, Stobaugh J, Moenne-Loccoz P, Rivera M (2009) *Biochemistry* 48:96–109
- Smulevich G, Miller MA, Kraut J, Spiro TG (1991) *Biochemistry* 30:9546–9558
- Smulevich G, Wang Y, Edwards SL, Poulos TL, English AM, Spiro TG (1990) *Biochemistry* 29:2586–2592
- Smulevich G, Paoli M, Burke JF, Sanders SA, Thorneley RNF, Smith AT (1994) *Biochemistry* 33:7398–7407
- Smulevich G, Feis A, Focardi C, Tams J, Welinder KG (1994) *Biochemistry* 33:15425–15432
- Que L (1988) Metal-tyrosinate proteins. In: Spiro TG (ed) *Biological applications of Raman spectroscopy*, vol 3. Wiley, New York, pp 491–521
- Hu S, Smith KM, Spiro TG (1996) *J Am Chem Soc* 118:12638–12646
- Nagai K, Kagimoto T, Hayashi A, Taketa F, Kitagawa T (1983) *Biochemistry* 22:1305–1311
- Nagai M, Yoneyama Y, Kitagawa T (1989) *Biochemistry* 28:2418–2422
- Adachi S, Nagano S, Ishimori K, Watanabe Y, Morishima I, Egawa T, Kitagawa T, Makino R (1993) *Biochemistry* 32:241–252
- Liu Y, Moenne-Loccoz P, Hildebrand DP, Wilks A, Loehr TM, Mauk AG, Ortiz de Montellano PR (1999) *Biochemistry* 38:3733–3743
- Eakanunkul S, Lukat-Rodgers GS, Sumithran S, Ghosh A, Rodgers KR, Dawson JH, Wilks A (2005) *Biochemistry* 44:13179–13191
- Aki Y, Nagai M, Nagai Y, Imai K, Aki M, Sato A, Kubo M, Nagatomo S, Kitagawa T (2010) *J Biol Inorg Chem* 15:147–158
- Howes BD, Feis A, Indiani C, Marzocchi MP, Smulevich G (2000) *J Biol Inorg Chem* 5:227–235
- Blumberg WE, Peisach J (1971) Probes of structure and function of macromolecules and membranes. In: Chance B, Yonetani T, Mildvan AS (eds) *Probes of enzymes and hemoproteins*. Academic, New York, pp 215–228
- Brautigan DL, Feinberg BA, Hoffman BM, Margolias E, Peisach J, Blumberg WE (1977) *J Biol Chem* 252:574–582
- Walker FA, Huynh BH, Scheidt WR, Osvath SR (1986) *J Am Chem Soc* 108:5288–5297
- Izadi N, Henry Y, Haladjian J, Goldberg ME, Wandersman C, Delepierre M, Lecroisey A (1997) *Biochemistry* 36:7050–7057
- Arnoux P, Haser R, Izadi N, Lecroisey A, Delepierre M, Wandersman C, Czjzek M (1999) *Nat Struct Biol* 6:516–520
- Nicoletti FP, Howes BD, Fittipaldi M, Fanali G, Fasano M, Ascenzi P, Smulevich G (2008) *J Am Chem Soc* 130:11677–11688
- Teixeira M, Campos AP, Aguiar AP, Costa HS, Santos H, Turner DL, Xavier AV (1993) *FEBS Lett* 317:233–236
- Palmer G (1985) *Biochem Soc Trans* 13:548–560
- Taylor CPS (1977) *Biochim Biophys Acta* 491:137–149
- Lama A, Pawaria S, Bidon-Chanal A, Anand A, Gelpi JL, Arya S, Martí M, Estrin DA, Luque FJ, Dikshit KL (2009) *J Biol Chem* 284:14457–14468
- Parrilli E, Giuliani M, Giordano D, Russo R, Marino G, Verde C, Tutino ML (2010) *Biochimie* 92:1003–1009
- Coletta M, Angeletti M, De Sanctis G, Cerroni L, Giardina B, Amiconi G, Ascenzi P (1996) *Eur J Biochem* 235:49–53
- De Sanctis G, Petrella G, Ciaccio C, Feis A, Smulevich G, Coletta M (2007) *Biophys J* 93:2135–2142
- Watts RA, Hunt PW, Hvitved AN, Hargrove MS, Peacock WJ, Dennis ES (2001) *Proc Natl Acad Sci USA* 98:10119–10124
- Dewilde S, Ebner B, Vinck E, Gilany K, Hankeln T, Burmester T, Kreiling J, Reinisch C, Vanfleteren JR, Kiger L, Marden MC, Hundahl C, Fago A, Van Doorslaer S, Moens L (2006) *J Biol Chem* 281:5364–5372
- Pesce A, Dewilde S, Nardini M, Moens L, Ascenzi P, Hankeln T, Burmester T, Bolognesi M (2004) *Micron* 35:63–65

52. Visca P, Fabozzi G, Petrucca A, Ciaccio C, Coletta M, De Sanctis G, Bolognesi M, Milani M, Ascenzi P (2002) *Biochem Biophys Res Commun* 294:1064–1070
53. Scott NL, Falzone CJ, Vuletich DA, Zhao J, Bryant DA, Lecomte JT (2002) *Biochemistry* 41:6902–6910
54. Falzone CJ, Christie Vu B, Scott NL, Lecomte JT (2002) *J Mol Biol* 324:1015–1029
55. Razzera G, Vernal J, Baruh D, Serpa VI, Tavares C, Lara F, Souza EM, Pedrosa FO, Almeida FC, Terenzi H, Valente AP (2008) *J Biol Inorg Chem* 13:1085–1096
56. Burmester T, Weich B, Reinhardt S, Hankeln T (2000) *Nature* 407:520–523
57. Burmester T, Ebner B, Weich B, Hankeln T (2002) *Mol Biol Evol* 19:416–421
58. Sowa AW, Guy PA, Sowa S, Hill RD (1999) *Acta Biochim Pol* 46:431–445
59. Hargrove MS, Brucker EA, Stec B, Sarath G, Arredondo-Peter R, Klucas RV, Olson JS, Phillips GN (2000) *Structure* 8:1005–1014
60. Kriegl JM, Bhattacharyya AJ, Nienhaus K, Deng P, Minkow O, Nienhaus GU (2002) *Proc Natl Acad Sci USA* 99:7992–7997
61. Smagghe BJ, Trent JT III, Hargrove MS (2008) *PloS ONE* 3:e2039

## Research Communication

# Ligand- and Proton-linked Conformational Changes of the Ferrous 2/2 Hemoglobin of *Pseudoalteromonas haloplanktis* TAC125

Daniela Giordano<sup>1</sup>, Roberta Russo<sup>1</sup>, Chiara Ciaccio<sup>2,3</sup>, Barry D. Howes<sup>4</sup>, Guido di Prisco<sup>1</sup>, Michael C. Marden<sup>5</sup>, Gaston Hui Bon Hoa<sup>5</sup>, Giulietta Smulevich<sup>4</sup>, Massimo Coletta<sup>2,3</sup> and Cinzia Verde<sup>1</sup>

<sup>1</sup>*Institute of Protein Biochemistry, CNR, Naples, Italy*

<sup>2</sup>*Department of Experimental Medicine and Biochemical Sciences, Università di Roma Tor Vergata, Rome, Italy*

<sup>3</sup>*Interuniversity Consortium for the Research on the Chemistry of Metals in Biological Systems, Bari, Italy*

<sup>4</sup>*Dipartimento di Chimica “Ugo Schiff”, Università di Firenze, Sesto Fiorentino (FI), Italy*

<sup>5</sup>*INSERM, U779, 78 rue du Général Leclerc, Le Kremlin Bicêtre, France*

---

### Summary

The spectroscopic and ligand-binding properties of a 2/2 globin from the Antarctic bacterium *Pseudoalteromonas haloplanktis* TAC125 have been studied in the ferrous state. It displays two major conformations characterized by CO-association rates that differ by a factor of 20, with relative fractions that depend on pH. A dynamic equilibrium is found between the two conformations, as indicated by an enhanced slower phase when lower CO levels were used to allow a longer time to facilitate the transition. The deoxy form, in the absence of external ligands, is a mixture of a predominant six-coordinate low spin form and a five-coordinate high-spin state; the proportion of low spin increasing at alkaline pH. In addition, at temperatures above the physiological temperature of 1 °C, an enhanced tendency of the protein to oxidize is observed. © 2011 IUBMB

IUBMB *Life*, 63(7): 566–573, 2011

---

**Keywords** Antarctic; hemoglobin; ligand binding; resonance Raman.

### INTRODUCTION

The hemoglobin (Hb) superfamily is composed of three phylogenetically distinct lineages (1). Two of these lineages include the proteins characterized by the 3/3  $\alpha$ -helical myoglobin (Mb)-like structure. The third lineage comprises “truncated” Hbs displaying the 2/2 topology (2). Although the function of 2/2 Hbs is not well understood, it has been proposed that they may be involved in intracellular O<sub>2</sub> storage or transfer, binding and detoxification of reactive nitrogen and O<sub>2</sub> species, enzymatic function(s), O<sub>2</sub> sensing (3, 4), and sulfide binding (5).

Additional Supporting Information may be found in the online version of this article.

Received 11 February 2011; accepted 7 April 2011

Address correspondence to: Cinzia Verde, Institute of Protein Biochemistry, CNR, Via Pietro Castellino 111, I-80131 Naples, Italy. Tel: +39 0816132710. Fax: +39 0816132710. E-mail: c.verde@ibp.cnr.it

ISSN 1521-6543 print/ISSN 1521-6551 online  
DOI: 10.1002/iub.492

A phylogenetic analysis led to the partition of 2/2 Hbs into three groups designated I or N, II or O, and III or P (3). Group II is by far the most populated, and some crystal structures of 2/2 Hbs belonging to group II [*Bacillus subtilis* (6), *Thermobifida fusca* (7), *Geobacillus stearothermophilus* (8), and *Mycobacterium tuberculosis* (9, 10)] are already available.

Multiple genes encoding 2/2 Hbs have been identified in the genome of the Antarctic bacterium *Pseudoalteromonas haloplanktis* TAC125 (11, 12).

Recent results demonstrate that the inactivation of the group II 2/2 Hb encoded by the *PSHAa0030* gene (hereafter named *Ph-2/2HbO*) makes the mutant bacterial strain sensitive to high-O<sub>2</sub> levels, hydrogen peroxide, and nitrosating agents (13). However, to date, the function of this protein is unknown.

In common with other group II 2/2 Hbs, the distal heme cavity of *Ph-2/2HbO* is characterized by the presence of a Trp residue in position G8 and two tyrosyl residues, TyrCD1 and TyrB10. However, unlike other bacterial Hbs, the ferric state, in addition to an aquo six-coordinated high-spin (HS) form, has multiple six-coordinated low-spin (LS) forms, where either TyrCD1 or TyrB10 can likely coordinate the heme iron (14).

In this work, we report the results obtained by spectroscopic and kinetic measurements on the Fe(II) forms of *Ph-2/2HbO*. In the pH range between pH 5.6 and 11.0, the protein is a mixture of 5cHS and 6cLS heme, the latter becoming dominant at alkaline pH.

### EXPERIMENTAL PROCEDURES

#### Protein Expression and Purification

The gene *PSHAa0030*-encoding *Ph-2/2HbO* was cloned and the recombinant protein expressed and purified as previously described (12, 14).

### Sample Preparation

The ferrous samples were prepared by adding 2  $\mu\text{l}$  of sodium dithionite (10 mg  $\text{ml}^{-1}$ ) to 50  $\mu\text{l}$  of deoxygenated buffered solution of Met-Hb. The carbomonoxy complex was prepared by flushing Met-Hb with nitrogen, then with CO, and reducing the protein as described above (15). The protein concentration of all samples, for both resonance Raman (RR) and electronic-absorption spectroscopy, was 30  $\mu\text{M}$  on a heme basis.

### Spectroscopy

Electronic-absorption spectra, measured with a double-beam Cary 5 spectrophotometer (Varian, Palo Alto, CA) using a 5-mm NMR tube and a 600  $\text{nm min}^{-1}$  scan rate, were recorded both before and after the RR measurements. No sample degradation was observed under the experimental conditions employed. The RR spectra were obtained using a 5-mm NMR tube and by excitation with the 413.1-nm line of a Kr<sup>+</sup> laser (Coherent, Innova 300 C, Santa Clara, CA) and the 441.6-nm line of a HeCd laser (Kimmon IK4121R-G). Backscattered light from a slowly rotating NMR tube was collected and focussed into a triple spectrometer, described in detail previously (15). The spectral resolution of the RR spectra cited in the figure captions is that calculated theoretically on the basis of the optical properties of the spectrometer. However, for the moderately broad experimental RR bands observed in this study (*ca.* 10  $\text{cm}^{-1}$ ), the effective spectral resolution will be lower in general.

All RR measurements were repeated several times under the same conditions to ensure reproducibility. To improve the signal/noise ratio, a number of spectra were accumulated and summed only if no spectral differences were noted. The RR spectra were calibrated with indene and  $\text{CCl}_4$  as standards to an accuracy of 1  $\text{cm}^{-1}$  for intense isolated bands.

### Kinetics of Ligand Binding and Dissociation by Stopped Flow

Kinetics of CO dissociation from CO-bound *Ph-2/2HbO* and of CO association to *Fe(II)-Ph-2/2HbO* were carried out at 20 °C and between pH 6.0 and 11.0, employing a rapid-mixing stopped-flow apparatus (Applied Photophysics, Salisbury, UK) with time resolution of 1 ms. CO-dissociation kinetics were carried out by mixing a CO-saturated *Fe(II)-Ph-2/2HbO* solution (final concentration,  $5.0 \times 10^{-6}$  M), in the presence of sodium dithionite (final concentration,  $1.1 \times 10^{-2}$  M), with a degassed buffer solution, containing  $\text{NaNO}_2$  (final concentration,  $5.0 \times 10^{-3}$  M; ref. 16).  $\text{O}_2$ -dissociation kinetics were carried out at pH 7.0 by first mixing deoxygenated protein (in the presence of 5 mM sodium dithionite) with the oxygenated buffer and then following the deoxygenation of *Fe(II)-O<sub>2</sub>-Ph-2/2HbO* (*i.e.*, oxygen pulse, see ref. 16). CO-association kinetics were undertaken over the same pH range by mixing unliganded *Fe(II)-Ph-2/2HbO* solution (final concentration,  $3.0 \times 10^{-6}$  M), in the presence of sodium dithionite, with a degassed buffer solution equilibrated with CO (the final concentration ranged between  $1.5 \times 10^{-5}$  M and  $5.0 \times 10^{-4}$  M; ref. 16).

Kinetic progress curves of ligand dissociation–association to *Fe(II)-Ph-2/2HbO* have been analyzed according to Eq. (1):

$$A_{\text{obs}} = A_0 + \sum_{i=1}^{i=n} \Delta A_i \cdot \exp(-i k_{\text{obs}} \cdot t) \quad (1)$$

where  $A_{\text{obs}}$  is the observed absorbance at 421 nm at time  $t$ ,  $A_0$  is the absorbance at  $t = 0$ ,  $n$  is the number of exponentials,  $\Delta A_i$  is the absorbance change associated to the  $i$ -th exponential,  $i k$  is the rate constant of the  $i$ -th exponential (either CO association or ligand dissociation rate constant). The same analytical approach has been applied to the kinetics of  $\text{O}_2$  dissociation at 414 nm.

The CO concentration dependence of  $k_{\text{obs}}$  was analyzed according to:

$$k_{\text{obs}} = k_{\text{on}} \cdot [\text{CO}] + k_{\text{off}} \quad (2)$$

where  $k_{\text{obs}}$  is the observed rate constant at a given CO concentration,  $k_{\text{on}}$  is the second-order CO association rate constant and  $k_{\text{off}}$  is the first-order CO dissociation rate constant.

The kinetic-energy barriers were determined on the basis of the temperature dependence of rate constant(s) (*i.e.*,  $k$ ) according to:

$$\frac{\partial \ln(k)}{\partial(1/T)} = -\frac{E_a}{R} \quad (3a)$$

where  $T$  is temperature in K,  $R$  is the gas constant and  $E_a$  is the Arrhenius activation energy. Further, the rate constant  $k$  is directly related to the activation free energy according to the following equation:

$$\ln k = \ln(\kappa T/h) - \Delta G^\ddagger/RT \quad (3b)$$

where  $\kappa$  is the Boltzmann's constant,  $h$  is the Planck's constant, and other parameters are the same as in Eq. (3a). It should be noted that, in  $\ln k$ , units of  $k$  are per sec. Thus, because  $\Delta H^\ddagger = E_a - RT$ , knowing the rate constant  $k$  at a given  $T$  and the temperature dependence of  $k$ , we can also determine the activation entropy according to:

$$T\Delta S^\ddagger = \Delta H^\ddagger - \Delta G^\ddagger \quad (3c)$$

### CO-bimolecular Recombination Rates by Laser Flash-photolysis

The kinetics of ligand binding to the heme iron was also measured by the laser flash-photolysis technique. The photolysis setup consists of a 10-ns ND:YAG (neodymium-doped yttrium aluminum garnet) laser, delivering pulses of 120 mJ at 532 nm (Quantel, France) and a detection beam. The standard detection wavelength was 436 nm, in the Soret band. The protein concen-

tration was 5  $\mu\text{M}$  on a heme basis. Samples were in 100 mM buffer in the pH range from 6.0 to 11.0, at 25  $^\circ\text{C}$ , and were equilibrated under CO (0.01, 0.1, or 1 atm) in 1-cm optical-pathlength cuvettes. Additional CO levels were obtained by mixing one of the standards (0.01, 0.1, or 1 atm CO) with nitro-

gen (17). A typical kinetic curve was obtained from the average of 10 measurements, with at least 4 sec lapsing between photolysis pulses to allow sample recovery. Before and after laser exposure, the samples were checked by visible absorption spectra. Simulation of a series of curves, using Eqs. (1) and (2), at different CO concentrations allows a determination of the CO on-rate.

Simulations were made with up to three phases, but only two dominant phases were retained, as the third component was small in amplitude and showed no clear pH or temperature dependence. The kinetic data were reproducible; the main error of about 20% is due to separation of the phases.

## RESULTS AND DISCUSSION

### Spectroscopy

The electronic-absorption spectrum of ferrous *Ph-2/2HbO*, in the pH range 5.8–10.9 at 25  $^\circ\text{C}$ , varied as a function of pH. In particular, the spectra were characterized by a mixture of a predominant 6cLS heme (Soret band at 421 and Q bands at 528 and 559 nm) and a 5cHS form (shoulder at about 440 nm; Fig. 1A). The fraction of the LS form increased with increasing pH from 5.8 to 11.0 (Fig. 1A, traces a–c).

Accordingly, the RR spectra in the high-frequency region, obtained in resonance with the Soret maximum at 440 nm (Fig. 1B, traces a–c) showed core size marker bands typical of a

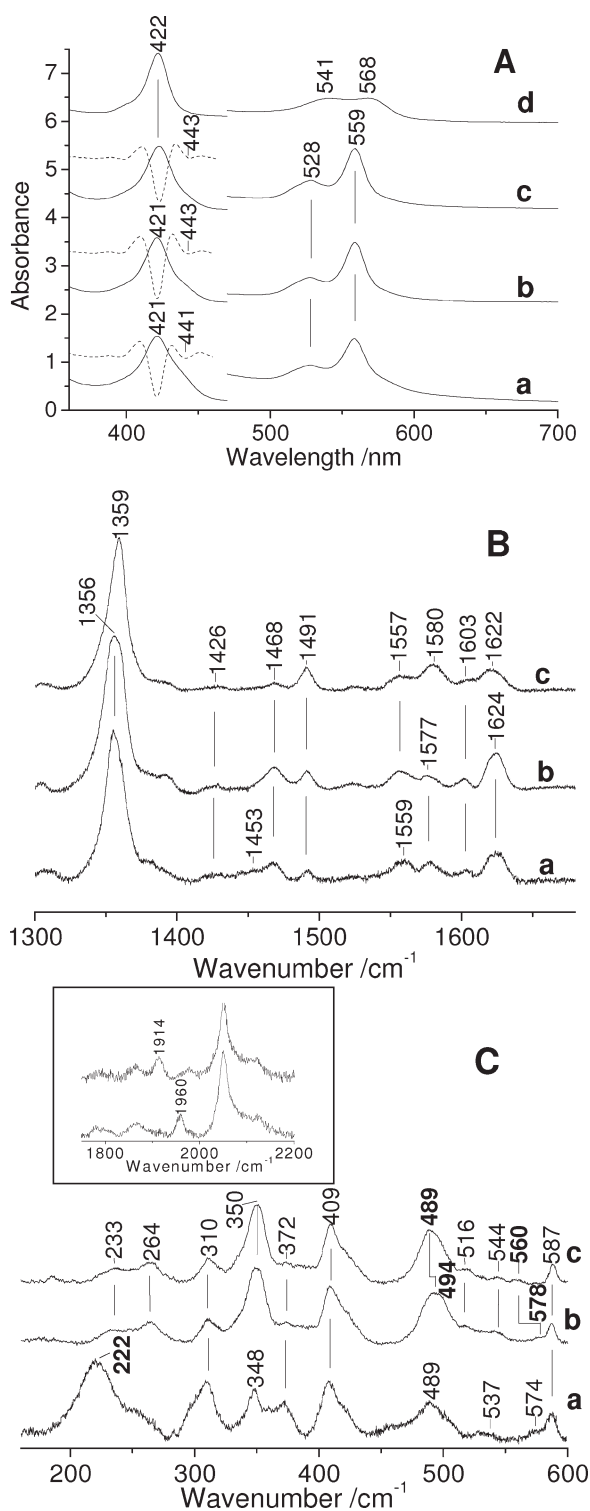


**Figure 1.** (A) Absorption spectra of the deoxy form of *Ph-2/2HbO* at pH 5.8 in 0.1 M MES (a), pH 7.6 in 0.1 M Tris-HCl (b), and pH 11.0 in 0.1 M CAPS (c), and the CO complex at pH 5.8 in 0.1 M MES (d); the spectrum of the CO complex is invariant in the pH range 5.8–10.9. The second derivative and absorption spectra are shown superimposed on the Soret region. The visible region was expanded fivefold. Spectra were shifted along the ordinate axis to allow better visualization. (B) RR spectra of the deoxy form recorded with the 441.6-nm excitation wavelength in the high-wavenumber region at pH 5.8 (a), 7.6 (b) and 11.0 (c). Experimental conditions: 15 mW laser power at the sample; 1  $\text{cm}^{-1}$  spectral resolution; average of two spectra with 5-min integration time (pH 5.6), average of two spectra with 10-min integration time (pH 7.6), 10-min integration time (pH 11.0). (C) RR spectra of the deoxy form (a) and its CO complex for  $^{12}\text{CO}$  (b) and  $^{13}\text{CO}$  (c) recorded with the 441.6- and 413.1-nm excitation wavelengths, respectively, in the low-wavenumber region at pH 7.6; the spectrum of the CO complex is invariant in the pH range 5.8–11.0. The inset shows the  $\nu(\text{CO})$  stretching mode at 1960  $\text{cm}^{-1}$ , which shifts to 1914  $\text{cm}^{-1}$  for the  $^{13}\text{CO}$  adduct. A cylindrical lens was used to focus the laser beam on the sample for the CO adduct. Experimental conditions: 1  $\text{cm}^{-1}$  spectral resolution; average of four spectra with 10-min integration time; laser power at the sample 15 mW (deoxy), 2 mW (CO adduct).

5cHS form ( $\nu_3$  at 1,468  $\text{cm}^{-1}$  and  $\nu_2$  at 1,559  $\text{cm}^{-1}$ ), predominant at acid pH, and a 6cLS form ( $\nu_3$  at 1,491  $\text{cm}^{-1}$ ,  $\nu_2$  at 1,580  $\text{cm}^{-1}$ ) which markedly increased at alkaline pH. Therefore, the low-frequency region of the RR spectra (Fig. 1C, trace a) yields information about the Fe-proximal His bond strength from the frequency of the corresponding  $\nu(\text{Fe-His})$  stretching mode, which is active only in the ferrous 5cHS form upon excitation in the Soret absorption band (18, 19). The intense band at 222  $\text{cm}^{-1}$ , whose intensity decreases at alkaline pH, was assigned to the  $\nu(\text{Fe-Im})$  stretching mode. Its frequency is similar to that of Mb.

A definitive determination of the nature of the sixth ligand is not possible, however, based on the results previously obtained for the ferric form (14), we suggest that either the TyrCD1-O<sup>-</sup> or TyrB10-O<sup>-</sup> are coordinated to the heme Fe(II) atom. In fact, although His is the most common residue which coordinates to the heme Fe, Tyr was found to coordinate in the Hb of *Herbaspirillum seropedicae* (20) and *Chlamydomonas* (21).

Upon addition of CO, the UV-visible absorption spectra (Fig. 1A, trace d; with Soret and Q bands at 422, 541, and 568 nm, respectively) and the high-frequency RR spectra obtained with 413.1 nm excitation (data not shown) were characteristic of the 6cLS form. The spectra did not change between pH 5.8 and 10.9. In the low-frequency region RR spectrum (Fig. 1C, traces b and c) two isotope-sensitive peaks were observed. The band at 494  $\text{cm}^{-1}$ , which shifted to 489  $\text{cm}^{-1}$  for the <sup>13</sup>CO complex, was assigned to a  $\nu(\text{Fe-C})$  stretching mode, and the band at 578  $\text{cm}^{-1}$ , which shifted to 560  $\text{cm}^{-1}$ , was assigned to the corresponding  $\delta(\text{Fe-C-O})$  bending mode. Accordingly, it was possible to identify one  $\nu(\text{CO})$  stretching mode at 1,960  $\text{cm}^{-1}$  (inset Fig. 1C), which shifted to 1,914  $\text{cm}^{-1}$  upon isotopic substitution. Therefore, in agreement with the isotopic (<sup>12</sup>CO-<sup>13</sup>CO) difference spectra (Supporting Information, Fig. S1), only one CO conformer was detected in the RR spectra of the CO complex of *Ph-2/2HbO*.

The presence of a bending mode is an indicator of off-axis interactions with nearby groups, which could be steric in character, but are more likely to be of an electrostatic nature. In addition, CO is an excellent probe for investigating the distal cavity of heme proteins because back-donation from the Fe  $d\pi$  to the CO $\pi^*$  orbitals is modulated by polar interactions (22). The electrostatic field generated by the polar distal pocket amino acids alters the electron distribution in the FeCO unit, changing the order of the C-O bond (23). The correlation plot between the  $\nu(\text{FeC})$  and  $\nu(\text{CO})$  frequencies of several heme proteins (Supporting Information, Fig. S2) suggests that the observed frequencies of the *Ph-2/2HbO* CO complex could be characteristic of a CO conformer in which polar interactions with the surrounding residues of the distal cavity are absent or very weak. However, our previous results on the ferric form showed that the distal cavity is characterized by the presence of a Trp in position G8 and two tyrosyl residues (TyrCD1 and TyrB10). Moreover, the ferric state, in addition to the aquo six-coordinated high-spin form, showed multiple six-coordinated

low-spin forms, where either TyrCD1 or TyrB10 can likely coordinate the iron. Therefore, an alternative explanation is that the nonbonding lone pair of the hydroxyl group of one of the two Tyr may be oriented toward the CO ligand, giving rise to negative polarity that weakens the back-bonding from Fe to CO, as previously suggested for the *T. fusca* WG8F mutant ( $\nu(\text{Fe-C})$  at 491  $\text{cm}^{-1}$ ,  $\nu(\text{CO})$  at 1,967  $\text{cm}^{-1}$ ) and the human Mb V68T mutant ( $\nu(\text{Fe-C})$  491  $\text{cm}^{-1}$ ,  $\nu(\text{CO})$  at 1,961  $\text{cm}^{-1}$ ; Supporting Information, Fig. S2; refs. 15, 22, and 24).

### Kinetics of CO Dissociation

CO dissociation was characterized at all pH values by a two-exponential pattern (Fig. 2A) with essentially pH-independent rates (but not the relative amplitudes), which ranged for the faster rate constant (*i.e.*,  $^f k_{\text{off}}$ ) around 1.0( $\pm$ 0.5)  $\text{sec}^{-1}$  and for the slower rate constant (*i.e.*,  $^s k_{\text{off}}$ ) around 0.03( $\pm$ 0.02)  $\text{sec}^{-1}$ . Interestingly, the percentage of the absorption amplitude for the faster CO dissociation process increased with pH, shifting from about 16% at pH 6.0 to about 39% at pH 11.0. This behavior suggested the coexistence of two CO-bound forms, whose relative percentage is pH-dependent, and the fast CO-dissociating form was stabilized by alkaline pH.

Furthermore, whereas  $^s k_{\text{off}}$  showed values closely similar to those observed in mammalian Mbs (16),  $^f k_{\text{off}}$  displayed an unusually fast CO-dissociation process, possibly reflecting drastic alteration of the heme coordination by proximal His (25). It is interesting to observe that in the 2/2HbO of *M. tuberculosis*, there is a biphasic CO-dissociation process, characterized by a  $^f k_{\text{off}}$  for the faster rate of  $4 \times 10^{-3} \text{sec}^{-1}$  and by a  $^s k_{\text{off}}$  for the slower rate of  $1.5 \times 10^{-3} \text{sec}^{-1}$  (26). These values are remarkably slower than those observed for the CO dissociation from Fe(II)-CO-*Ph-2/2HbO*, suggesting that in this case a conformational strain is exerted on the axial coordinating ligands. However, it should be outlined that values for  $k_{\text{off}}$  similar to those observed for fast values of Fe(II)-CO-*Ph-2/2HbO* have been reported for globin-coupled sensors from *Azotobacter vinelandii* (27) and *Geobacter sulfurreducens* (28).

### Kinetics of CO Association by Stopped Flow

CO association by stopped flow showed a single exponential pattern at all pH values (Fig. 2B), and the observed rate constant was linearly dependent on CO concentration (data not shown), allowing the bimolecular CO-binding rate constant to be obtained according to Eq. (2).

Values of  $k_{\text{on}}$  ( $=4.5(\pm 1.0) \times 10^5 \text{M}^{-1} \text{s}^{-1}$ ) were pH independent, and the best nonlinear least-squares fitting of data according to Eq. (2) was obtained imposing the value of  $^s k_{\text{off}}$  obtained at the corresponding pH. Therefore, starting from unliganded Fe(II)-*Ph-2/2HbO*, only one CO-binding species was observed, whereas the CO-bound form displayed the coexistence of two Fe(II)-CO-*Ph-2/2HbO* forms. Indeed, such behavior suggests the possibility of a ligand-linked equilibrium between two conformations, that is largely displaced in favor of

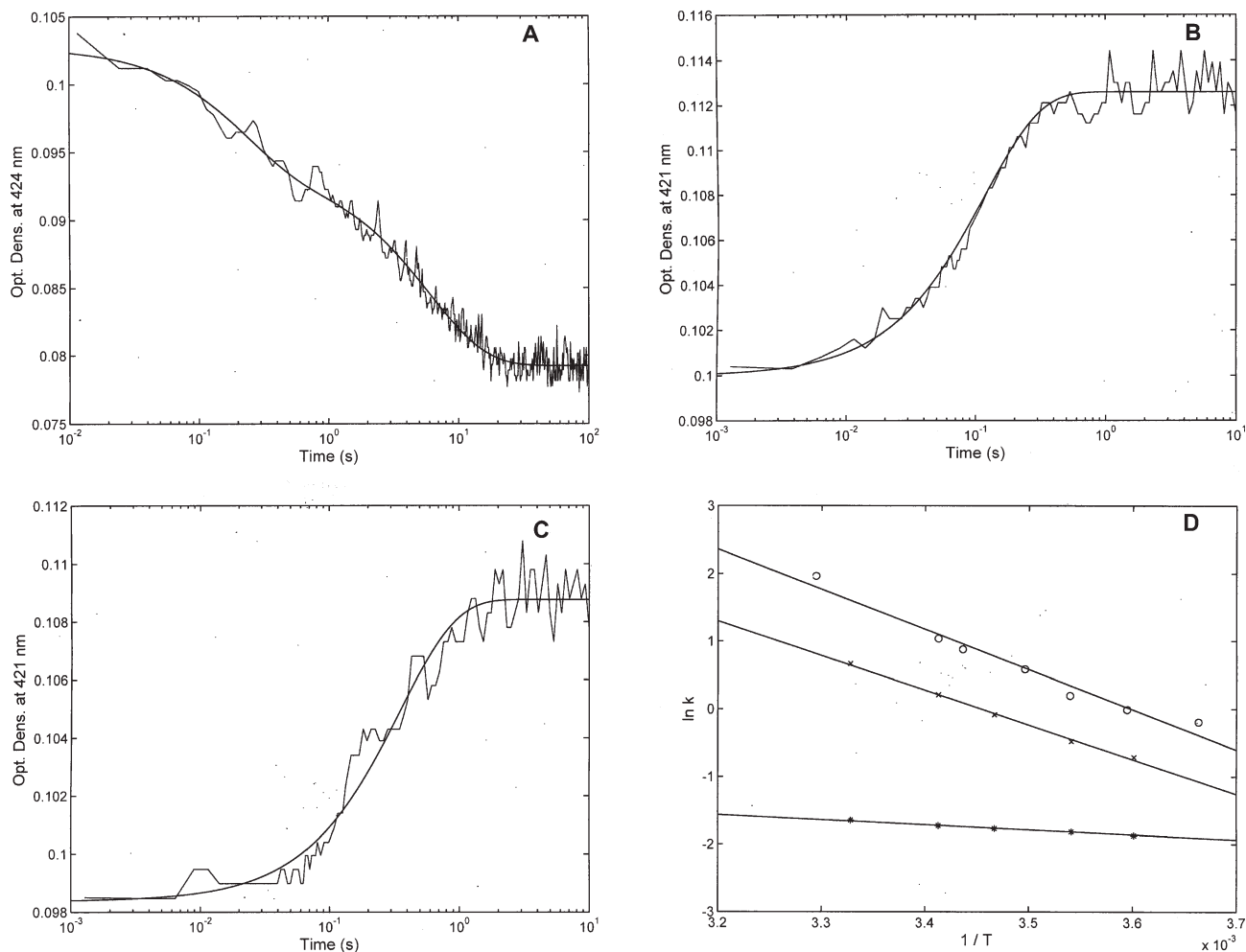


**Figure 2.** Kinetic progress curves for CO dissociation at 424 nm (A), CO association at 421 nm with final [CO] = 25  $\mu$ M (B) and O<sub>2</sub> dissociation at 421 nm (C). Continuous curves represent nonlinear least-squares fitting of data employing Eq. (1). Temperature dependence (D) of the kinetics of O<sub>2</sub> dissociation from Fe(II)-O<sub>2</sub>-Ph-2/2HbO (o), of CO dissociation from <sup>4</sup>Fe(II)-CO-Ph-2/2HbO (x) and from <sup>5</sup>Fe(II)-CO-Ph-2/2HbO (\*) at pH 7.0. Continuous lines are the nonlinear least-squares fitting of data according to Eq. (3a).

a single conformation (observed by stopped flow) in the unliganded form, whereas in the CO-bound form, they were both populated to a significant extent. It is worth remarking that in the case of *M. tuberculosis* 2/2HbO, it is possible to observe a biphasic CO-binding behavior, which is characterized by association rate constants slower than those observed for Fe(II)-Ph-2/2HbO (26). Further, also in the case of 2/2HbO from *Mycobacterium leprae*, which is six-coordinated (29), there is a very slow CO-binding rate constant. All these data seem to indicate that in the case of Fe(II)-Ph-2/2HbO, where there is a relatively fast bimolecular process, the six-coordination is characterized by a very weak bond energy, and the dissociation of the sixth endogenous axial ligand is much faster than the CO association rate. Therefore, the six-coordination observed in both the UV-Vis and RR deoxy spectra is quickly replaced by the exogenous ligand CO.

### CO-rebinding Kinetic Profile and Determination of $k_{on}$ CO Rates at Different pH

The CO-rebinding kinetics following nanosecond laser photolysis of Ph-2/2HbO were recorded as a function of CO concentration at different pH values and at 25 °C.

A two-exponential decay model was sufficient to explain the kinetic curves. With this model, two CO-dependent kinetic phases were obtained. Table 1 reports the CO-association constants obtained from Eq. (2) for the fast (*i.e.*,  $^f k_{on}$ ) and slow rates (*i.e.*,  $^s k_{on}$ ) at different pH values. The data demonstrate that  $^f k_{on}$  is very fast, in the range of  $10^7$  M<sup>-1</sup> sec<sup>-1</sup>, and close to that of human neuroglobin (17), whereas  $^s k_{on}$  is compatible to the rates obtained for Mb, in the range of  $10^5$  M<sup>-1</sup> sec<sup>-1</sup> (30). Therefore, CO binding observed by stopped flow refers to the slower population (Table 1, and above).

**Table 1**

CO-association rate constants obtained by laser-flash photolysis at different pH values at 25 °C (in parentheses the relative percentage of the two rate constants at 1 atm CO)<sup>a</sup>

pH	<sup>f</sup> k <sub>on</sub> (10 <sup>7</sup> M <sup>-1</sup> sec <sup>-1</sup> )	<sup>s</sup> k <sub>on</sub> (10 <sup>5</sup> M <sup>-1</sup> sec <sup>-1</sup> )
6.0	0.8 ± 0.1 (25)	4.6 ± 0.9 (75)
7.6	1.2 ± 0.2 (29)	6.9 ± 1.3 (71)
8.5	1.2 ± 0.2 (35)	7.8 ± 1.5 (65)
11.0	1.2 ± 0.2 (52)	5.8 ± 1.1 (48)

<sup>a</sup>Weighted standard deviations are determined from five different experiments.

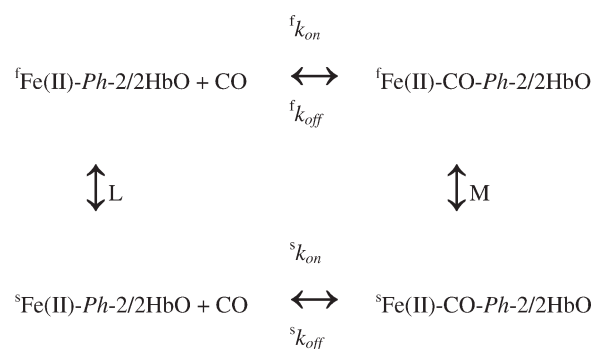
The CO-dependent kinetic phases are unusual for a 2/2 bacterial Hb of group II. In the 2/2HbO of *M. tuberculosis*, the slow phase is in the range of 10<sup>4</sup> M<sup>-1</sup> sec<sup>-1</sup>, whereas the fast phase is in the range of 10<sup>5</sup> M<sup>-1</sup> sec<sup>-1</sup> (26). Both proteins display two conformations that differ greatly in ligand association rate, suggesting that these proteins may switch between two distinct functional levels.

### pH Dependence of the Amplitude of the Fast and Slow Phases of CO Binding

Table 1 shows that the amplitude of the slow phase dominated (75%) at pH 6.0, but decreased to 48% at pH 11.0. There is apparently an equilibrium between the two conformations, and pH strongly modulates such an equilibrium. The amplitude of the fast phase increased with increasing pH, whereas the amplitude of the slow phase decreased in such a way that at pH 11.0, each conformation accounted for almost 50%.

On the basis of stopped flow and laser photolysis data, we can reasonably envisage the existence in Fe(II)-*Ph*-2/2HbO of a ligand- and pH-linked conformational transition between two tertiary arrangements. The unliganded form showed a large predominance of the slow-reacting form, which was characterized by the following kinetic parameters at pH 7.0 and 20 °C:  $k_{on} = 4.25(\pm 0.5) \times 10^5 \text{ M}^{-1} \text{ sec}^{-1}$  and  $k_{off} = 0.023 \pm 0.004 \text{ sec}^{-1}$ . Upon CO binding the equilibrium was partially displaced (in a pH-dependent fashion) toward a fast-reacting form (coexisting with the slow reacting forms predominant in the unliganded form), which was characterized by the following parameters at

pH 7.6 and 25 °C:  $k_{on} = 1.16(\pm 0.32) \times 10^7 \text{ M}^{-1} \text{ sec}^{-1}$  and  $k_{off} = 0.45 \pm 0.06 \text{ sec}^{-1}$ . This mechanism may be sketched according to the following Scheme



where <sup>f</sup>Fe(II)-*Ph*-2/2HbO and <sup>f</sup>Fe(II)-CO-*Ph*-2/2HbO are the unliganded and the CO-bound forms, respectively, of the fast-reacting species, whereas <sup>s</sup>Fe(II)-*Ph*-2/2HbO and <sup>s</sup>Fe(II)-CO-*Ph*-2/2HbO are the unliganded and the CO-bound forms, respectively, of the slow-reacting species,  $L = [{}^s\text{Fe(II)-}Ph\text{-2/2HbO}]/[{}^f\text{Fe(II)-}Ph\text{-2/2HbO}]$  and  $M = [{}^s\text{Fe(II)-CO-}Ph\text{-2/2HbO}]/[{}^f\text{Fe(II)-CO-}Ph\text{-2/2HbO}]$  are the equilibrium constants of the tertiary conformational equilibrium in the unliganded and in the CO-bound forms, respectively. Therefore, the kinetic process observed by stopped flow may correspond to the CO binding to <sup>s</sup>Fe(II)-*Ph*-2/2HbO.

Remarkably, while the reactivity of <sup>s</sup>Fe(II)-*Ph*-2/2HbO by stopped-flow seemed essentially pH-independent, the extent of the two phases rather than the rate constants of <sup>f</sup>Fe(II)-*Ph*-2/2HbO (by laser photolysis, see Table 1) appeared to be slightly proton linked both for the association and the dissociation rate constants. However, this proton linkage does not support any relevant role played by pH on the functional modulation over the physiological pH range (*i.e.*, between pH 6.5 and 8.0).

Furthermore, at a given pH value the amplitude of the slow phase increased as the CO concentration decreased (Supporting Information, Fig. S3), suggesting that after photolysis there is competition between CO rebinding of <sup>f</sup>Fe(II)-*Ph*-2/2HbO and the transition between <sup>f</sup>Fe(II)-*Ph*-2/2HbO and <sup>s</sup>Fe(II)-*Ph*-2/2HbO (corresponding to equilibrium L, see Scheme I). This behavior is perfectly in line with the mechanism sketched in Scheme I, suggesting that  $L > M$  and the existence of a CO-linked tertiary equilibrium.

**Table 2**

Activation parameters for CO association to <sup>s</sup>Fe(II)-*Ph*-2/2HbO, CO dissociation from <sup>f</sup>Fe(II)-CO-*Ph*-2/2HbO and <sup>s</sup>Fe(II)-CO-*Ph*-2/2HbO and O<sub>2</sub> dissociation from Fe(II)-O<sub>2</sub>-*Ph*-2/2HbO at 1 °C

	$\Delta G^\ddagger$ (kJ mol <sup>-1</sup> )	$\Delta H^\ddagger$ (kJ mol <sup>-1</sup> )	$\Delta S^\ddagger$ (e.u.)
<sup>s</sup> Fe(II)- <i>Ph</i> -2/2HbO	43.3 ± 6.1	42.2 ± 5.8	-4.3 ± 0.6
<sup>f</sup> Fe(II)-CO- <i>Ph</i> -2/2HbO	67.5 ± 8.4	41.9 ± 7.9	-93.4 ± 11.3
<sup>s</sup> Fe(II)-CO- <i>Ph</i> -2/2HbO	72.2 ± 8.9	5.6 ± 0.8	-243.2 ± 35.6
Fe(II)-O <sub>2</sub> - <i>Ph</i> -2/2HbO	68.6 ± 8.1	49.2 ± 6.1	-70.8 ± 8.8

The activation enthalpy for CO dissociation from the two CO-bound forms is drastically different ( ${}^f\Delta H^\ddagger = 41.9 \pm 6.3$  kJ mol $^{-1}$  and  ${}^s\Delta H^\ddagger = 5.57 \pm 0.83$  kJ mol $^{-1}$ ), clearly indicating a remarkable structural difference between the two forms. On the other hand, the activation enthalpy for CO association to the slow-reacting form by stopped-flow ( ${}^s\Delta H^\ddagger = 42.2 \pm 5.7$  kJ mol $^{-1}$ ) is similar to that observed for the fast CO-dissociating species.

Table 2 reports the activation parameters for CO association and dissociation at 1 °C, namely the physiological temperature of this hemoprotein. It is clear from these values that the activation enthalpy is very small for CO dissociation from  ${}^s\text{Fe(II)-CO-Ph-2/2HbO}$ , much smaller than that for CO association to  ${}^s\text{Fe(II)-Ph-2/2HbO}$ , underlying the occurrence of an endothermic CO binding to this form. Furthermore, the behavior of the activation entropy was much more negative for CO dissociation from  ${}^s\text{Fe(II)-CO-Ph-2/2HbO}$  than for its association, implying a remarkable entropy gain upon equilibrium CO binding. Such behavior, which has been observed previously in CO binding to trout HbI (31), though to a smaller extent, indicates that upon CO binding the slow-reacting form undergoes a gross conformational change involving burying of hydrophobic residues. It is also worth outlining that the slight difference for CO-dissociation rate constants between the two forms reflects two drastically different dissociation pathways. Thus, although  ${}^f\text{Fe(II)-CO-Ph-2/2HbO}$  shows a fairly high-activation enthalpy (Table 2), suggesting a physical barrier to the exit of the ligand (possibly due to residues of the distal side of the heme),  ${}^s\text{Fe(II)-CO-Ph-2/2HbO}$  displays a prevalent activation-entropy contribution, because the enthalpic barrier is drastically reduced. Such a feature indeed suggests a marked conformational change between the two forms, which affects the CO-dissociation pathway, possibly involving hydrophobic residues, which become more exposed to the solvent.

### Kinetics of O<sub>2</sub> Dissociation as a Function of Temperature

Kinetics of O<sub>2</sub> dissociation displayed a single kinetic process at pH 7.0 (Fig. 2C), clearly suggesting that the tertiary conformational equilibrium is different, such that the fully oxygenated form is largely displaced in favor of one of the two tertiary arrangements. The rate constant measured at 25 °C ( $k = 4.2 \pm 0.6$  sec $^{-1}$ ) is similar to that observed in other mammalian Mbs (16), being fully compatible with a role in O<sub>2</sub> diffusion (32).

To test whether this unlikely role (for a bacterial organism, whose size and cellular organization guarantees sufficient O<sub>2</sub> supply simply by diffusion without a molecular carrier) is still feasible at the environmental temperatures, where these organisms live (*i.e.*, 1 °C), we investigated the temperature dependence of O<sub>2</sub> dissociation (Fig. 2D). The relationship between temperature and the O<sub>2</sub>-dissociation rate constant indicates a fairly high-activation enthalpy ( $\Delta H^\ddagger = 49.2(\pm 6.1)$  kJ mol $^{-1}$ ),

similar to that observed for the CO dissociation from  ${}^f\text{Fe(II)-CO-Ph-2/2HbO}$  (Fig. 2D). At 274 K (*i.e.*, 1 °C), the O<sub>2</sub>-dissociation rate constant ( $k = 0.73 \pm 0.09$  sec $^{-1}$ ) indicates a fairly high-activation free energy ( $\Delta G^\ddagger = 68.6(\pm 8.1)$  kJ mol $^{-1}$ ), which clearly implies that the activation entropy is negative ( $\Delta S^\ddagger = -70.8(\pm 8.8)$  e.u.). Remarkably, these parameters mirror those observed for CO dissociation from  ${}^f\text{Fe(II)-CO-Ph-2/2HbO}$ , possibly suggesting that in the O<sub>2</sub>-bound form the tertiary equilibrium is largely displaced in favor of the fast-reacting form.

Therefore, similar to the fast-reacting form of the CO-bound molecule, the first step of O<sub>2</sub> release is accompanied by quite large loss of entropy (bound state relative to the top of the barrier), though significantly smaller than that for CO dissociation from  ${}^s\text{Fe(II)-CO-Ph-2/2HbO}$ , suggesting that also in this case, there is a large functional change. The very high free energy barrier is also in agreement with such behavior.

### CONCLUSIONS

*Ph-2/2HbO* displays multiple conformations and a partial six-coordination, which are key factors that need to be considered when determining its functional properties. However, in the reduced state, the six-coordination, likely due to a tyrosyl residue, seems very weak and does not disturb the ligand-binding reaction. As for neuroglobin, potential *in vivo* interactions could influence the function via the strength of the six-coordination. A shift in the equilibrium between the two conformations could also provide a large change in the ligand affinities. The difference in activation enthalpies of the two states could also indicate a mechanism to compensate local changes in temperature.

### ACKNOWLEDGEMENTS

This study is financially supported by the Italian Ministry of University and Research (MIUR PRIN 2007SFZXZ7 to C.V., G.S., and M.C.), the Italian National Programme for Antarctic Research (PNRA) and INSERM (France). It is in the framework of the SCAR programme Evolution and Biodiversity in the Antarctic (EBA), the project CAREX (Coordination Action for Research Activities on Life in Extreme Environments), European Commission FP7 call ENV.2007.2.2.1.6. DG and RR acknowledge CNR (for Short-Term Mobility fellowships), and CAREX (for Transfer of Knowledge grants). The authors thank the Centre de Ressources Biologiques de l'Institut Pasteur, Paris (<http://www.crbip.pasteur.fr>) for supplying the *P. haloplanktis* CIP 108707 strain.

### REFERENCES

1. Vinogradov, S. N., Hoogewijs, D., Bailly, X., Arredondo-Peter, R., Guertin, M., Gough, J., Dewilde S., Moens, L., and Vanfleteren J. R. (2005) Three globin lineages belonging to two structural classes in genomes from the three kingdoms of life. *Proc. Natl. Acad. Sci. USA* **102**, 11385–11389.

2. Pesce, A., Couture, M., Dewilde, S., Guertin, M., Yamauchi, K., Ascenzi, P., Moens, L., and Bolognesi, M. (2000) A novel two-over-two alpha-helical sandwich fold is characteristic of the truncated hemoglobin family. *EMBO J.* **19**, 2424–2434.
3. Wittenberg, J. B., Bolognesi, M., Wittenberg, B. A., and Guertin, M. (2002) Truncated hemoglobins: a new family of hemoglobins widely distributed in bacteria, unicellular eukaryotes, and plants. *J. Biol. Chem.* **277**, 871–874.
4. Wu, G., Wainwright, L. M., and Poole, R. K. (2003) Microbial globins. *Adv. Microb. Physiol.* **47**, 255–310.
5. Nicoletti, F. P., Comandini, A., Bonamore, A., Boechi, L., Boubeta, F., Feis, A., Smulevich, G., and Boffi, A. (2010) Sulfide binding properties of truncated hemoglobins. *Biochemistry* **49**, 2269–2278.
6. Giangiacomo, L., Ilari, A., Boffi, A., Morea, V., and Chiancone, E. (2005) The truncated oxygen-avid hemoglobin from *Bacillus subtilis*. *J. Biol. Chem.* **280**, 9192–9202.
7. Bonamore, A., Ilari, A., Giangiacomo, L., Bellelli, A., Morea, V., and Boffi, A. (2005) A novel thermostable hemoglobin from the actinobacterium *Thermobifida fusca*. *FEBS J.* **272**, 4189–4201.
8. Ilari, A., Kjølgaard, P., von Wachenfeldt, C., Catacchio, B., Chiancone, E., and Boffi, A. (2007) Crystal structure and ligand binding properties of the truncated hemoglobin from *Geobacillus stearothermophilus*. *Arch. Biochem. Biophys.* **457**, 85–94.
9. Milani, M., Savard, P. Y., Ouellet, H., Ascenzi, P., Guertin, M., and Bolognesi, M. (2003) A TyrCD1/TrpG8 hydrogen bond network and a TyrB10TyrCD1 covalent link shape the heme distal site of *Mycobacterium tuberculosis* hemoglobin O. *Proc. Natl. Acad. Sci. USA* **100**, 5766–5771.
10. Milani, M., Pesce, A., Nardini, M., Ouellet, H., Ouellet, Y., Dewilde, S., Bocedi, A., Ascenzi, P., Guertin, M., Moens, L., Friedman, J. M., Wittenberg, J. B., and Bolognesi, M. (2005) Structural bases for heme binding and diatomic ligand recognition in truncated hemoglobins. *J. Inorg. Biochem.* **99**, 97–109.
11. Médigue, C., Krin, E., Pascal, G., Barbe, V., Bernsel, A., Bertin, P. N., Cheung, F., Cruveiller, S., D'Amico, S., Duilio, A., Fang, G., Feller, G., Ho, C., Mangenot, S., Marino, G., Nilsson, J., Parrilli, E., Rocha, E. P., Rouy, Z., Sekowska, A., Tutino, M. L., Vallenet, D., von Heijne, G., and Danchin, A. (2005) Coping with cold: the genome of the versatile marine Antarctic bacterium *Pseudoalteromonas haloplanktis* TAC125. *Genome Res.* **15**, 1325–1335.
12. Giordano, D., Parrilli, E., Dettai, A., Russo, R., Barbiero, G., Marino, G., Lecointre, G., di Prisco, G., Tutino, M. L., and Verde, C. (2007) The truncated hemoglobins in the Antarctic psychrophilic bacterium *Pseudoalteromonas haloplanktis* TAC125. *Gene* **398**, 69–77.
13. Parrilli, E., Giuliani, M., Giordano, D., Russo, R., Marino, G., Verde, C., and Tutino, M. L. (2010) The role of a 2-on-2 haemoglobin in oxidative and nitrosative stress resistance of Antarctic *Pseudoalteromonas haloplanktis* TAC125. *Biochimie* **92**, 1003–1009.
14. Howes, B. D., Giordano, D., Boechi, L., Russo, R., Mucciacciaro, S., Ciaccio, C., Sinibaldi, F., Fittipaldi, M., Marti, M. A., Estrin, D. A., di Prisco, G., Coletta, M., Verde, C., and Smulevich, G. (2011) The peculiar heme pocket of the 2/2 hemoglobin of cold adapted *Pseudoalteromonas haloplanktis* TAC125. *J. Biol. Inorg. Chem.* **16**, 299–311.
15. Droghetti, E., Nicoletti, F. P., Bonamore, A., Boechi, L., Mañez, P. A., Estrin, D. A., Boffi, A., Smulevich, G., and Feis, A. (2010) Heme pocket structural properties of a bacterial truncated hemoglobin from *Thermobifida fusca*. *Biochemistry* **49**, 10394–10402.
16. Antonini, E. and Brunori, M. (1971) *Hemoglobin and Myoglobin in Their Reactions with Ligands*. North-Holland, Amsterdam.
17. Uzan, J., Dewilde, S., Burmester, T., Hankeln, T., Moens, L., Hamdane, D., Marden, M. C., and Kiger, L. (2004) Neuroglobin and other hexa-coordinated hemoglobins show a weak temperature dependence of oxygen binding. *Biophys. J.* **2**, 1196–1204.
18. Hori, H. and Kitagawa, T. (1980) Iron-ligand stretching band in the resonance Raman spectra of ferrous iron porphyrin derivatives. Importance as a probe band for quaternary structure of hemoglobin. *J. Am. Chem. Soc.* **102**, 3608–3613.
19. Stein, P. and Spiro, T. G. (1980) Hydrogen-bond and deprotonation effects on the resonance Raman iron-imidazole mode in deoxy hemoglobin models: implication for hemoglobin cooperativity. *J. Am. Chem. Soc.* **102**, 7795–7797.
20. Razzera, G., Vernal, J., Baruh, D., Serpa, V. I., Tavares, C., Lara, F., Souza, E. M., Pedrosa, F. O., Almeida, F. C., Terenzi, H., and Valente, A. P. (2008) Spectroscopic characterization of a truncated haemoglobin from the nitrogen-fixing bacterium *Herbaspirillum seropedicae*. *J. Biol. Inorg. Chem.* **13**, 1085–1096.
21. Couture, M., Das, T. K., Lee, H. C., Peisach, J., Rousseau, D. L., Wittenberg, B. A., Wittenberg, J. B., and Guertin, M. (1999) *Chlamydomonas* chloroplast ferrous hemoglobin. Heme pocket structure and reaction with ligands. *J. Biol. Chem.* **274**, 6898–6910.
22. Spiro, T. G. and Wasbotten, I. H. (2005) CO as a vibrational probe of heme protein active sites. *J. Inorg. Biochem.* **99**, 34–44.
23. Phillips, G. N. Jr., Teodoro, M. L., Li, T., Smith, B., and Olson, J. S. (1999) Bound CO is a molecular probe of electrostatic potential in the distal pocket of myoglobin. *J. Phys. Chem. B* **103**, 8817–8829.
24. Cameron, A. D., Smerdon, S. J., Wilkinson, A. J., Habash, J., Helliwell, J. R., Li, T., and Olson, J. S. (1993) Distal pocket polarity in ligand binding to myoglobin: deoxy and carbonmonoxide forms of a threonine 68(E11) mutant investigated by X-ray crystallography and infrared spectroscopy. *Biochemistry* **32**, 13061–13070.
25. Coletta, M., Ascenzi, P., and Brunori, M. (1988) Kinetic evidence for a role of heme geometry on the modulation of carbon monoxide reactivity in human hemoglobin. *J. Biol. Chem.* **263**, 18286–18289.
26. Ouellet, H., Juszcak, L., Dantsker, D., Samuni, U., Ouellet, Y. H., Savard, P. Y., Wittenberg, J. B., Wittenberg, B. A., Friedman, J. M., and Guertin, M. (2003) Reactions of *Mycobacterium tuberculosis* truncated hemoglobin O with ligands reveal a novel ligand-inclusive hydrogen bond network. *Biochemistry* **42**, 5764–5774.
27. Thijs, L., Vinck, E., Bolli, A., Trandafir, F., Wan, X., Hoogewijs, D., Coletta, M., Fago, A., Weber, R. E., van Doorslaer, S., Ascenzi, P., Alam, M., Moens, L., and Dewilde, S. (2007) Characterization of a globin-coupled sensor with a gene-regulating function. *J. Biol. Chem.* **282**, 37325–37340.
28. Pesce, A., Thijs, L., Nardini, M., Desmet, F., Sisinni, L., Gourlay, L., Bolli, A., Coletta, M., van Doorslaer, S., Wan, X., Alam, M., Ascenzi, P., Moens, L., Bolognesi, M., and Dewilde, S. (2009) HisE11 and HisF8 provide bis-histidyl heme hexa-coordination in the globin domain of *Geobacter sulfurreducens* globin-coupled sensor. *J. Mol. Biol.* **386**, 246–260.
29. Visca, P., Fabozzi, A., Petrucca, C., Ciaccio, C., Coletta, M., De Sanctis, G., Bolognesi, M., Milani, M., and Ascenzi, P. (2002) The truncated hemoglobin from *Mycobacterium lepre*. *Biochem. Biophys. Res. Commun.* **294**, 1064–1070.
30. Springer, B. A., Sligar, S. G., Olson, J. S., and Phillips, G. N. Jr. (1994) Mechanisms of ligand recognition in myoglobin. *Chem. Rev.* **94**, 699–714.
31. Wyman, J., Gill, S. J., Noll, L., Giardina, B., Colosimo, A., and Brunori, M. (1977). The balance sheet of hemoglobin. Thermodynamics of CO binding by hemoglobin trout I. *J. Mol. Biol.* **109**, 195–205.
32. Wittenberg, J. B. (1966) The molecular mechanism of hemoglobin-facilitated oxygen diffusion. *J. Biol. Chem.* **241**, 104–114.

## Research Communication

# Structure and Dynamics of Antarctic Fish Neuroglobin Assessed by Computer Simulations

Ignacio Boron<sup>1,2</sup>, Roberta Russo<sup>3</sup>, Leonardo Boechi<sup>2</sup>, C.-H. Christina Cheng<sup>4</sup>, Guido di Prisco<sup>3</sup>, Darío A. Estrin<sup>2</sup>, Cinzia Verde<sup>3</sup> and Alejandro D. Nadra<sup>1,5</sup>

<sup>1</sup>Departamento de Química Biológica, Facultad de Ciencias Exactas y Naturales, Universidad de Buenos Aires, Ciudad de Buenos Aires, Argentina

<sup>2</sup>Departamento de Química Inorgánica, Analítica y Química-Física (INQUIMAE-CONICET), Facultad de Ciencias Exactas y Naturales, Universidad de Buenos Aires, Ciudad de Buenos Aires, Argentina

<sup>3</sup>Institute of Protein Biochemistry, CNR, Via Pietro Castellino 111, I-80131 Naples, Italy

<sup>4</sup>Department of Animal Biology, University of Illinois, Urbana, IL, USA

<sup>5</sup>Departamento de Fisiología, Biología Molecular y Celular, Facultad de Ciencias Exactas y Naturales, Universidad de Buenos Aires, Ciudad de Buenos Aires, Argentina

---

### Summary

Neuroglobin (Ngb) is a heme protein, highly conserved along evolution, predominantly found in the nervous system. It is up-regulated by hypoxia and ischemia and may have a neuroprotective role under hypoxic stress. Although many other roles have been proposed, the physiological function is still unclear. Antarctic icefishes lack hemoglobin and some species also lack myoglobin, but all have Ngb and thus may help the elucidation of Ngb function. We present the first theoretically derived structure of fish Ngb and describe its behavior using molecular dynamics simulations. Specifically, we sequenced and analyzed Ngbs from a colorless-blooded Antarctic icefish species (*Chaenocephalus aceratus*) and a related red-blooded species (*Dissostichus mawsoni*). Both fish Ngbs are 6-coordinated but have some peculiarities that differentiate them from mammalian counterparts: they have extensions in the N and C termini that can interact with the EF loop, and a gap in the alignment that changes the CD-region structure/dynamics that has been found to play a key role in human neuroglobin. Our results suggest that a single mutation between both fish Ngbs is responsible for significant difference in the behavior of the proteins. The functional role of these characteristics is discussed. © 2011 IUBMB

IUBMB *Life*, 63(3): 206–213, 2011

**Keywords** neuroglobin; evolution; hemeproteins; protein function; protein structure; structural biology.

### INTRODUCTION

Neuroglobin (Ngb) is a heme protein, evolutionarily conserved, predominantly found in the brain and retina of vertebrates (1). It is transcriptionally upregulated by hypoxia and ischemia; *in vivo* and *in vitro* evidence suggests a neuroprotective role of Ngb during hypoxic stress (2, 3). Although many other roles have been envisaged, including scavenging of reactive nitrogen and oxygen species (4), signal transduction (5), and regulation of apoptotic pathways (6), the physiological function is still unclear. Protein dynamics, ligand binding, and its migration in the protein matrix have been investigated in great detail using time resolved techniques, providing important insights into structural and dynamic properties in the reactivity of mammalian Ngbs (7, 8). Nevertheless, the full understanding of the biochemical mechanisms explaining how Ngb may perform its function seems hindered by the (multiple) ligand-binding features.

Despite low-amino acid sequence identity (ca. 20%) between human Ngb and myoglobin (Mb), the 3D structure displays the classical globin fold (9), which is endowed with several unique properties. Ngb binds small gaseous ligands (oxygen, CO and NO) at the 6-coordination position of the heme iron. In the absence of an exogenous ligand, the heme iron (in the ferric and ferrous form) is 6-coordinated (6c), with distal HisE7 occupying the sixth coordination site. Distal His can be readily replaced by the external ligands. Another prominent feature of

---

Received 6 January 2011; accepted 9 February 2011

Address correspondence to: Dr. Alejandro D. Nadra, Departamento de Química Biológica, Facultad de Ciencias Exactas y Naturales, Universidad de Buenos Aires, Ciudad de Buenos Aires, Argentina. Tel: +54-11-45763300 ext 205. Fax: 54-11-45763342. E-mail: anadra@qi.fcen.uba.ar

the Ngb structure is a huge cavity, open toward the exterior that affords potential transit to ligands. Additionally, in human Ngb, two cysteyle residues in the CD region, Cys46-CD7 and Cys55-D5, may form an internal disulfide bond that modulates oxygen affinity (10). This regulation was not observed in zebrafish Ngb, where the first cysteine is shifted by two positions (11), or in murine Ngb, where Cys46-CD7 is absent (12).

Ngb was originally identified in mammals but is widespread in all nonmammalian vertebrates, e.g., the zebrafish *Danio rerio* and other teleost fishes (11). Mammalian and zebrafish Ngbs share about 50% sequence identity and their oxygen-binding properties are similar (11).

Recently, we have characterized the Ngb gene in fishes of the Antarctic ocean (13, 14) and cloned and sequenced the Ngb cDNA from the brain of an icefish *Chaenocephalus aceratus* (family Channichthyidae) and from the retina of the closely related, red-blooded *Dissostichus mawsoni* (family Nototheniidae). Both species belong to the suborder Notothenioidei, the predominant teleost group in the Antarctic ichthyofauna. Antarctic icefishes (16 species) lack hemoglobin, and six of the species also lack Mb. Elucidation of the icefish Ngb structure may potentially shed light on the physiological function of Ngb, especially considering apparent Ngb localization in tissues of increased oxidative metabolism and mitochondrial activity (15). The highest Ngb level was found in the retina, which has the highest oxygen-consuming rate in the body (16). Unique among vertebrates, Antarctic colorless-blooded icefishes of the family Channichthyidae lack erythrocytes and hemoglobin, and thus oxygen supply largely occurs through circulatory and diffusive flux (17). Although loss of globin genes in icefishes is due to relaxed selection in the oxygen-rich Antarctic marine environment is a matter of debate, but interestingly they have not lost the Ngb gene or its transcription.

In this study, we analyze the Ngb from the Antarctic icefish *C. aceratus* and the red-blooded nototheniid *D. mawsoni* as well as other teleost Ngbs in comparison with mammalian Ngbs. We performed homology modeling and molecular dynamics simulations (MDS) and described the first theoretical model of fish Ngb and its behavior according to MDS. Both Antarctic notothenioid Ngbs are 6-coordinated but show peculiarities that differentiate them from mammalian counterparts.

## EXPERIMENTAL PROCEDURES

### *Ngb* Sequence

The amino acid sequences of *C. aceratus* and *D. mawsoni* Ngb were derived from cDNA sequences. The cDNA sequences were obtained by RT-PCR amplification of total RNA from retina of *D. mawsoni* and from whole brain of *C. aceratus* using appropriate primers. Briefly, total RNA was isolated using Ultraspec RNA isolation reagent (Biotecx, TX). Lock-dock oligo-dT30 primed and reverse-transcribed first strand cDNA was PCR-amplified with a notothenioid-specific 5'UTR primer,

5'GTGTGCATCTCTAGCCGAGGAATCC3' and 5'GGAATCC TGTCTCCAACAGTTGTGTCCC3' for *C. aceratus* and *D. mawsoni*, respectively, paired with a degenerate teleost 3' UTR primer 5'GACCYCAYTCAMAGAGCAAATGTACAGCG3'. The cloning and sequencing process leading to the design of notothenioid-specific 5'UTR primers were detailed elsewhere (Girodano et al., 2010, submitted). In *silico* translation of the cDNA sequences provided the Ngb protein sequences used for homology modeling and were submitted to UniProt Knowledgebase under accession numbers P86880 (*C. aceratus*) and P86881 (*D. mawsoni*).

### Multiple Sequence Alignment and Structure Modeling

Antarctic fish Ngb sequences together to those of mammalian and other fish species downloaded from Swiss-prot (18) were aligned by the 3DCoffee program (19) following standard parameters. The model of 6c *D. mawsoni* Ngb was generated with the Modeller9 program (20), using the human X-ray structure (PDB entry 1OJ6) as a template. The resulting structure was then used as starting point to generate the complete set of simulations.

### Classical Molecular Dynamics

The initial structure explained above was placed in a pre-equilibrated octahedral TIP3 water box. The standard protonation state at physiological pH was assigned to ionisable amino acid residues. Special attention was paid to protonation of His residues, which were assigned on the basis of the hydrogen bond pattern with neighboring residues. For distal HisE7 and proximal HisF8, protonation was chosen to be in the Nd position. Equilibration of the system (~25,000 atoms) and running parameters were performed as described (21). All simulations were performed at 300 K and pressures of 1 bar using Berendsen thermostat and barostat. The Amber99 force field (22) was used for all residues but not for the heme, whose parameters had been developed and thoroughly tested by our team in previous work (23–26). All simulations were performed with the PMEMD module of the AMBER9 package (27). Equilibration consisted of energy minimization of the initial structures, followed by slow heating up to 300 K (4 steps of 50 ps at 150, 200, 250, and 300 K). The structure was considered to be stabilized after a 20-ns MD run of the 6c *D. mawsoni* Ngb. From this equilibrated structure, the other structures were generated by deleting the His-Fe bond (5c-state) and/or introducing the two point mutations that differentiate the two Antarctic Ngbs, followed by the same four-step equilibration protocol. For each structure, 80-ns long MD production runs were performed where the backbone root mean square distance does not exceed 1.9 Å with respect to the initial frame. Trajectories were analyzed from frames collected at 2-ps intervals.

### Essential Dynamics

Dynamical differences between *D. mawsoni* and *C. aceratus* Ngbs in their 5c state were studied using essential dynamics

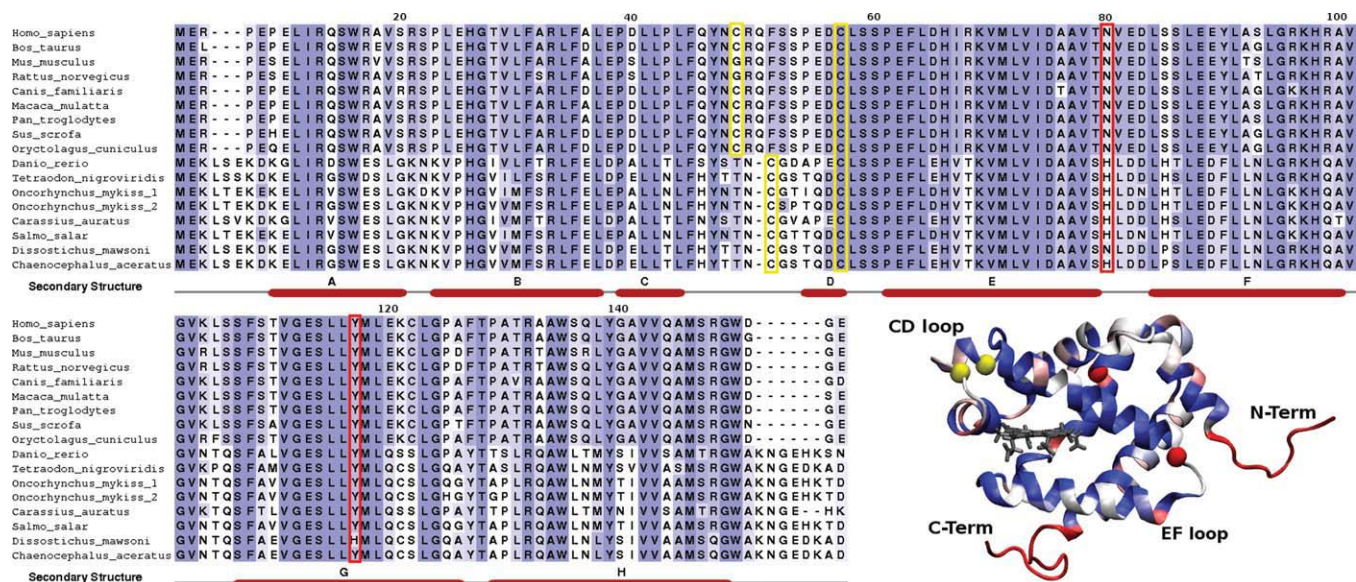


**Figure 1.** Sequence alignment of mammal and fish Ngbs. Residues are shaded according to sequence conservation. Relevant positions, e.g., mutations between Antarctic fish proteins or conserved Cys residues, are boxed. A scheme of the secondary structure found in human Ngb with helices A-H is below the alignment. Inset: Modeled structure of fish Ngb colored by sequence conservation with human Ngb. N- and C-terminal extensions are in red, residues 80 and 117 in red circles and Cys in yellow circles. Numbering is according to fish Ngb. [Color figure can be viewed in the online issue, which is available at [wileyonlinelibrary.com](http://wileyonlinelibrary.com).]

(ED) analysis (28). ED analysis was performed with the ptraj module of the AMBER suite and consisted in the diagonalization of the covariance matrices of atomic positions along the trajectory. From them we obtained the eigenvectors that define the essential motions of the protein. To analyze the configurational space explored by the proteins, projections of their essential modes onto the last 50 ns of the MD trajectory were performed. Only backbone atoms were considered.

## RESULTS

### Mammalian vs. Fish Neuroglobins

When compared with mammalian counterparts in a multiple sequence alignment (Fig. 1), fish Ngbs display some striking peculiarities. They all show three- and six-residue extensions, composed of charged residues, in their N and C termini, respectively. The extra residues protrude toward the EF loop causing potentially relevant interactions, as discussed below. The alignment also shows a gap (position 51) in the CD region, which may be involved in aiding heme coordination and shows correlated motions with the so-called His-gate (21, 29). As shown in Fig. 2A, in fish Ngbs, the average Cys-Cys distance in the CD loop is several-Å shorter than in the human protein, in which Cys46-CD7 and Cys55-D5 are known to form a disulfide bridge and appear to be involved in redox-state sensing (11, 21, 30). Thus, although the residues are in the reduced form, they remain very close to each other during the time scale of the simulations (Fig. 2B). This short distance allows the protein to adopt a conformation, which is more suitable to form a disulfide

bridge than in human Ngb, where a more important rearrangement is needed.

Apart from these differences, conservation is high in the rest of the Ngb sequences between mammals and fish, with Antarctic fish Ngbs about 55% identical to human, as well as between members of each group. Notably, sequence conservation is significantly higher among mammals than among fish species as previously described (31).

### Red- vs. Colorless-Blooded Antarctic Fish Ngb

Sequence analysis of *D. mawsoni* and *C. aceratus* Ngbs shows that the only differences between these proteins are at positions 80 and 117, the icefish having His and Tyr and red-blooded *D. mawsoni* Asn and His, respectively. Both residues are located away from the heme, exposed to the solvent and distant from the dynamically relevant CD corner.

As shown by MDS, the two proteins differ in loop structure and flexibility (Figs. 2C and 2D and Table 1). Moreover, different interactions are established between the EF loop and its N-terminal region of *D. mawsoni* Ngb and the corresponding regions of *C. aceratus*. This interaction, absent in human Ngb, helps to stabilize an incipient  $\alpha$ -helical structure in the N-terminal region. In *D. mawsoni* Ngb, formation of the H bond between Lys9:HD2 and Asn80:O involves disruption of that between Asn80:O and Asp83:H, and *vice versa* (Figs. 2C and 2D). In contrast, in *C. aceratus* Ngb, the EF loop and N-terminal interaction is present but is less specific and fluctuates contacting different residues.

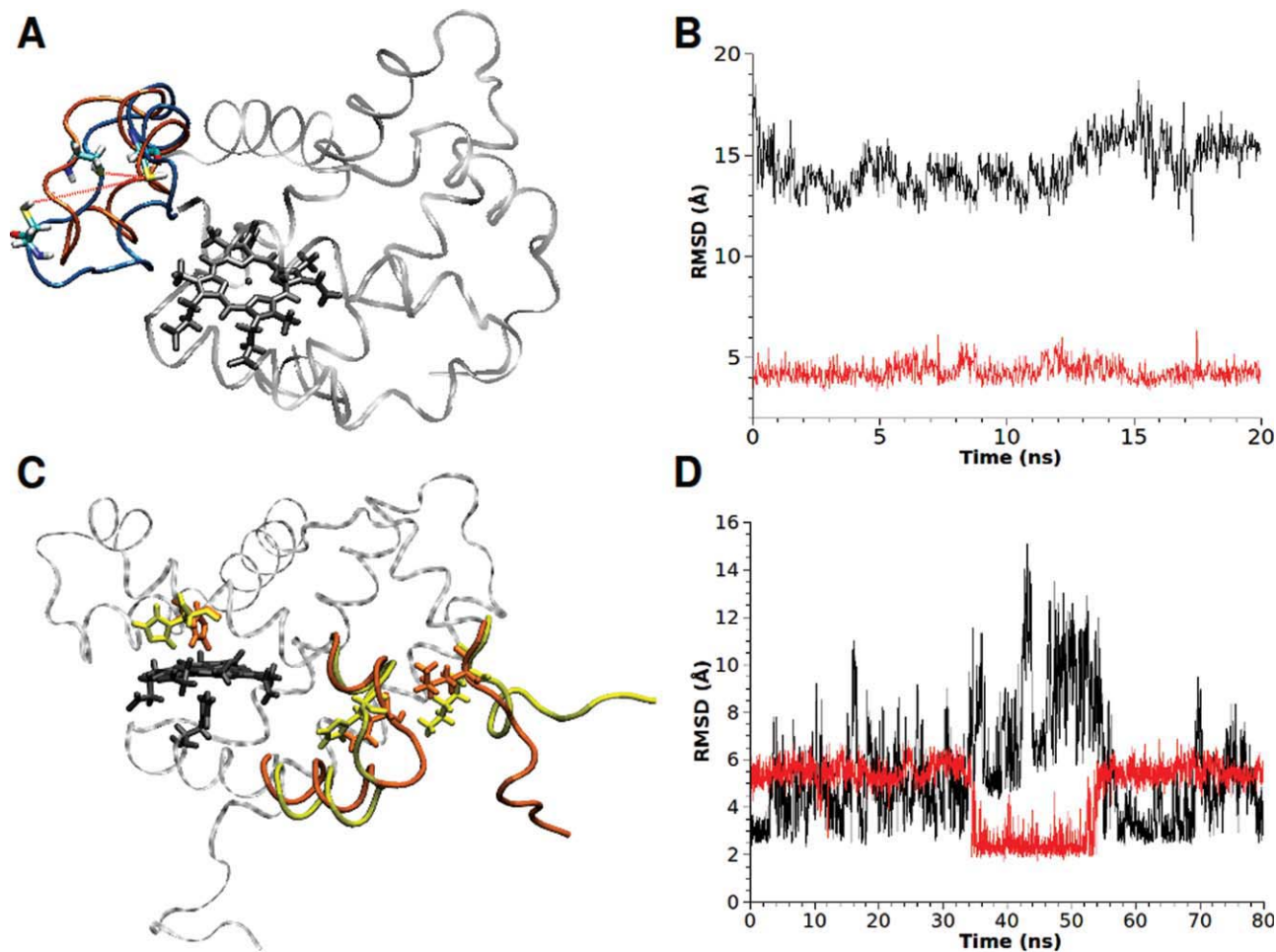


**Figure 2.** Peculiarities of Antarctic fish Ngbs. **A:** Comparison between Cys-Cys average distance in *D. mawsoni* Ngb (orange) and human Ngb (blue) at the CD loop. In human Ngb, the disulfide formation requires a relevant rearrangement of the CD region (14.4-Å average distance); in *D. mawsoni* Ngb, the two Cys are close (4.2-Å average distance) and in adequate orientation to form a bond. Similar values were obtained in *C. aceratus* Ngb (not shown). **B:** Time trace of the Cys-Cys distance along 20 ns for human (black) and *D. mawsoni* (red) Ngb. **C:** Backbone representation of *D. mawsoni* Ngb (orange) and *C. aceratus* Ngb (yellow), highlighting the changes in EF-loop conformation and its interaction with the N-terminal region in colored sticks. **D:** Time trace for two selected distances in *D. mawsoni* Ngb (Asn80:O-Asp83:H in red; Lys9:HD2-Asn80:O in black) illustrating the interaction between the EF loop and N termini. [Color figure can be viewed in the online issue, which is available at [wileyonlinelibrary.com](http://wileyonlinelibrary.com).]

A static view of the conformation adopted by the proteins can be obtained by comparing average structures (Fig. 2, Table 1). Root mean square deviation (RMSD) values clearly show that the EF loop of *C. aceratus* and *D. mawsoni* Ngbs significantly differ and that this difference is independent of the coordination state (Table 1). Furthermore, this difference is not only static but also affects the dynamics of the protein (Fig. 3), where root mean square fluctuations (RMSF) and ED projections show a remarkably higher flexibility in the *C. aceratus* EF loop, whereas in *D. mawsoni* Ngb, the overall flexibility is spread along different loops (Figs. 3A and 3B).

In the distal site, the main consequence is that His is able to open in a “His-gate”-like movement only in *C. aceratus* Ngb in

the time frame under consideration. Notably, the His opening modifies the CD-region conformation and flexibility. RMSD values for this region (Table 1) show that *C. aceratus* Ngb is significantly different in the 5c state after His opening. Furthermore, RMSF values and ED analysis show that CD region becomes less flexible (Figs. 3A and 3B). All these conformational and dynamical differences are dictated by the replacement of Asn 80 by His, as they can be reverted by mutating these residues. This experiment consisted in converting *C. aceratus* Ngb to *D. mawsoni* Ngb at position 80 after the conformational change that the loop suffer was acquired and stabilized. Within 5 ns after reversion, the EF loop readopted the conformation consistent with the corresponding residue at position 80. This

**Table 1**  
RMSD between average structures for both fish Ngbs

			<i>C. aceratus</i> Ngb		<i>D. mawsoni</i> Ngb	
			5c	6c	5c	6c
CD region	<i>C. aceratus</i> Ngb	5c		<b>0.64</b>	<b>0.75</b>	<b>0.77</b>
		6c	<b>0.82</b>		0.82	0.79
	<i>D. mawsoni</i> Ngb	5c	<b>0.96</b>	0.79		0.53
		6c	<b>0.92</b>	0.74	0.54	
EF region	<i>C. aceratus</i> Ngb	5c		0.8	<b>0.81</b>	<b>0.8</b>
		6c	0.82		<b>0.52</b>	<b>0.45</b>
	<i>D. mawsoni</i> Ngb	5c	<b>0.96</b>	<b>0.79</b>		0.54
		6c	<b>0.92</b>	<b>0.74</b>	0.54	

Average structures for both fish Ngbs either in the 5c or the 6c states for the last 50 ns were compared and RMSD calculated. We focused our analysis in the conformation of the CD region (upper) and the EF region (lower). The values above the diagonal inform on the RMSD excluding the loop regions (residues 40–60 for the CD region and residues 75–95 for the EF region), while those below the diagonal inform on the total RMSD. Highlighted in bold are values where differences between including and excluding CD or EF regions are higher, implying a significantly different loop conformation between protein species.

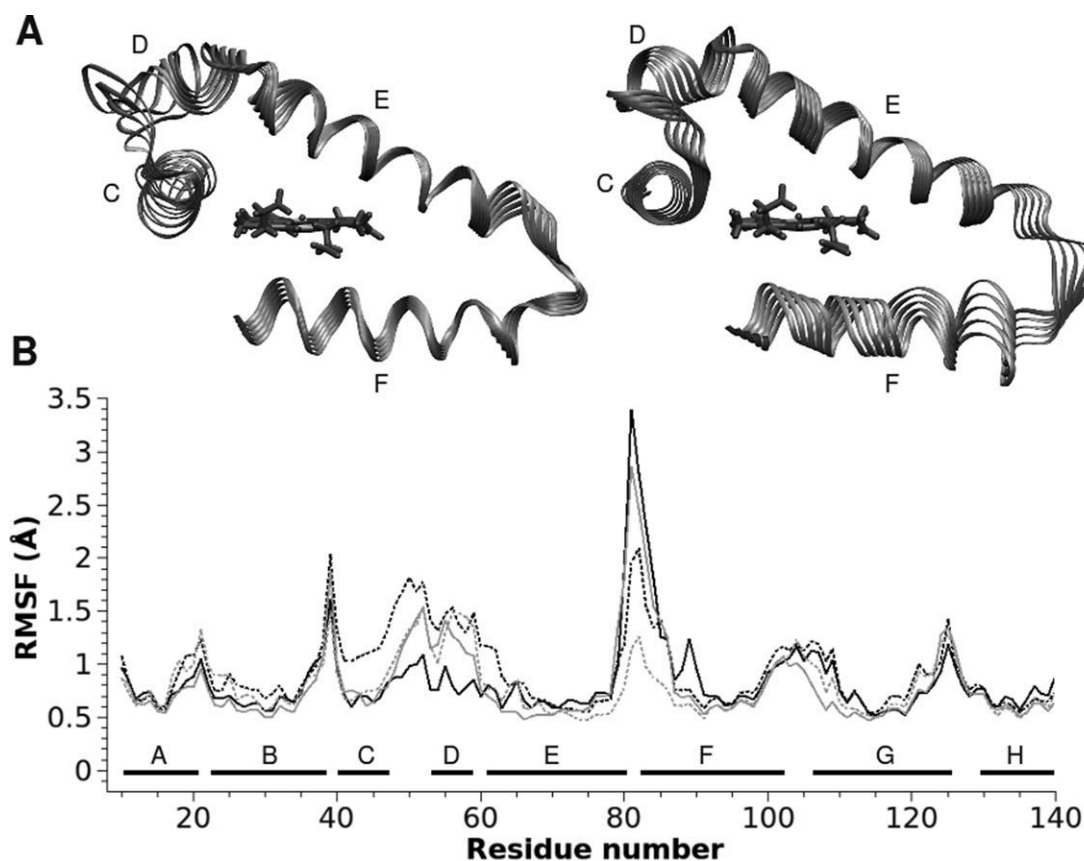


**Figure 3.** Dynamical differences between fish Ngbs. A: Projection of the normal mode with highest amplitude in *D. mawsoni* (left) and *C. aceratus* (right). B: Root mean square fluctuations along the last 50 ns in *D. mawsoni* (dotted line) and *C. aceratus* (continuous line). 5c-species are in black and 6c-species in gray.

implies that the single mutation modifies EF loop conformation and dynamics and propagates, through the heme-coordinating His, up to the CD region in the opposite part of the protein.

## DISCUSSION

Isolation and environmental history have shaped a unique Antarctic marine biota. Many fish groups became extinct because of the constraints of increasingly cold and icy conditions, and the cold-adapted and antifreeze-protected notothenioids emerged as the predominant teleost taxon (32, 33). In the modern notothenioid family Channichthyidae, mutational events led to remnant  $\alpha$ -globin genes and complete deletion of the genes encoding the  $\beta$  globins of hemoglobin (34–36). Six of the 16 icefish species including *C. aceratus* also fail to produce cardiac Mb (37). The lack of these globins is closely correlated with compensatory changes in the icefish anatomy, e.g., larger heart and gills and blood volume (38).

Because oxygen transport and supply must be achieved without hemoglobin and Mb, icefishes are an excellent system to investigate possible enhancement of other factors to compensate for the loss of these essential hemoprotein functions. Icefishes serve as the natural knock-outs for functional studies of oxygen-binding hemoproteins and the correlated nitrogen-monoxide-oxygenase activity. Current research in mammals suggests that nearly all icefish hallmark traits are linked to high levels of NO (39).

To our knowledge, this is the first structural modeling and MD study on such proteins from Antarctic fish. When compared with mammals, fish Ngbs display some striking peculiarities in regions considered relevant for protein function: (i) Ngbs of Antarctic and temperate fish have extensions of charged amino-acid residues at the N and C termini. In the zebrafish *D. rerio*, the N-terminal region was demonstrated to be implied in cell-penetrating capability (40). These extra residues extend toward the EF loop; (ii) Antarctic and temperate fish Ngbs are shorter by one residue in the CD region, involved in heme coordination and in the “His-gate.” The shorter loop approaches the two Cys that form the disulfide bridge in human Ngb so that the Cys-Cys distance is several Å shorter. The residues remain very close during the simulations, allowing easier formation of the disulfide bridge than in human Ngb. Disulfide formation in human Ngb has been experimentally shown to decrease protein flexibility (41), particularly, in the CD region. This in turn enhances O<sub>2</sub> affinity about 10-fold by stabilizing the 5c state, making the protein adopt a conformation prone to bind exogenous ligands (10, 21).

The UV-vis spectra of ferric and ferrous form of both *C. aceratus* and *D. mawsoni* Ngbs proteins are typical of 6c-state (Giordano et al., unpublished) in analogy with other Ngbs (42). Preliminary results obtained using multiple steered molecular dynamics and the Jarzynski equality as in Nadra et al. (21) show that the 6c-state is preferred in both Ngbs by about 6 kcal mol<sup>-1</sup>. Unexpectedly, but consistent with the Cys-Cys distance,

the overall conformation of the 5c state for both proteins is much more similar to the oxidised state of human Ngb (with the Cys residues forming an intramolecular disulfide bond).

A single amino-acid replacement appears sufficient to induce much higher flexibility in *C. aceratus* Ngb in comparison with red-blooded *D. mawsoni*. MDS analysis suggests that the Asn→His substitution in position 80 produces changes in the conformational and dynamical features in the icefish protein. In the distal domain, the main consequence is the “His-gate”-like movement, causing rearrangement of the CD region that correlates with EF-loop movements. These differences are dictated by this replacement, because they disappear by reversal mutation. No effect is associated to the Tyr→His replacement at position 117.

Adaptive changes appear restricted to regions that influence conformational mobility. This finding has important implications for rates of protein evolutionary adaptation, because a single substitution is sufficient for potential functional shifts. As these sequence differences are far from the active site or previously described relevant regions for protein function, in principle, we did not expect these mutations to be very functionally relevant. To our surprise, this appeared to be true only for the Tyr117→His mutation but not for His80→Asn. The latter is located in the EF loop, which connects the helices, which include heme-coordinated His, and is very close to the N-terminal extension. Although this loop is less variable in sequence than the CD region, it displays flexibility (21, 29) and may indeed have a relevant role in heme coordination.

These results support the general hypothesis that alterations in protein conformational mobility can happen through one/few substitutions, providing insights into the evolutionary rates at which adaptive change may occur (43, 44). They also indicate that a small change in the primary structure, namely a short-term response, may be very efficient as such for generating an adaptive response to a challenge.

However, prudence should be exercised in assigning a general value to these conclusions. First, one needs to be cautious in interpreting whether the single change in primary structure is due to adaptation or phylogenetic variation (or both, as they are not mutually exclusive). Nonetheless, we must take the icefish exceptional oxygen-transport system into account. In the icefish brain and retina, the delivery of oxygen by diffusion could be highly insufficient. Thus, Ngb may also have the task to fulfil the role of a classical oxygen carrier, and the conformational flexibility of Ngb can be included into the suite of anatomical and physiological compensations that icefish had to engineer as a result of the evolutionary loss of hemoglobin and Mb. To support this hypothesis, Ngb concentration and oxygen affinity should be measured for these species and be high enough to accomplish the proposed function. Second, His 80 is present in all fish sequences except in *D. mawsoni*. However, in these sequences, additional substitutions distributed in key positions in the structure may well mask the effect at position 80 in icefish Ngb.

## ACKNOWLEDGEMENTS

The authors thank Marcelo Martí and Luciana Capece for helpful discussion and technical advice. This work was partially supported by the University of Buenos Aires (20020090300117), Agencia Nacional de Promoción Científica y Tecnológica (PICT 732), CONICET (PIP 02508), European Union Project FP7-Nostress and Italian National Programme for Antarctic Research (PNRA). It is in the framework of the SCAR programme Evolution and Biodiversity in the Antarctic (EBA), the project CAREX (Coordination Action for Research Activities on Life in Extreme Environments), European Commission FP7 call ENV.2007.2.2.1.6. RR acknowledges CNR (Short-Term Mobility fellowship) and CAREX (Transfer of Knowledge grants). L.B. and I.B. are fellows from CONICET. D.A.E., and A.D.N. are members of CONICET. C-HCC acknowledges support from US National Science Foundation Grant OPP 0636696. The protein sequence data reported in this paper will appear in the UniProt Knowledgebase under the accession numbers P86880 (*C. aceratus*) and P86881 (*D. mawsoni*).

## REFERENCES

- Burmester, T., Weich, B., Reinhardt, S., and Hankeln, T. (2000) A vertebrate globin expressed in the brain. *Nature* **407**, 520–523.
- Sun, Y., Jin, K., Peel, A., Mao, X. O., Xie, L., and Greenberg, D. A. (2003) Neuroglobin protects the brain from experimental stroke in vivo. *Proc. Natl. Acad. Sci. USA* **100**, 3497–3500.
- Greenberg, D. A., Jin, K., and Khan, A. A. (2008) Neuroglobin: an endogenous neuroprotectant. *Curr. Opin. Pharm.* **8**, 20–24.
- Brunori, M., Giuffrè, A., Nienhaus, K., Nienhaus, G. U., Scandurra, F. M., and Vallone, B. (2005) Neuroglobin, nitric oxide, and oxygen: functional pathways and conformational changes. *Proc. Natl. Acad. Sci. USA* **102**, 8483–8488.
- Wakasugi, K., Nakano, T., and Morishima, I. (2003) Oxidized human neuroglobin acts as a heterotrimeric G $\alpha$  protein guanine nucleotide dissociation inhibitor. *J. Biol. Chem.* **278**, 36505–36512.
- Khan, A.A., Mao, X. O., Banwait, S., Jin, K., and Greenberg, D. A. (2007) Neuroglobin attenuates  $\beta$  amyloid neurotoxicity in vitro and transgenic Alzheimer phenotype in vivo. *Proc. Natl. Acad. Sci. USA* **104**, 19114–19119.
- Kriegel, J. M., Bhattacharyya, A. J., Nienhaus, K., Deng, P., Minkow, O., and Nienhaus, G. U. (2002) Ligand binding and protein dynamics in neuroglobin. *Proc. Natl. Acad. Sci. USA* **99**, 7992–7997.
- Abbruzzetti, S., Faggiano, S., Bruno, S., Spyrikis, F., Mozzarelli, A., Dewilde, S., Moens, L., and Viappiani, C. (2009) Ligand migration through the internal hydrophobic cavities in human neuroglobin. *Proc. Natl. Acad. Sci. USA* **106**, 18984–18989.
- Pesce, A., Dewilde, S., Nardini, M., Moens, L., Ascenzi, P., Hankeln, T., Burmester, T., and Bolognesi, M. (2003) Human brain neuroglobin structure reveals a distinct mode of controlling oxygen affinity. *Structure* **11**, 1087–1095.
- Hamdane, D., Kiger, L., Dewilde, S., Green, B. N., Pesce, A., Uzan, J., Burmester, T., Hankeln, T., Bolognesi, M., Moens, L., and Marden, M. C. (2003) The redox state of the cell regulates the ligand binding affinity of human neuroglobin and cytoglobin. *J. Biol. Chem.* **278**, 51713–51721.
- Fuchs, C., Heib, V., Kiger, L., Haberkamp, M., Roesner, A., Schmidt, M., Hamdane, D., Marden, M. C., Hankeln, T., and Burmester, T. (2004) Zebrafish reveals different and conserved features of vertebrate neuroglobin gene structure, expression pattern, and ligand binding. *J. Biol. Chem.* **279**, 24116–24122.
- Vallone, B., Nienhaus, K., Matthes, A., Brunori M., and Nienhaus, G. U. (2004) The structure of carbonmonoxy neuroglobin reveals a heme-sliding mechanism for control of ligand affinity. *Proc. Natl. Acad. Sci. USA* **101**, 17351–17356.
- Cheng, C.-H. C., di Prisco, G., and Verde, C. (2009a) Cold-adapted Antarctic fish: the discovery of neuroglobin in the dominant suborder Notothenioidei. *Gene* **433**, 100–101.
- Cheng, C.-H. C., di Prisco, G., and Verde, C. (2009b) The “icefish paradox”. Which is the task of neuroglobin in Antarctic haemoglobin-less icefish? *IUBMB Life* **61**, 184–188.
- Hankeln, T., Wystub, S., Laufs, T., Schmidt, M., Gerlach, F., Saaler-Reinhardt, S., Reuss, S., and Burmester, T. (2004) The cellular and subcellular localization of neuroglobin and cytoglobin—a clue to their function? *IUBMB Life* **56**, 671–679.
- Schmidt, M., Giessel, A., Laufs, T., Hankeln, T., Wolfrum, U., and Burmester, T. (2003) How does the eye breathe? Evidence for neuroglobin-mediated oxygen supply in the mammalian retina. *J. Biol. Chem.* **278**, 1932–1935.
- Cheng, C.-H. C. and Detrich, H. W., III. (2007) Molecular ecophysiology of Antarctic notothenioid fishes. *Philos. Trans. R. Soc. Lond. B Biol. Sci.* **362**, 2215–2232.
- Boeckmann, B., Bairoch, A., Apweiler, R., Blatter, M.-C., Estreicher, A., Gasteiger, E., Martin, M. J., Michoud, K., O’Donovan, C., Phan, I., Pilboud, S., and Schneider, M. (2003) The Swiss-Prot Protein Knowledgebase and its supplement TrEMBL in 2003. *Nucleic Acids Res.* **31**, 365–370.
- Notredame, C., Higgins, D. G., and Heringa, J. (2000) T-Coffee: a novel method for fast and accurate multiple sequence alignment. *J. Mol. Biol.* **302**, 205–217.
- Sali, A. and Blundell, T. L. (1993) Comparative protein modeling by satisfaction of spatial restraints. *J. Mol. Biol.* **234**, 779–815.
- Nadra, A. D., Marti, M. A., Pesce, A., Bolognesi, M., and Estrin, D. A. (2008). Exploring the molecular basis of heme hexacoordination in human neuroglobin. *Proteins* **71**, 695–705.
- Cheatham, T. E., III, Cieplak, P., and Kollman, P. A. (1999) A modified version of the Cornell et al. force field with improved sugar pucker phases and helical repeat. *J. Biomol. Struct. Dyn.* **16**, 845–862.
- Marti, M. A., Crespo, A., Capece, L., Boechi, L., Bikiel, D. E., Scherlis, D.A., and Estrin, D. A. (2006) Dioxigen affinity in heme proteins investigated by computer simulation. *J. Inorg. Biochem.* **100**, 761–770.
- Bidon-Chanal, A., Marti, M. A., Crespo, A., Milani, M., Orozco, M., Bolognesi, M., Luque, F. J., and Estrin, D. A. (2006) Ligand-induced dynamical regulation of NO conversion in *Mycobacterium tuberculosis* truncated hemoglobin-N. *Proteins* **64**, 457–464.
- Capece, L., Marti, M. A., Bidon-Chanal, A., Nadra, A., Luque, F.J., and Estrin, D. A. (2009) High pressure reveals structural determinants for globin hexacoordination: neuroglobin and myoglobin cases. *Proteins* **75**, 885–894.
- Boechi, L., Mañez, P. A., Luque, F. J., Marti, M. A., and Estrin, D. A. (2010) Unraveling the molecular basis for ligand binding in truncated hemoglobins: the trHbO *Bacillus subtilis* case. *Proteins* **78**, 962–970.
- Pearlman, D. A., Case, D. A., Caldwell, J. W., Ross, W. S., Cheatham, T. E., III, DeBolt, S., Ferguson, D., Seibel, G., and Kollman, P. (1995) AMBER, a package of computer programs for applying molecular mechanics, normal mode analysis, molecular dynamics and free energy calculations to simulate the structural and energetic properties of molecules. *Comput. Phys. Commun.* **91**, 1–41.
- Amadei, A., Linssen, A. B., and Berendsen, H. J. (1993) Essential dynamics of proteins. *Proteins* **17**, 412–425.
- Anselmi, M., Brunori, M., Vallone, B., and Di Nola, A. (2007) Molecular dynamics simulation of deoxy and carboxy murine neuroglobin in water. *Biophys. J.* **93**, 434–441.

30. Astudillo, L., Bernad, S., Derrien, V., Sebban, P., and Miksovska, J. (2010) Probing the role of the internal disulfide bond in regulating conformational dynamics in neuroglobin. *Biophys. J.* **99**, L16–L18.
31. Awenius, C., Hankeln, T., and Burmester, T. (2001) Neuroglobins from the zebrafish *Danio rerio* and the pufferfish *Tetraodon nigroviridis*. *Biochem. Biophys. Res. Commun.* **287**, 418–21.
32. Eastman, J. T. (1993) *Antarctic Fish Biology: Evolution in a Unique Environment*, Academic Press, San Diego, 322 p.
33. Eastman, J. T. (2005) The nature of the diversity of Antarctic fishes. *Polar Biol.* **28**, 93–107.
34. Cocca, E., Ratnayake-Lecamwasam, M., Parker, S. K., Camardella, L., Ciaramella, M., di Prisco, G., and Detrich, H. W., III. (1995) Genomic remnants of  $\alpha$ -globin genes in the hemoglobinless Antarctic icefishes. *Proc. Natl. Acad. Sci. USA* **92**, 1817–1821.
35. di Prisco, G., Cocca, E., Parker, S. K., and Detrich, H. W., III. (2002) Tracking the evolutionary loss of hemoglobin expression by the white-blooded Antarctic icefishes. *Gene* **295**, 185–191.
36. Near, T. J., Parker, S. W., and Detrich, H. W., III. (2006) A Genomic fossil reveals key steps in hemoglobin loss by the Antarctic icefishes. *Mol. Biol. Evol.* **23**, 2008–2016.
37. Sidell, B. D. and O'Brien K. M. (2006) When bad thing happen to good fish: the loss of hemoglobin and myoglobin expression in Antarctic icefishes. *J. Exp. Biol.* **209**, 1791–1802.
38. Egginton, S., Skilbeck, C., Hoofd, L., Calvo, J., and Johnston, I. A. (2002) Peripheral oxygen transport in skeletal muscle of Antarctic and sub-Antarctic notothenioid fish. *J. Exp. Biol.* **205**, 769–779.
39. Beers, J. M., Borley, K. A., and Sidell, B. D. (2010) Relationship among circulating hemoglobin, nitric oxide synthase activities and angiogenic poise in red- and white-blooded Antarctic notothenioid fishes. *Comp. Biochem Physiol A Mol. Integr. Physiol.* **156**, 422–429.
40. Watanabe, S. and Wakasugi, K. (2008) Zebrafish neuroglobin is a cell-membrane-penetrating globin. *Biochemistry* **47**, 5266–5270.
41. Ishikawa, H., Kim, S., Kwak, K., Wakasugi, K., and Fayer, M. D. (2007) Disulfide bond influence on protein structural dynamics probed with 2D-IR vibrational echo spectroscopy. *Proc. Natl. Acad. Sci. USA* **104**, 19309–19314.
42. Dewilde, S., Kiger, L., Burmester, T., Hankeln, T., Baudin-Creuz, V., Aerts, T., Marden, M. C., Caubergs, R., and Moens, L. (2001) Biochemical characterization and ligand binding properties of neuroglobin, a novel member of the globin family. *J. Biol. Chem.* **276**, 38949–38955.
43. Fields, P. A. and Somero, G. N. (1998) Hot spots in cold adaptation: localized increases in conformational flexibility in lactate dehydrogenase A4 orthologs of Antarctic notothenioid fishes. *Proc. Natl. Acad. Sci. USA* **95**, 11476–11481.
44. Somero, G. N. (2010) The physiology of climate change: how potentials for acclimatization and genetic adaptation will determine winners and losers. *J. Exp. Biol.* **213**, 912–920.